High resolution multi-nuclear 1 and 2D NMR characterization of stannous halide complexes of Rh(I/III) in aqueous and non-aqueous solutions

By

SHANI BARKHUYSEN, MSc (Stellenbosch)

Dissertation submitted to the Faculty of Science at Stellenbosch University in fulfilment of the requirements for the degree of

DOCTOR OF PHILOSOPHY

Supervisor: Professor Klaus R. Koch

March 2016

Declaration

By submitting this thesis electronically, I declare that the entirety of the work contained herein is my own, original work, that I am the sole author thereof (save to the extent explicitly otherwise stated), that reproduction and publication thereof by Stellenbosch University will not infringe any third party rights and that I have not previously in its entirety or in any part submitted it for obtaining any qualification.

March 2016

.

Acknowledgements

I would sincerely like to thank

- First and foremost, my supervisor, Professor Klaus R. Koch. Without your support and guidance, motivation and understanding this thesis would not have been possible. Thank you for always believing in me.

- Dr. Wilhelmus J. Gerber for his time, advice and insightful conversations.

- Dr. Izak Kotze at the University of the Witwatersrand for all his time and assistance with 2D NMR spectroscopy.

- Anglo Platinum and NRF Scarce Skills for funding.

- NMR lab staff, Elsa Malherbe and Dr. Jaco Brand, for always being willing to help with the NMR.

- The technical staff of the Analytical Chemistry department, Shafiek Mohammed and Roger Lawrence. I would also like to give special thanks to Deidre Davids for always being there and for helping me since my 3rd year of BSc studies.

- The PGM research group for their friendship, support and the fun times we had together.

- My parents for their love, support and motivation throughout my studies.

- My husband, for always being there for me, believing in me and helping me to believe in myself.

- God for giving me the strength persevere.

List of Abbreviations

PGM(s)	Platinum Group Metal(s)
NMR	Nuclear Magnetic Resonance
UV/Vis	Ultra violet visible
ICP-OES	Inductively Coupled Plasma - Optical Emission Spectrometry
HMQC	Heteronuclear Multiple-Quantum Correlation
AQ336	Aliquat-336 (methyltrioctylammonium chloride)
PEG-400	Polyethylene glycol-400
Chloroform-*d* / $CDCl_3$-*d*	deuterated chloroform
MIBK	Methyl iso-butyl ketone
Diϕ400	$C_6H_5NHC(O)$-$O\{(CH_2CH_2O)_{8/9}\}$-$(O)CHNC_6H_5$ podand
D_2O	deuterium oxide
v/v	volume/volume
K	Kelvin
°C	Degree Celsius
ppm	parts per million (NMR)
Hz	Hertz, s^{-1}
$\delta(^{195}Pt)$	chemical shift of ^{195}Pt NMR signal
$\delta(^{119}Sn)$	chemical shift of ^{119}Sn NMR signal
γ	gyromagnetic ratio
$^2J(^{119/117}Sn\text{-}^{195}Pt)$	condensed form for $^2J(^{119}Sn\text{-}^{119}Sn)$ and $^2J(^{117}Sn\text{-}^{119}Sn)$ satellites
ax	axial
eq	equatorial
NSA	Natural Statistical Abundance
c/t	*cis/trans*

Conference Proceedings

This work was presented at the following conference:

Analitika, September 2014, Stellenbosch, Poster presented

Title: Speciation of stannous chloride complexes of rhodium(I/III) with high-resolution ^{119}Sn and ^{103}Rh (indirect) NMR spectroscopy.

[**Royal Society of Chemistry,** B**est student poster prize**]

Abstract

A detailed high-resolution multi-nuclear NMR study the stannous halide complexes of Rh(I/III) in aqueous and non-aqueous solutions has been undertaken. In this study the series of $[Rh^{III}(SnX_3)_nX_{6-n}]^{3-}$ (X = Cl^-/Br^-, n = 1 – 6) anions, the $[Rh^{I}(SnX_3)_5]^{4-}$ (X = Cl^-/Br^-) and the $[Rh^{III}H(SnX_3)_5]^{3-}$ (X = Cl^-/Br^-) complex anion have been synthesized and characterized by means of high-resolution ^{119}Sn NMR spectroscopy in both aqueous and non-aqueous phases. It is shown in this work that, in contrast to the tacitly accepted kinetically labile nature of these Rh(III)-Sn(II) species, these do not undergo rapid *inter*- and *intra*-molecular exchange of the SnX_3^- ligands rapidly on the NMR time scale and are indeed kinetically inert.

In aqueous HCl, the ^{119}Sn NMR spectra display up to 9 (of an expected 10) main sets of ^{119}Sn resonances split into doublets due to $^1J(^{103}Rh\text{-}^{119}Sn)$ (^{103}Rh: I = ½, 100 %) in addition to $^2J(^{117/119}Sn\text{-}^{119}Sn)$ coupling satellites. A detailed investigation of the resonances at $\delta(^{119}Sn)$ = -278.2 and -202.5 ppm reveals that the $^2J(^{119}Sn\text{-}^{119}Sn)$ satellites are not symmetrically distributed around the respective main signals. The set of resonances at -278.2 ppm was previously assigned to a kinetically labile *cis*-$[Rh^{III}(SnCl_3)_4Cl_2]^{3-}$ complex anion, whereas the signal at -202.5 ppm was unassigned. We now find that the ^{119}Sn NMR signals at -278.2 ppm and -202.5 ppm can be assigned to the equatorial and axial *isotopomers* of *cis*-$Rh^{III}(SnCl_3)_4Cl_2]^{3-}$, respectively. This implies that the *cis*-$Rh^{III}(SnCl_3)_4Cl_2]^{3-}$ complex anion is kinetically inert and results in two resonances due to the observed $^{119}SnCl_3^-$ ligand in the *axial* (*trans* to$SnCl_3^-$) position not being magnetically equivalent to the $^{119}SnCl_3^-$ ligand in the *equatorial* (*trans* to Cl^-) position. This is supported by a detailed analysis of the $^2J(^{119}Sn\text{-}^{119}Sn)_{cis,ax\text{-}eq}$ coupling in the various possible *isotopomers* of this complex, as well as the good agreement between the simulated spectra generated by a computer program gNMR50 and the spectra experimentally recorded. Moreover, the experimental ratio of $(\nu_A - \nu_B)/J_{AB} \sim 8.2$ suggests second order $^2J(^{119}Sn\text{-}^{119}Sn)$ coupling effects accounts for the asymmetrical $^2J(^{119}Sn\text{-}^{119}Sn)_{cis,ax\text{-}eq}$ satellites. Similarly the ^{119}Sn NMR spectra of other $[Rh^{III}(SnCl_3)_nCl_{6-n}]^{3-}$ (n = 1 - 5) species are consistent with kinetically inert complexes, including the $[Rh^{III}(SnCl_3)_6]^{3-}$ species detected for the 1st time in solution. The ^{119}Sn NMR signals of all the species in the series of $[Rh^{III}(SnCl_3)_nCl_{6-n}]^{3-}$ (n = 1 - 6) complex anions, as well as $[Rh^{I}(SnCl_3)_5]^{4-}$ and the $[Rh^{III}H(SnCl_3)_5]^{3-}$ have been correctly assigned.

The analogous series of $[Rh^{III}(SnBr_3)_nBr_{6-n}]^{3-}$ (n = 3 – 5) were prepared and characterized for the first time. Investigation of the stannous bromide complexes of rhodium(I/III) in HBr solutions furnished the assignment of 3 new $[Rh^{III}(SnBr_3)_nBr_{6-n}]^{3-}$ (n = 3 – 5) species. Moreover, the distinctive isotopomer pairs of these complex anions were assigned. It is thus established that these species, as with the analogous chlorido species, are kinetically inert and do not undergo rapid *intra*- or *inter*-molecular exchange on the NMR time-scale. Comparison between the ^{119}Sn NMR parameters of the stannous chlorido and stannous bromido species shows that the $^1J(^{103}Rh\text{-}^{119}Sn)$ coupling constant is smaller for the $[Rh^{III}(SnBr_3)_nBr_{6-n}]^{3-}$ (n = 3 – 5) species than the $[Rh^{III}(SnCl_3)_nCl_{6-n}]^{3-}$ species which suggests that the $^{103}Rh\text{-}SnBr_3^-$ bond length is longer than the $^{103}Rh\text{-}SnCl_3^-$ bond length.

^{119}Sn NMR spectroscopy showed that the kinetically inert $[Rh^{III}(SnCl_3)_nCl_{6-n}]^{3-}$ (n = 1 - 6) and $[Rh^{III}H(SnCl_3)_5]^{3-}$ complex anions, together with the $[Rh^{I}(SnCl_3)_5]^{4-}$, are extracted into non-aqueous solutions using methyl isobutyl ketone (MIBK) and methyltrioctylammonium chloride (AQ336) in chloroform. With a Rh:Sn mole ratio of more than 1:10, the $[Rh^{III}H(SnCl_3)_5]^{3-}$ complex anion predominates the non-aqueous solutions, however additional signals are always observed. A detailed ^{1}H and ^{119}Sn NMR study of the *isotopologues* and *isotopomers* of the $[Rh^{III}H(SnCl_3)_5]^{3-}$ species extracted into MIBK was undertaken. From the ^{119}Sn NMR spectrum, and with the aid of gNMR50 to simulate the spectra, two *isotopomers* (axial $^{119}SnCl_3^-$ and equatorial $^{119}SnCl_3^-$) and six *isotopologues* were assigned and characterized. Twelve respective *isotopologues* and *isotopomers* were assigned in the ^{1}H NMR spectrum of the $[Rh^{III}H(SnCl_3)_5]^{3-}$ complex anion. However, this was only achieved with the aid of a simulated ^{1}H NMR spectrum with gNMR50, wherein the ^{1}H NMR parameters were used to record a indirectly detected ^{103}Rh,^{1}H HMQC NMR spectrum for this species and the $\delta(^{103}Rh)$ was determined to be -1191 ppm. This is the first ^{103}Rh chemical shift value reported for these Rh(III)-Sn(II) species. Decreasing the stannous(II)chloride concentration, and thus the Rh:Sn mole ratio, in the aqueous phase results in the disappearance of the $[Rh^{III}H(SnCl_3)_5]^{3-}$ complex anion, accompanied by the formation of more ^{119}Sn NMR signals upfield of the hydrido species. These species correspond well to the kinetically inert species in the aqueous phase and is assigned accordingly. A detailed *isotopologue/isotopomer* study of all the species observed in the non-aqueous phases resulted in the assignment of 7 possible species: $[Rh^{III}(SnCl_3)_nCl_{6-n}]^{3-}$ (n = 2 – 6), including the $[Rh^{III}(SnCl_3)_6]^{3-}$ species not previously observed, $[Rh^{III}H(SnCl_3)_5]^{3-}$ and $[Rh^{I}(SnCl_3)_5]^{4-}$.

Moreover, 5 *isotopomer* pairs, as well as the respective *isotopologues*, for these species were identified and assigned for the first time.

Opsomming

‘n In-diepte hoë-resolusie, multi-kern KMR studie van die tin(II)halied komplekse van Rh(I/III) in beide waterige en nie-waterige oplossings is onderneem. Tydens hierdie studie is die reeks $[Rh(SnX_3)_nX_{6-n}]^{3-}$ (X = Cl^-/Br^-, n = 1 – 6) kompleksanione, die $[Rh(SnX_3)_5]^{4-}$ (X = Cl^-/Br^-) kompleksanioon en die $[RhH(SnX_3)_5]^{3-}$ (X = Cl^-/Br^-) kompleks anioon met hoë-resolusie ^{119}Sn KMR in beide waterige en nie-waterige oplossings geïdentifiseer en gekarakteriseer. Daarenbowe is bewys dat, in teenstelling met die stilswyend aanvaarde *stereo*-chemies nie-rigiede aard van die Rh(III)-Sn(I) spesies, hierdie spesies nie vinnige *inter*- en *intra*-molekulêre uitruiling van die SnX_3^- (X = Cl^- or Br^-) ligande op die KMR tydskaal ondergaan nie en dus dat hieride spesies wel *stereo*-chemies rigied is.

In waterige soutsuur oplossings word tot nege (van die verwagte tien) hoof stelle ^{119}Sn seine, elkeen verdeel in dublette weens $^1J(^{103}Rh\text{-}^{119}Sn)$ (^{103}Rh: I = ½, 100 %) en omring met $^2J(^{117/119}Sn\text{-}^{119}Sn)$ satelliete, in die ^{119}Sn KMR spektra vertoon. ‘n Meer in diepte ondersoek van die ^{119}Sn seine by -278.2 en -202.5 ppm het onthul dat die $^2J(^{119}Sn\text{-}^{119}Sn)$ satelliete nie simmetries rondom die hoof seine versprei is nie. Die ^{119}Sn KMR sein by -278.2 ppm was voorheen toegeskryf aan ‘n *stereo*-chemies rigiede *cis*-$[Rh^{III}(SnCl_3)_4Cl_2]^{3-}$ kompleksanioon, terwyl die sein by -202.5 ppm nie geïdentifiseerd was nie. Tydens hierdie studie is egter gewys dat die ^{119}Sn KMR seine by -278.2 ppm en -202.5 ppm aan die ekwatoriale en aksiale isotopomere van die *cis*-$[Rh^{III}(SnCl_3)_4Cl_2]^{3-}$ kompleksanioon onderskeidelik toegeskryf kan word. Dit impliseer dus dat die *cis*-$[Rh^{III}(SnCl_3)_4Cl_2]^{3-}$ kompleksanioon *stereo*-chemies rigied is en gevolglik dat twee afsonderlike seine verkry word vir die isotopomere waarin die waargenome $SnCl_3^-$ ligande in die aksiale (*cis* aan Cl^-) en ekwatoriale (*trans* aan Cl^-) posisies is, aangesien hierdie twee ^{119}Sn atome nie magneties ekwivalent is nie. Hierdie toeskrywing word ondersteun deur ‘n gedetailleerde analise van die $^2J(^{119}Sn\text{-}^{119}Sn)_{cis,ax\text{-}eq}$ koppeling in die verskillende moontlike isotopomere van hierdie kompleks, sowel as simulasies van die verwagte spektra met behulp van ‘n rekenaar program, gNMR50, wat goed ooreenstem met die eksperimenteel verkreide spektra. Verder dui die eksperimenteel verkreide verhouding van $(\nu_A - \nu_B) / J_{AB} \sim 8{,}2$ daarop dat die asimmetriese $^2J(^{119}Sn\text{-}^{119}Sn)_{cis,eq\text{-}ax}$ satelliete toegeskryf kan word aan tweede orde $^2J(^{119}Sn\text{-}^{119}Sn)$ koppelingseffekte. Net so is die ^{119}Sn KMR spektra van ander $[Rh^{III}(SnCl_3)_nCl_{6-n}]^{3-}$ (n = 1 - 5) spesies ook in ooreenstemming met *stereo*-chemies rigiede komplekse, insluitende die van die $[Rh^{III}(SnCl_3)_6]^{3-}$ spesies, wat vir die eerste keer in

oplossings geïdentifiseer en gekarakteriseer is. Die ^{119}Sn KMR seine van die reeks $[Rh^{III}(SnCl_3)_nCl_{6-n}]$ 3- (n = 1-6) anione, sowel as $[RH^{I}(SnCl_3)_5]^{4-}$ en die $[Rh^{III}H(SnCl_3)_5]^{3-}$ is korrek toegedien.

Tydens hierdie studie is die reeks $[Rh^{III}(SnBr_3)_nBr_{6-n}]^{3-}$ (n = 3 - 5) spesies is vir die eerste keer voorberei en gekarakteriseer deur middel van hoë-resolusie ^{119}Sn KMR. Ondersoek van die tin(II)bromied komplekse van rodium(I/III) in HBr oplossings het gelei to die toedeling van 3 nuwe $[Rh^{III}(SnBr_3)_nBr_{6-n}]^{3-}$ (n = 3 - 5) spesies. Daarenbowe is die isotopomeerpare ($^{119}SnBr_3^-$ *trans* tot $SnBr_3^-$ of *trans* tot Br^-) van elk van hierdie kompleksanione geïdentifeseer en gekarakteriseer. Dit is dus vasgestel dat hierdie spesies, soos gevind met die ooreenstemmende chloried spesies, *stereo*-chemies rigied is en nie vinnige *intra*- of *inter*-molekulêre uitruiling op die KMR tydskaal ondergaan nie.

Vergelyking tussen die ^{119}Sn KMR parameters van die tin(II)chloride en tin(II)bromide Rh(III) spesies toon dat die $^1J(^{103}Rh\text{-}^{119}Sn)$ koppelings-konstante kleiner is vir die $[Rh^{III}(SnBr_3)_nBr_{6-n}]^{3-}$ (n = 3 - 5) spesies as vir die $[Rh^{III}(SnCl_3)_nCl_{6-n}]^{3-}$ spesies wat daarop dui dat die $^{103}Rh\text{-}SnBr_3^-$ bindingslengte langer is as die $^{103}Rh\text{-}SnCl_3^-$ bindingslengte.

^{119}Sn KMR spektroskopie het getoon dat die *stereo*-chemies rigiede $[Rh^{III}(SnCl_3)_nCl_{6-n}]^{3-}$ (n = 1 - 6) en $[Rh^{III}H(SnCl_3)_5]^{3-}$ komplekse anione, asook die $[Rh^{I}(SnCl_3)_5]^{4-}$ spesies, in metiel iso-butiel ketoon (mibk) en metiel tri-oktiel ammonium chloried (Aliquat-336 of AQ336) in chloroform in geekstraeer word. Alhoewel die $[Rh^{III}H(SnCl_3)_5]^{3-}$ kompleksanioon die oorheersende spesies in die nie-waterige oplossings is wanneer 'n Rh:Sn molverhouding van meer as 1:10 gebruik is, word daar altyd steeds addisionele seine waargeneem. 'n Gedetailleerde ^{1}H en ^{119}Sn KMR studie van die isotopoloë en isotopomere van die $[Rh^{III}H(SnCl_3)_5]^{3-}$ spesies in MIBK is onderneem. Vanaf die verkrygde ^{119}Sn KMR spektrum, en met die hulp van gNMR50 om die spektra te simuleer, is twee isotopomere (aksiale (*trans* tot Cl^-) $^{119}SnCl_3^-$ en ekwatoriale (*trans* tot $SnCl_3^-$) $^{119}SnCl_3^-$) en ses isotopoloë geïdentifiseer en gekarakteriseer. Daarteenoor is twaalf onderskeie isotopoloë en isotopomere in die ^{1}H KMR spektrum van die $[Rh^{III}H(SnCl_3)_5]^{3-}$ kompleksanion geïdentifiseer. Die karakterisering van hierdie isotopoloe en isotopomere was egter slegs moontlik met die hulp van 'n gNMR50 gesimuleerde ^{1}H KMR spectrum. Die ^{1}H KMR parameters is gebruik vir ‘n indirekte metode om ^{103}Rh te analiseer: ^{103}Rh, ^{1}H “HMBK” KMR. Die ^{103}Rh, ^{1}H KMR spektrum vir hierdie

spesies het een sein getoon met δ(^{103}Rh) = -1191 dpm. Dit is die eerste ^{103}Rh chemiese verskuiwing waarde wat vir hierdie Rh(III)-Sn(II) spesies berig is.

Die vermindering van die Rh:Sn molverhouding in die waterige fase het tot gevolg gehad dat die $[Rh^{III}H(SnCl_3)_5]^{3-}$ kompleksanioon minder word, terwyl meer ^{119}Sn KMR seine veld-op van die hydrido spesies gevorm word. Hierdie spesies stem goed ooreen met die *stereo*-chemies rigiede spesies in die waterige fase en is dienooreenkomstig toegedien. 'n Gedetailleerde isotopoloog/isotopomeer studie van al die waargeneem in die nie-waterige fases spesies gelei het tot die toedeling van 7 moontlike spesies: $[Rh^{III}(SnCl_3)_nCl_{6-n}]^{3-}$ (n = 2 - 6), insluitend die $[Rh^{III}(SnCl_3)_6]^{3-}$ spesies nie voorheen waargeneem is nie, $[Rh^{III}H(SnCl_3)_5]^{3-}$ en $[Rh^{I}(SnCl_3)_5]^{4-}$. Verder is daar 5 isotopomeerpare, asook die onderskeie isotopoloë vir hierdie spesies geïdentifiseer vir die eerste keer.

Table of Contents

CHAPTER V: Stannous chloride complexes of rhodium(I/III) in non-aqueous solutions

CHAPTER VI: General Discussion and Conclusions

List of Figures

Figure 4.7 The ^{119}Sn NMR spectrum of (A) the $[Rh(SnCl_3)_5Cl]^{3-}$ species is shown, as well as the assignment of the two respective *isotopomers* and (B) the $[Rh(SnBr_3)_5Br]^{3-}$ species with $\delta(^{119}Sn)$ = -267.6 ppm and -324.4 ppm, split into doublets due to $^1J(^{103}Rh\text{-}^{119}Sn)$ = 523 Hz (a) and 562 Hz (b), respectively. The spectrum is tentatively assigned to the respective species as shown. (C) The simulated spectrum using gNMR50.

Figure 4.8 The simulated ^{119}Sn NMR spectrum and the respective $^1J(^{103}Rh\text{-}^{119}Sn)$ and $^2J(^{119/117}Sn\text{-}^{119}Sn)$ spin-couplings of the set of signals at (A) $\delta(^{119}Sn)$ = -324.4 ppm and at (B) $\delta(^{119}Sn)$ = -267.6 ppm. The $\Delta\nu_{½}$ is set to 10 Hz to increase resolution.

Figure 5.1 ^{119}Sn NMR spectrum of the $[RhH(SnCl_3)_5]^{3-}$ species that was extracted into methyl isobutylketone (MIBK) from an aqueous solution containing $[Rh(SnCl_3)_5]^{4-}$ at 25 °C.

Figure 5.2 The expanded ^{119}Sn NMR spectra of the sets of signals at -13.3 ppm and 80 ppm. The $^1J(^1H\text{-}^{119}Sn)_{cis}$ and $^1J(^1H\text{-}^{119}Sn)_{trans}$ spin couplings are indicated by symbols a and 'a' respectively. The $^1J(^{103}Rh\text{-}^{119}Sn)$ spin couplings are indicated by the symbols b and 'b' and the $^2J(^{119/117}Sn\text{-}^{119}Sn)$ spin couplings are indicated by the symbols c and 'c'. The relative integrals of the respective peaks are 1 to 4.

Figure 5.3 The ^{119}Sn NMR spectra of the sets of signals at -13.3 ppm and 80 ppm obtained (A) experimentally and (B) simulated using gNMR50. The good correlation between the experimental and simulated spectra allowed for the assignment of the $^2J(^{117}Sn\text{-}^{119}Sn)_{trans,eq\text{-}eq}$ satellites of the $[RhH(SnCl_3)_5]^{3-}$ complex anion, which was complicated by the overlap of these satellites with the set of signals at $\delta(^{119}Sn)$ = 80.0 ppm assigned to the $[RhH(SnCl_3)_5]^{3-}$ *isotopomer* where the observed $^{119}SnCl_3^-$ ligand is *trans* to ^{1}H

Figure 5.4 The simulated ^{119}Sn NMR spectrum of (A) the set of signals at $\delta(^{119}Sn)$ = -13.3 ppm assigned to the 'equatorial' $[RhH(SnCl_3)_5]^{3-}$ complex anion where the observed $^{119}SnCl_3$ ligand is *trans* to another $^{119}SnCl_3$ ligand and (B) the set of signals at $\delta(^{119}Sn)$ = 80.0 ppm assigned to the 'axial' $[RhH(SnCl_3)_5]^{3-}$ complex anion where the observed $^{119}SnCl_3$ ligand is *trans* to Cl^-. The width at half height of the signals was set to 5 Hz to improve the resolution of the signals in order to assign the all the respective ^{1}J and ^{2}J spin couplings, indicated by symbols a to d.

Figure 5.5 ^{1}H NMR spectrum of A) the $[Rh^{III}H(SnCl_3)_5]^{3-}$ species that was extracted into methyl isobutylketone (MIBK) from an aqueous solution containing $[Rh^I(SnCl_3)_5]^{4-}$ at 25 °C. The symbol a indicates the $^1J(^{103}Rh\text{-}^{119}Sn)$ spin coupling, and symbols b and c indicates the $^2J(^{119/117}Sn\text{-}^1H)$ spin couplings. B) Simulated ^{1}H NMR spectrum of the $[RhH(SnCl_3)_5]^{3-}$ species using the NMR parameters obtained from the experimental spectrum.

Figure 5.6 The simulated ^{1}H NMR spectrum of the set of signals at $\delta(^1H)$ = -12.78 ppm assigned to the $[Rh^{III}H(SnCl_3)_5]^{3-}$ complex anion where (A) shows an expansion of the $^2J(^{119/117}Sn\text{-}^1H)_{cis}$ satellites and (B) an expansion of the $^2J(^{119/117}Sn\text{-}^1H)_{trans}$ satellites. The width at half height of the signals was set to

List of Tables

List of Schemes

Scheme 3.5 A schematic representation of the *cis*-$[Rh(SnCl_3)_4Cl_2]^{3-}$ complex anion where the ^{119}Sn nucleus is a) in the equatorial and b) in the axial position. All coordinated chlorido ligands of $SnCl_3^-$ are left out for clarity.

Scheme 3.6 Schematic representation of the *cis*-$[Rh(SnCl_3)_4Cl_2]^{3-}$ complex that shows all the various $^2J(^{117}Sn\text{-}^{119}Sn)$ and $^2J(^{119}Sn\text{-}^{119}Sn)$ couplings observed for the respective *isotopomers* and *isotopologues* possible for this complex. All coordinated chlorido ligands of $SnCl_3^-$ are left out for clarity.

Scheme 3.7 A schematic representation of two *isotopomers* of the $Rh(SnCl_3)_5Cl]^{3-}$ complex anion, as well as its possible ^2J scalar couplings, where the observed $^{119}SnCl_3^-$ ligand is a) in the axial (*trans* to Cl^-) and b) in the equatorial (*cis* to Cl^-) position. In (a) the $^{119}Sn_{ax}$ ligand (blue) can scalar couple to either a $^{117}Sn_{eq}$ ligand, $^2J(^{117}Sn_{eq}\text{-}^{119}Sn_{ax})$, or to a $^{119}Sn_{eq}$ ligand, $^2J(^{119}Sn_{eq}\text{-}^{119}Sn_{ax})$. In (b) the $^{119}Sn_{eq}$ ligand (blue) can scalar couple to either a $^{117}Sn_{ax}$ or a $^{119}Sn_{ax}$ ligand, $^2J(^{117}Sn_{ax}\text{-}^{119}Sn_{eq})$ and $^2J(^{119}Sn_{ax}\text{-}^{119}Sn_{eq}$, or to a $^{117}Sn_{eq}$ ligand, $^2J(^{117}Sn_{eq}\text{-}^{119}Sn_{eq})$. All coordinated chlorido ligands of $SnCl_3^-$ are left out for clarity.

Scheme 3.8 A schematic representation of a) the $Rh(SnCl_3)_6]^{3-}$ complex anion and its possible *isotopomers* where the ^{119}Sn nucleus is b) in the axial and c) in the equatorial position. All Cl^- ions are left out for clarity

Scheme 4.1 Schematic representation of (a) the $[^{103}Rh(^{i}SnBr_3)_n(^{119}SnBr_3)_{3-n}Br_3]^{3-}$ (n = 0 – 2) and (b) the $[^{103}Rh(^{i}SnBr_3)_n(^{119}SnBr_3)(^{117}SnBr_3)_{2-n}Br_3]^{3-}$ (n = 0,1) *isotopologues* of *fac*-$[Rh(SnBr_3)_3Br_3]^{3-}$ complex anion resonating at $\delta(^{119}Sn)$ = -407.2 ppm. All coordinated bromido ligands of $SnBr_3^-$ are left out for clarity. The $^{119}Sn/^{i}Sn$ label on atoms means that that atom can represent either ^{119}Sn or ^{i}Sn in a specific *isotopologue*.

Scheme 4.2 A schematic representation of the *cis*-$[Rh(SnBr_3)_4Br_2]^{3-}$ complex where the observed $^{119}SnBr_3^-$ ligand is (A) in the axial position and (B) in the equatorial position. If the observed ^{119}Sn is in the axial position (*trans* to another $^{i}SnBr_3^-$ ligand) it has a different chemical shift to the case when it is in the equatorial (*trans* to a Br^-), supporting the suggestion that these species are kinetically inert. The $^1J(^{103}Rh\text{-}^{119}Sn)$ couplings in the different *isotopomers* are indicated with the symbols ‘a’ and ‘d’, respectively, which correspond to the splitting indicated by symbols ‘a’ and ‘d’ in Figure 4.6B. Similarly, the possible $^2J(^{119/117}Sn\text{-}^{119}Sn)$ scalar couplings are indicated with symbols ‘b’, ‘c’, ‘e’, ‘f’ and ‘g’ and correspond to respective satellites shown in Figure 4.6B. All coordinated bromido ligands of $SnBr_3^-$ are left out for clarity

Scheme 4.3 A schematic representation of two *isotopomers* of $Rh(SnBr_3)_5Br]^{3-}$ complex anion where the observed $^{119}SnBr_3^-$ ligand is a) in the axial (*trans* to Br^-) and b) in the equatorial (*cis* to Br^-) position. Moreover, the expected $^2J(^{119/117}Sn\text{-}^{119}Sn)$ spin-couplings for each *isotopomer* are indicated on the scheme. All coordinated bromido ligands of $SnBr_3^-$ are left out for clarity.

Scheme 5.1 Schematic representation of two *isotopomers* and *isotopologues* of the $[RhH(SnCl_3)_5]^{3-}$ species. The observed ^{119}Sn nucleus is encircled. All Cl^- ligands of the $SnCl_3^-$ ligand are left out for clarity.

Scheme 5.2 Schematic representation of two different *isotopomers* of the $[RhH(SnCl_3)_5]^{3-}$ species where the $^{119}SnCl_3^-$-ligand is (a) *cis* and (b) *trans* to the observed ^1H nucleus.

Scheme 5.3 Schematic representation of the kinetically inert $[Rh(SnCl_3)_6]^{3-}$ species.

Scheme 5.4 Schematic representation of the *isotopomer* of the $[Rh(SnCl_3)_5Cl]^{3-}$ complex anion where the observed ^{119}Sn nucleus is in the equatorial position. All coordinated chlorido ligands of $SnCl_3^-$ are left out for clarity.

Chapter I

General Introduction and Background

Chapter I

General Introduction and Background

> *"My inquiries having terminated more successfully than I had expected, I design in the present Memoir to prove the existence, and to examine the properties, of another metal, hitherto unknown, which may not improperly be distinguished by the name of* ***Rhodium****, from the rose-colour of a dilute solution of the salts containing it."*
>
> William Hyde Wollaston.

More than two centuries ago, in 1803, Dr. William Hyde Wollaston studied 'platina', samples of dense silver metal from South America, and discovered that several other metals were present in this substance.[1] This discovery was greatly aided by the chemical reaction of stannous chloride (muriate of tin) with the complexes of the platinum group metals, which are highly coloured in acid solution. In the words of Wollaston "the action of muriate of tin upon the solutions of these metals, is also totally different" and platinum and palladium complexes could be distinguished by the intense colours they produce ranging from blue to green, yellow and blood-red. It was found that samples of 'Platina' contained platinum, palladium, iridium, osmium and rhodium.

Rhodium is one of the rarest elements on earth, with only 0.0002 ppm estimated to be in the earth's crust, and with negligible amounts found in seawater or the atmosphere.[2] Rhodium is also one of the most expensive rare metals, however, the demand of this rare metal is ever increasing due to its favourable properties such as its resistance to corrosion and its reflective exterior, resulting in rhodium being electroplated onto white gold and platinum jewellery to give it that shiny finish and to prevent tarnish of the surface. Moreover, with the recent increase in the demand of LCD glass for TVs and mobile devices, the demand for rhodium has also increased.[3] The chemical industry also caused an increase in the demand of rhodium due to their high catalytic activity toward toward dehydrogenation, hydrogen transfer reactions as well as the isotopic exchange of hydrogen. However, the primary use of rhodium is for auto-catalyst and a recent report by Johnson Matthey showed that in 2013 78.8 % of the demand for rhodium came from the auto sector, Figure 1.1a.[3]

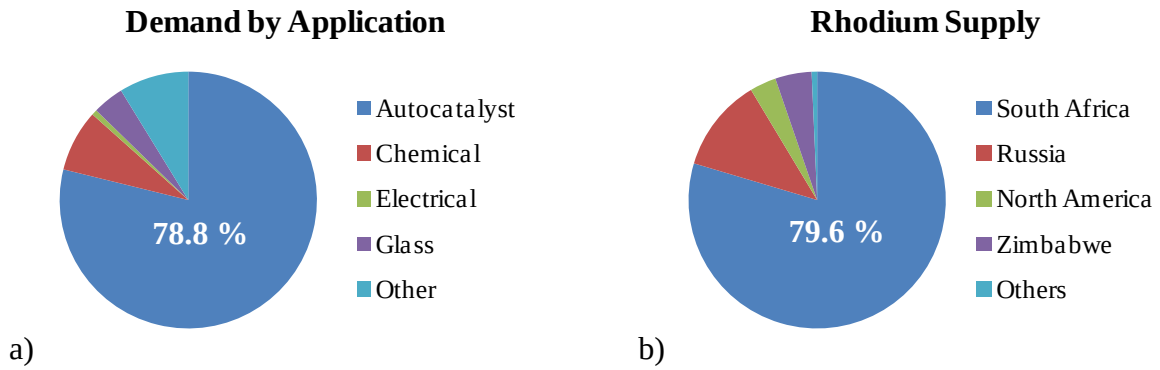

a) b)

Figure 1.1 From the various applications that contribute to the high demand of rhodium, a, it is clear that the primary use of rhodium is by the auto-catalyst sector. The countries that supply rhodium is shown in b and it is evident that South Africa is the primary producers of rhodium. [3]

Rhodium is obtained by the mining of platinum and palladium; however the industrial extraction of rhodium is very expensive due to its rarity and high melting point. Thus, only approx. 25 tons of rhodium is extracted per year in comparison to 2,500 tons of gold. South Africa is the largest producer of rhodium, Figure 1.1b, supplying almost 80 % of the world's rhodium.[3] However, the high cost of PGMs and their limited natural resources stresses the importance of recycling these metals. Between 2008 and 2012 approximately 20 – 30 % of the rhodium's total annual supply came from recycling automotive catalytic converters. With the ever-growing demand for rhodium and with its limited natural resources, it is important to find efficient and cost-effective separation processes to recover rhodium with high purity from diverse secondary resources. Solvent extraction and ion exchange have been proposed for this purpose.[4,5]

The separation and purification of rhodium from the other PGMs, however, is extremely difficult due to its chemical behaviour in chloride media.[6] Rhodium form octahedral aquo-chlorido complexes of the general formula $[RhCl_n(H_2O)_{6-n}]^{3-n}$ (n = 5 or 6) in concentrated chloride media. These highly charged complexes are nearly impossible to extract[7] due to the steric hindrance of the octahedral complex and the difficulty of packing two or three cationic organic molecules around a relatively small single ion.[6] Moreover, the $[RhCl_n(H_2O)_{6-n}]^{3-n}$ (n = 5 or 6) complexes are kinetically inert, rendering the replacement of Cl^- or H_2O in the inner coordination sphere by extractants unsuccessful.

It has been shown by several authors that the addition of tin(II)chloride to acidic solutions of rhodium greatly increases the extractability of rhodium into the organic phase using various different methods, so aiding in the separation thereof from other platinum group metals (PGMs).[6,8,9]

1.1 Reaction of Stannous Halides with Rhodium in aqueous acidic solutions

In 1918 Ivanov reported that Rhodium(III) salts a hydrochloric acid solution slowly turned red when tin(II) chloride was added to the solution.[10] This reaction was readily adopted as a qualitative spot test for trace levels of rhodium[11,12] and was later used for quantitative measurements using colourimetry.[13,14] However, accurate quantification is complicated by interferences by other PGMs.[14] This difficulty was overcome by Ayres and co-workers who reported a spectrophotometric method for the determination of rhodium,[15,16] without knowledge about the nature of the coloured Rh-tin compounds formed. Moreover, this spectrophotometric method enabled Ayres and co-workers to simultaneously determine rhodium and platinum in solution. The addition of tin(II) chloride to a hydrochloric acid solution of platinum(II/IV) resulted in an absorbance maximum at 403 μm[17,18] compared to an absorbance maximum at 475 μm obtained for the corresponding solution with Rh(III) and Sn(II).[16] In a similar study, Berman and Ironside[19] reported that the reaction of tin(II) bromide with rhodium salts in hydrobromic acid produced an intense yellow coloured solution that was suitable for the spectrophotometric determination of rhodium and has an absorbance maximum at 427 μm. Using this method, Berman and Ironside could determine the concentration of rhodium in the presence of equal quantities of iridium. Thus, using spectrophotometric methods rhodium could be quantified in the presence of other elements such as platinum,[16] iridium[19,20] and uranium[21] without prior separation. Even though this method of quantification gave little insight as to the nature of these coloured Rh-Sn species, Sandell[22] reported the formation of a red and a yellow form of rhodium, which indicated the formation of two different species. The “red form” was observed in solutions of 2 M HCl and had an absorption maximum at 480 nm, whereas on dilution with water the solution turned yellow with the absorption maxima being blue-shifted to 435 nm. Sandell[22] suggested that reduction of rhodium to a lower oxidation state (but not to colloidal metal) occurs, and that the formation of one or more chlorido complexes is involved. However, the first significant

attempts to isolate and determine the structure of the Rh-Sn species responsible for such coloured solutions only took place in 1963 by Davies *et. al.*[23]

1.1.1 Determination of nature of coloured Rh-Sn species

Davies *et. al.* showed for the Rh(III) and tin(II) chloro-system, using visible absorption spectroscopy with Job's method, that a Rh:Sn ratio of 1:3 is required for the formation of the red complex.[23] Furthermore, addition of bulky cations such as tetramethylammonium chloride to the coloured solutions resulted in the formation of orange-yellow precipitates, the microanalytical data of which suggested the formation of the $[(CH_3)_4N]_4[Rh_2Sn_4Cl_{14}]$ species. The reaction between rhodium(III)chloride and tin(II)chloride in 3 M HCl was suggested to be as follows:

$$2RhCl_3 + 6SnCl_3^- \rightleftharpoons [Rh_2Sn_4Cl_{14}]^{4-} + 2SnCl_5^- \qquad 1.1$$

Thus three equivalents of tin(II) are required per molecule of Rh(III): one molecule was thought to reduce the Rh(III) to Rh(I), and two $SnCl_3^-$ ions were thought to be necessary for complexation.[24] The resulting binuclear anion, believed to be a square planar Rh(I) complex, was postulated to be formed either by $SnCl_3^-$ coordination or with solvated tin(II) chloride, illustrated in Scheme 1.1.

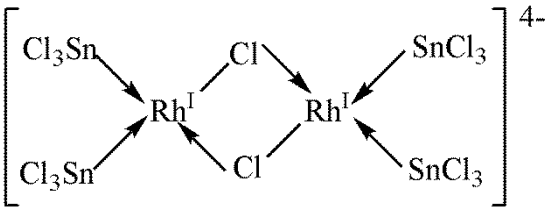

Scheme 1.1 Anionic complex suggested by Davies *et al.* to form on reaction of tin(II) chloride with Rh(III).[23,24]

The assignment by Davies *et. al.* was supported by the far-infrared spectrum reported by Adams and Chandler[25] wherein they assigned the stretching frequencies at 363 (w) and 336 (ms) cm^{-1} to $SnCl_3$. This is contrary to a π-$C_5H_5W(CO_3)SnCl_3$ species, which were reported to be complexes of tin(IV).[26,27]

As mentioned above, spectrophotometric studies of this Rh-Sn(II)-chloride system shows that there are two species possible: solutions with low concentrations of $SnCl_3^-$ (Rh:Sn mole ratio of less than 4) shows absorption maxima at 419 mμ and 310 mμ,[20,21] whereas a shift to higher wavelengths was observed in the spectrum of solutions with a large excess $SnCl_3^-$ with absorption maxima at 470 mμ and 330 mμ.[16,17,21,26] Furlani *et. al.*[28] showed that the proportions of these two species are dependent on mainly the relative $SnCl_3^-$:Cl^- mole ratio and not the Rh:$SnCl_3^-$ mole ratio. Moreover, by contrast to the results obtained by Davies *et. al.*,[23] Furlani *et. al.*[28] postulated that in tin-rich hydrochloric acid solutions containing rhodium(III), a mononuclear d^8-rhodium(I) anion with a tetragonal planar structure, shown in Scheme 1.2, was formed which could be extracted into iso-amyl alcohol.

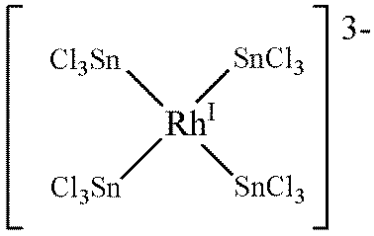

Scheme 1.2 Anionic Rh(I) complex suggested by Furlani *et. al.*[28] to form on reaction of tin(II) chloride with Rh(III).

In a similar study, Furlani *et. al.* reportedly isolated the $[IrCl_2(SnCl_3)_4]^{3-}$ complexes from both aqueous solutions and iso-amyl alcohol extracts.[29] This is in contrast to the $[Ir_2Cl_6(SnCl_3)_4]^{4-}$ species isolated by Young and co-workers.[24] Further support for this mononuclear species, $[IrCl_2(SnCl_3)_4]^{3-}$, was obtained from a number of four-coordinated rhodium(I) complexes containing carbon monoxide or organic ligands such as norbornadiene, triphenylphosphine and triphenylarsine in addition to the hallogenostannate(II) ligands have been reported by Furlani *et. al.*[27,28] Up to this point, characterization of the Rh-Sn species formed in solution was based on the assumption that rhodium(III) would be reduced to rhodium(I) by tin(II), with concomitant oxidation to tin(IV). However, for several complexes such as $[RhCl_3(SnCl_3)(norbornadiene)_2]$,[30] $[RhCl_2(SnCl_3)(PhMe_2As)_3]$[27] and $[RhCl(SnCl_3)_2py_3]$[31] the authors showed these to be d^6 six-coordinate Rh(III) complexes with coordinated $SnCl_3^-$ ligands and not rhodium(I) complexes.

In the 1980's Kimura and co-workers[32,33] also studied the reaction of tin(II) chloride with rhodium(III) chloride, and similarly to Sandell[22] obtained both a yellow and a red solution

depending on conditions. However, where Sandell believed the yellow solutions to be due to a single Rh-Sn species, Kimura *et. al.*[32,33] isolated three complexes from the yellow Rh-Sn solutions using tetramethylammonium chloride. These were characterized as a new series of six-coordinated rhodium(III) $[(CH_3)_4N]_3[Rh(SnCl_3)_nCl_{6-n}]$ (n = 2, 3, 4) complexes. This suggested that under certain experimental conditions tin(II)chloride does not reduce rhodium(III) to rhodium(I) compounds. A species isolated from a purple solution, on the other hand, was considered to be a five-coordinate rhodium(I) species formulated as $[M(NH_3)_6]_3[Rh(SnCl_3)_5][SnCl_3]Cl_4 \cdot 4H_2O$ (M = Rh(III) or Ir(III)).[32,33] Furthermore, Kimura *et. al.*[32,33] reported that in the presence excess Br^- anions in hydrochloric acid solutions a $[Rh(SnCl_3)_3Cl_3]^{3-}$ complex is rapidly converted to the $[Rh(SnBr_3)_3Br_3]^{3-}$ complex. Elemental analysis data, as well as IR data supported this by the disappearance of the Rh-Cl stretching vibrations at 303 and 275 cm^{-1} in the IR spectrum, due to the formation of a bromido Rh-Sn species. Both the $[Rh(SnCl_3)_3Cl_3]^{3-}$ and the $[Rh(SnBr_3)_3Br_3]^{3-}$ species were considered to be in the facial conformation as it is thought to be thermodynamically more stable than the *mer*-isomer due to the known π-acceptor properties of $SnCl_3^-$ as a ligand.[34]

In 1979, Antonov *et. al.*[35] isolated a $Cs_3[RhCl_4(SnCl_3)_2]$ complex in addition to a series of $(Me_4N)_3[RhX_n(SnX_3)_{6-n}]$ (X = Cl^-/Br^-, n = 1, 2, 3) complexes, all of which were octahedral rhodium(III) complexes. The structure of these species was determined using, among other techniques, ^{119}Sn Mössbauer and far infrared spectroscopy. The infrared and Mössbauer spectra confirmed that the SnX_3^- ligand was coordinated to a rhodium(III) centre through a tin atom.[31,36] The decrease in the Mössbauer chemical shift (δ) observed in the ^{119}Sn Mössbauer spectra on going from the salt, $[Me_4N][SnX_3]$, to the Rh(III)-Sn(II) species indicated an decrease in the density of the $5s^2$ electrons on the tin(II) atom as a result of the σ-donor interaction of the SnX_3^- ligands with the rhodium(III) ion.[31,37] The corresponding increase in the quadrupole splitting (ϵ) is due to the π-acceptor interaction of the SnX_3^- ligand coordinated to the metal ion. These authors found that the Mössbauer chemical shift and quadrupole splitting values for the six-coordinate Rh(III)-Sn(II)Cl_3 species isolated were practically the same as the published values of the Rh(I)-Sn(II) complexes previously formulated as $[Rh_2Cl_2(SnCl_3)_4]^{4-}$, $[Rh(SnCl_3)_4]^{3-}$ and $[Rh(SnCl_3)_5]^{4-}$.[20,21,35,38] The Rh(III)-Sn(II) and Rh(I)-Sn(II) species obtained using practically the same experimental conditions, lead Antonov and co-workers[25] to suggest that the cited authors[20,21,35,38] were in fact also dealing with trichlorostannato complexes of Rh(III) and not Rh(I) as they reported.

A year later Kimura and Sakurai managed to isolate a violet salt from an aged purple solution that was suitable for single crystal X-ray diffraction analysis.[39] The crystal structure, given in Scheme 1.3, shows the complex, $[Rh(SnCl_3)_4SnCl_4]^{5-}$, to be trigonal bipyramidal, with one of the three Sn atoms in the equatorial plane having a distorted trigonal bipyramidal form, and the other four Sn atoms having distorted tetrahedral arrangements. The diffraction data showed that the salt consisted of three cations, $[Rh(NH_3)_6]^{3+}$, two kinds of anions, $[Rh^{I}(SnCl_3)_4(SnCl_4)]^{4-}$ and $[SnCl_6]^{4-}$, together with four molecules of water of crystallization and is formulated as $[Rh(NH_3)_6]_3[Rh^{I}(SnCl_3)_4(SnCl_4)][SnCl_6]\cdot 4H_2O$.

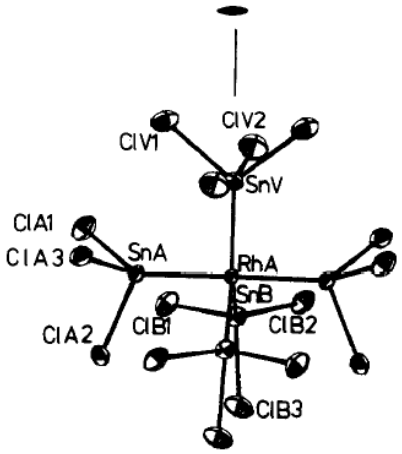

Scheme 1.3 Crystal structure of $[Rh(SnCl_3)_4(SnCl_4)]^{4-}$ reported by Kimura *et. al.* [39]

This was the first direct evidence for the true structure of these Rh-Sn species. However, the X-ray data reported was not good. To date this is the only crystal structure in the literature for such trichlorostannato complexes of rhodium(I), which shows the difficulty of obtaining such crystals.

In 1977 Lasigne and Wells reported high resolution and high sensitivity methods in pulse Fourier-transform ^{119}Sn NMR spectroscopy are particularly useful for the characterization of inorganic tin species, especially for *in situ* solutions.[40] Subsequently, Moriyama *et. al.*[41] used ^{119}Sn NMR to study the rhodium-tin complexes formed in aqueous HCl solutions and showed that the series of six-coordinate $[Rh^{III}(SnCl_3)_nCl_{6-n})]^{3-}$ (n = 1 – 5) existed in solution, as well as a mononuclear Rh(I) species $[Rh(SnCl_3)_5]^{4-}$, with 5 $SnCl_3^-$ ligands coordinated to the rhodium. The $[Rh(SnCl_3)_5]^{4-}$ species was obtained in solutions with a Rh:Sn mole ratio ≥ 6 in HCl. Since then it has been shown by means of high resolution ^{119}Sn NMR spectroscopy that several Rh(III)-Sn(II) complexes are in equilibrium in solutions of tin(II)chloride and

rhodium(III)chloride, as well as a Rh(I)-Sn(II) complex, depending on the relative Rh:Sn mole ratio and HCl concentration. It is thus evident that both Rh(III) and Rh(I) complex anions with $SnCl_3^-$ as ligand can be formed although not all these species in solution have yet been fully characterized.

1.2 Nature of SnX_3^- Ligand in Transition Metal-Tin Complexes

The coordination of one ligand to a central metal ion has an influence on the nature of the bonding between that metal ion and every other ligand. For square-planar and octahedral d^6/d^8 metal ion complexes this influence can be divided into two broad categories: *cis*- and *trans*-effect. The *trans*-effect was first recognized by Chernyaev[42] almost a century ago, and for many years this was the only way the influence of one ligand on the properties of another could be observed experimentally. Later the conceptual siblings, the *trans* influence and the *cis* effect and *cis* influence, came to light. Care should be taken to avoid ambiguity when referring to the *trans*-effect and *trans*-influence. The former, perhaps better referred to as kinetic *trans* effect (KTE), is a *kinetic effect* that relates to the influence of a coordinated group upon *the rate of substitution* of ligands *trans* to it.[43] The latter, also referred to as structural *trans* effect (STE), describes the extent to which that ligand weakens the bond *trans* to it in the equilibrium state of the substrate. Thus, the *trans effect* is a kinetic transition state effect when ligand substitution in a metal complex takes place, while the *trans influence* is a thermodynamic ground state effect in a given complex. (A typical *trans effect* order is shown of page 11). Similarly, ligands coordinated *cis* to each other also influence the kinetics or thermodynamics of their *cis*-neighbours.[43] While extensive knowledge has been accumulated for the *trans*-effect the *cis*-effect has received less attention.[43] These *trans/cis*-directing effects of ligands are dependent on the electronic nature of the ligand.

It is thus clear that the coordination chemistry of stannylenes (SnR_2 compounds) and the electronic properties thereof play a big role in the formation of tin-transition metal complexes. Stannylenes (Sn(II)) use two of their π-electrons in covalent bonding and these possess two electrons which constitute a lone pair, which can be used to from an adduct with a Lewis acid.[44] There are also low-lying empty p and d orbitals, which, when these participate in hybridization of other orbitals of tin, result in 'empty' orbitals with suitable symmetry and orientation for π-bonding, and subsequently for complex formation with 'soft' acids such

transition metals. Several hybridization geometries have been established for stannylenes as shown in Scheme 1.4, of which the $5sp^3$-tetrahedral hybridization is most prevalent for when stannylenes form tin-transition metal complexes.

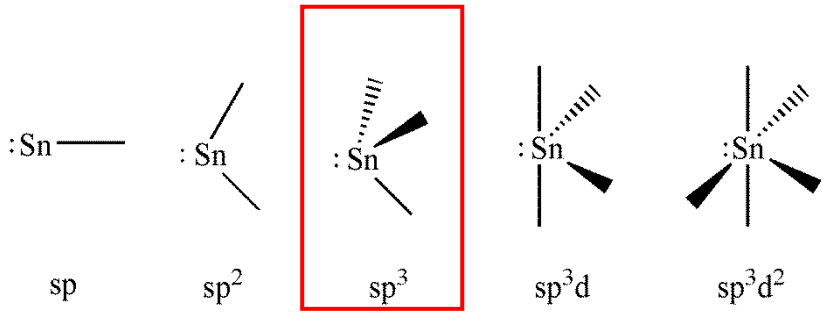

Scheme 1.4 Hybridization geometries available for stannylenes. The sp^3-hybridization, shown in the red block, is the most prevalent for tin-transition metal complexes.[44]

Although several studies of the SnX_3^- (X = Cl^-/Br^-) moiety as a ligand have shown that it usually coordinates to the transition metal ion via the lone pair of the tin(II) atom in SnX_3^-,[44-48] there is still much controversy regarding the detailed electronic nature of the SnX_3^- (X = Cl^-/Br^-) ligand and its effect on an octahedral transition-metal coordination complex.

In a study of fluorophenyl platinum(II) square-planar complexes, Parshall showed that ^{19}F NMR shielding parameters of fluorophenyl platinum complexes are sensitive criteria of the δ-donor and π-acceptor ability of the ligand *trans* to the phenyl group.[49,50] In this regard it was reported that the $SnCl_3^-$ ligand is a weak σ-donor and a strong π-acceptor ligand. Graham *et al.*[51] came to similar conclusion analyzing the approximate C-O stretching force constants in octahedral $(SnCl_3)Mn(CO)_5$ complexes, calculated using the Cotton-Kraihanzel[52-54] approximation. Although both the methods used by Parshall and Graham were criticized by Hartley[55], their results appears still to be generally accepted. Moreover, it was reported that ligands of the strong π-acceptor type tend to be σ-donors while strongly σ-withdrawing ligands tend to be π-donors. This is in accordance with the findings of Graham and Parshall and is perhaps a consequence of a synergic character of the metal-ligand bond, in which a drift of π-electrons is assumed to be in the opposite direction to that of σ-electron density.[56]

There is, however, ambiguity when it comes to the relative σ-donor and π-acceptor abilities of $SnCl_3^-$ compared to that of the $SnBr_3^-$ ligand. Stokely *et. al.*[57] obtained identical Fe-Sn bond lengths in the $(\eta^5\text{-}C_5H_5)Fe(CO)_2(SnX_3)$ (X = Cl^-/Br^-) compounds, from which they

concluded that there is no difference in the relative σ-donor/π-acceptor abilities of $SnCl_3^-$ and $SnBr_3^-$. Conversely, Antonov *et al.*[35] reported that $SnBr_3^-$ is both a stronger σ-donor and slightly stronger π-acceptor than $SnCl_3^-$. A decrease in the Mössbauer isomer shift ($\delta^{119}Sn$) was observed on going from the free SnX_3^- ion in $[Me_4N][SnX_3]$ (X = Cl^-/Br^-) compared to the coordinated SnX_3^- as ligand in $(Me_4N)_3[RhX_n(SnX_3)_{6-n}]$ (X = Cl^-/Br^-, n = 1, 2, 3) complexes. This decrease indicates a marked decrease in the density of the $5s^2$ electrons of the SnX_3^- ligand as a result of the σ-donor interaction of the SnX_3^- ligand with the Rh(III) ion. The increase in the quadrupole splitting (ϵ) on the other hand is indicative of the π-acceptor interaction of SnX_3^- ligand as a result of coordination to the metal ion, where the d-electrons of Rh(III) form a π-bond with the π* (anti-bonding) orbitals of the SnX_3^- ligand. It is from the relative differences in the isomer shifts (Δδ) and quadrupole splittings (Δϵ) between the free SnX_3^- ion compared to the coordinated SnX_3^- ligand in $(Me_4N)_3[RhX_n(SnX_3)_{6-n}]$ (X = Cl^-/Br^-, n = 1, 2, 3) complexes, that Antonov *et al.*[35] concluded that the $SnBr_3^-$ ligand is a relatively stronger σ-donor and slightly stronger π-acceptor than $SnCl_3^-$ toward Rh(III). There is however, yet another opinion regarding the electronic nature of these two ligands. Based on the X-ray data obtained for the *cis*-$[PtX_2(SnX_2)_2]^{2-}$ (X = Cl^-/Br^-) as well as on ^{119}Sn and ^{195}Pt NMR data obtained for these complexes and $[Pt(SnX_3)_5]^{3-}$, Nelson and co-workers[58] characterized $SnCl_3^-$ as a better σ-donor and/or π-acceptor than $SnBr_3^-$ toward Pt(II). Firstly, the Pt-Sn bond length were found to be longer for the $SnBr_3^-$ ligand complexes and secondly the $^1J(^{119}Sn\text{-}^{195}Pt)$ coupling constants were larger for the $SnCl_3^-$ complexes than for the $SnBr_3^-$ complexes. A recent, detailed high resolution ^{195}Pt NMR study by Barkhuysen and Koch of the series of $[PtSn_5Cl_nBr_{15-n}]^{3-}$ (n = 0 – 15) complexes showed that with each substitution of a Cl^- ion with a Br^- to a spin-active ^{119}Sn nucleus, the $^1J(^{119}/^{117}SnCl_{3-n}Br_n\text{-}^{195}Pt)$ (n = 0 – 3) coupling constant decreased with ± 4.5 %.[59] This decrease in the coupling constant suggests that $SnCl_3^-$ is indeed a better σ-donor and/or π-acceptor toward Pt(II) than $SnBr_3^-$, as suggested by Nelson.[58] Although consensus on the relative electronic properties of $SnCl_3^-$ and $SnBr_3^-$ has not yet been reached, both these are shown to be strong π-acceptors. It is this strong π-acceptor ability of the SnX_3^- ligand and the consequent d_π-d_π back-bonding between the transition metal and tin(II) that is thought to cause the relatively high *trans* directing properties of SnX_3^-ligands coordinated to PGM metal ions.[24,54,60]

Lindsey *et al.*[61] studied the kinetic *trans*-effect of the $SnCl_3^-$ ligand by the same criteria described by Chatt and co-workers[62,63] wherein they related the *trans*-effect of a ligand to the

shift in the ν(Pt-H) and the ^{1}H NMR chemical shift in hydrides of the type *trans*-[PtHL(PR_3)$_2$]. From this study Lindsey *et. al*.[61] estimated that the *trans-effect* of $SnCl_3^-$ lies between NCS^- and CN^-, the two ligands with the highest *trans-effect* in the Chatt series:[64]

$$Cl < Br < I < NCS < SnCl_3 < CN$$

In contrast to the strong kinetic *trans*-effect of the SnX_3^- ligand, Rüegger *et. al*. found the structural *trans*-influence thereof to be quite moderate, similar to that of olefins, based on $^{1}J(^{119}Sn\text{-}^{195}Pt)$ coupling constants measured for the (PPN)[Pt($SnCl_3$)$_3$L$_2$] complexes containing similar L ligands.[65] Albinati *et. al.*[66] studied the effect of the $SnCl_3^-$ ligand on the $^{2}J(Pt\text{-}CH_3)$ coupling constants in *trans*-[Pt($SnCl_3$)(CH_3)(PEt_3)$_2$] complexes. These results supported the suggestion of Rüegger *et al*. that the $SnCl_3^-$ ligand has only a moderate structural *trans* influence, similar to that of an olefin. Moreover, the mutual influence of ligands in *trans*-[HPtX(PPh_3)$_2$] and *trans*-[XPt(SnX_3)(PPh_3)$_2$] (X = Cl^-/Br^-) compounds was determined by comparing the relationship between the ν(Pt-H) wavenumbers and the δ(Pt-H) chemical shift parameters resulting in a structural *trans* influence for these ligands in the order:[66]

$$Cl^- < Br^- <<< SnBr_3^- < SnCl_3^-$$

This strong structural *trans* influence of $SnCl_3^-$ and $SnBr_3^-$ certainly contributes greatly to the high catalytic activity, as well as facile ligand-exchange (*trans-effect*) reactions, observed for PGM-tin halide complexes. It is quite evident, however, that the majority of the knowledge pertaining to the *trans*-effect involves square-planar Pt(II) complexes and although valuable information is obtainable from these complexes, care should be taken not to apply the classic trans-influence (STE) model based on Pt(II) chemistry to all systems.[67] Furthermore, reports concerning the kinetic *trans* effect of in octahedral complexes are relatively scarce by comparison to reports concerning structural *trans*-influence.[68] In a recent review of the *trans-influence* and *trans-effect* in octahedral complexes, it was stated that the electronic effects require consideration of the σ- and π-bonding properties of both the metal center and the ligands.[68] Thus, there are several uncertainties regarding the relative importance of the kinetic *trans*-effect compared to the *trans*-influence of the $SnCl_3^-$ ligand in the substitution reactions

involved in the formation of a series of $[Rh(SnCl_3)_nCl_{6-n}]^{3-}$ (1 – 5) complexes from $[Rh(H_2O)_{6-n}Cl_n]^{(3-n)+}$ and $SnCl_3^-$ in aqueous hydrochloric acid solutions.

1.3 Application of multinuclear NMR spectroscopy to study nature of Rh-Sn Species

Even though the first nuclear magnetic resonance (NMR) signal was detected in 1938 in a molecular beam,[69] chemists only started showing interest therein in 1950, after it had been discovered that the precise resonance frequency of a nucleus depends critically on its chemical/electron environment.[70-73] The discovery of this so-called *chemical shift* set the stage for use of NMR as an extremely sensitive probe of the structure of molecules, and what seemingly started off as an interesting study of a physical phenomenon developed into a indispensable technique for the elucidation of molecular structures of organic and inorganic species today. The introduction of superconducting magnets, Fourier-transform methods and multiple-pulse excitation makes NMR the most efficient spectroscopic method for the determination of molecular structures and conformations of complex molecules in solution. During the 1970's and 1980's rapid development of a wide range of 1D and 2D NMR techniques took place thanks to the advances made in both radiofrequency generation and data handling technology.[74-77] The most important development was Fourier-transform NMR spectroscopic methods, for which Richard Ernst received the Nobel Prize in Chemistry 1991, and indirect detection methods resulted in a dramatic increase in the NMR sensitivity allowing for less sensitive nuclei to be be observed.[78] The four types of measureable NMR parameters of molecules in solution that are of importance for structure elucidation of a species are: chemical shift (δ), scalar spin-spin coupling constants (J), resonance peak intergral areas of NMR signals and the relaxation times.[79]

The chemical shift measured for a particular compound is an indication of the degree of magnetic shielding induced by electrons surrounding the nucleus in question, which in turns gives information regarding the electron density surrounding that nucleus.[80] The relationship between the Larmour Frequency (ν_A), the applied magnetic field (B_0), magnetic shielding constant (σ_i) and the gyromagnetic ratio (γ) is:

$$\nu_A = \frac{\gamma}{2\pi} B_0(1 - \sigma_i) \qquad 1.2$$

However, this analysis is complicated by the fact that there are several factors that may contribute to the shielding (σ_i) of a nucleus in a molecular environment:

$$\sigma_i = \sigma_i^{dia} + \sigma_i^{para} + \sigma_{ij} \qquad 1.3$$

where σ_i^{dia} represent the diamagnetic shielding of the nucleus being considered and is a first-order term that can be calculated from the electronic ground state. The σ_i^{para} term is a second-order perturbation term which represents the temperature-independent paramagnetic shielding (due to non-local electrons circulating around a nucleus).[79] Both these contributions to shielding arise from the local electron cloud, whereas σ_{ij} represents all the contributions from remote sources. The diamagnetic shielding term σ_i^{dia} describes the local electronic density around the nucleus and it accounts for the unperturbed spherical motion of the electrons. The σ_i^{dia} shielding term also is dominant in proton NMR spectroscopy. The paramagnetic shielding term σ_i^{para} depends not only on the electron density at the nucleus, but is also related to an electronic excitation energy, ΔE^{-1} and a non-s-orbital expansion term, $\langle r_d^{-3} \rangle$, as is shown in the Ramsey[81] equation as revised by Juranic:[82]

$$\sigma^{para} = -\frac{8\mu_0\mu_B^2}{\pi}\langle r_d^{-3}\rangle F \frac{\beta}{\Delta E} \qquad 1.4$$

The term μ_0 refers to the permeability of vacuum, μ_B is the Bohr magneton and $\langle r_d^{-3} \rangle$ refers to the *d* orbital radius of the free ion and is constant for a given oxidation state. The parameter ΔE represents the average excitation energy between the electrons in the ground state and a low lying excited state. The quantity β represent the *nephelauxetic* ratio. From equation 1.4 it can be deduced that σ_i^{para} is proportional to $1/\Delta E$ and thus that a decrease in ΔE will result in an increase in the paramagnetic shielding value. The chemical shift thus provides important information regarding the chemical environment of the nucleus.

Additionally, the spin-spin coupling between nuclei is also important for the assignment of structure, sometimes even more so that the chemical shift values, and can be understood in terms of the Fermi contact expression used by Pople and Santry:[83]

$$^1J(A,B) \propto \gamma_A\gamma_B\left|\Psi_{ns_A}(0)\right|^2\left|\Psi_{ns_B}(0)\right|^2\pi_{A,B} \qquad 1.5$$

$$\pi_{A,B} = \sum_i^{occ}\sum_j^{unocc}(\epsilon_j - \epsilon_i)^{-1}c_{i,A}c_{j,A}c_{i,B}c_{j,B} \qquad 1.6$$

The symbols γ represent the gyromagnetic ratios of nuclei, the terms $|\Psi_{ns}(0)|^2$ are the valence s-electron densities at the nuclei, A and B, and $\pi_{A,B}$ is the mutual polarizability. The $\pi_{A,B}$ expression contains the s coefficients of the atomic orbitals used in the linear combinations that make up the occupied and unoccupied molecular orbitals, as well as a difference term ($\epsilon_j - \epsilon_i$) where ϵ_i is the energy of an occupied and ϵ_j an unoccupied molecular orbital. The major influences on spin-spin coupling, J, are the *s*-character of the bond between the two coupling nuclei and the ΔE.

Since the reaction of tin(II) halide with rhodium(III) halides in acidic solutions to yield highly coloured complexes is the essential objective of this study a brief discussion of the NMR active elements, ^{119}Sn, ^{103}Rh and ^{1}H, is necessary here.

1.3.1 Direct ^{119}Sn NMR spectroscopy

^{119}Sn NMR spectroscopy in particular has proven to be extremely powerful tool for the elucidation of structures of transition-metal tin complexes which cannot be studied in solution by any other technique from a structural point of view.[44] The element tin has *ten natural occurring isotopes* the most of all the elements, of which three are NMR-active with I = ½: ^{119}Sn (natural abundance = 8.59 %), ^{117}Sn (natural abundance = 7.68 %) and ^{115}Sn (natural abundance = 0.34 %), Table 1.1.[80]

Table 1.1 Natural Abundances and magnetic properties of the stable tin isotopes.

Tin Isotope	Natural Abundance / %	Spin	Gyromagnetic ratio[a] γ/2π MHz T^{-1}	Receptivity (^{13}C = 1)
^{112}Sn	0.97	0		
^{114}Sn	0.66	0		
^{115}Sn	0.34	½	-13.922	0.715
^{116}Sn	14.54	0		
^{117}Sn	7.68	½	-15.168	19.9
^{118}Sn	24.22	0		
^{119}Sn	8.59	½	-15.569	25.6
^{120}Sn	32.58	0		
^{122}Sn	4.63	0		
^{124}Sn	5.79	0		

[a] γ/2π ^{1}H is 42.467

Although both ^{119}Sn and ^{117}Sn can easily be used to characterise tin complexes with NMR spectroscopy, ^{119}Sn has the higher receptivity relative to ^{13}C and is therefore the preferred nucleus for study by NMR.

The ^{119}Sn NMR spectrum of tin-transition metal complexes has an unusually large chemical shift range of greater than 2000 ppm.[44,80] It was shown in Equation 1.3 that several factors contribute to the shielding of a nucleus, so that changes in chemical shift for ^{119}Sn are largely determined by the paramagnetic shielding term, σ^{para}, which according to Equation 1.4, is inversely proportional ΔE. The ΔE, which represents the average energy difference between the ground state and a low lying excited state, is highly influenced by the σ-donor/π-acceptor properties of a ligand. The $SnCl_3^-$ ligand is considered to be a weak σ-donor and strong π-acceptor.[58,59] Thus, on coordination to a transition metal much of the electron density on the metal brought by σ donation is returned to the $SnCl_3^-$ ligand through π-back bonding, which effects the magnitude of the average excitation energy, ΔE. These changes in the magnitude of the average excitation energy, ΔE, affects the shielding arising from the local electron cloud, σ^{para}. However, many more factors come into play, such as the solvent, concentration and temperature effects that might affect the chemical shift. Therefore, interpretation of the chemical shift, $\delta(^{119}Sn)$, obtained for ^{119}Sn is limited to a semi-quantitative or qualitative level. Nonetheless, the relative chemical shifts $\delta(^{119}Sn)$ observed, respective scalar J coupling constants between I = ½ nuclei, as well as the relative signal intensities measured may still be used to determine the stoichiometry of a complex, particularly for Rh-Sn complexes, and the electronic environment in which it finds itself.

The characterization of rhodium-tin complexes with ^{119}Sn NMR spectroscopy, in particular, is particularly convenient in that rhodium only has one natural occurring isotope, ^{103}Rh, with I = ½. The following advantages have been highlighted by Moriyama *et. al*.:[84]

1) Coordination of the Sn-ligand to rhodium is evidenced by the main ^{119}Sn NMR resonance signal being split into a doublet due to $^1J(^{103}Rh\text{-}^{119}Sn)$ spin coupling.
2) In the event of more than one Sn-ligand being coordinated to rhodium, $^2J(^{117}Sn\text{-}^{119}Sn)$ satellites would be observed, which provides information on the stoichiometry and fluxional behaviour of the complex.

3) The NMR parameters $\delta(^{119}Sn)$, $^{1}J(^{103}Rh\text{-}^{119}Sn)$ and $^{2}J(^{117}Sn\text{-}^{119}Sn)$ are useful in assigning the observed ^{119}Sn NMR resonance signals to the Rh-Sn complexes from which they arise.

Moreover, it was shown that the experimentally measured peak intensity ratio, $I_{(satellite)}/I_{(main)}$, can be related to the statistical probability of a number of Sn-ligands being coordinated to rhodium. Moriyama *et. al.*[84] used this to assign the respective ^{119}Sn NMR resonance signals to the series of $[Rh(SnCl_3)_nCl_{6-n}]^{3-}$ (n = 1 – 5) complex anions.

Moriyama *et. al.* found that both the ^{119}Sn chemical shifts and the $^{1}J(^{103}Rh\text{-}^{119}Sn)$ coupling constants are very sensitive to changes within the coordination sphere of a particular Rh-$SnCl_3$ complex. The relatively large $^{1}J(^{103}Rh\text{-}^{119}Sn)$ coupling constants can, according to Pople and Santry's equations,[83] be ascribed to the high mutual polarizability of the s-orbitals on Rh and Sn, a high *s*-character in the bond, and the relatively large gyromagnetic ratios (γ) of ^{119}Sn. The ^{119}Sn NMR data obtained by several groups[44,84] for Rh-Sn species has led to the following empiricisms:

1. Increase in the number of coordinated Sn-ligands results in the successive de-shielding of the ^{119}Sn nucleus indicated by the downfield shift of $\delta(^{119}Sn)$
2. Increase in the number of coordinated Sn-ligands results in a decrease in the magnitude of the $^{1}J(^{103}Rh\text{-}^{119}Sn)$ coupling constant
3. $^{2}J(^{117}Sn\text{-}^{119}Sn)_{trans} > {}^{2}J(^{117}Sn\text{-}^{119}Sn)_{cis}$

Application of ^{119}Sn NMR spectroscopy for the elucidation of Rh-Sn species has enabled the elucidation of the structure of species *in situ*, not possible by any other method.

1.3.2 Indirect $^{103}Rh(^{1}H)$ NMR spectroscopy

Even though ^{103}Rh is one of the few nuclei with I = ½ that has a natural abundance of 100 %, it has a very small magnetic moment (μ = -0.1522), sometimes a long relaxation time and low resonance frequencies, which makes it difficult to observe with direct NMR techniques.[79] Moreover, although the relative receptivity of ^{103}Rh is high enough to directly detect ^{103}Rh, its large chemical shift range (12 000 ppm) makes it difficult to cover the entire

range in a single measurement. Thus, this technique will require several NMR experiments using different spectral widths to avoid 'folding-back' of signals into a spectral window, especially if the expected chemical shift of a the given Rh-containing species is unknown. Thus, direct ^{103}Rh NMR is a time-consuming process that requires very long experimental acquisitions.

Insensitive Nuclei Enhanced by Polarization Transfer (INEPT) was developed to enhance the signals from a nucleus with a relatively low magnetic moment (such as ^{103}Rh) that is directly coupled to a nucleus with a large magnetic moment (usually ^{1}H), by exploiting polarization transfer from the more sensitive nucleus to the ^{103}Rh.[79] INEPT is thus a 1D NMR technique that can enhance the sensitivity of the insensitive nucleus by a factor of $\eta = \gamma_H/\gamma_{X,}$ which for ^{103}Rh amounts to a factor of 31.6. Currently, however, the best method to observe ^{103}Rh is by the two-dimensional indirect detection method Heteronuclear Multiple-Quantum Coherence (HMQC). This widely used HMQC pulse-sequence, designed and first used by Bax *et. al.*,[85] was originally intended for ^{1}H{^{15}N} detection, but has since been adopted for indirect detection of nuclei such as ^{103}Rh.[86] HMQC experiments require a non-zero scalar $J_{(M\text{-}S)}$ coupling with $J_{(M\text{-}S)} > 1/T_2$ (where M is the insensitive, low-γ spin ½ transition metal nucleus such as ^{103}Rh, S is the sensitive, high γ spin ½ nucleus such as ^{1}H and T_2 is the spin-spin relaxation time). Using HMQC as a indirect detection method for ^{103}Rh, (^{1}H,^{103}Rh), provides a maximum possible enhancement of $(\gamma_H/\gamma_{Rh})^{5/2}$ = 5680 times over simple ^{103}Rh{^{1}H} observation and 590 times for (^{31}P,^{103}Rh){^{1}H} observation, using the method of Bax *et. al.*[85] Clearly indirect detection (^{1}H,^{103}Rh) NMR is an especially useful method for the characterization of rhodium and other transition metal (I = ½) hydrides.[87]

As with ^{119}Sn NMR spectroscopy, the ^{103}Rh chemical shift is largely determined by the paramagnetic shielding term, σ^{para}, which according to the Ramsey equation (Equation 1.4) is principally determined by two terms:[81,88] the average energy difference between filled and empty d-orbitals, ΔE, and $\langle r^{-3} \rangle_d$ where r is the average radius of a valence level d orbital. The ΔE is influenced by weak/strong properties of of ligands and increases according to the spectrochemical series, whereas r is influenced by hard/soft properties and increases according to the nephelauxetic series.[88,89] The δ(^{103}Rh) chemical shifts are commonly referenced to the absolute frequency Ξ(^{103}Rh) = 3.16 MHz in a field in which the protons of

TMS resonate at exactly 100 MHz.[90] However, sometimes arbitrary reference substances such as $RhCl_6^{2-}$ are also used, although these can be converted to the $\Xi(^{103}Rh)$ scale.

1.4 Research Aims and Objectives

The characteristic intense colours generated in solution when stannous chloride reacts with chlorido complexes of the platinum group metals (Pt, Rh, Ir, Pd, Ru and Os) was key in the discovery and identification of these noble elements in the early 17th century by Wollaston *et. al*.[1] Interest in these complexes has greatly increased in view of their analytical colorimetric applications[10,15-18] and their interesting catalytic activity toward hydrogenation and isomerization reactions.

Tin chloride complexes of Rh(III/I) have been the subject of several previous studies showing that several $[RhCl_{6-n}(SnCl_3)_n]^{3-}$ (n = 1 – 6), as well as $[Rh(SnCl_3)_5]^{4-}$ complex anions, the latter due to the reduction of Rh(III) by tin(II), can simultaneously be present in solution. As part of our interest in the favourable effects on the extraction of Rh(III/I) in analytical and hydrometallurgical applications I have carried out a detailed speciation study of this complex system. Previously Koch *et. al.*[8,9] reported that extraction of the Rh(I) complex anion, $[Rh(SnCl_3)_5]^{4-}$, into Aliquat-336/$CDCl_3$ is accompanied by a gradual colour change from red to yellow. This yellow species was assigned to the $[RhH(SnCl_3)_5]^{3-}$ complex anion using ^{119}Sn NMR spectroscopy; nevertheless several unidentified species in such solutions remain to be characterized.

In this context, this study involves a detailed high-resolution ^{119}Sn NMR spectroscopy study of the nature of these Rh-Sn complex anions, as a function of the Rh(III):Sn(II) mole ratio, the $[H^+]$ and the Sn:Cl mole ratio in aqueous and non-aqueous solutions.

Specific aims of study

1. Study in more detail the speciation of chlorido Rh-Sn species in hydrochloric acid/aqueous solutions by means of UV/vis and high resolution ^{119}Sn NMR spectroscopy, with the aim to confirm tentative assignments using high magnetic fields.

2. Synthesis and characterization of the analogous bromido Rh-Sn species in HBr by means of ^{119}Sn NMR spectroscopy.

3. An investigation of the speciation of the extracted Rh(III/I)-Sn(II) complexes into various organic solutions and determining the speciation by means of high resolution 1D and 2D ^{119}Sn and ^{103}Rh NMR spectroscopy.

Chapter II

Experimental, Methods of analysis and Preliminary investigations

Chapter II

Experimental, Methods of analysis and Preliminary investigations

In this chapter the synthesis of the series of $[Rh(SnCl_3)_nCl_{6-n}]^{3-}$ (n = 1 – 6) complex anions, the $[Rh(SnCl_3)_5]^{4-}$ complex anions and the series of $[Rh(SnBr_3)_nBr_{6-n}]^{3-}$ (n = 5 – 3) complex anions in acidic aqueous solutions, as well as the extraction of these complex anions into various organic phases by means of several different solvent extraction techniques, are described. Moreover, the methods used to characterize these complexes in both aqueous and organic media will be discussed. An NMR simulation program, gNMR50, was used to validate the assignments made in the ^{119}Sn, ^{1}H and ^{103}Rh NMR spectra, respectively. In order to establish the optimal experimental conditions under which the respective species are formed, preliminary UV-Vis spectroscopy experiments were carried out before NMR experiments were performed, the results of which are discussed here.

2.1 Synthesis and preliminary UV-vis analysis of the series of $[Rh(SnCl_3)_nCl_{6-n})]^{3-}$ (n = 1 – 6) and $[Rh(SnCl_3)_5]^{4-}$ complex anions

All solutions were prepared using boiled ultrapure Milli-Q water (MQ › 18MΩ) which was cooled and stored under nitrogen to eliminate dissolved oxygen. Concentrated hydrochloric (32 %), perchloric acid and hydrobromic acid (48 %) (analytical grade) were also saturated with nitrogen by bubbling the gas through the acid for at least 15 minutes prior to use.

2.1.1 General synthesis of the series of $[Rh(SnCl_3)_nCl_{6-n}]^{3-}$ (n = 1 – 6) and $[Rh(SnCl_3)_5]^{4-}$ complex anions in aqueous acidic solutions

All aqueous phase solutions were freshly prepared for each investigation. The general procedure followed was to calculate the mass of $SnCl_2{\cdot}2H_2O$ needed for the specific experiment and to dissolve the weighed amount of $SnCl_2{\cdot}2H_2O$ salt in the required volume of concentrated hydrochloric acid (to give the correct concentration after final dilution). The calculated amount

of $RhCl_3 \cdot 3H_2O$ was then added to the solution and diluted to volume with water. Unless stated otherwise, the solutions were allowed to equilibrate for 24 hours under N_2. The same synthesis procedure was used to prepare solutions for both the preliminary UV-vis and the NMR experiments, with only the initial concentrations of the reagents used differing. The initial rhodium concentration needed for the NMR experiments were typically thousand fold more than that required for the UV-vis experiments. Care was taken to exclude oxygen during the dilution and equilibration process of the aqueous phase.

2.1.2 Synthesis procedure for preliminary UV-vis analysis

The reaction of Rh(III) with Sn(II) in acidic aqueous media can yield several 6-coordinated $[Rh(SnCl_3)_nCl_{6-n}]^{3-}$ (n = 1 - 6) as well as the trigonal bipyramidal $[Rh(SnCl_3)_5]^{4-}$ complex anion, depending on the specific experimental conditions used.[41] In order to determine the influence of the hydrochloric acid concentration as well as the rhodium(III) to tin(II) mole ratio on the resulting species, preliminary UV-vis analyses were done. Therefore, for these preliminary UV-Vis analyses, the rhodium(III) concentration was first kept constant at 5×10^{-4} M, while the HCl concentration and the Rh(III):Sn(II) mole ratio were varied, respectively.

A rhodium stock solution with a concentration of 20 mM was prepared by dissolving 0.1317 g of $RhCl_3 \cdot H_2O$ in 25 mL concentrated HCl (32 %). The solution was refluxed at 70 °C for three days to ensure that the predominant rhodium species present in solution before the addition of $SnCl_2 \cdot 2H_2O$ are the $[RhCl_6]^{3-}$ and $[RhCl_5(H_2O)]^{2-}$ species.[91]

First, solutions with a Rh:Sn mole ratio of 1:10 were prepared in order to ensure the formation of a purple-red solution which is indicative of the $[Rh(SnCl_3)_5]^{4-}$ species. The UV/vis spectrum recorded for this species by Ayres *et. al.*,[16] Figure 2.1, shows an absorbance maximum at 475 mμ. Therefore, to determine the influence of the HCl concentration on the Rh(III)-Sn(II) species formed in solution, a stock solution with a rhodium concentration of 10 mM and a Rh(III):Sn(II) mole ratio of 1:10 in 6 M HCl was prepared. This was done by dissolving 0.0112 g of $SnCl_2 \cdot 2H_2O$ in 2.9467 mL of the rhodium stock solution, diluting it to 4.242 mL with H_2O and topping up to 5 mL with 6 M HCl. In order to obtain solutions with

HCl concentrations varying from 0.5 M to 6 M, with increments of 0.5 M, the solution was diluted with the respective required amounts of HCl and H_2O to obtain a final rhodium concentration of 0.4 mM. The solutions were left to equilibrate for 24 hours under N_2. However, even after 24 hours of equilibration time all the solutions remained yellow, contrary to the red solutions expected to be obtained with a Rh:Sn mole ratio of 1:10. The resulting UV/vis spectra of the yellow solutions are shown in Figure 2.2.

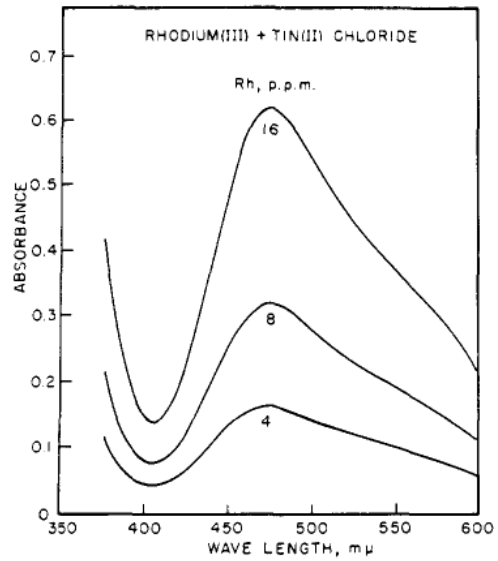

Figure 1. Spectral curves for rhodium(III) solutions color-developed with tin(II) chloride

Figure 2.1 UV/vis spectra recorded by Ayres *et. al.*[16] for rhodium-tin solutions wherein the initial rhodium concentration was varied from 4 to 8 to 16 ppm. An absorbance maximum is obtained at λ_{max} = 475 mμ.

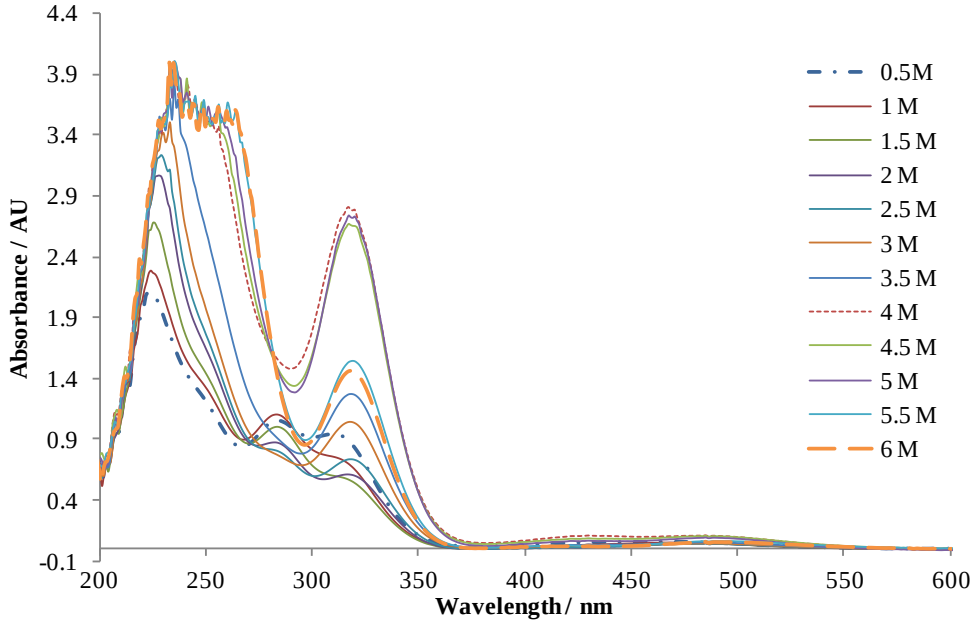

Figure 2.2 Dependence of Rh-Sn complexes on HCl concentration (M). The initial rhodium concentration is kept constant at 0.4 mM and a Rh to Sn mole ratio of 1:10 was used while the HCl concentration was varied from 0.5 to 6 M. All solutions were allowed to equilibrate for 24 hours under N_2.

At the same time a second set of solutions were prepared in which the HCl concentration was kept constant at 4 M HCl and the Rh:Sn mole ratios were varied from 1:1 to 1:20. The 20 mM rhodium stock solution was used to prepare these samples and the amount of $SnCl_2 \cdot 2H_2O$ required for each respective solution was calculated and added before the solution was diluted to obtain a final HCl concentration of 4 M. The resulting UV/vis spectra are shown in Figure 2.3.

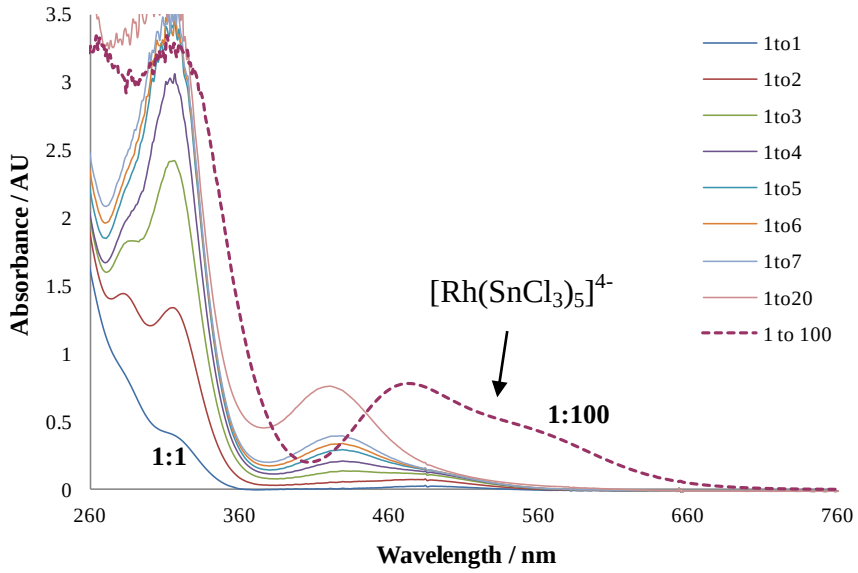

Figure 2.3 Dependence of Rh-Sn complexes on the Rh:Sn mole ratio used. The final HCl concentration of all the solutions was 4 M and the initial rhodium concentration is kept constant at 0.4 mM. The Rh to Sn mole ratio was varied from 1:1 to 1:100. All solutions were allowed to equilibrate for 24 hours under N_2.

Evidently, no absorbance maxima is observed at 475 nm for either series of solutions, thus the red $[Rh(SnCl_3)_5]^{4-}$ species is not present in any of the solutions. Rather, the spectra observed in Figure 2.2 and Figure 2.3 are characteristic of the electronic spectra of the series of $[Rh(SnCl_3)_nCl_{6-n}]^{3-}$ species.[9]

With a Rh:Sn mole ratio of 1:10 and a starting rhodium concentration of 0.4 mM, the tin(II) concentration is 4 mM. Thus, even with the lowest HCl concentration used, 0.5 M HCl, the concentration of free chloride ions which compete for coordination to the Rh-centre are 100 fold higher than that of the $SnCl_3^-$ ions. It is therefore evident that it is not only the Rh:Sn mole ratio that is of importance for the formation of these Rh-Sn species, but rather the Rh:Sn:Cl mole ratio. Therefore, the required amount of $SnCl_2 \cdot 2H_2O$ was added to the solution with a Rh:Sn mole ratio of 1:20 in 4 M HCl to obtain a Rh:Sn mole ratio of 1:100.

The solution was again left to equilibrate for 24 hours under N_2. A purple-red solution was obtained and the UV/vis spectrum recorded for the solution is shown in Figure 2.3. This spectrum is characteristic of the five-coordinate $[Rh(SnCl_3)_5]^{4-}$ species. Therefore, it is clear that when working with such low rhodium concentrations, the Sn:Cl mole ratio plays an very important role in the Rh-Sn species that are formed.

To determine the influence of the initial rhodium concentration, a series of samples were prepared with a Rh:Sn mole ratio of 1:100 and the HCl concentration was kept constant at 4 M, but the initial rhodium concentration was varied from 0.1 mM to 0.4 mM, Figure 2.4A.

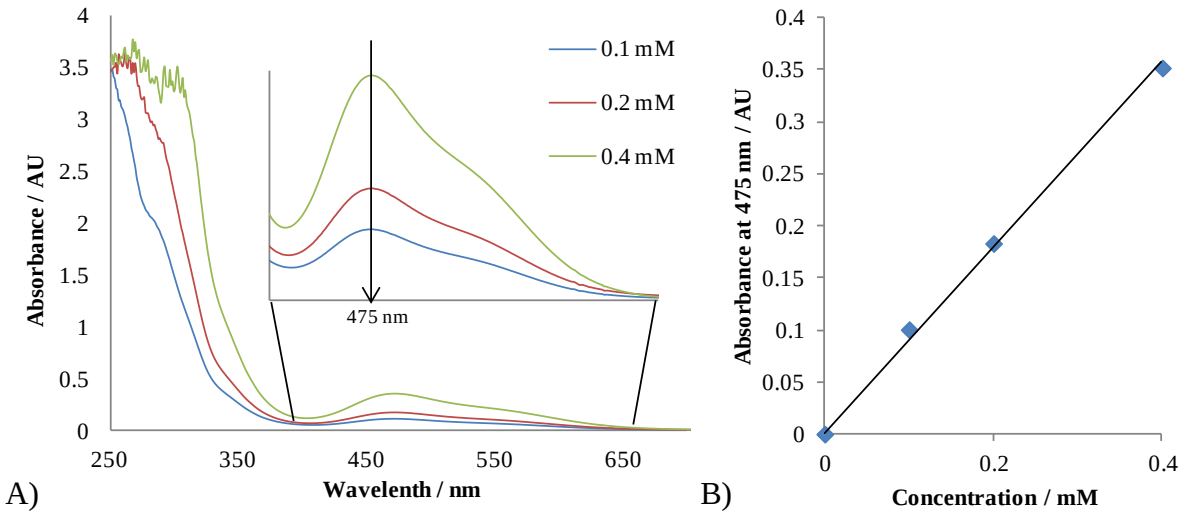

Figure 2.4 UV/vis spectra of Rh to Sn ratio of 1 to 100 in 4 M HCl, different Rh concentrations. The dependence of the Rh-Sn complexes on the initial rhodium concentration used is shown in (A) wherein the Rh:Sn mole ratio and HCl concentration were kept constant at 1 to 100 and 4 M while the initial rhodium concentration was varied from 0.1 mM to 0.4 mM. In (B) the absorbance at 475 nm is plotted against the initial rhodium concentration. The straight line obtained is indicative thereof that the Beer Lambert Law is obeyed. All solutions were allowed to equilibrate for 24 hours under N_2

From Figure 2.4A it is clear that as the initial rhodium concentration is increased the absorbance maximum at 475 nm also increases. According to the Beer Lambert Law, the absorbance of a species is directly proportional to the concentration of that species, equation 1.1:

$$A = \varepsilon l c \qquad 1.1$$

where A is the absorbance (no units), ε is the molar absorbtivity of the species, *l* is the path length of the sample and c is the concentration of species. Therefore, the straight line that is

obtained when plotting the absorbance at 475 nm against the initial rhodium concentration of the solution, Figure 2.4, shows that the Beer Lambert Law is obeyed.

2.2 Synthesis of the series of $[Rh(SnBr_3)_nBr_{6-n})]^{3-}$ (n = 1 – 6) and $[Rh(SnBr_3)_5]^{4-}$ complex anions

Initially the same method of synthesis used for the $[Rh(SnCl_3)_5]^{4-}$ species were attempted wherein $SnBr_2$ and HBr were used instead of $SnCl_2$ and HCl. However, no species were observed in the ^{119}Sn NMR spectrum. To exclude the possibility of halide exchange between Cl^- and Br^- and the formation of several species, as was reported for the analogous $[Pt(SnCl_3)_5]^{3-}$ species when it came in contact with Br^-, the starting Rh compound was changed from $RhCl_3 \cdot 3H_2O$ to a $Rh(NO_3)_3 \cdot xH_2O$ solution. The concentration of the $Rh(NO_3)_3 \cdot xH_2O$ solution was determined to be 0.3 M by ICP-OES. The general procedure followed was to calculate the mass of $SnBr_2$ needed for the specific experiment and to dissolve the weighed amount of $SnBr_2$ salt in the required volume of concentrated hydrobromic acid (to give the correct concentration after final dilution). The calculated amount of the $Rh(NO_3)_3 \cdot xH_2O$ solution was then added to the Sn solution and diluted to volume with water. Unless stated otherwise, the solutions were allowed to equilibrate for 24 hours under N_2. The same synthesis procedure was used to prepare solutions for both the preliminary UV-vis and the NMR experiments, with only the initial concentrations of the reagents used, differing. The initial rhodium concentration needed for the NMR experiments were typically thousand fold more than that required for the UV-vis experiments. Care was taken to exclude oxygen during the dilution and equilibration process of the aqueous phase.

Various attempts were made to obtain mixed chlorido-bromido Rh-Sn species, but unfortunately the ^{119}Sn NMR spectra obtained for the solutions showed no signals.

2.3 Extraction of $[Rh(SnCl_3)_nCl_{6-n}]^{3-}$ (n = 1 – 6) and $[Rh(SnCl_3)_5]^{4-}$ complex anions

Previously Koch *et. al.* reported that extraction of the Rh(I) complex anion, $[Rh(SnCl_3)_5]^{4-}$, into Aliquat-336/$CDCl_3$ is accompanied by a gradual colour change from red to yellow.[8] This yellow species was assigned to the $[RhH(SnCl_3)_5]^{3-}$ complex anion using ^{119}Sn NMR spectroscopy; nevertheless several unidentified species remain to be characterized. Therefore, after the synthesis

and analysis of the aqueous Rh-Sn solutions, the $[Rh(SnCl_3)_nCl_{6-n}]^{3-}$ (n = 1 – 6) and $[Rh(SnCl_3)_5]^{4-}$ complex anions were extracted into various organic phases.

2.3.1 Extraction with an anion exchanger: Aliquat 336

The $[Rh(SnCl_3)_nCl_{6-n}]^{3-}$ (n = 1 – 6) and $[Rh(SnCl_3)_5]^{4-}$ complex anions were extracted into chloroform-*d* using methyltrioctylammonium chloride (Aliquat-336), illustrated in Scheme 2.1, as ion-exchanger. Three and four molar equivalents of Aliquat-336 are needed to extract 1 mole of $[Rh(SnCl_3)_nCl_{6-n}]^{3-}$ (n = 1 – 6) and $[Pt(SnCl_3)_5]^{3-}$ respectively, Scheme 2.2 and Scheme 2.3. Therefore a solution of 30 % (v/v) Aliquat-336 in chloroform-*d* was prepared by weighing off the required mass of Aliquat-336 and adding it to chloroform-*d*. The organic phase (0.5 mL) was added to the aqueous Rh-Sn solutions (0.5 mL) and the mixture was stirred slowly for 15 minutes. For aqueous solutions with hydrochloric acid concentrations of 3 M or higher, the extraction was accompanied by a colour change from deep red/purple to bright yellow, which was indicative of the formation of the $[RhH(SnCl_3)_5]^{3-}$ complex anion.

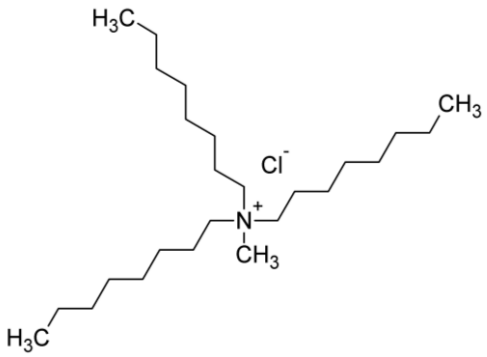

Scheme 2.1 Structure of the ion-exchanger, trioctylammonium chloride, used to extract the respective Rh-Sn complexes into chloroform-*d*.

$$[RhCl_n(SnCl_3)_{6-n}]^{3-}_{aq} + 3\overline{R_3NMe^+Cl^-} \rightleftharpoons 3Cl^-_{(aq)} + \overline{(R_3NMe^+)_3[RhCl_n(SnCl_3)_{6-n}]^{3-}}$$

Scheme 2.2 Reaction scheme for the extraction of $[Rh(SnCl_3)_nCl_{6-n}]^{3-}$ (n = 1 – 6) into chloroform-*d* using Aliquat-336 as ion-exchanger.

$$[Rh(SnCl_3)_5]^{4-}_{aq} + 4\overline{R_3NMe^+Cl^-} \rightleftharpoons 4Cl^-_{(aq)} + \overline{(R_3NMe^+)_4[Rh(SnCl_3)_5]^{4-}}$$

Scheme 2.3 Reaction scheme for the extraction of $[Rh(SnCl_3)_5]^{4-}$ into chloroform-*d* using Aliquat-336 as ion-exchanger.

The solutions were left to stand overnight to allow essentially all the coloured complexes to be extracted into the organic phase by the reaction showed in Scheme 2.2 and Scheme 2.3. The organic phase of the respective solutions was transferred into NMR tubes for ^{119}Sn NMR analysis.

2.3.2 Extraction with Methyl *iso*-Butyl Ketone

The $[Rh(SnCl_3)_nCl_{6-n}]^{3-}$ (n = 1 – 6) and $[Rh(SnCl_3)_5]^{4-}$ complex anions were extracted into methyl iso-butyl ketone (MIBK) by simply shaking the aqueous phase with equal volume of MIBK for 30 minutes. Regardless of the HCl concentration in the aqueous phase, extraction with MIBK resulted in a colour change from deep red/purple to bright yellow, illustrated in Scheme 2.4. This is indicative of the formation of the hydride Rh-Sn complex, $[RhH(SnCl_3)_5]^{3-}$, in the organic phase.

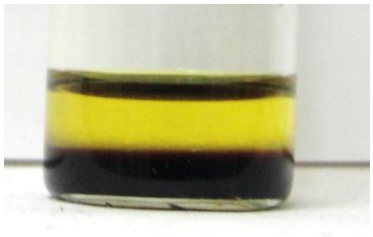

Scheme 2.4 Colour change from deep purple (the lower aqueous phase) to bright yellow (the upper organic phase) on extraction of the $[Rh(SnCl_3)_5]^{4-}$ with MIBK.

The bright yellow solution was transferred to a NMR tube for ^{119}Sn, ^{1}H and ^{103}Rh{^{1}H} NMR analysis.

2.3.3 Extraction with model polyurethane compound: Diϕ400

In order to extract the desired Rh-Sn species into the organic phase using the model polyurethane compound, referred to as podands, the latter needed to be synthesized. It was previously shown by Iris Hall[9] that the $C_6H_5NHC(O)\text{-}O\{(CH_2CH_2O)_{8/9}\}\text{-}(O)CHNC_6H_5$ podand (Diφ400U) is the most effective podand for the extraction of these Rh-Sn species. In light of this the Diφ400U "podand" was synthesized and used to extract the Rh-Sn species into chloroform.

2.3.3.1 Synthesis of Diϕ400 (model polyurethane compound)

To synthesize the model polyurethane compound Diϕ400, polyethylene glycol 400 (PEG-400) and phenyl isocyanate was added together in a 1:2 mole ratio in dichloromethane (DCM), as illustrated in Scheme 2.5.

Therefore, 2 mL (0.0184 mol) phenyl isocyanate was added to 2 mL DCM (dichloromethane) in one reaction vile and 4.36 mL (0.00966 mol, 5 % excess) PEG-400 was added to 4.5 mL DCM in another reaction vile. The 4 mL phenyl isocyanate solution was transferred to a 3-neck round bottom flask and the PEG-400 solution was transferred to a dripping funnel. The PEG-400 solution was added drop wise to the phenyl isocyanate solution, where after the mixed solution was stirred for 20 hours. The resulting solution was washed with water, dried under vacuum at 80 °C and washed with ethanol to remove excess water.

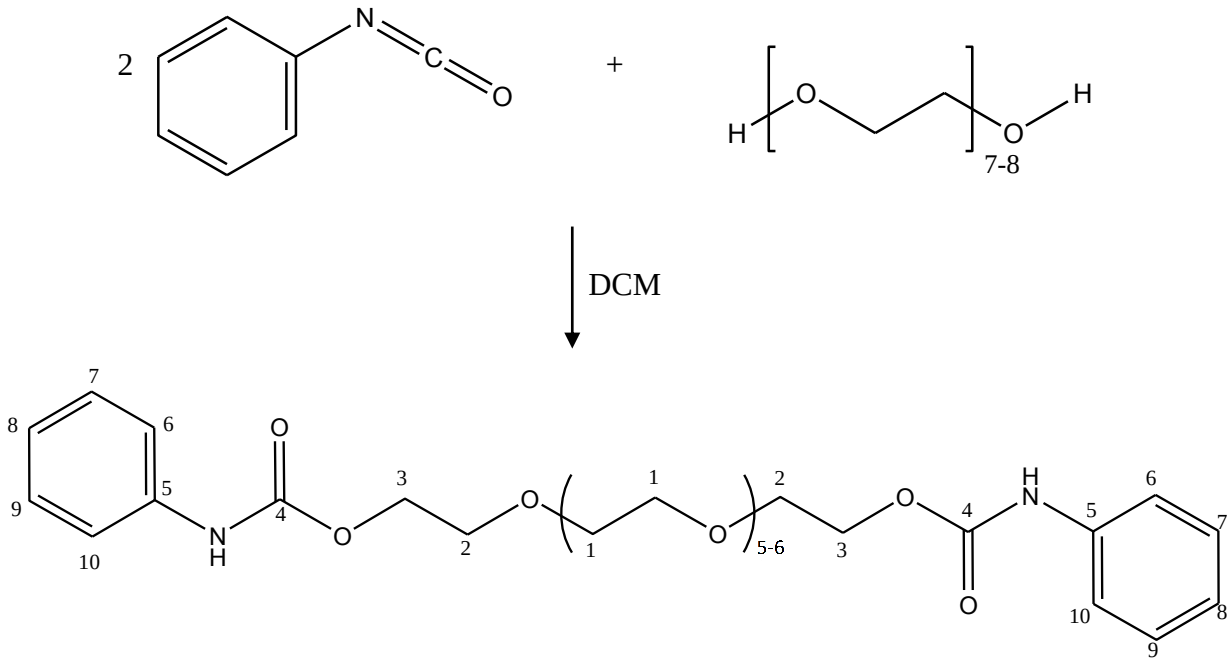

Scheme 2.5 Reaction scheme for the synthesis of the model polyurethane compound $C_6H_5NHC(O)$-$O\{(CH_2CH_2O)_{8/9}\}$-$(O)CHNC_6H_5$. A 2:1 mole ratio of phenyl isocyanate to PEG-400 is required for the reaction.

The Diϕ400 podand was characterized by means of ^{13}C NMR spectroscopy.

2.3.3.2 ^{13}C NMR characterization of the Diϕ400 podand

The ^{13}C NMR spectrum of the Diϕ400 compound is shown in Figure 2.5 and the NMR parameters are given in Table 2.1.

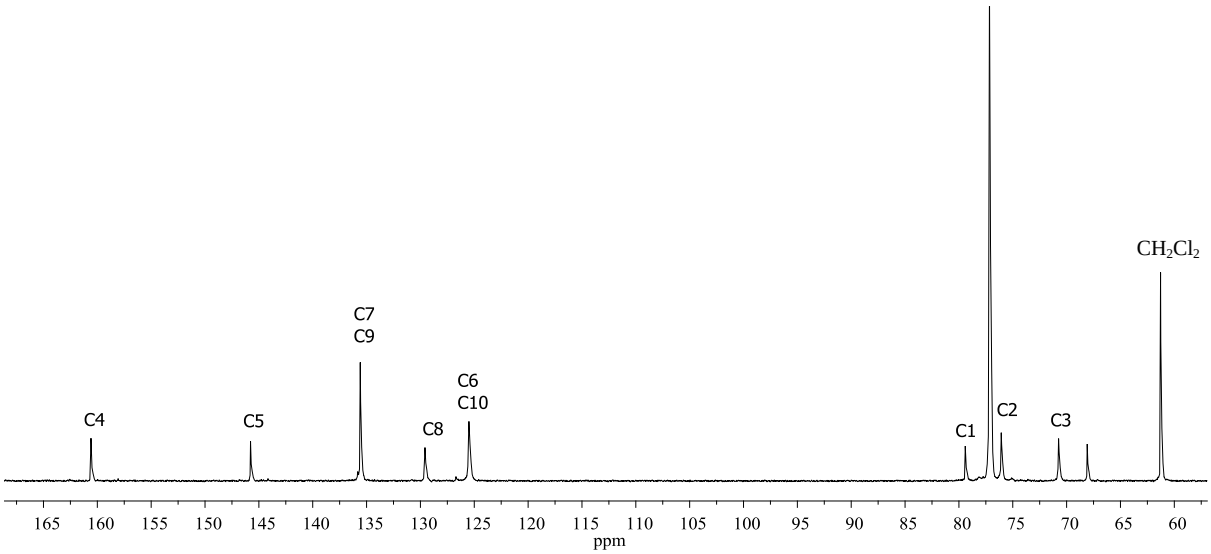

Figure 2.5 ^{13}C NMR spectrum of the $C_6H_5NHC(O)$-$O\{(CH_2CH_2O)_{8/9}\}$-$(O)CHNC_6H_5$ podand (Diφ400U) in *d*-chloroform at 25 °C.

Table 2.1 The assignment of the ^{13}C NMR spectrum of the Diφ400U podand based on the predicted ^{13}C NMR spectrum.

	Experimental δ(^{13}C)/ppm	Predicted δ(^{13}C)/ppm
C1	79.4	70.2
C2	67.7	69.1
C3	70.7	62.1
C4	160.6	153.9
C5	145.7	135.9
C6	125.5	121.6
C7	135.6	129.0
C8	129.6	124.4
C9	135.6	129.0
C10	125.5	121.6

*The predicted spectrum does not account for solvent effects. The experimental results were obtained from a solution of the Diφ400U podand dissolved in *d*-chloroform.

The δ(^{13}C) values also compare well to that reported by I. Hall[9] for this podand. Therefore this podand was used as is for the extraction of the Rh-Sn species.

Unfortunately, only broad unresolved ^{119}Sn NMR signals were obtained when this podand was used to extract the Rh-Sn complexes and are therefore not discussed in Chapter 5.

2.4 Experimental

2.4.1 Reagents

Rhodium(III)chloride, (99.9+ %, $RhCl_3 \cdot 3H_2O$, Johnson-Matthey Chemicals limited), tin(II)chloride ($SnCl_2 \cdot 2H_2O$, Sigma-Aldrich and $SnCl_2$, Sigma-Aldrich) and tin(II)bromide ($SnBr_2$, Sigma-Aldrich) were of reagent grade quality and were stored in a dessicator prior to use. Potassium chloride (KCl, 99.5%, Sigma Aldrich) was also of reagent grade quality and used as is. A rhodium nitrate ($Rh(NO_3)_3 \cdot xH_2O$, Johnson Matthey) solution was used for the synthesis of the bromido Rh-Sn species. All aqueous solutions were prepared using ultrapure Milli-Q water (MQ › 18MΩ) that was degassed with nitrogen for at least an hour prior to use in order to remove O_2. The hydrochloric acid (HCl, 32%, Riedel-de Haën), perchloric acid ($HClO_4$, 70 %, Sigma Aldrich) and hydrobromic acid (HBr, 48%, Associated Chemical enterprises) were also degassed with nitrogen prior to use. Chloroform-*d* ($CDCl_3$, 99.8%, Merck) and deuterium oxide (D_2O, 99.9 %, Sigma-Aldrich) were used as solvents to obtain a lock signal for NMR measurements of the organic and aqueous solutions, respectively. Methyltrioctylammonium chloride (Aliqaut-336, $CH_3N[(CH_2)_7CH_3]_3Cl$, Aldrich) was used as ion-pairing reagent to extract complexes into chloroform-*d*. Methyl iso-butylketone (MIBK, Sigma Aldrich) was used to extract the Rh-Sn complexes. Phenyl isocyanate (>98 %, Sigma Aldrich), poly(ethylene glycol) 400 (PEG400, Sigma-Aldrich) and dichloromethane (DCM, >99.8 %, Sigma-Aldrich) were used to synthesize the Diφ400U podand. Isopropanol (C_3H_80, Sigma-Aldrich) was HPLC grade and used as is.

2.4.2 Titrimetric Determination of Tin(II)

Although tin can be assayed successfully by atomic absorption, the method does not differentiate between tin(II) and tin(IV). However, for the purpose of this study it is important to determine the quantity of tin(II) in particular in our stannous chloride solutions. Therefore a well-documented titrimetric method for the analysis of tin(II) in hydrochloric acid by oxidation with potassium iodate was adopted.

The potassium iodate solution reacts quantitatively with stannous tin Sn(II) in the presence of concentrated hydrochloric acid with the oxidation thought to proceed through the following steps:

$$3\ SnCl_2 + 1\ KIO_3 + 6\ HCl \rightleftharpoons 3\ SnCl_4 + 1\ KI + 3\ H_2O \quad 2.4.1$$

$$1\ KIO_3 + 5\ KI + 6\ HCl \rightleftharpoons 6\ KCl + 3\ H_2O + 3\ I_2 \quad 2.4.2$$

$$2\ KIO_3 + 2\ I_2 + 6\ HCl \rightleftharpoons 1\ KCl + 3\ H_2O + 5\ ICl \quad 2.4.3$$

The overall reaction thus given by:

$$2SnCl_2 + KIO_3 + 6HCl \rightleftharpoons 2SnCl_4 + KCl + ICl + 3H_2O \quad 2.4.4$$

Thus 1 mole KIO_3 is equivalent to 2 mole $SnCl_2$. In accordance with the published method 1.5 g $SnCl_2 \cdot 2H_2O$ was weighed out and dissolved in a small volume of concentrated hydrochloric acid to prevent the rapid oxidization of Sn(II) to Sn(IV) by oxygen in the atmospheric air and then made up to 250 mL in a volumetric flask. From this solution, 25 mL was removed and added to another 250 mL volumetric flask to which 30 mL concentrated HCl, 20 mL H_2O as well as 5 mL of an immiscible organic solvent, chloroform, was added. The solution was then titrated with standard 0.1 M KIO_3 whilst gently shaking the bottle. Once the violet colour of the iodine, formed as a by-product during the reaction, has reached its maximum intensity, a stopper was inserted and the solution was shaked thoroughly. From there titration was slowly continued until the end-point of the reaction was reached, which is marked by the disappearance of the last trace of this violet colour from the organic phase. Iodine chloride (ICl) is not extracted and imparts a yellowish colour to the aqueous phase. The titration was done in triplicate and it was determined that 98 % of the $SnCl_2 \cdot 2H_2O$ salt is Sn(II).

2.4.3 Determination of Rhodium by Inductively Coupled Plasma-Optical Emission Spectrometry (ICP-OES)

The rhodium concentration of the samples prepared using either the $RhCl_3 \cdot 3H_2O$ salt or the $Rh(NO_3)_3 \cdot xH_2O$ solution was determined using a Spectro Arcos ICP-OES which

incorporated the use of a Burgener T2002 Nebulizer and Cyclonic spray chamber. The samples were transferred to the nebulizer by PEEK tubing with internal diameter equal to 0.12 mm. The nebulizer flow rate, auxiliary gas flow rate coolant flow and RF power were set to 0.6 $mL.min^{-1}$, 2 $L.min^{-1}$, 16 $L.min^{-1}$ and 1550 W, respectively.

Firstly, standard curves were constructed for rhodium using a series of standard solutions with rhodium concentrations of 0 ppm, 0.468 ppm, 9.362 ppm, 46.846 ppm, 93.615 ppm and 468.07 ppm in a 3 M hydrochloric acid matrix. The respective standard curves obtained using four different emission lines, λ = 233.477, 249.077, 252.053 and 343.489 nm, are shown in Figure 2.6. From the slopes obtained it is evident that the λ = 343.5 nm emission line is the most sensitive resonance line with the lowest background noise and was thus the line used to determine the rhodium concentration in the various samples.

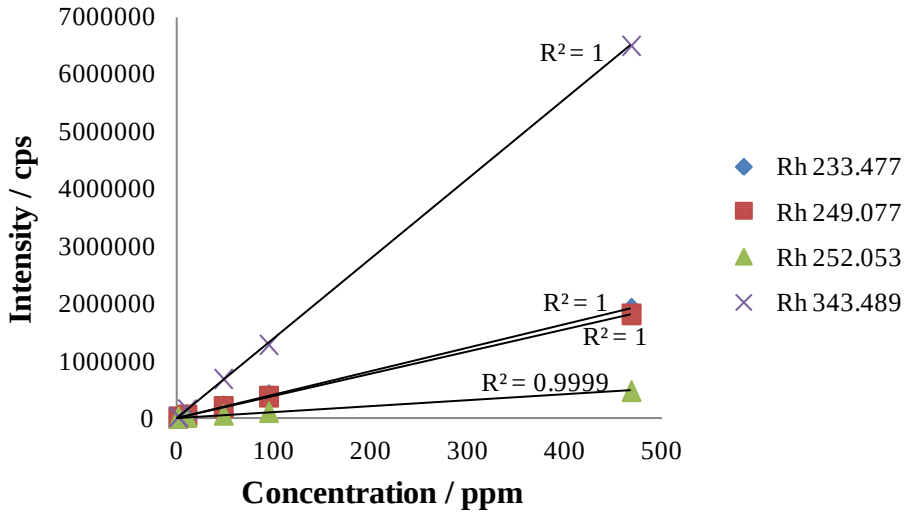

Figure 2.6 Calibration curve constructed for rhodium using four different emission lines: λ = 233.477, 249.077, 252.053 and 343.489 nm.

For the preparation of the series of $[Rh(SnCl_3)_nCl_{6-n}]^{3-}$ (n = 1 – 6) complex anions and the $[Rh(SnCl_3)_5]^{4-}$ complex anion the $RhCl_3 \cdot 3H_2O$ salt obtained from Johnson-Matthey was used as starting material. As the concentration of the standard solutions of rhodium ranged from 0.468 ppm to 468.07 ppm a rhodium solution of 100 ppm was required. Moreover, in order to conform to the matrix of the standard solutions the 100 ppm sample needed to be prepared in 3 M HCl.

Therefore a 25 mL 20 mM (2058.2 ppm) rhodium solution was prepared by weighing out 0.1317 g of the $RhCl_3 \cdot 3H_2O$ salt and transferring it to a 25 mL volumetric flask which was then filled up to the line with 3 M HCl. In order to obtain a rhodium concentration of 100 ppm the solution was diluted *ca.* 20 times by pipetting 0.4859 mL out and into a 10 mL volumetric flask which was then filled to the line with 3 M HCl.

From the standard curves constructed the rhodium concentration was determined to be 97.184 ppm. Thus the starting solution had a rhodium concentration of 19.4368 mM and not 20 mM as was thought. This discrepancy was taken into consideration for all the experiments for which the $RhCl_3 \cdot 3H_2O$ salt was used.

For the preparation of the series of $[Rh(SnBr_3)_nBr_{6-n}]^{3-}$ (n = 3 – 5) complex anions a $Rh(NO_3)_3$ solution received from Johnson-Matthey was used. However, no indication was given as to what the rhodium concentration of the solution is. Subsequently, the solution was diluted 200 and 400 times respectively, again ensuring that the final hydrochloric acid is 3 M. Using the calibration curve constructed with the λ = 343.489 nm emission line the rhodium concentration of the 400 and 200 times diluted solutions were determined to be 150.636 and 76.309 ppm, respectively. Thus, the rhodium concentration of the $Rh(NO_3)_3$ solution received was determined to be 0.3 M.

2.4.4 UV/Vis spectroscopy

All UV-Vis spectra were recorded on an Agilent 8453 Ultraviolet-visible spectrometer at 20 °C using a 0.5 cm quartz cell. Solutions in the sample and blank cells were similar in every respect except that the latter contained no rhodium-stannous halide solutions. The spectra were run between 190 and 1500 nm at a scan speed of 200 nm/min.

2.4.5 ^{119}Sn NMR spectroscopy

All ^{119}Sn NMR spectra were recorded at 223.7 MHz using a Varian INOVA 600 MHz spectrometer at 20 °C and a 5 mm broad-band probe, unless stated otherwise. All chemical shifts are quoted relative to an external reference of neat $Sn(CH_3)_4$ sealed in a 1 mm capillary surrounded by ^2H_2O. Spectra were recorded under conditions of optimal resolution using an

excitation pulse of 2.0 µs, with an acquisition time 1.016 s, and no relaxation delay was applied. The T_1 values for the ^{119}Sn NMR nuclei in these systems were measured to be 0.1 – 0.5 s, so that essentially quantitative resonance intensities are obtained. Broad band ^{1}H-decoupling was applied in all measurements. A line broadening factor of 20 Hz was applied in processing, resulting in an effective line-width at half height. Spectral widths of up to 2000 ppm were used.

2.4.6 ^{103}Rh NMR spectroscopy

^{103}Rh NMR experiments were recorded on a Bruker DRX 400 spectrometer (using a 5 mm triple resonance inverse (TBI) probe with a dedicated ^{31}P channel and extended decoupler range) operating at the proton frequency of 400.13 MHz.

Indirect detection method: ^{103}Rh-^{1}H spectra were obtained by indirect detection using the pulse program 'hmqcf3ph' shown in Figure 2.7.

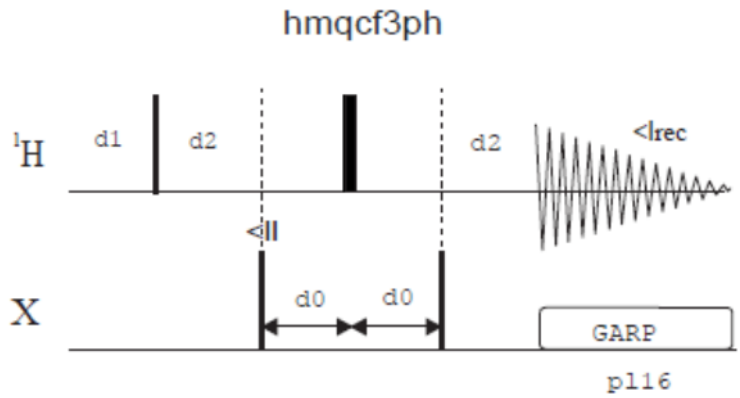

Figure 2.7 The pulse program 'hmqcf3ph' used for the ^{103}Rh-^{1}H NMR spectroscopy for the indirect detection of ^{103}Rh.

The spectral width in f2 (^{1}H) varied between 2 and 3 ppm according to specific circumstances while the spectral width in f1(^{103}Rh) were gradually decreased in order to obtain better resolution of the generated ^{103}Rh NMR signal obtained. The exact δ(^{1}H), pw90 and decp90 of the $[RhH(SnCl_3)_5]^{3-}$ species in MIBK were determined before the 2D NMR experiment was started. The pw90 of ^{1}H was measured to be 13.7 µs and the decp90 of ^{103}Rh was measured to be 75µs. The time domain (TD) was set to 2048, the number of increments (ni) to 64 and power to 11.2 and 145 for f1 and f2, respectively.

2.4.7 NMR simulation program gNMR50

NMR spectroscopy is a powerful tool for the analysis of a sample and the characterization of species. However, in some cases the NMR spectra become so complicated that simple analysis of the sample is not possible. In such cases, using a simulation program to simulate the NMR spectrum can be very helpful. One such program is gNMR50 which allows you to interpret and simulate your data.[92]

Simulation in the strict sense is the calculation of an NMR spectrum from a set of parameters such as chemical shifts, coupling constants etc. Computer simulation of a NMR spectrum is particularly useful in the interpretation of 'simple' NMR spectra that do not adhere to "first-order" rules. For "second-order" spectra simulation is the only practical way to predict the appearance of a spectrum from its basic parameters.

For the work done in this thesis, gNMR50 was used to confirm tentative assignments made in ^{119}Sn and ^{1}H NMR spectra that were too complicated to assign by simple analysis. The methodology used was to first draw the structure of the tentatively assigned $[Rh(SnCl_3)_nCl_{6-n})]^{3-}$ (n = 1 – 6) complex anion in question, import the structure into gNMR50, enter the experimentally measured NMR parameters such as chemical shift and spin-coupling values and then simulate the spectrum. As a 'proof-of-principle' the ^{119}Sn and ^{195}Pt NMR spectra of the trigonal bipyramidal $[Pt(SnCl_3)_5]^{3-}$ complex anion, that was fully characterized previously in this group, is simulated.[59] Although the Rh-Sn species are being investigated, the Pt-Sn system was chosen deliberately for the 'proof-of-principle' as the ^{119}Sn NMR spectrum of $[Pt(SnCl_3)_5]^{3-}$ is fully understood and the ^{119}Sn NMR parameters are exactly know. The experimentally measured ^{119}Sn and ^{195}Pt NMR parameters are summarized in Table 2.2.

Table 2.2 Experimental ^{119}Sn and ^{195}Pt NMR parameters measured for the $[Pt(SnCl_3)_5]^{3-}$ complex anion.[7]

NMR paramater	Experimental Values
$\delta(^{195}Pt)$ / ppm	-5904.6
$\delta(^{119}Sn)$ / ppm	-123.4
$^{1}J(^{195}Pt\text{-}^{119}Sn)$ / Hz	15 864
$^{1}J(^{195}Pt\text{-}^{119}Sn)$ / Hz	15 160
$^{1}J(^{195}Pt\text{-}^{115}Sn)$ / Hz	13 921
$^{2}J(^{117}Sn\text{-}^{119}Sn)$ / Hz	6060

The structure of the trigonal bipyramidal $[Pt(SnCl_3)_5]^{3-}$ is drawn in ChemDraw Ultra 8.0, Figure 2.8, and the .cdx file is imported into gNMR50, Figure 2.9. The structure will appear in window A in Figure 2.9A. Each nucleus (excluding halides) is numbered, Sn = 1, 3 - 6 and Pt = 2.

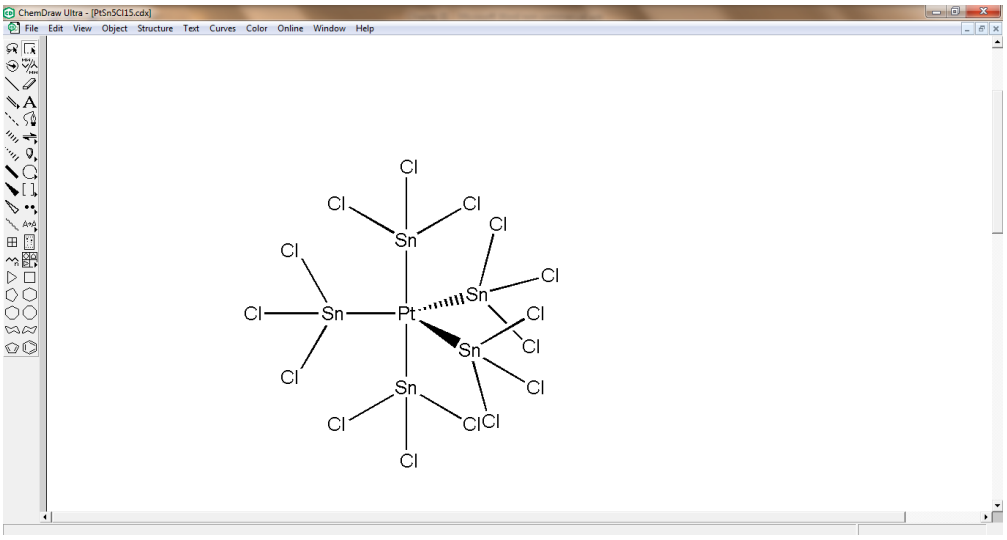

Figure 2.8 The structure of $[Pt(SnCl_3)_5]^{3-}$ drawn in ChemDraw 8.0 before it is imported into gNMR50.

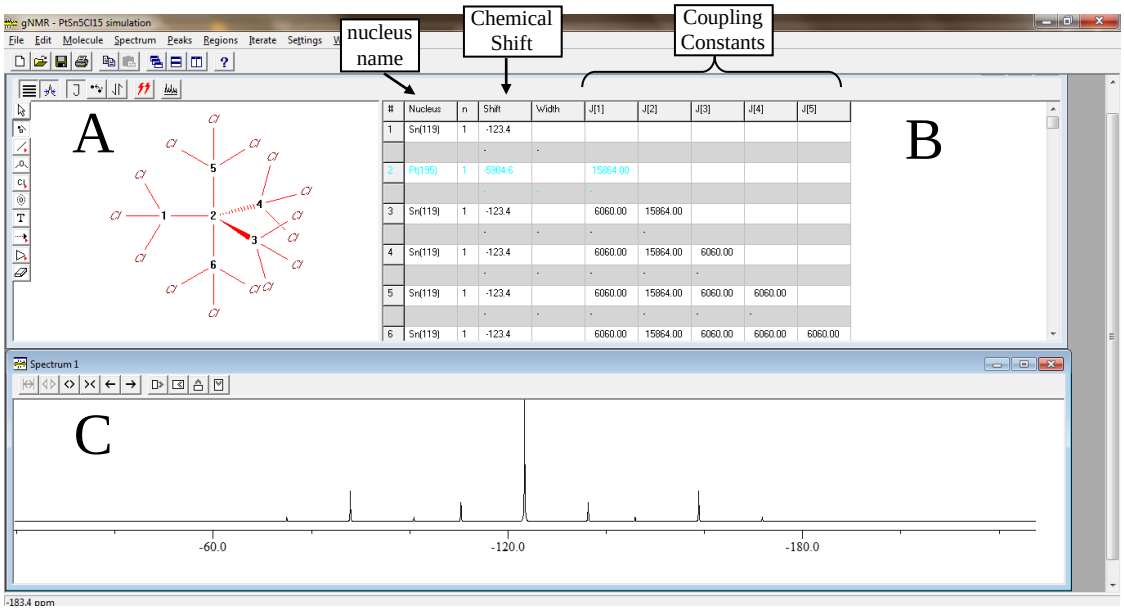

Figure 2.9 Interface of gNMR50. Once a structure is imported into gNMR50 it will appear in window A. To the right of the structure, in window B, the molecule spreadsheet is given. All the NMR parameters are entered into this spreadsheet. The simulated spectrum is given in window C.

In window B in Figure 2.9 a molecule spreadsheet is given into which the relevant NMR data can be entered. The 'nucleus name' column is automatically completed when the structure is

imported into window A. gNMR recognizes two types of names: single-isotope names and natural abundance isotope mixture names. For platinum, for example, the former would be written as 195Pt whereas the latter is written as Pt(195). If the isotope mixture name is used, gNMR50 will generate a mixture of *isotopomers* for the molecule. Thus, Pt(195) will generate a mixture containing 33.8% ^{195}Pt and 66.2 % of species with a magnetically-inactive platinum nucleus. Similarly, if the nucleus name Sn(119) is used, gNMR50 will generate a mixture of *isotopomers* containing 8.59 % ^{119}Sn, 7.68 % ^{117}Sn, 0.34 % ^{115}Sn and 83.39 % species not containing any of these nuclei. Therefore, if the natural abundances of all the isotopes in the molecule must be considered for the simulation, the natural abundance isotope mixture names must be used.

The next column of importance is the 'chemical shift' column. In this field the chemical shift values measured for each nucleus in the experimentally obtained spectrum, as listed in Table 2.2, is given in ppm. The rightmost part of the molecule spreadsheet is a matrix that displays the respective coupling constants experimentally measured, Table 2.2. For example, the entry in column 2, row 3 corresponds to J_{23}, the coupling between 2 (Pt) and 3 (Sn), in other words ^{1}J(^{195}Pt-^{119}Sn). In the case of *isotopomer* mixtures, as is most of the species in this work with tin having three NMR-active isotopes, the coupling constants will be different for each isotope in the mixture. Therefore, a 'main isotope' must be agreed upon and the coupling constant for that isotope is entered. For example, if Sn(119) is used as nucleus name, gNMR uses the natural abundance mixture, but assume that all supplied coupling constants refer to the main isotope, ^{119}Sn. Conversion to values for the other isotopes are then done automatically. Therefore only the coupling constant measured for ^{1}J(^{119}Sn-^{195}Pt) = 15 864 Hz is entered into the matrix and gNMR50 will automatically generate the ^{1}J(^{117}Sn-^{195}Pt) and ^{1}J(^{115}Sn-^{195}Pt) coupling constants when simulating the NMR spectrum.

Once all the chemical shift and spin-coupling values are entered the spectrum is simulated. Window C in Figure 2.9 shows the ^{119}Sn NMR spectrum simulated from the data given in Table 2.2. From here the frequency limit can be changed in order to increase or decrease the resolution of the spectrum and the line widths of the signals can be changed. The simulated spectrum can now be compared to the experimentally obtained spectrum to determine if the assignment can be confirmed, Figure 2.10.

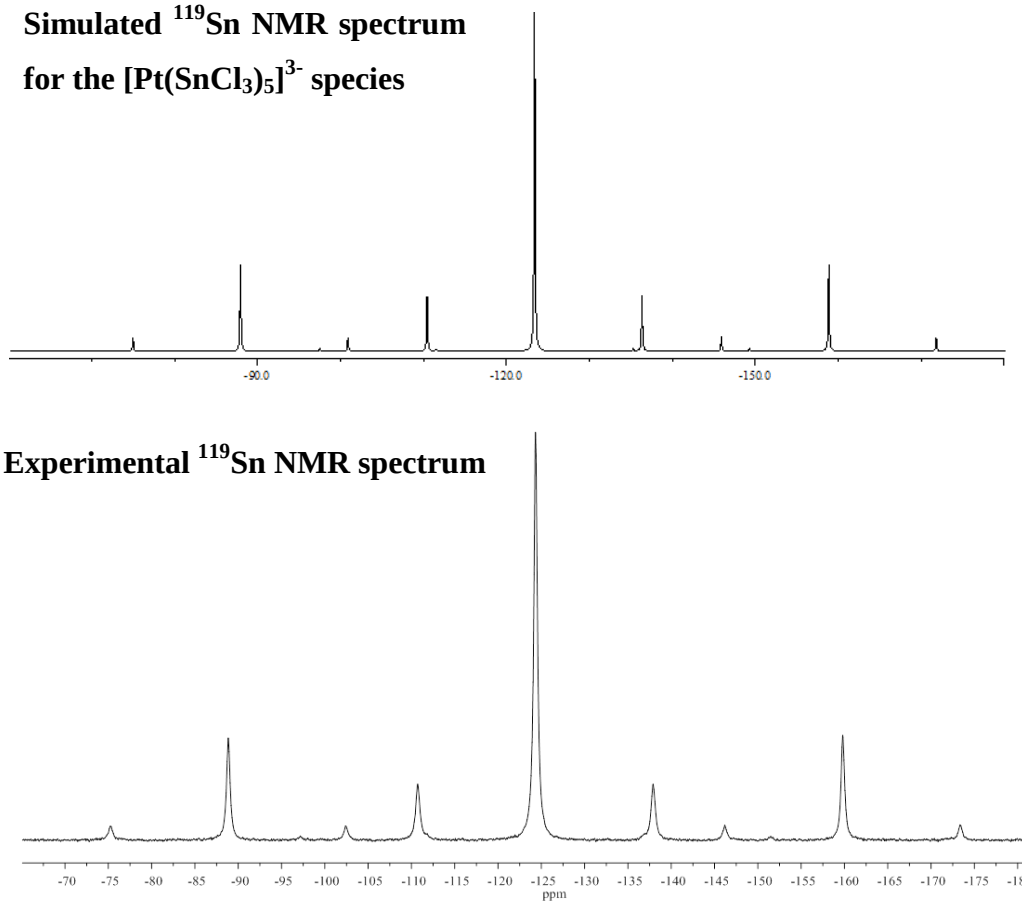

Figure 2.10 Comparison between the simulated ^{119}Sn NMR spectrum of $[Pt(SnCl_3)_5]^{3-}$ and the experimentally obtained ^{119}Sn NMR spectrum thereof.

Moreover, the observed nucleus can be changed from ^{119}Sn to ^{195}Pt (or any other NMR-active nucleus) and the spectrum can be re-calculated to give you the ^{195}Pt NMR spectrum, which can then be compared to the experimentally obtained spectrum.

The use of gNMR50 to simulate these complex NMR spectra holds several advantages and allows for a confirmation of the assignments based on 1st order ^{n}J(X-Y) coupling observed in these $[Rh(SnX_3)_nX_{6-n}]^{3-}$ (n = 1 – 6, X = Cl^-/Br^-), $[Rh(SnCl_3)_5]^{4-}$ and $[RhH(SnCl_3)_5]^{3-}$ species.

Chapter III

Speciation of stannous chloride complexes of rhodium(I/III) in acidic aqueous solutions with high-resolution ^{119}Sn NMR spectroscopy

Chapter III

Speciation of stannous chloride complexes of rhodium(I/III) in acidic aqueous solutions with high-resolution ^{119}Sn NMR spectroscopy

3.1 Introduction

In the early 1960's Young and co-workers[23,24] were the first to isolate a Rh-Sn species, $[Rh_2Cl_2(SnCl_3)_4]^{4-}$, wherein the $SnCl_3^-$ moiety, as a ligand, was directly coordinated to the central rhodium and described it as a bridged $[Rh^I_2Cl_2(SnCl_3)_4]^{4-}$ species. It was postulated by Young *et. al.*[24] and others[93] that, even in solutions where the tin concentration is of the same order as that of rhodium, one molecule of tin(II) is used to reduce rhodium(III) to rhodium(I) thus resulting in the formation of Rh(I)-Sn(II) species. This proposal of reduction of rhodium(III) by tin(II) was supported by Furlani *et. al.*[28] who also isolated a Rh(I) complex, $[AsPh_4]_3[Rh(SnCl_3)_4]\cdot SnCl_2$, but this was done from solutions containing effective Rh:Sn mole ratios of 1:100-500. Conversely, Kimura *et. al.*[33,39] isolated a series of rhodium(III) species, $[N(CH_3)_4]_3[Rh(SnCl_3)_nCl_{6-n}]$ (n = 1 – 4), from solutions with a effective Rh:Sn mole ratio of 1:1-4, showing that reduction did not take place under these conditions. The existence of the $[N(CH_3)_4]_3[Rh(SnCl_3)_nCl_{6-n}]$ (n = 2 – 5) species was confirmed by ^{119}Sn Mössbauer spectroscopy and showed that the Sn(II) species are covalently coordinated to rhodium.[94,35]

Burke and Lauterbur[95] were the first to report that ^{119}Sn NMR spectroscopy is a useful tool for the characterization of tin compounds, with ^{119}Sn having a spin = ½ and a natural abundance of 8.68 %, and used it for their study of the mixed halide tin(IV) $SnCl_nBr_{4-n}$ (n = 1 – 3) species. In the early 1980's, Moriyama *et. al.* showed by means of ^{119}Sn NMR spectroscopy that a series of $[Rh(SnCl_3)_nCl_{6-n}]^{3-}$ (n = 1 – 5) complex anions exist in solution,[41] not all of which were unambiguously characterized. Investigation of the effect of the effective Rh:Sn mole ratio on the distribution of these species showed that with ratios of 1:1-5 six main doublet ^{119}Sn NMR resonance signals at -991.6, -654.4, -411.1, -281.4, -204.3 and -100.5 ppm were observed and assigned to the $[Rh(SnCl_3)_nCl_{6-n}]^{3-}$ (n = 1 – 5) complex anions respectively. The signal at -281.4 ppm, however, was not assigned but was shown to form part of the trend observed for the series of rhodium(III)-Sn(II) species. On the other hand, when a effective Rh:Sn mole ratio of 1:6 was used, a doublet peak at -8.5 ppm, with a

relatively large Rh-Sn coupling constant became dominant and was tentatively assigned to the reduced, trigonal bipyramidal $[Rh^{I}(SnCl_3)_5]^{4-}$ species. This redox process was supported by the conversion of one mole of $SnCl_2$ to tin(IV) per mole of $RhCl_3$, as evidenced by the Sn(IV) signals at -620 ppm. From this it is clear that several equilibria can simultaneously exist in solution:[41]

$$[Rh^{III}Cl_6]^{3-} + SnCl_3^- \rightleftharpoons [Rh(SnCl_3)Cl_5]^{3-} + Cl^- \quad 3.1.1$$

$$[Rh(SnCl_3)Cl_5]^{3-} + SnCl_3^- \rightleftharpoons \textit{cis/trans}\text{-}[Rh(SnCl_3)_2Cl_4]^{3-} + Cl^- \quad 3.1.2$$

$$\textit{c/t}\text{-}[Rh(SnCl_3)_2Cl_4]^{3-} + SnCl_3^- \rightleftharpoons \textit{fac/mer}\text{-}[Rh(SnCl_3)_3Cl_3]^{3-} + Cl^- \quad 3.1.3$$

$$[Rh^{III}(SnCl_3)_5Cl]^{3-} + SnCl_3^- \rightleftharpoons [Rh^{I}(SnCl_3)_5]^{4-} + Cl^- \quad 3.1.4$$

It was however reported by Saito *et. al.* that these Rh(III)-Sn(II) complexes are kinetically labile and that the $SnCl_3^-$-ligands undergo fast *intra*-molecular scrambling on the NMR time-scale.[41] Therefore the *stereo*-chemical *cis/trans* or *fac/mer* isomers of the series of $[Rh(SnCl_3)_nCl_{6-n}]^{3-}$ (n = 1 – 5) and $[Rh(SnCl_3)_5]^{4-}$ species could not be identified and thus that the stepwise substitution of a Cl^- by a $SnCl_3^-$ was simplified to be:

$$[Rh^{III}Cl_6]^{3-} \longrightarrow [Rh(SnCl_3)Cl_5]^{3-} \longrightarrow [Rh(SnCl_3)_2Cl_4]^{3-} \longrightarrow [Rh(SnCl_3)_3Cl_3]^{3-} \longrightarrow$$
$$[Rh(SnCl_3)_4Cl_2]^{3-} \longrightarrow [Rh^{III}(SnCl_3)_5Cl]^{3-} \longrightarrow \longrightarrow [Rh^{I}(SnCl_3)_5]^{4-}$$

where the final step indicates the reduction of Rh(III) to Rh(I) by excess $Sn(II)Cl_2$. High resolution ^{119}Sn NMR spectroscopy has proven to be extremely useful tool for the elucidation of the structure of these Rh(III)/(I)-Sn(II)halide complex anions. Rhodium has one isotope, ^{103}Rh, which is NMR active and of the 10 natural occurring tin isotopes, three are NMR active, Table 3.1.

Table 3. 1 Natural Abundances and magnetic properties of rhodium and tin isotopes with I = ½.

NMR-active isotope	Natural Abundance / %	Spin	Gyromagnetic Ratio	Receptivity ($^{13}C = 1$)
^{103}Rh	100	½	-1.3455	0.186
^{119}Sn	8.68	½	-15.869	25.6
^{117}Sn	7.67	½	-15.168	19.9
^{115}Sn	0.35	½	-13.922	0.715

In light of this ^{119}Sn NMR spectroscopy of these Rh-Sn species hold several advantages:[41] (1) coordination of a $^{119}SnCl_3$-ligand to the central rhodium is evidenced by the occurrence of a doublet, where the ^{119}Sn NMR signal is split due to spin coupling to ^{103}Rh (I = ½, natural abundance = 100 %), (2) coordination of two or more tin-ligands to the central rhodium is evidenced by the appearance of satellites due to spin coupling to ^{117}Sn (I = ½, natural abundance = 7.67 %) and (3) NMR parameters such as chemical shift, $\delta(^{119}Sn)$, and the respective coupling constants, $^1J(^{103}Rh\text{-}^{119}Sn)$ and $^2J(^{117}Sn\text{-}^{119}Sn)$, are useful for the assignment of species.

In a previous ^{195}Pt NMR study it was shown that a detailed analysis of the *isotopologue* and *isotopomer* distribution of aqua-chlorido Pt(IV) species led to the unambiguous identification and assignment of the isotopic stereoisomers of $[PtCl_5(H_2O)]^-$ and *cis/trans*-$[PtCl_4(H_2O)_2]$.[95] Subsequently, as part of my MSc, the detailed high resolution ^{195}Pt and ^{119}Sn NMR study of the heteroleptic $[Pt(Sn_5Cl_nBr_{15-n})]^{3-}$ (n = 0 – 15) complexes resulted not only in the unambiguous assignment of all 16 possible species, but also the assignment of 120 *isotopologues* of the series of complexes.[59]

To the best of our knowledge a detailed analysis of the *isotopologues* and *isotopomers* of the series of $[Rh(SnCl_3)_nCl_{6-n}]^{3-}$ (n = 1 – 6) and $[Rh(SnCl_3)_5]^{4-}$ complexes has not been done. The number of magnetically equivalent $^{119}SnX_3^-$ ligands coordinated to the central rhodium atom reflected by the intensities or relative areas of the respective $^2J(^{117}Sn\text{-}^{119}Sn)$ satellites which are expected to be equal to the natural statistical abundance (NSA) of the specific *isotopologue* or *isotopomer* of the species from which they arise.* The term *isotopologue* refers to chemical species that differ only in isotopic composition of their molecules or ions,

* The relative experimental signal areas obtained with ^{119}Sn and ^{103}Rh NMR for different isotopologues should to a good approximation be equal to the natural statistical abundances (NSA) of the respective isotopologues as the change in standard reaction Gibbs energy for the interconvertion between isotopologues of the $[Rh(SnCl_3)_nCl_{6-n}]^{3-}$ (n = 1 – 5) and $[Rh(SnCl_3)_5]^{4-}$ complex anions is relatively small.

whereas the term *isotopomers* are isomers of *isotopologues* with the same isotopic composition, but differing in their position in the molecule or ion.[97]

These two terms are illustrated for the $[Rh(SnX_3)_4X_2]^{3-}$ (X = Cl^-/Br^-) complex anion in Scheme 3.1, where (a) and (b) are *isotopologues* of each other when a ^{119}Sn isotope in (a) $[^{103}Rh(^{i}Sn^{35/37}Cl_3)_3(\mathbf{^{119}Sn}^{35/37}Cl_3)^{35/37}Cl_2]^{3-}$ is simply replaced by a ^{117}Sn isotope in (b) $[^{103}Rh(^{i}Sn^{35/37}Cl_3)_3(\mathbf{^{117}Sn}^{35/37}Cl_3)^{35/37}Cl_2]^{3-}$. On the other hand, the complex illustrated in (c) is a *isotopomer* of the isotopologue $[^{103}Rh(^{i}Sn^{35/37}Cl_3)_3(\mathbf{^{119}Sn}^{35/37}Cl_3)^{35/37}Cl_2]^{3-}$ (a). These have the same isotopic composition, but the ^{119}Sn isotope is either in the equatorial (*trans* to Cl^-) position, (a), or in the axial (*cis* to Cl^-) position, (c).

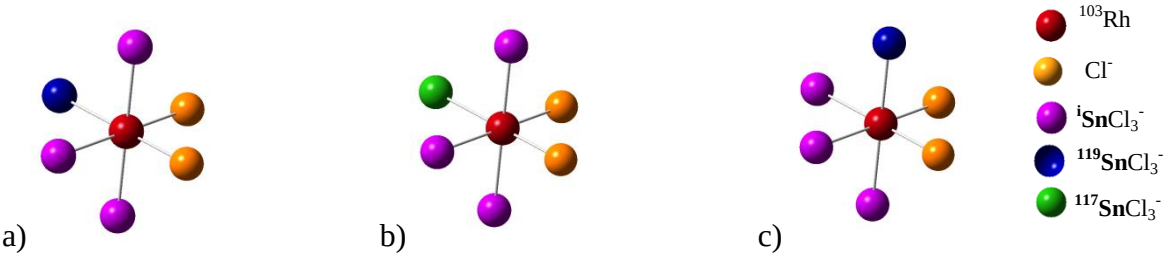

Scheme 3.1 A schematic representation of an example of *isotopologues* and *isotopomers* of the $[Rh(SnCl_3)_4Cl_2]^{3-}$ complex anion, where (a) and (b) are *isotopologues* of each other and (a) and (c) are *isotopomers* of each other. (^{i}Sn represents all the magnetically inactive isotopes of Sn)

The natural statistical abundance (NSA) of each isotopologue can be calculated using Equation 3.1 where n_x is the number of isotope x present in the specific isotopologue (e.g. x = ^{119}Sn) and ρ_x is the natural abundance of isotope x (e.g. $\rho_x = 0.0868$).[44]

$$\rho(n_1 n_2 \dots n_x) = \frac{(\sum_{i=1}^{x} n_i)!}{n_1! n_2! \dots n_x!} \rho_1^{n_1} \cdot \rho_2^{n_2} \cdot \rho_x^{n_x} \qquad 3.1.5$$

As part of the interest in the favourable effects of stannous chloride on the extraction of Rh(III/I) in analytical and hydrometallurgical applications[8,9,98] a detailed ^{119}Sn NMR speciation study of this complex system in aqueous hydrochloric acid solutions has been carried out. From Equations 3.1.1 to 3.1.4 on page 40 it is evident that the mass action of the Cl^- ions may have an effect on the speciation of the Rh-Sn species. Therefore, in order to control the effect of the Cl^- ions this study was extended to the use of perchloric acid instead of hydrochloric acid, in order to decrease the free Cl^- concentration.

3.2 Results and Discussion

3.2.1 Speciation of the series of $[Rh(SnCl_3)_nCl_{6-n}]^{3-}$ (n = 1 – 6) and $[Rh(SnCl_3)_5]^{4-}$ complex anions in acidic aqueous solutions with H^+ concentrations between 0.5 and 6 M

3.2.1.1 $[Rh(SnCl_3)_5]^{4-}$ complexes in aqueous solutions

A 0.5 M rhodium solution with a Rh:Sn mole ratio was prepared by dissolving the required amount of $SnCl_2 \cdot 2H_2O$ in concentrated HCl under nitrogen atmosphere, to prevent oxidation of Sn(II) to Sn(IV), adding the required amount of $RhCl_3 \cdot 3H_2O$ and diluting to obtain a final HCl concentration of 3 M. The deep red/purple solution was allowed to reach equilibrium by stirring it overnight under N_2 atmosphere. The ^{119}Sn NMR spectrum acquired for this solution is shown in Figure 3.1.

The main feature of this ^{119}Sn NMR spectrum is the broadish signal at $\delta(^{119}Sn)$ = 9.39 ppm, split into a doublet due to $^1J(^{103}Rh\text{-}^{119}Sn)$ spin coupling, indicated by the symbol 'a', and flanked by its $^2J(^{117}Sn\text{-}^{119}Sn)$ satellites, indicated by the symbol 'b'. The measured I(satellite)/I(main) ratio of 16.6 % compares well with the calculated NSA of 16.3 % for an Rh-Sn complex with five $SnCl_3^-$-ligands coordinated to the central rhodium atom. Moreover, the chemical shift position, $\delta(^{119}Sn)$ = -9.39 ppm, as well as the $^1J(^{103}Rh\text{-}^{119}Sn)$ and $^2J(^{117}Sn\text{-}^{119}Sn)$ coupling constants measured to be 809.1 and 3624.2 Hz, respectively, compare well to the values reported in literature by Moriyama *et. al.* for the trigonal bipyramidal $[Rh(SnCl_3)_5]^{4-}$ complex anion.[41] Hence, the main set of ^{119}Sn NMR signals at -9.39 ppm is assigned to the $[^{103}Rh(^{i}SnCl_3)_n(^{119}SnCl_3)_{5-n}]^{4-}$ (n = 0 – 4)[†] *isotopologues* and the $^2J(^{117}Sn\text{-}^{119}Sn)$ satellites to the series of $[^{103}Rh(^{i}SnCl_3)_n(^{119}SnCl_3)_{4-n}(^{117}SnCl_3)]^{4-}$ (n = 0 – 3,) *isotopologues*. However, only one pair of $^2J(^{117}Sn\text{-}^{119}Sn)$ satellites are observed which suggests that fast intramolecular scrambling occurs on the NMR time-scale rendering the ^{119}Sn nucleus in the axial position magnetically equivalent to one in the equatorial position. Thus no *isotopomers* are observed in the ^{119}Sn NMR spectrum of the $[Rh(SnCl_3)_5]^{4-}$ complex anion, which is in agreement with what was previously reported in literature.[41,8,9,98] The minor species at $\delta(^{119}Sn)$ = -99.21 ppm in the spectrum in Figure 3.1 will be discussed later in Section 3.2.1.3.3, page 61.

[†] The notation '^{i}Sn' refers to all 7 isotopes of Sn that are not magnetically active.

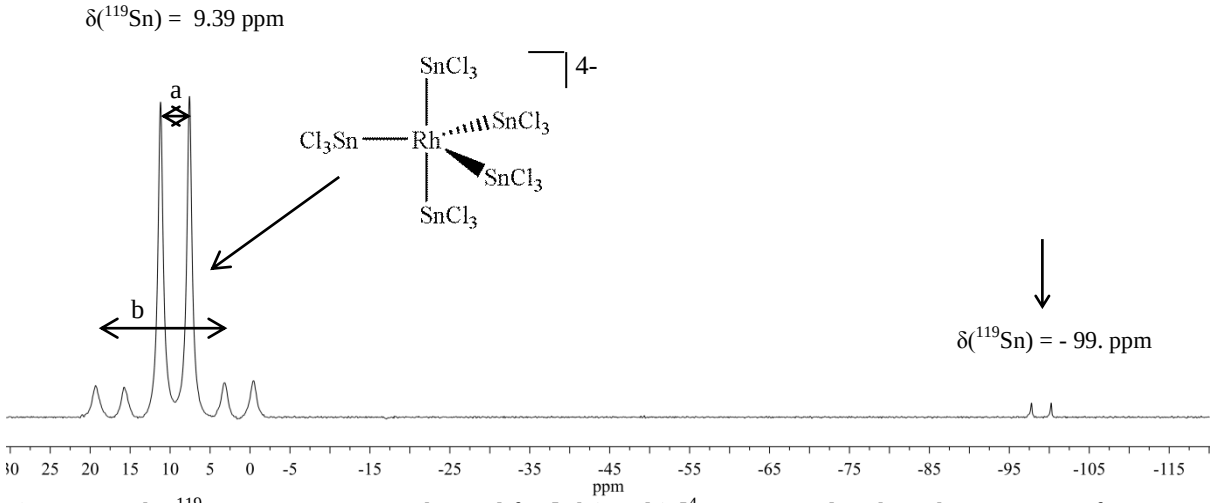

Figure 3.1 The ^{119}Sn NMR spectrum obtained for $[Rh(SnCl_3)_5]^{4-}$ in 3 M HCl with a Rh to Sn ratio of 1:8 at 25 °C. The main signal is split into a doublet, indicated by 'a', due to $^{1}J(^{103}Rh\text{-}^{119}Sn)$ coupling = 809.1 Hz and is flanked by $^{2}J(^{117}Sn\text{-}^{119}Sn)$ = 3624.2 Hz satellites as indicated by 'b'. The species at $\delta(^{119}Sn)$ = -99.2 ppm is assigned later.

As a matter of interest a ^{117}Sn NMR spectrum of the same solution was acquired under exactly the same conditions and an almost identical splitting pattern was obtained, with the exception that the $^{1}J(^{103}Rh\text{-}^{119}Sn)$ coupling constant is 770.1 Hz compared to the $^{1}J(^{103}Rh\text{-}^{119}Sn)$ coupling constant of 809.1 Hz.

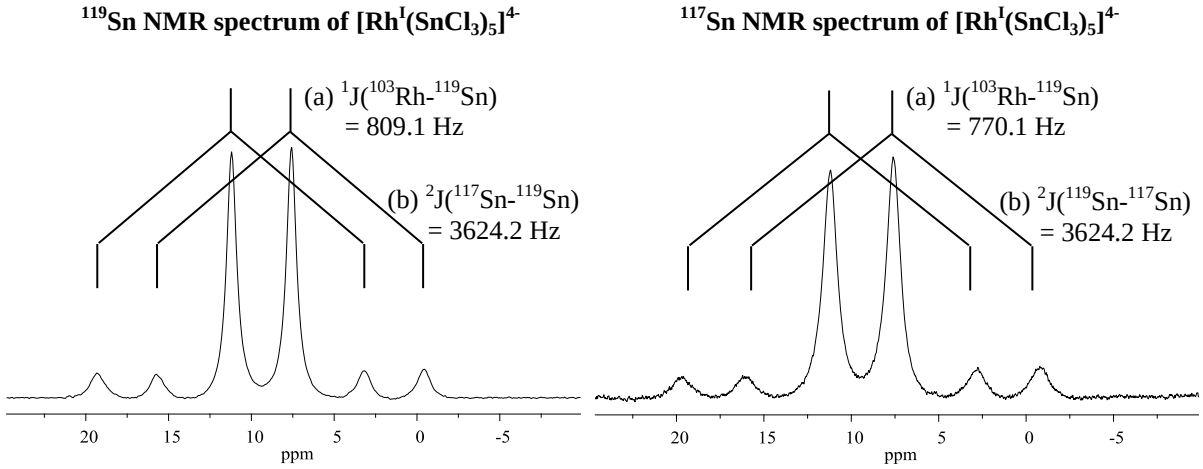

Figure 3.2 Comparison between the ^{119}Sn and ^{117}Sn NMR spectra of the $[Rh(SnCl_3)_5]^{4-}$ species at -9.39 ppm. The $^{1}J(^{103}Rh\text{-}^{117}Sn)$ coupling constant is 770.1 Hz compared to the $^{1}J(^{103}Rh\text{-}^{119}Sn)$ coupling constant of 809.1 Hz, both couplings indicated by (a) in the respective spectra. The $^{2}J(^{117}Sn\text{-}^{119}Sn)$ coupling constant, indicated by (b) in the respective spectra, are as expected the same.

The ratio of these two values, 809.1/770.1 = 1.048, compares well to the ratio of the gyromagnetic ratios of ^{119}Sn and ^{117}Sn, $\gamma(^{119}Sn)/(\gamma(^{117}Sn)$ = 1.046, which confirms the assignment of the $^{1}J(^{103}Rh\text{-}^{117}Sn)$ coupling and thus also the assignment of the $[Rh(SnCl_3)_5]^{4-}$

species on the ^{117}Sn NMR spectrum. Hence, either ^{119}Sn or ^{117}Sn NMR spectroscopy can be used to characterize these species. However, since ^{119}Sn is slightly higher in abundance and thus has a slightly higher NMR-receptivity compared to ^{117}Sn, Table 3.1, ^{119}Sn NMR was used for the remainder of the experiments.

3.2.1.2 The effect of HCl concentration on the speciation of Rh-Sn complexes

From Equations 3.1.1 to 3.1.4 on page 40 it is apparent that the Cl^- concentration is expected to have a significant effect on the equilibria of the reactions. Therefore, the $[Rh(SnCl_3)_nCl_{6-n}]^{3-}$ species distribution was evaluated as a function of hydrochloric acid concentration [HCl]/M. In this regard, 3 solutions with 0.5, 3 and 6 M HCl were prepared in which the [Rh] = 0.5 M and the effective Rh:Sn mole ratio = 1:6 was kept constant. The solutions were allowed to equilibrate for at least 24 hours under N_2 atmosphere before acquiring the ^{119}Sn NMR spectra of each solution. The ^{119}Sn spectra are shown in Figure 3.3a, b and c.

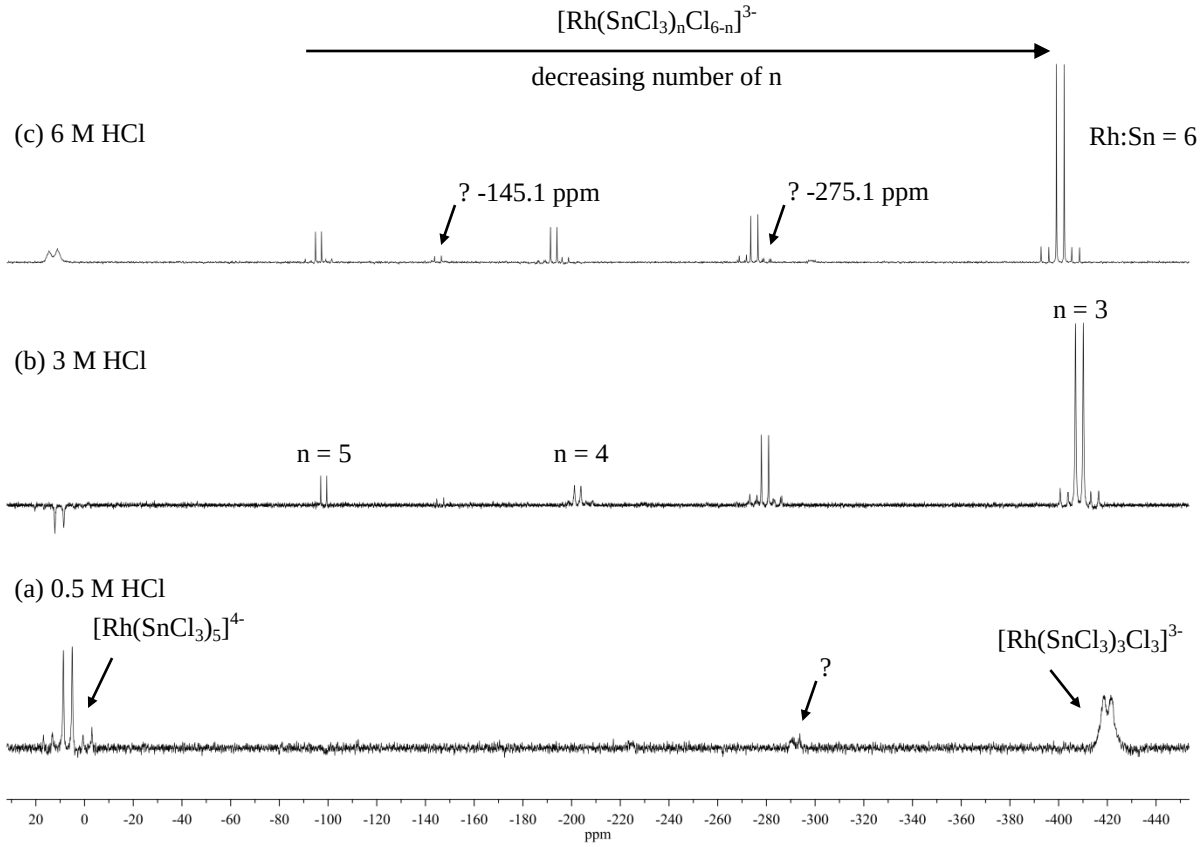

Figure 3.3 Variation of the ^{119}Sn NMR spectrum of the aqueous solution of $RhCl_3 \cdot 3H_2O$ and $SnCl_2 \cdot 2H_2O$ with HCl concentration: (a) 0.5 M HCl, (b) 3 M HCl and (c) 6 M HCl. The effective Rh:Sn mole ratio was kept constant at 1:6 and spectra were measured at 25 °C.

These spectra confirm that the distribution of species was indeed very sensitive to change in the HCl concentration from 0.5 to 6 M, Figure 3.3. The spectrum of the solution with a hydrochloric acid concentration of 0.5 M, Figure 3.3(a), shows three sets of ^{119}Sn NMR resonances; the major broad doublet at -420 ppm with $^{1}J(^{103}Rh\text{-}^{119}Sn)$ = 714 Hz and a minor peak at -293 ppm together with a well-resolved doublet at 9.4 ppm with $^{1}J(^{103}Rh\text{-}^{119}Sn)$ = 810 Hz. From the measured $\delta(^{119}Sn)$ and $^{1}J(^{103}Rh\text{-}^{119}Sn)$ values, the two sets of signals at -420 and 9.4 ppm were tentatively assigned to the $[Rh^{III}(SnCl_3)_3Cl_3]^{3-}$ and the $[Rh^{I}(SnCl_3)_5]^{4-}$ species, respectively, as listed in Table 3.2. The very broad signal obtained for the $[Rh^{III}(SnCl_3)_3Cl_3]^{3-}$ species suggests that the species is undergoing a dynamic process such as ligand exchange, for example, on the NMR time-scale. By contrast to these broad signals, sharp signals are obtained for the $[Rh^{I}(SnCl_3)_5]^{4-}$ complex anion in 0.5 M HCl, which is indicative of the system being in equilibrium. Moreover, it is interesting to note that only the $[Rh^{III}(SnCl_3)_3Cl_3]^{3-}$ and the $[Rh^{I}(SnCl_3)_5]^{4-}$ species are present in this solution, which suggests that $[Rh^{III}(SnCl_3)_3Cl_3]^{3-}$ species is thermodynamically favoured species in the series of Rh(III)-Sn(II) complexes under these conditions.

As the hydrochloric acid concentration is increased, the ^{119}Sn resonance signals due to the $[Rh^{III}(SnCl_3)_3Cl_3]^{3-}$ species become better resolved whilst those of the $[Rh^{I}(SnCl_3)_5]^{4-}$ become significantly broader, Figure 3.3(c). Moreover, the increase in the hydrochloric acid concentration is accompanied by the formation of four additional sets of ^{119}Sn NMR signals at -275.1, -193.8, -145.1 and -102.3 ppm, respectively. The $\delta(^{119}Sn)$/ppm and $^{1}J(^{103}Rh\text{-}^{119}Sn)$/Hz values of the species at $\delta(^{119}Sn)$ = -193.8 and -102.3 ppm compare well with those reported by Moriyama *et. al.*[41] for the $[Rh^{III}(SnCl_3)_4Cl_2]^{3-}$ and $[Rh^{III}(SnCl_3)_5Cl]^{3-}$ species, Table 3.2.

Table 3.2 ^{119}Sn NMR parameters of the rhodium-tin species observed in acidic aqueous solutions.

	Rh-Sn Complexes	Oxidation number of Rhodium	δ(^{119}Sn)/ ppm[a]	^{1}J(^{103}Rh-^{119}Sn)/ Hz[b]
1	$[Rh(SnCl_3)Cl_5]^{3-}$	III	- (-991.6)[c]	- (864)
2	$[Rh(SnCl_3)_2Cl_4]^{3-}$	III	- (-654.4)[c]	- (796)
3	$[Rh(SnCl_3)_3Cl_3]^{3-}$	III	-420.2 (-411.1)	714 (718)
4	*d*	III	-275.1 (-281.4)	664 (664)
5	$[Rh(SnCl_3)_4Cl_2]^{3-}$	III	-193.8 (-204.3)	589 (590)
6	*e*	III	-145.1	620
7	$[Rh(SnCl_3)_5Cl]^{3-}$	III	-102.3 (-100.5)	555 (547)
8	$[Rh(SnCl_3)_5]^{4-}$	I	9.4 (8.5)	810 (806)

[a] Values in brackets are δ(^{119}Sn) values reported by Moriyama *et. al.*[41] [b] Values in brackets are ^{1}J(^{103}Rh-^{119}Sn) coupling constants reported by Moriyama *et. al.*[41] [c] These species were not observed with current experimental conditions. [d] Structure unassigned, previously observed by Moriyama *et. al.*[41] [e] Structure unassigned, not previously reported.

Inspection of the published ^{119}Sn NMR spectra at 37.1 MHz from Moriyama *et. al.*[41] did not reveal such detail as the spectra shown in Figure 3.3c. Moreover, the resonances at δ(^{119}Sn) = -275.1 and -145.1 ppm were not correctly assigned and this will be discussed at a later stage in Sections 3.2.1.3.2 and 3.2.1.3.3, respectively.

It is clear from Figure 3.3 that an increase in the hydrochloric acid concentration favours the formation of the rhodium(III)-Sn(II) complexes, $[Rh^{III}(SnCl_3)_nCl_{6-n}]^{3-}$ (n = 1 – 3), over that of the reduced $[Rh^{I}(SnCl_3)_5]^{4-}$ species, and dominate at 0.5 M HCl. This trend can be rationalized by the increasing number of free Cl^- ions in solution which compete with the $SnCl_3^-$ ligand for coordination to the rhodium center and subsequently hamper the formation of the $[Rh^{I}(SnCl_3)_5]^{4-}$ complex anion. Thus, despite the addition of an excess of $SnCl_2$ with respect to Rh, the high Sn:Cl mole ratios obtained when working in high hydrochloric acid concentrations appears to suppress the formation of the $[Rh^{I}(SnCl_3)_5]^{4-}$ species and results in predominantly the $[Rh^{III}(SnCl_3)_nCl_{6-n}]^{3-}$ (n = 3 – 5) complex anions in solution favouring those with lower values of 'n' as the Cl^- concentration increases. This is consistent with the proposed equilibrium reactions 3.1.1 to 3.1.4 on page 40.

Although the chemical shift values and ^{1}J(^{103}Rh-^{119}Sn) / Hz coupling constants measured for the respective species in Figure 3.3 compare well to the values previously reported by Moriyama *et. al.*,[41] listed in Table 3.2, and the corresponding assignments of the

$[Rh^{III}(SnCl_3)_nCl_{6-n})]^{3-}$ are tentatively made. The minor ^{119}Sn NMR signals at 275.1 and -145.1 ppm shown in Figure 3.3c could not be assigned due to their low concentrations.

3.2.1.3 Speciation of the $[Rh(SnCl_3)_nCl_{6-n}]^{3-}$ (n = 3 – 5) complex anions in 6 M HCl

The concentration of the species between $\delta(^{119}Sn)$ = -50 and -450 ppm in Figure 3.3(c) are too low in concentration to obtain good ^{119}Sn NMR signals at reasonable signal to noise ratios (SN) to allow for reliable assignments. In order to increase the abundance of the $[Rh(SnCl_3)_nCl_{6-n}]^{3-}$ (n = 3 – 5) species between $\delta(^{119}Sn)$ = -50 and -450 ppm, the effective Rh:Sn mole ratio was decreased to 1:5 in a hydrochloric acid concentration of 6 M, to ensure a large excess of Cl^- ions.

The ^{119}Sn NMR spectrum acquired for this solution after 24 hours of equilibration at room temperature under N_2 is shown in Figure 3.4. This spectrum shows six main sets of ^{119}Sn resonances, each of which is split into a doublet due to $^1J(^{103}Rh\text{-}^{119}Sn)$/Hz spin coupling confirming that all six signals are due to $[Rh^{III}(SnCl_3)_nCl_{6-n}]^{3-}$ (n = 1 – 5) and $[Rh^{I}(SnCl_3)_5]^{4-}$ species.

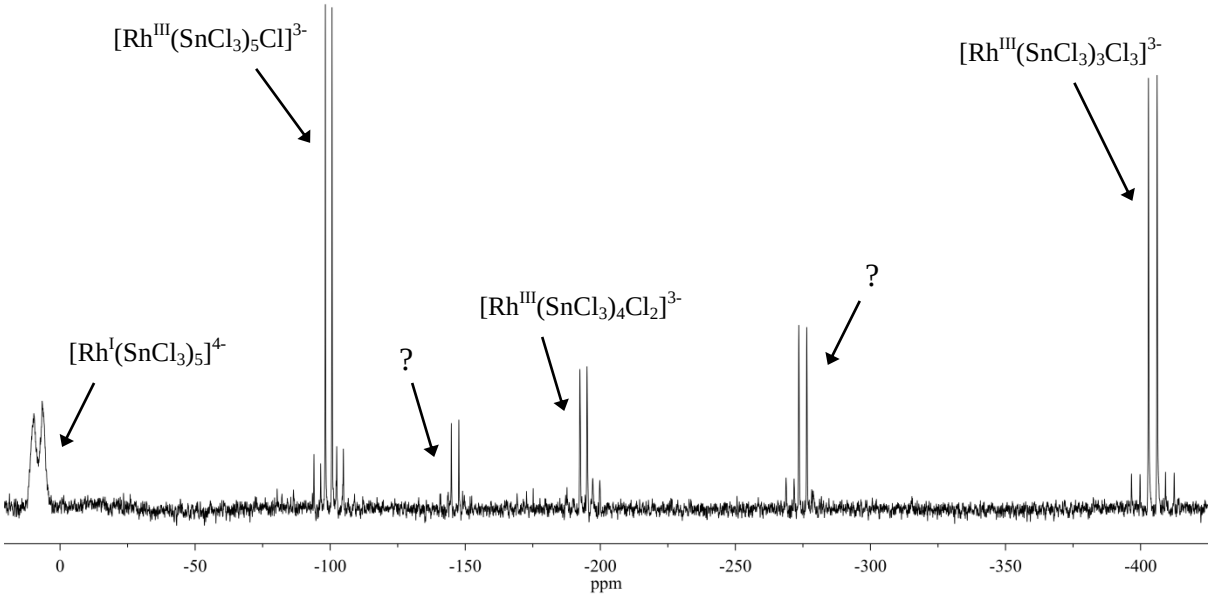

Figure 3.4 The ^{119}Sn NMR spectrum acquired for a 0.5 M Rh solution with a effective Rh:Sn mole ratio of 1:5 in 6 M HCl at 25 °C. Six main doublets are observed, each flanked by its respective satellites.

From the chemical shifts and $^{1}J(^{103}Rh\text{-}^{119}Sn)$/Hz coupling constants measured for the ^{119}Sn NMR signals in Figure 3.4, the assignments of the $[Rh^{III}(SnCl_3)_nCl_{6-n}]^{3-}$ (n = 3 – 5) and the $[Rh^{I}(SnCl_3)_5]^{4-}$ species previously made by Moriyama *et. al.*[41] could be confirmed. On the other hand, the two sets of signals at $\delta(^{119}Sn)$ = -145.1 and -275.1 ppm have not previously been reported or assigned, and thus require further investigations.

In a previous study of the Pt-Sn species,[59] it was shown that a plot of $\delta(^{119}Sn)$/ppm against $^{1}J(^{195}Pt\text{-}^{119}Sn)$/Hz is indicative of systematic trends in the series of species. Therefore, to identify the ^{119}Sn NMR signals at -145.1 and -275.1 ppm, the $^{1}J(^{103}Rh\text{-}^{119}Sn)$/Hz coupling constant of each species in Figure 3.4 was measured and plotted against its corresponding $\delta(^{119}Sn)$/ppm value. The resulting trend is displayed in Figure 3.5a and is comparable to the one Moriyama *et. al.*[41] reported for some of the series of $[Rh(SnCl_3)_nCl_{6-n}]^{3-}$ (n = 1 – 5) species. This suggests that the unassigned species may form part of the series of Rh(III)-Sn(II) species. Moreover, plotting the $^{2}J(^{117}Sn\text{-}^{119}Sn)$/Hz coupling constant of each species against its $\delta(^{119}Sn)$/ppm value in Figure 3.5b, shows that the $^{2}J(^{117}Sn\text{-}^{119}Sn)$/Hz coupling constant of the unassigned species at $\delta(^{119}Sn)$ = -145.1 ppm is almost equal to that of the $[Rh(SnCl_3)_5Cl]^{3-}$ species at $\delta(^{119}Sn)$ = -102.3 ppm, with $^{2}J(^{117}Sn\text{-}^{119}Sn)$ = 1882 Hz. This suggests that these two sets of signals are related to each other or might result from a single species. Similarly, the $^{2}J(^{117}Sn\text{-}^{119}Sn)$/Hz coupling constant of the unassigned species at -275.1 ppm is virtually equal to that of the $[Rh^{III}(SnCl_3)_4Cl_2]^{3-}$ species at -193.8 ppm.

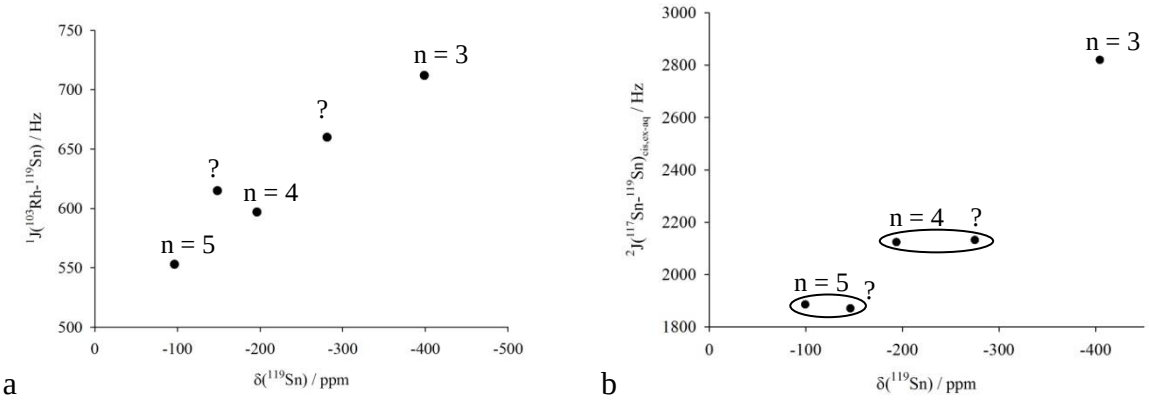

Figure 3.5 Plot of (a) $^{1}J(^{103}Rh\text{-}^{119}Sn)$ as a function of $\delta(^{119}Sn)$ and (b) $^{2}J(^{117}Sn\text{-}^{119}Sn)$ as a function of $\delta(^{119}Sn)$. The numeral values correspond to "n" in the series of $[Rh(SnCl_3)_nCl_{6-n}]^{3-}$ (n = 3 – 5) species.

A more detailed examination of each individual set of ^{119}Sn NMR resonance signals observed in Figure 3.4 shows that the signals at $\delta(^{119}Sn)$ = -102.3, -145.1, -198.4 and -275.1 ppm also

exhibit 'asymmetrical' $^{2}J(^{117}Sn\text{-}^{119}Sn)$ coupling patterns (satellites). 'Asymmetrical' satellites such as these have not been reported in any of the literature for the series of $[Rh(SnCl_3)_nCl_{6-n}]^{3-}$ (n = 1 – 5) complex anions.[41] However, a similar asymmetrical distribution of the $^{2}J(^{119}Sn\text{-}^{119}Sn)_{ax\text{-}eq}$ satellites have been reported for the kinetically inert $[RhH(SnCl_3)_5]^{3-}$ complex anion, and was ascribed to second order coupling effects/distortions in the spectrum.[9,33]

In light of this a detailed re-assignment of the species in the ^{119}Sn NMR spectrum in Figure 3.4 was carried out. To facilitate this process the ^{119}Sn NMR spectrum is divided into four different sections: A, B, C and D in Figure 3.6 and elucidation of this spectrum will be dealt with section for section. In this context gNMR50 was used to compare the simulated and experimental ^{119}Sn NMR spectra, to confirm unambiguous assignments.

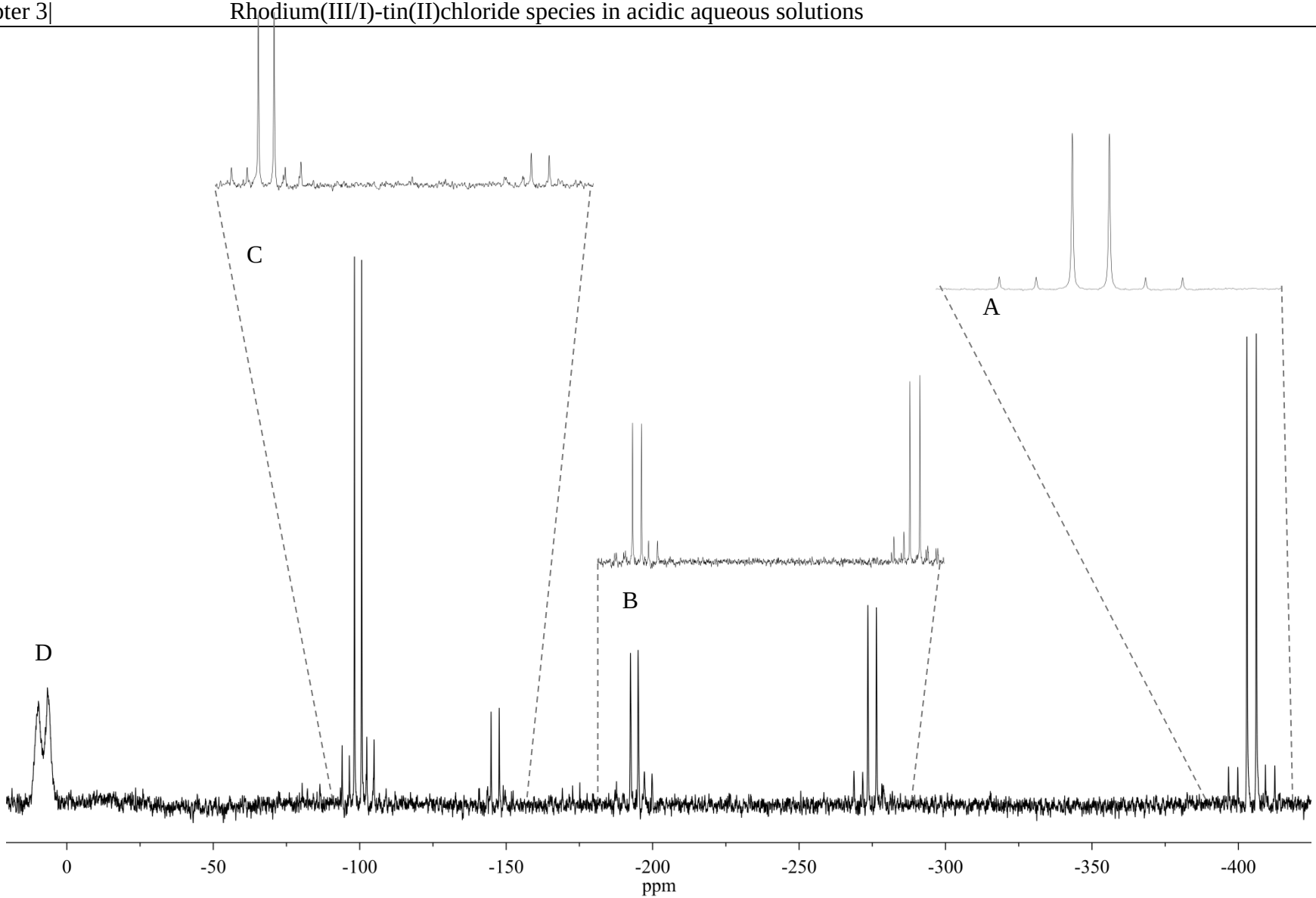

Figure 3.6 The ^{119}Sn NMR spectrum acquired for a 0.5 M Rh solution with a effective Rh:Sn mole ratio of 1:5 in 6 M HCl at 25 °C. Six main doublets are observed, each flanked by its respective satellites.

3.2.1.3.1 Spectral Section A of resonances at δ(^{119}Sn) = - 411.3 ppm

An expansion of Section A in Figure 3.6 is given below in Figure 3.7 and shows the species at δ(^{119}Sn) = -411.3 ppm. The signal is split into a doublet due to spin coupling with a coupling constant of 716 Hz and is flanked by its ^{2}J(^{117}Sn-^{119}Sn) satellites with a coupling constant of 2817 Hz.

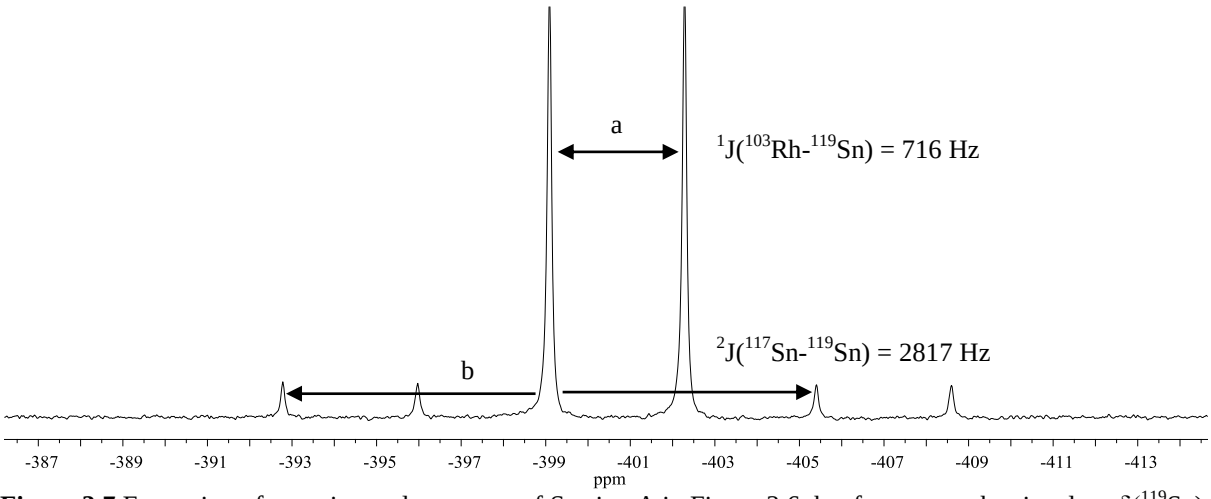

Figure 3.7 Expansion of experimental spectrum of Section A in Figure 3.6 that focuses on the signals at δ(^{119}Sn) = -411.3 ppm. Symbol 'a' indicate ^{1}J(^{103}Rh-^{119}Sn) spin coupling, whereas symbol 'b' indicates ^{2}J(^{117}Sn-^{119}Sn) spin coupling.

The chemical shift position, as well as the ^{1}J(^{103}Rh-^{119}Sn) and ^{2}J(^{117}Sn-^{119}Sn) coupling constants, correspond well to those previously reported for the $[Rh^{III}(SnCl_3)_3Cl_3]^{3-}$ complex anion.[41] Furthermore, the ^{2}J(^{117}Sn-^{119}Sn) satellite intensities were measured to be 8 %, which is in good agreement with the natural statistical abundance (NSA) of 8.3 % calculated, using Equation 3.1.5 on page 42, for a Rh-Sn complex anion with 3 magnetically equivalent $SnCl_3^-$ -ligands. The main ^{119}Sn resonance signal is thus assigned to the $[^{103}Rh(^{i}SnCl_3)_n(^{119}SnCl_3)_{3-n}Cl_3]^{3-}$ (n = 0 – 2) *isotopologue*, whereas the ^{2}J(^{117}Sn-^{119}Sn) satellites are assigned to the $[^{103}Rh(^{i}SnCl_3)_n(^{119}SnCl_3)_{2-n}(^{117}SnCl_3)Cl_3]^{3-}$ (n = 0, 1) isotopologue of the $[Rh^{III}SnCl_3)_3Cl_3]^{3-}$ complex anion. In addition to these *isotopologues*, there are two possible stereo-*isomers*, *fac*- and *mer*-, for the $[Rh^{III}(SnCl_3)_3Cl_3]^{3-}$ complex anion, illustrated in Scheme 3.2, which creates the expectation of two separate sets of ^{119}Sn NMR resonance signals. Yet, only one set of signals are observed in the ^{119}Sn NMR spectrum of this species, which is in good agreement with what was previously reported for *fac*-$[Rh(SnCl_3)_3Cl_3]^{3-}$ by Moriyama *et. al.*.[41]

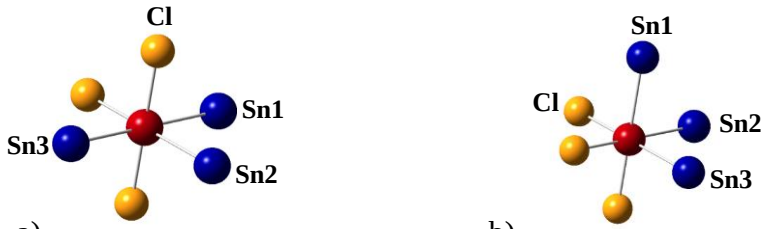

Scheme 3.2 A schematic representation of a) the *mer*- isomer and b) the *fac*-isomer of the $[Rh(SnCl_3)_3Cl_3]^{3-}$ complex anion. All Cl^- ions of the $SnCl_3^-$ ligands are left out for clarity.

Moriyama *et. al.*[41] suggested that either the $SnCl_3^-$ and Cl^- ligands undergo fast *intra*-molecular scrambling on the NMR time-scale which results in only one set of ^{119}Sn NMR resonance signals for both the *fac*- and *mer*- isomers, or alternatively that only the *fac*-isomer is present in solution, as the latter is the only isomer that has been isolated.[33,39,41] Entertaining the proposal of only *one* isomer, either the *mer*- or the *fac*-isomer, being in solution, a closer look at the ^{119}Sn NMR spectral pattern was taken.

The *mer*-isomer, shown in Scheme 3.2a, has one $SnCl_3^-$-ligand, Sn2, *trans* to a chlorido ligand and *cis* to the other two $SnCl_3^-$-ligands, with the other two $SnCl_3^-$-ligands, Sn1 and Sn2, being *trans* to each other and *cis* to a chlorido ligand. Thus, both $^2J(^{117}Sn\text{-}^{119}Sn)_{cis}$ and $^2J(^{117}Sn\text{-}^{119}Sn)_{trans}$ satellites should be observed in the ^{119}Sn NMR spectrum of the *mer*-$[Rh^{III}(SnCl_3)_3Cl_3]^{3-}$ species. On the other hand, in the case of the *fac*-$[Rh^{III}(SnCl_3)_3Cl_3]^{3-}$ isomer, Scheme 3.2b, all three $SnCl_3^-$-ligands (Sn1, Sn2 and Sn3) are *trans* to a chlorido-ligand (*cis* to each other) rendering them magnetically equivalent. Therefore, only $^2J(^{117}Sn\text{-}^{119}Sn)_{cis}$ satellites would be expected to be observed in the ^{119}Sn NMR spectrum of the *fac*-$[Rh^{III}(SnCl_3)_3Cl_3]^{3-}$ species. This spectral pattern agrees well with that obtained for the set of signals at $\delta(^{119}Sn)$ = -411.3 ppm, Figure 3.7, where only one set of $^2J(^{117}Sn\text{-}^{119}Sn)$ satellites with a coupling constant of 2817 Hz is observed. It is thus reasonable to suggest that the set of signals at $\delta(^{119}Sn)$ = -411.3 ppm can be assigned to the *fac*-$[Rh(SnCl_3)_3Cl_3]^{3-}$ species where the main signal is split into a doublet due to $^1J(^{103}Rh\text{-}Sn)$/Hz scalar coupling in the $[^{103}Rh(^iSnCl_3)_n(^{119}SnCl_3)_{3-n}Cl_3]^{3-}$ (n = 0 – 2) isotopologue, and is flanked by one pair of $^2J(^{117}Sn\text{-}^{119}Sn)_{cis}$ satellites due to coupling in the $[^{103}Rh(^iSnCl_3)_n(^{119}SnCl_3)(^{117}SnCl_3)_{2-n}Cl_3]^{3-}$ (n = 0, 1) isotopologue, illustrated in Scheme 3.3a and b respectively.

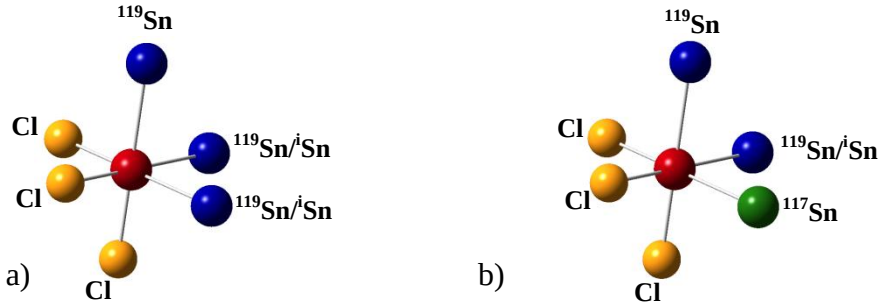

Scheme 3.3 A schematic representation of the *isotopologues* of the *fac*-$[Rh(SnCl_3)_3Cl_3]^{3-}$ species (Figure 3.7): a) $[^{103}Rh(^{i}SnCl_3)_n(^{119}SnCl_3)_{3-n}Cl_3]^{3-}$ (n = 0 – 2) and b) $[^{103}Rh(^{i}SnCl_3)_n(^{119}SnCl_3)_{2-n}(^{117}SnCl_3)Cl_3]^{3-}$ (n = 0, 1). All coordinated chlorido ligands of $SnCl_3^-$ are left out for clarity. $^{119}Sn/^{i}Sn$ refers to to the ligand being either $^{119}SnCl_3^-$ or $^{i}SnCl_3^-$.

It is thus proposed here that the signals at $\delta(^{119}Sn)$ = -411.3 ppm should be assigned to a kinetically inert *fac*-$[Rh^{III}(SnCl_3)_3Cl_3]^{3-}$ species. Although the series of $[Rh(SnCl_3)_nCl_{6-n}]^{3-}$ (n = 1 – 5) is tacitly believed to be *stereo*-chemically non-rigid, this proposition of a kinetically inert *fac*-$[Rh^{III}(SnCl_3)_3Cl_3]^{3-}$ species is supported by a study by Koch *et. al.*[8,9,98] wherein it was reported that the hydrido Rh(III)-Sn(II) species, $[Rh^{III}H(SnCl_3)_5]^{3-}$, is kinetically inert, proving that kinetically inert Rh(III)-Sn(II) species do exist in solution.

3.2.1.3.2 Spectral Section B of resonances between $\delta(^{119}Sn)$ = -193.8 and -275.1 ppm

The set of resonances at $\delta(^{119}Sn)$ = -193.8 ppm had previously been assigned to a kinetically labile $[Rh(SnCl_3)_4Cl_2]^{3-}$ complex anion,[41] whereas a signal at $\delta(^{119}Sn)$ = -275.1 ppm was unassigned. However, a detailed investigation of the ^{119}Sn NMR resonances at -193.8 and -275.1 ppm also reveals asymmetrical distribution of the $^{2}J(^{117}Sn\text{-}^{119}Sn)$ satellites around the respective main signals shown in Figure 3.8A on page 59.

The ^{119}Sn resonances at $\delta(^{119}Sn)$ = -193.8 ppm, Figure 3.8A, are split into a doublet due to $^{1}J(^{103}Rh\text{-}^{119}Sn)$ = 590 Hz (a), and is flanked by two sets of $^{2}J(^{117/119}Sn\text{-}^{119}Sn)$ satellites‡ with coupling constants of 2140 Hz (b) and 2240 Hz (c), respectively. The former are 'symmetrically' arranged about the main resonance signal, whereas the latter is asymmetrically arranged about the main signal. The $^{1}J(^{103}Rh\text{-}^{119}Sn)$ measured for the asymmetrical $^{2}J(^{117/119}Sn\text{-}^{119}Sn)$ satellites, indicated by symbol ('a') = 590 Hz, in Figure 3.8A, are equal to that measured for the main signal, (a) = 590 Hz, which confirms

‡ $^{2}J(^{117/119}Sn\text{-}^{119}Sn)$ is a general formula that is used when it is not yet clear whether it is $^{2}J(^{117}Sn\text{-}^{119}Sn)$ or $^{2}J(^{119}Sn\text{-}^{119}Sn)$ satellites that are being discussed. The specific notation will be used once assignment has been confirmed.

that these are indeed satellites of the same complex anion and not merely another, overlapping minor separate complex.

The ^{119}Sn resonance at $\delta(^{119}Sn)$ = -275.1 ppm is split into a doublet due to $^{1}J(^{103}Rh\text{-}^{119}Sn)$ = 664 Hz (d), and is flanked by three sets of $^{2}J(^{117/119}Sn\text{-}^{119}Sn)$ satellites indicated by symbols (e), (f) and (g) in Figure 3.8A. Two of these sets of satellites, with coupling constants of 2143 Hz (e) and 2455 Hz (g), are symmetrically arranged about the main set of signals, whereas the third, with a coupling constant of 2243 Hz (f), is asymmetrically arranged about the main ^{119}Sn NMR resonance. The values of the $^{1}J(^{103}Rh\text{-}^{119}Sn)$ spin-coupling measured for the asymmetrical $^{2}J(^{117/119}Sn\text{-}^{119}Sn)$ satellites, ('d' = 664 Hz), are equal to that measured for the main signal, (d = 664 Hz), which confirms that these are indeed satellites of the same complex anion, or set of coupled spin systems in the same molecule.

Asymmetrical satellites such as these have previously been reported by Koch *et. al.*[8,9,98] for the kinetically inert hydride species, $[RhH(SnCl_3)_5]^{3-}$. Two different ^{119}Sn NMR signals were reported for the ^{119}Sn nuclei in the axial, $\delta(^{119}Sn)$ = 78.7 ppm, and equatorial, $\delta(^{119}Sn)$ = -14.1 ppm, positions as these occur in two different magnetic environments in the kinetically inert species. The asymmetric satellites observed were found to arise from second order effects due to $^{2}J(^{119}Sn\text{-}^{119}Sn)$ coupling from a $^{119}SnCl_3^-$ ligand in the axial position to a $^{119}SnCl_3^-$ ligand *cis* to it, in the equatorial position. The difference in the chemical shifts of the ^{119}Sn nuclei in the two respective positions is so small relative to the $^{2}J(^{119}Sn\text{-}^{119}Sn)_{cis,ax\text{-}eq}$ coupling that second order effects occur. Koch *et. al.* also reported the following trend in the respective coupling constants observed: $^{2}J(^{117}Sn\text{-}^{119}Sn)_{trans,eq\text{-}eq} > {}^{2}J(^{117}Sn\text{-}^{119}Sn)_{cis,eq\text{-}eq} > {}^{2}J(^{119}Sn\text{-}^{119}Sn)_{cis,ax\text{-}eq} > {}^{2}J(^{117}Sn\text{-}^{119}Sn)_{cis,ax\text{-}eq} > {}^{1}J(^{103}Rh\text{-}^{119}Sn)_{eq} > {}^{2}J(^{1}H\text{-}^{119}Sn)_{cis,ax\text{-}eq}$.

Therefore, assuming that this complex anion $[Rh^{III}(SnCl_3)_4Cl_2]^{3-}$ is kinetically inert, not undergoing rapid exchange between axial and equatorial $SnCl_3^-$ ligands, the spectrum can be understood as follows. The ^{119}Sn resonance signals at -275.1 ppm and -193.8 ppm either belong to two separate isomers of similar structure or one species in which the $^{119}SnCl_3^-$ ligands are coordinated to a Rh(III) center in magnetically different positions of a kinetically inert complex. The two possible isomers to consider are the *cis*- and *trans*-$[Rh(SnCl_3)_4Cl_2]^{3-}$ anions, illustrated in Scheme 3.4(a) and (b), respectively. For the *trans*-$[Rh^{III}(SnCl_3)_4Cl_2]^{3-}$ complex, Scheme 3.4(b), all the ^{119}Sn nuclei are magnetically equivalent and thus would be

expected to result in one set of ^{119}Sn NMR signals with no asymmetric $^{2}J(^{117/119}Sn\text{-}^{119}Sn)$ satellites.

On the other hand, for the *cis*-$[Rh^{III}(SnCl_3)_4Cl_2]^{3-}$ species, (a), the ^{119}Sn nucleus can either be *cis* to a chlorido-ligand or *trans* to a chlorido-ligand, giving rise to two magnetically non-equivalent ^{119}Sn nuclei with different chemical shifts, should the species be kinetically inert.

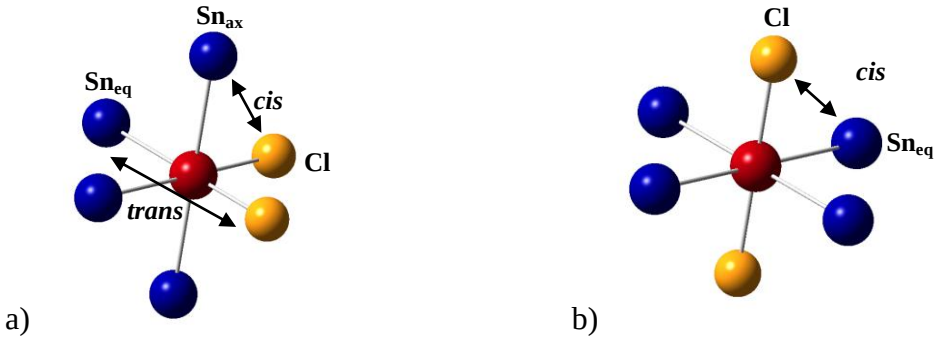

Scheme 3.4 A schematic representation of a) the *cis*- isomer and b) the *trans*-isomer of the $[Rh(SnCl_3)_4Cl_2]^{3-}$ complex anion. All coordinated chlorido ligands of $SnCl_3^-$ are left out for clarity.

Moreover, for the *cis*-isomer (a), the ^{119}Sn nucleus has a 50/50 chance of either being in the axial or equatorial position, which agrees well with the 1:1 ratio experimentally obtained upon integration of the sets of signals at $\delta(^{119}Sn)$ = -275.1 and 193.8 ppm. Therefore, it is reasonable to suggest that these two sets of ^{119}Sn resonances are due to a $^{119}SnCl_3^-$ ligand being either in the equatorial (*trans* to Cl^-) or the axial position *trans* to another $SnCl_3^-$ of the *cis*-$[Rh(SnCl_3)_4Cl_2]^{3-}$ isomer, and they are not magnetically equivalent resulting in non-first order coupling, Scheme 3.5a and b. To establish which is which requires the consideration of all the possible *isotopologues* of magnetically active $^{117/119}$Sn nuclei.

First consider the ^{119}Sn nucleus in equatorial position, Scheme 3.5a. The ^{119}Sn resonance signal is expected to be split into a doublet due to coupling to ^{103}Rh (natural abundance = 100%, I = ½), $^{1}J(^{103}Rh\text{-}^{119}Sn)$. Coupling of the ^{119}Sn nucleus in the equatorial position to ^{117}Sn (natural abundance = 7.61 %, I = ½) will result in two sets of doublets of doublet satellites for the $[^{103}Rh(^{119}SnCl_3)_x(^{117}SnCl_3)_y(SnCl_3)_zCl_2]$ (x + y + z = 4) *isotopologues* which arise as follows: 1) *cis* $^{2}J(^{117}Sn\text{-}^{119}Sn)$ coupling to ^{117}Sn in the equatorial position and 2) *cis* $^{2}J(^{117}Sn\text{-}^{119}Sn)$ coupling to ^{117}Sn in the axial position. Moreover, in the case of kinetically

inert complex anions, the equatorial and axial ^{119}Sn ligands will *not* be magnetically equivalent, and thus result in a third set of satellites due to $^{2}J(^{119}Sn\text{-}^{119}Sn)_{cis,eq\text{-}ax}$ spin-coupling. This splitting pattern corresponds well to that observed for the set of ^{119}Sn NMR signals at -275.1 ppm seen in the experimental spectrum of Figure 3.8A.

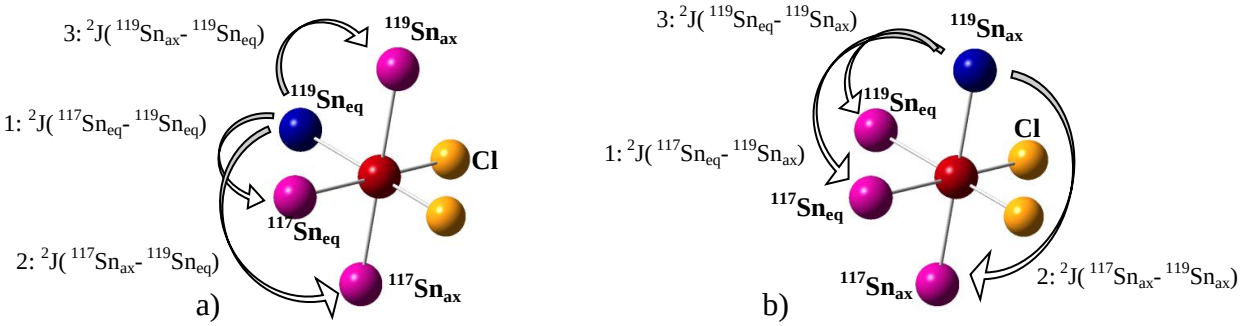

Scheme 3.5 A schematic representation of the *cis*-$[Rh(SnCl_3)_4Cl_2]^{3-}$ complex anion where the ^{119}Sn nucleus is a) in the equatorial and b) in the axial position. All coordinated chlorido ligands of $SnCl_3^-$ are left out for clarity.

Now consider the ^{119}Sn nucleus in the the axial position, Scheme 3.5b. The ^{119}Sn resonance signal is expected to be split into a doublet due to $^{1}J(^{103}Rh\text{-}^{119}Sn)$ coupling, with coupling to ^{117}Sn resulting in *two sets* of doublet of doublet satellites for the $[^{103}Rh(^{119}SnCl_3)_x(^{117}SnCl_3)_y(SnCl_3)_zCl_2]$ (x + y + z = 4) *isotopologues*: 1) $^{2}J(^{117}Sn\text{-}^{119}Sn)_{cis,eq\text{-}ax}$ and 2) $^{2}J(^{117}Sn\text{-}^{119}Sn)_{trans,ax\text{-}ax}$. Again one may also expect to see $^{2}J(^{119}Sn\text{-}^{119}Sn)_{cis,ax\text{-}eq}$ coupling that would result in a third set of doublet of doublet satellites. This splitting pattern corresponds well to that observed for the set of ^{119}Sn NMR signals at -193.8 ppm.

From this, the two sets of ^{119}Sn resonance signals at -193.8 and -275.1 ppm can tentatively be assigned to the axial and equatorial *isotopomers* of *cis*-$Rh(SnCl_3)_4Cl_2]^{3-}$, respectively. The axial ^{119}Sn resonance signal at -193.8 ppm, with $^{1}J(^{103}Rh\text{-}^{119}Sn)$ = 590.0 Hz, is flanked by one set of symmetrical $^{2}J(^{117}Sn\text{-}^{119}Sn)_{cis,eq\text{-}ax}$ satellites, 2240 Hz, and one set of asymmetrical satellites, 2240 Hz, tentatively ascribed to $^{2}J(^{119}Sn\text{-}^{119}Sn)_{cis,eq\text{-}ax}$ coupling.

The magnitude of the coupling of the measured $^{2}J(^{119}Sn\text{-}^{119}Sn)_{cis,eq\text{-}ax}$ satellites should conform to the expected $^{2}J(^{117}Sn\text{-}^{119}Sn)_{cis,eq\text{-}ax}$ values, estimated from the equation below where γ refers to the gyromagnetic ratios of $\gamma(^{119}Sn)$ and $\gamma(^{117}Sn)$ (Table 3.1):

$$\frac{^2J(^{119}Sn - ^{119}Sn)_{cis,ax-eq}}{^2J(^{117}Sn - ^{119}Sn)_{cis,ax-eq}} = \frac{\gamma(^{119}Sn)}{\gamma(^{117}Sn)}$$

$$^2J(^{119}Sn - ^{119}Sn)_{cis,ax-eq} = 1.047 \text{ x } 2139.9 = 2239.5 \text{ Hz}$$

This calculated value of 2239.5 Hz and the experimental $^2J(^{117}Sn\text{-}^{119}Sn)$ value of 2240 Hz are in excellent agreement, supporting the assignment of these asymmetric satellites to $^2J(^{117}Sn\text{-}^{119}Sn)_{cis,eq\text{-}ax}$ coupling in the respective *isotopologues*. However, it was mentioned earlier that one would expect to see $^2J(^{117}Sn\text{-}^{119}Sn)_{trans,ax\text{-}ax}$ satellites, yet none is observed. This may be due to the $^2J(^{117}Sn\text{-}^{119}Sn)_{trans,ax\text{-}ax}$ satellites being too low in intensity to be observed in the experimental ^{119}Sn NMR signal as a very low signal to noise ratio was obtained.

The tentatively assigned equatorial ^{119}Sn resonance signal at -275.1 ppm, with $^1J(^{103}Rh\text{-}^{119}Sn)$ = 664.1 Hz, flanked by two sets of symmetrical satellites, $^2J(^{117}Sn\text{-}^{119}Sn)_{cis,eq\text{-}eq}$,= 2455.0 Hz and $^2J(^{117}Sn\text{-}^{119}Sn)_{cis,ax\text{-}eq}$,= 2143.0 Hz, and one set of asymmetrical $^2J(^{119}Sn\text{-}^{119}Sn)_{cis,eq\text{-}ax}$ satellites of 2243.1 Hz. Using a similar approach as above with $\gamma(^{119}Sn)$ and $\gamma(^{117}Sn)$, the calculated value of $^2J(^{119}Sn\text{-}^{119}Sn)_{cis,eq\text{-}ax}$ coupling of 2242.8 Hz agrees well with the measured coupling for the asymmetrical satellites, 2243 Hz.

From the results obtained two conclusions can be drawn: 1) ^2J spin-coupling between ^{117}Sn and ^{119}Sn nuclei is always 1st order, in other words such *isotopologues* follow ideal Pascal rules, but 2) for ^2J coupling between two ^{119}Sn nuclei that are not magnetically equivalent second order effects as was described come into play. First order analysis of NMR spectra[79] is usually considered applicable when $(\nu_A - \nu_B)/J_{AB} > 7$. In this case, the frequency separation between the two sets of ^{119}Sn NMR signal, axial and equatorial ^{119}Sn, is measured to be 18 149.8 Hz. Thus, using the equation mentioned:

$$\frac{\nu_A - \nu_B}{J_{AB}} = \frac{61498.9 - 43349.1}{2239.5} = 8.1$$

Although this value is slightly greater than 7, a ratio between 7 and 20 implies that second order distortions may be expected. Therefore, it is to be expected that the ^{119}Sn NMR spectrum of species simultaneously containing ^{119}Sn nuclei in both the axial and equatorial

positions will show some degree of form of second order distortion. Moreover, the 'roofing' effect as to which was eluded to earlier, is consistent with second order trends in which signal intensities increase towards the midpoint between axial and equatorial resonances.

In order to finally validate these assignments simulation programme, gNMR50, was used to simulate the ^{119}Sn NMR spectra of the axial and equatorial *cis*-$[Rh(SnCl_3)_4Cl_2]^{3-}$ species. The chemical shift and coupling values obtained from the experimental ^{119}Sn NMR spectrum, Table 3.3 were used as input to simulate the ^{119}Sn NMR spectrum shown in Figure 3.8B.

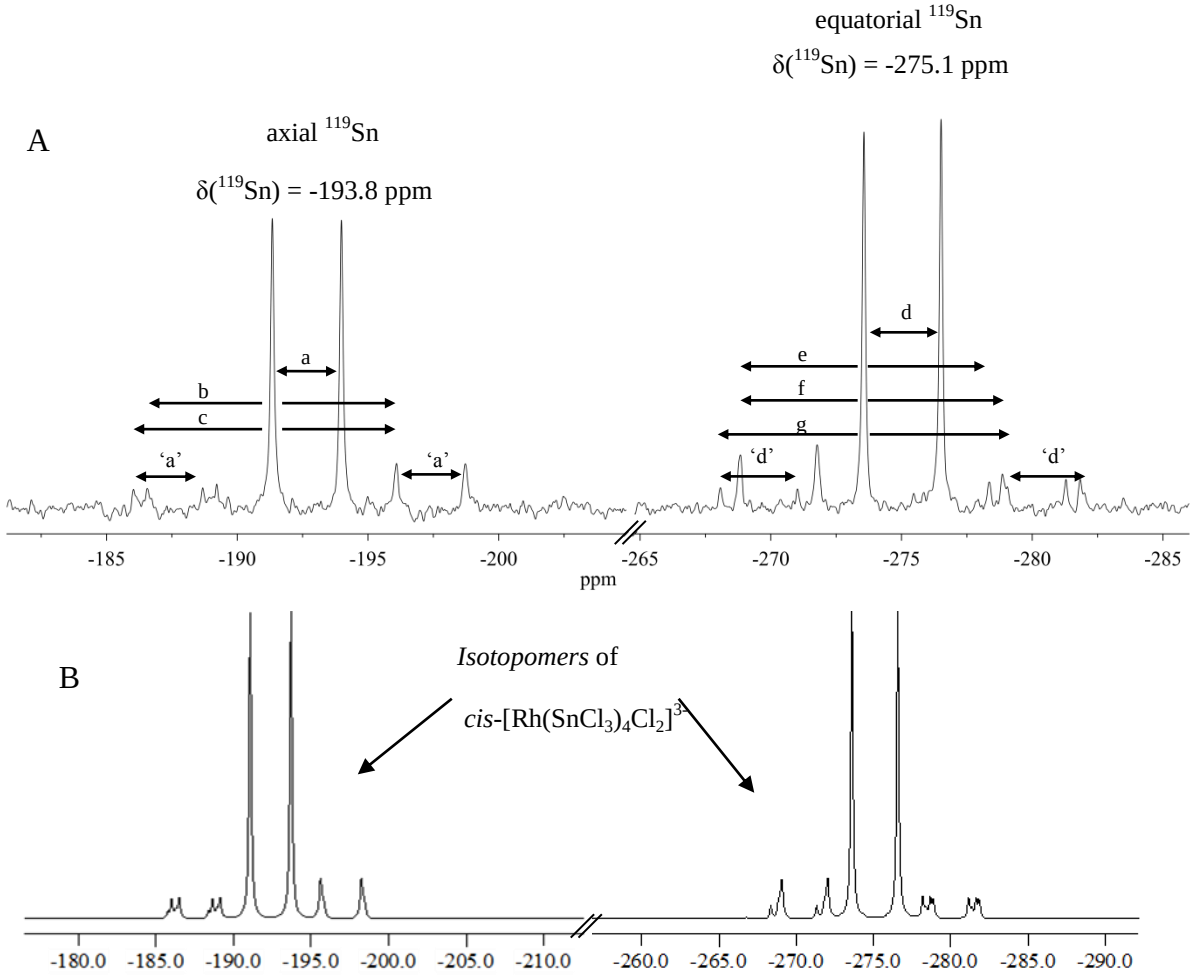

Figure 3.8 An expansion of Section B in Figure 3.6 is given in Spectrum A and focuses on the signals at δ(^{119}Sn) = -193.8 and -275.1 ppm. Symbols 'a' and 'd' indicate ^{1}J(^{103}Rh-^{119}Sn) coupling in both species and symbols 'b-c' and 'e-g' indicate respective ^{2}J(Sn-Sn) satellites that are discussed in detail in text. Computer simulated ^{119}Sn NMR spectrum of the axial and equatorial $SnCl_3^-$ resonances of the *cis*-$[Rh(SnCl_3)_4Cl_2]^{3-}$ species. In Spectrum B the ^{119}Sn NMR spectrum simulated with gNMR50 and using the NMR parameters measured in Spectrum A is given.

The simulated ^{119}Sn NMR spectrum, Figure 3.8B, is virtually identical to the experimental spectrum with similar asymmetrical $^{2}J(^{119}Sn\text{-}^{119}Sn)_{cis,ax\text{-}eq}$ (2240 Hz) satellites, thus confirming the proposed assignment of the ^{119}Sn NMR signals at -275.1 ppm and -193.8 ppm to the equatorial and axial *isotopomers* of a simple complex anion *cis*-$Rh(SnCl_3)_4Cl_2]^{3-}$ as shown below in Scheme 3.6. The NMR parameters of the respective *isotopologues* and *isotopomers* observed in the experimental ^{119}Sn NMR spectrum of this complex anion are listed in Table 3.3.

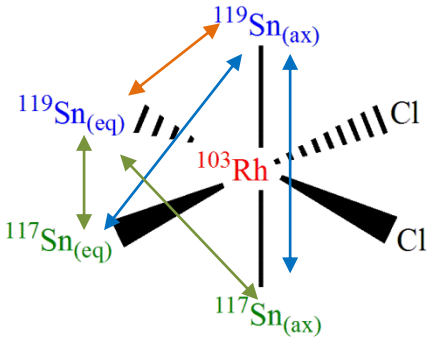

.

$\delta(^{119}Sn_{ax})$ = -193.8 ppm

$\delta(^{119}Sn_{eq})$ = -275.1 ppm

$^{2}J(^{117}Sn_{(eq)}\text{-}^{119}Sn_{(eq)})_{(cis)}$ = 2455 Hz

$^{2}J(^{119}Sn_{(ax)}\text{-}^{119}Sn_{(eq)})_{(cis)}$ = 2240 Hz

$^{2}J(^{117}Sn_{(ax)}\text{-}^{119}Sn_{(eq)})_{(cis)}$ = 2143 Hz

$^{2}J(^{117}Sn_{(eq)}\text{-}^{119}Sn_{(ax)})_{(cis)}$ = 2140 Hz

$^{2}J(^{117}Sn_{(ax)}\text{-}^{119}Sn_{(ax)})_{(trans)}$ = ?

Scheme 3.6 Schematic representation of the *cis*-$[Rh(SnCl_3)_4Cl_2]^{3-}$ complex that shows all the various $^{2}J(^{117}Sn\text{-}^{119}Sn)$ and $^{2}J(^{119}Sn\text{-}^{119}Sn)$ couplings experimentally observed for the respective *isotopomers* and *isotopologues* possible for this complex. All coordinated chlorido ligands of $SnCl_3^-$ are left out for clarity.

Table 3.3 ^{119}Sn NMR parameters of the *isotopologues* observed for the equatorial and axial *isotopomers* of the *cis*-$[Rh(SnCl_3)_4Cl_2]^{3-}$ species.

Rh-Sn *isotopologue*	**$\delta(^{119}Sn)$ /ppm**	**$^{1}J(^{103}Rh\text{-}^{119}Sn)$ /Hz**	**$^{2}J(^{117}Sn\text{-}^{119}Sn)$ /Hz**
Isotopomer: Observed $^{119}SnCl_3^-$ ligand in the equatorial position, *trans* to Cl^-			
$[^{103}Rh(^{i}SnCl_3)_3(^{119}SnCl_3)Cl_2]^{3-}$	$-275.1_{(eq)}$	$664_{(eq)}$	- $^{2}J(^{119}Sn\text{-}^{119}Sn)_{(cis,eq\text{-}ax)}$ = 2240
$[^{103}Rh(^{i}SnCl_3)_2(^{119}SnCl_3)_2Cl_2]^{3-}$	$-275.1_{(eq)}$	$664_{(eq)}$	
$[^{103}Rh(^{i}SnCl_3)_2(^{119}SnCl_3)(^{117}SnCl_3)Cl_2]^{3-}$	$-275.1_{(eq)}$	$664_{(eq)}$	$2455_{(cis,eq\text{-}eq)}$ $2143_{(cis,ax\text{-}eq)}$
Isotopomer: Observed $^{119}SnCl_3^-$ ligand in the axial position, *trans* to $SnCl_3^-$			
$[^{103}Rh(^{i}SnCl_3)_3(^{119}SnCl_3)Cl_2]^{3-}$	$-193.8_{(ax)}$	$589_{(ax)}$	- $^{2}J(^{119}Sn\text{-}^{119}Sn)_{(cis,eq\text{-}ax)}$ = 2240
$[^{103}Rh(^{i}SnCl_3)_2(^{119}SnCl_3)_2Cl_2]^{3-}$	$-193.8_{(ax)}$	$589_{(ax)}$	
$[^{103}Rh(^{i}SnCl_3)_2(^{119}SnCl_3)(^{117}SnCl_3)Cl_2]^{3-}$	$-193.8_{(ax)}$	$589_{(ax)}$	$2140_{(cis,eq\text{-}ax)}$ $?_{(trans,ax\text{-}ax)}$

It is thus evident that, contrary to the tacitly accepted *stereo-chemically non-rigid* nature of these Rh(III)-Sn(II) species,[33,39,41] all and in particular the *cis*-$[Rh(SnCl_3)_4Cl_2]^{3-}$ species do not undergo rapid *inter*- and *intra*-molecular exchange of the $SnCl_3^-$ ligands, but is kinetically inert with the consequence that the ^{119}Sn nucleus in the *axial* position is not magnetically equivalent to ^{119}Sn in the *equatorial* position. Thus, assignments made by Moriyama *et. al.*[41] are shown to be incorrect and the peaks at -193.8 and -275.1 ppm are due to the *cis*-$[Rh(SnCl_3)_4Cl_2]^{3-}$ complex anion.

3.2.1.3.3 Section C: Spectral zone comprising of δ(^{119}Sn) = -145.1 and -102.3 ppm

Figure 3.9 shows similar asymmetrical sets of ^{2}J($^{117/119}$Sn-^{119}Sn) satellites for the δ(^{119}Sn) peaks at -145.1 and -102.3 ppm, as observed for the *cis*-$[Rh(SnCl_3)_4Cl_2]^{3-}$ species described above. The set of ^{119}Sn NMR signals at -102.3 ppm have previously been assigned to a presumed kinetically labile $[Rh(SnCl_3)_5Cl]^{3-}$ complex anion,[41] whereas the resonance signals at -145.1 ppm was not assigned.

The same methodology used above was applied to elucidate the ^{119}Sn NMR signals in Section C of Figure 3.6, the expansion of which is given below in Figure 3.9A.

A) Experimental ^{119}Sn NMR of signals at δ(^{119}Sn) = -102.3 and -145.1 ppm

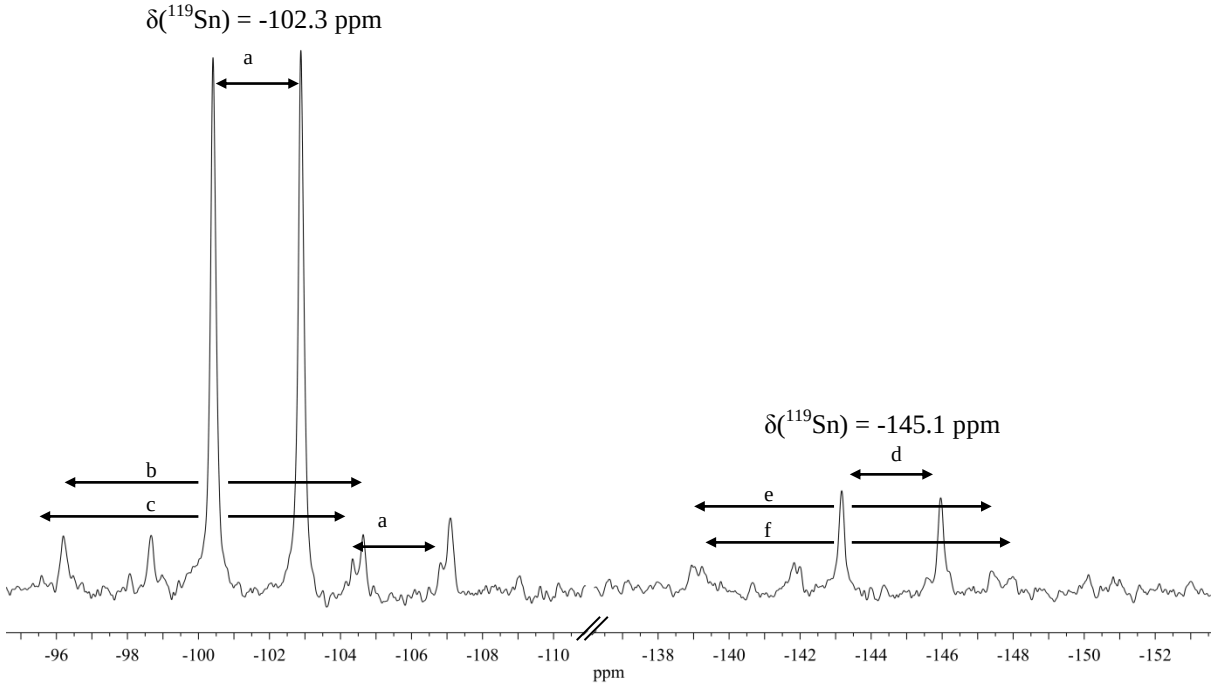

B) Simulated ^{119}Sn NMR for $[Rh(SnCl_3)_5Cl]^{3-}$

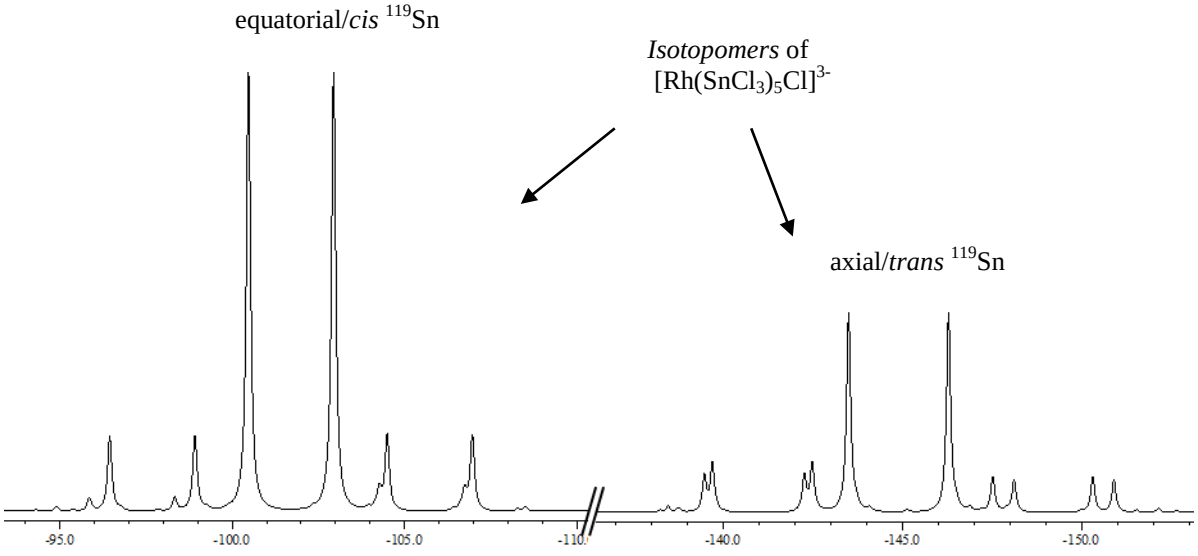

Figure 3.9 Enlargement of Section C in Figure 3.6 is shown in A and focuses on the signals at δ(^{119}Sn) = -102.3 and -145.1 ppm. Symbols 'a' and 'd' indicate ^{1}J(^{103}Rh-^{119}Sn) coupling in both species and symbols 'b-c' and 'e-f' indicate respective ^{2}J(Sn-Sn) satellites discussed in detail in text. The simulated ^{119}Sn NMR spectrum obtained for the $[Rh(SnCl_3)_5Cl]^{3-}$ species, using gNMR50 is given in B**.** The experimentally measured δ(^{119}Sn), ^{1}J(^{103}Rh-^{119}Sn) and ^{2}J(Sn-Sn) were used to simulate the spectrum.

The ^{119}Sn resonance signals at -102.3 and 145.1 ppm, Figure 3.9A, are split into doublets with coupling constants of 555 Hz (a) and 620 Hz (d), respectively, due to coupling of ^{119}Sn to ^{103}Rh (natural abundance = 100%, I = ½). Each main signal is flanked by a symmetrical set

of satellites with $^{2}J(Sn\text{-}Sn)$ = 1882 Hz, indicated by symbols 'b' and 'e' in Figure 3.9A, and one set of satellites with $^{2}J(^{117/119}Sn\text{-}^{119}Sn)$ = 1963 Hz indicated by symbols 'c' and 'f', asymmetrically distributed around the main signals. The signal:satellite ratio for the set of signals at -102.3 ppm was measured to be 1:0.30 which agrees well with the natural statistical abundance (32.6 %) calculated for the $[Rh(SnCl_3)_5Cl]^{3-}$ species using Equation 3.1. Unfortunately, with the poor S/N ratio, it was not possible to accurately measure the areas of the ^{119}Sn NMR satellite signals observed for the species at -145.1 ppm. Integration of the respective sets of signals at -102.3 and -145.1 ppm in Figure 3.9A shows an area ratio of 4:1.

As the ^{119}Sn NMR resonance at -102.3 ppm is assigned to the $[Rh(SnCl_3)_5Cl]^{3-}$ complex anion, it is reasonable to suggest that, similar to the $[Rh(SnCl_3)_4Cl_2]^{3-}$ species, the two sets of resonances in Figure 3.9A are observed due to two *isotopomers* of this species where the $SnCl_3^-$-ligand is either in the axial position (*trans* to the chlorido ligand) or in the equatorial position (*cis* to a chlorido ligand) as is shown in Scheme 3. 7a and b, respectively.

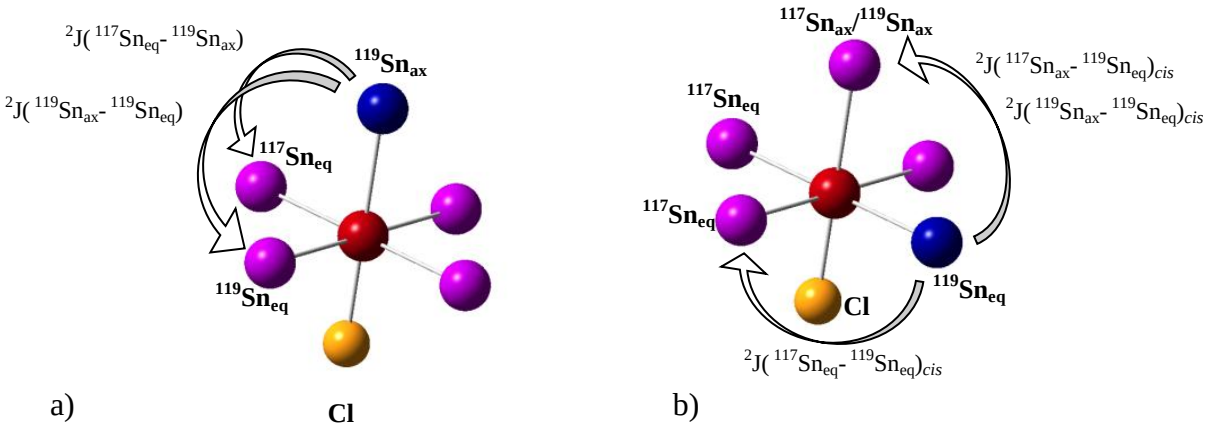

Scheme 3. 7 A schematic representation of two *isotopomers* of the $Rh(SnCl_3)_5Cl]^{3-}$ complex anion, as well as its possible ^{2}J scalar couplings, where the observed $^{119}SnCl_3^-$ ligand is a) in the axial (*trans* to Cl^-) and b) in the equatorial (*cis* to Cl^-) position. In (a) the $^{119}Sn_{ax}$ ligand (blue) can scalar couple to either a $^{117}Sn_{eq}$ ligand, $^{2}J(^{117}Sn_{eq}\text{-}^{119}Sn_{ax})$, or to a $^{119}Sn_{eq}$ ligand, $^{2}J(^{119}Sn_{eq}\text{-}^{119}Sn_{ax})$. In (b) the $^{119}Sn_{eq}$ ligand (blue) can scalar couple to either a $^{117}Sn_{ax}$ or a $^{119}Sn_{ax}$ ligand, $^{2}J(^{117}Sn_{ax}\text{-}^{119}Sn_{eq})$ and $^{2}J(^{119}Sn_{ax}\text{-}^{119}Sn_{eq}$, or to a $^{117}Sn_{eq}$ ligand, $^{2}J(^{117}Sn_{eq}\text{-}^{119}Sn_{eq})$. All coordinated chlorido ligands of $SnCl_3^-$ are left out for clarity.

.

The ^{119}Sn nucleus has a 1 in 5 chance of being *trans* to the chlorido ligand (axial) compared to it having a 4 in 5 chance of being *cis* to the chlorido ligand (equatorial). This agrees well with the 4 to 1 ratio obtained by integrating the respective sets of signals at -102.3 and -145.1 ppm in Figure 3.9A. It is thus reasonable to suggest that the set of resonances at -102.3 and -

145.1 ppm can be assigned to the axial and equatorial *isotopomers* of the $[Rh(SnCl_3)_5Cl]^{3-}$ species, respectively, in which the ^{119}Sn nuclei in the respective positions are not magnetically equivalent. The $^{2}J(Sn\text{-}Sn)$ spin-couplings observed for respective *isotopologues* are illustrated in Scheme 3. 7. Using the equation on page 58 the $^{2}J(^{119}Sn\text{-}^{119}Sn)_{cis,ax\text{-}eq}$ coupling constant is calculated to have a magnitude of 1968.5 Hz, which compares well with the experimentally measured 1963 Hz. Also, a value of 4.2 (lower than 7) was obtained with Equation 3.3, which indicates that second order coupling distortions are probable and therefore explains the asymmetrical distribution of these satellites. Moreover, the simulated ^{119}Sn NMR spectrum obtained for these species, using gNMR50, is shown in Figure 3.9B (intensity ratios not to scale). The excellent agreement between the simulated ^{119}Sn NMR spectrum, Figure 3.9B, and the experimental ^{119}Sn NMR spectrum, Figure 3.9A, along with all the other abovementioned evidence, allows for the unambiguous assignment of the resonance signals at -102.3 and -145.1 ppm to the equatorial (^{119}Sn *cis* to Cl^-) and axial (^{119}Sn *trans* to Cl^-) *isotopomers* of the $[Rh(SnCl_3)_5Cl]^{3-}$ complex anion. The detailed NMR parameters of this species and its *isotopologues* are shown in Table 3.4.

Table 3.4 ^{119}Sn NMR parameters of the *isotopologues* observed for the equatorial and axial *isotopomers* of the $[Rh(SnCl_3)_5Cl]^{3-}$ complex.

Rh-Sn isotopologue	**$\delta(^{119}Sn)$ /ppm**	**$^{1}J(^{103}Rh\text{-}^{119}Sn)$ /Hz**	**$^{2}J(^{117}Sn\text{-}^{119}Sn)$ /Hz**
Isotopomer: Observed $^{119}SnCl_3^-$ ligand in the equatorial position, *trans* to $SnCl_3^-$			
$[^{103}Rh(^{i}SnCl_3)_4(^{119}SnCl_3)Cl]^{3-}$	$-102.3_{(eq)}$	$555_{(eq)}$	-
$[^{103}Rh(^{i}SnCl_3)_3(^{119}SnCl_3)_2Cl]^{3-}$	$-102.3_{(eq)}$	$555_{(eq)}$	$^{2}J(^{119}Sn\text{-}^{119}Sn)_{(cis,ax\text{-}eq)} = 1962$
$[^{103}Rh(^{i}SnCl_3)_3(^{119}SnCl_3)(^{117}SnCl_3)Cl]^{3-}$	$-102.3_{(eq)}$	$555_{(eq)}$	$1883_{(cis,ax\text{-}eq)}$
Isotopomer: Observed $^{119}SnCl_3^-$ ligand in the axial position, *trans* to Cl^-			
$[^{103}Rh(^{i}SnCl_3)_4(^{119}SnCl_3)Cl]^{3-}$	$-145.1_{(ax)}$	$620_{(ax)}$	-
$[^{103}Rh(^{i}SnCl_3)_3(^{119}SnCl_3)_2Cl]^{3-}$	$-145.1_{(ax)}$	$620_{(ax)}$	$^{2}J(^{119}Sn\text{-}^{119}Sn)_{(cis,eq\text{-}ax)} = 1963$
$[^{103}Rh(^{i}SnCl_3)_3(^{119}SnCl_3)(^{117}SnCl_3)Cl]^{3-}$	$-145.1_{(ax)}$	$620_{(ax)}$	$1883_{(cis,eq\text{-}ax)}$ $?_{(trans,eq\text{-}eq)}$

In summary, each set of ^{119}Sn NMR signals in Figure 3.6 has successfully been assigned to an *isotopomer* of a species in the series of $[Rh(SnCl_3)_nCl_{6-n}]^{3-}$ (n = 3 – 5) complex anions, including the two sets of signals at -275.1 and -145.1 ppm which have not been assigned in literature. From these assignments it is evident that these $[Rh^{III}(SnCl_3)_nCl_{6-n}]^{3-}$ (n = 1 – 5) complex anions are kinetically inert and do not undergo *inter*- or *intra*-molecular exchange

on the NMR time-scale, which is in contrast to what is reported in literature. Moreover, several *isotopologues* are characterized for each *isotopomer*. This is in contrast to what is reported in the literature. All the *isotopomers* and *isotopologues* of the series of $[Rh(SnCl_3)_nCl_{6-n}]^{3-}$ (n = 1 – 5) complexes assigned in the ^{119}Sn NMR spectra in Figure 3.6 are assigned and characterized for the first time as such an in depth analysis of the *isotopologues* and *isotopomers* of these Rh-Sn species have never been reported.

3.2.1.4 Speciation of the series $[Rh(SnCl_3)_nCl_{6-n}]^{3-}$ (n = 3 – 5) complex anions in 6 M $HClO_4$ (i.e. chloride ion deficient solution)

Illustrated in Equations 3.1.1 to 3.1.4 the Rh-Sn solutions made up in 6 M HCl contain large excess chloride ions that compete with the $SnCl_3^-$-moiety for coordination to the rhodium center. To determine how the coordination of chloride ions influence the speciation and the ^{119}Sn NMR spectra of the $[Rh(SnCl_3)_nCl_{6-n}]^{3-}$ species, a 0.5 M Rh solution with an effective Rh:Sn mole ratio of 1:5 was prepared in 6 M $HClO_4$. Enough LiCl was however added to the solution to ensure that the $SnCl_2$ is converted into the $SnCl_3^-$-moiety which is needed to bind to the rhodium center, with the final Rh:Sn:Cl mole ratio being 1:5:18. The ^{119}Sn NMR spectrum obtained for this solution is shown in Figure 3.10.

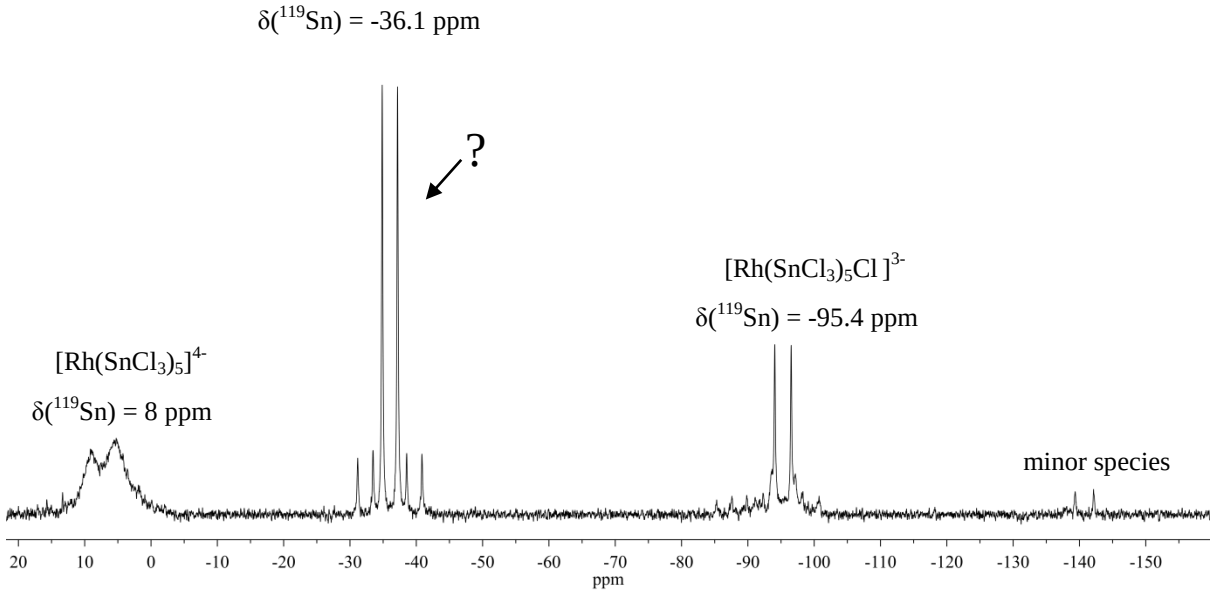

Figure 3.10 ^{119}Sn NMR spectrum acquired for a 0.5 M Rh solution with an effective Rh:Sn mole ratio of 1:5 in 6 M $HClO_4$ at 25 °C. Three main doublets are observed, each flanked by its respective satellites, and one minor species is observed.

The ^{119}Sn NMR spectrum of this solution in 6 M $HClO_4$ shows 3 main sets of peaks (doublets with satellites) which is indicative of several Rh-Sn complex anions. The broad unresolved doublet at 8 ppm is assigned to the $[Rh^{I}(SnCl_3)_5]^{4-}$ complex anion based on the chemical shift, as well as the $^{1}J(^{103}Rh\text{-}^{119}Sn)$ = ± 800 Hz, as discussed in Section 3.2.1.1 . The broadness of this set of signals is ascribed to the relatively slow *intra*- and *inter*-molecular ligand exchange on the NMR time-scale under these experimental conditions. Similarly, the ^{119}Sn NMR resonance signal at -95.4 ppm with $^{1}J(^{103}Rh\text{-}^{119}Sn)$ = 553 Hz is assigned to the *isotopomer* of the $[Rh(SnCl_3)_5Cl]^{3-}$ complex anion where ^{119}Sn nucleus is in the axial position, *trans* to the chlorido-ligand. However, the set of ^{119}Sn NMR resonance signals at -36.1 ppm, has never been reported in literature and require a more in depth discussion. To facilitate the elucidation of $\delta(^{119}Sn)$ = -36.1 ppm an enlargement thereof is shown in Figure 3.11.

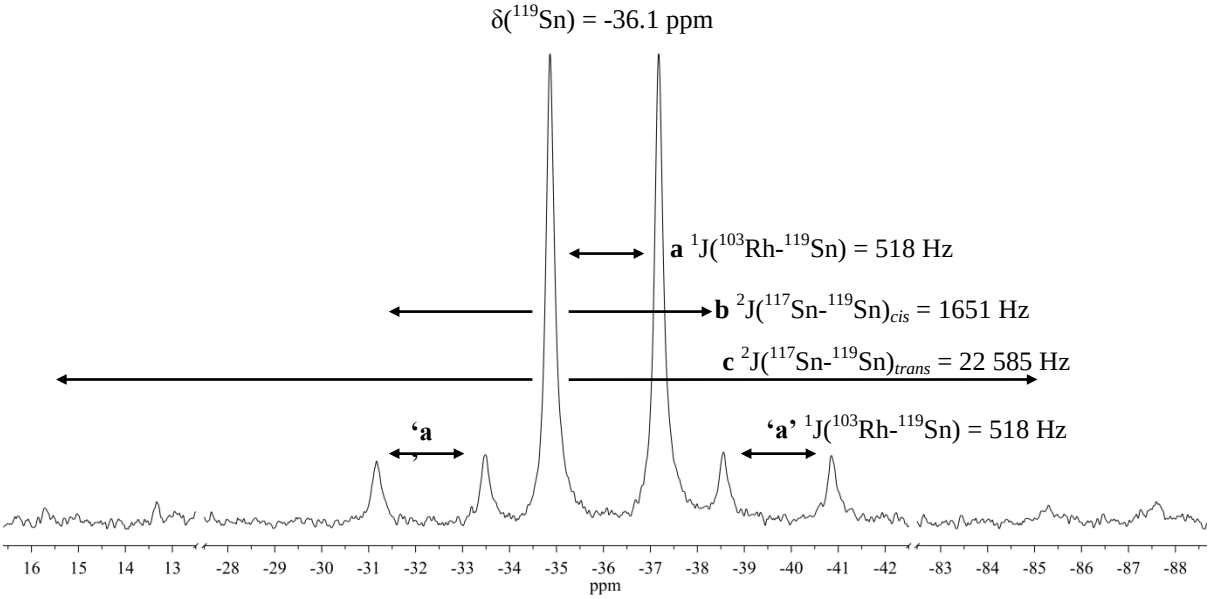

Figure 3.11 Expansion of the signals at $\delta(^{119}Sn)$ = -36.1 ppm. Symbol 'a' indicates $^{1}J(^{103}Rh\text{-}^{119}Sn)$ coupling, symbol 'b' $^{2}J(^{117}Sn\text{-}^{119}Sn)_{cis}$ and 'c' $^{2}J(^{117}Sn\text{-}^{119}Sn)_{trans}$ satellites.

The spectrum consists of a main signal and two types of satellite signals. The main signal is split into a doublet due to $^{1}J(^{103}Rh\text{-}^{119}Sn)$ coupling, indicated by the symbol **a** in Figure 3.11, with $^{1}J(^{103}Rh\text{-}^{119}Sn)$ = 518 Hz. The first set of $^{2}J(^{117}Sn\text{-}^{119}Sn)$ satellites with a doublet of doublet multiplicity has a coupling constant of 1651 Hz, **b** in Figure 3.11. Although the doublet of doublet signals, indicated by **c** in Figure 3.11, are very low in intensity, they are symmetrically distributed around the main doublet and the $^{1}J(^{103}Rh\text{-}^{119}Sn)$ measured for these signals are equal to that measured for the main doublet, 518 Hz. This confirms that these are indeed $^{2}J(^{117/119}Sn\text{-}^{119}Sn)$ satellites of the complex anion at $\delta(^{119}Sn)$ = -36.1 ppm with a

coupling constant of 22 585 Hz. When the $^{1}J(^{103}Rh\text{-}^{119}Sn)$ is plotted against the $\delta(^{119}Sn)$ = 36.1 ppm, Figure 3.12a, it is evident that this species conforms to the same trend that was observed for the series of $[Rh(SnCl_3)_nCl_{6-n}]^{3-}$ (n = 1 – 5) complex anions.

Plotting the coupling constant of the $^{2}J(^{117/119}Sn\text{-}^{119}Sn)$ satellites indicated by 'b' in Figure 3.11 against $\delta(^{119}Sn)$ = -36.1 ppm, shows that these satellites conform to the trend observed for the $^{2}J(^{117}Sn\text{-}^{119}Sn)_{cis}$ satellites of the series of $[Rh(SnCl_3)_nCl_{6-n}]^{3-}$ (n = 3 – 5), Figure 3.12b.

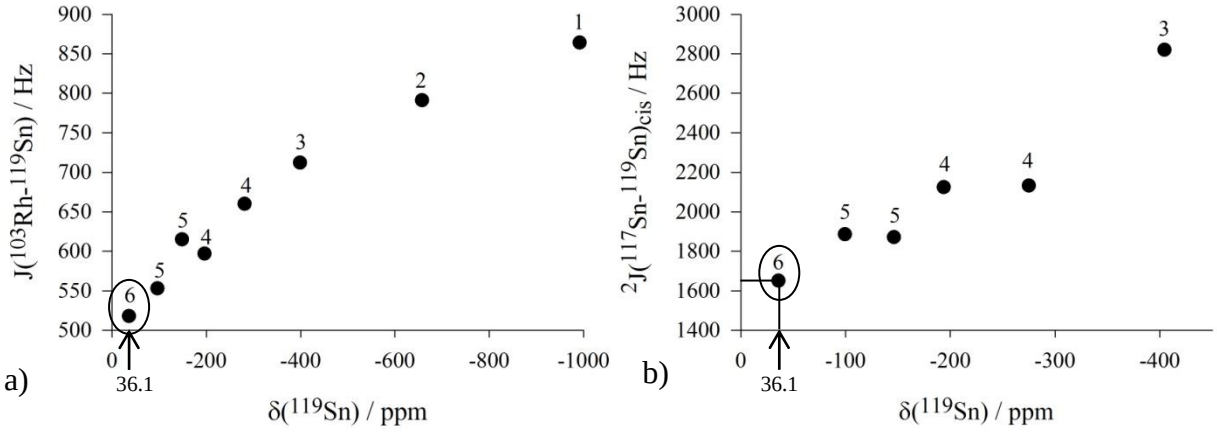

Figure 3.12 Plot of (a) $^{1}J(^{103}Rh\text{-}^{119}Sn)$ as a function of $\delta(^{119}Sn)$ and (b) $^{2}J(^{117}Sn\text{-}^{119}Sn)$ as a function of $\delta(^{119}Sn)$. The numeral values correspond to "n" in the series of $[Rh(SnCl_3)_nCl_{6-n}]^{3-}$ (n = 1 – 6) species.

Figure 3.12 suggests that the set of signals at $\delta(^{119}Sn)$ = 36.1 ppm arises from a species with six $SnCl_3^-$-ligands coordinated to the rhodium center. Although such a species has not been reported for either rhodium or platinum complexes, Saito *et. al*. has reported that a octahedral $[Ru^{II}(SnCl_3)_6]^{3-}$ complex anion was formed[100] in 3 M HCl solutions with a Ru:Sn ratio of 1:10.

The splitting pattern observed for the ^{119}Sn NMR spectrum of the rhodium-tin complex in Figure 3.11 is similar to the one reported for the $[Ru(SnCl_3)_6]^{3-}$ complex anion. It is therefore reasonable to suggest that an analogous Rh-Sn species, $[Rh(SnCl_3)_6]^{3-}$, can exist in solution. Thus the set of signals at $\delta(^{119}Sn)$ = 36.1 in Figure 3.9 are assigned to the six-coordinated Rh-Sn species that can be formulated as the isoelectronic $[Rh(SnCl_3)_6]^{3-}$ complex anion, illustrated in Scheme 3.8a. Two possible *isotopomers* of this species, one with $^{117}SnCl_3^-$ ligand *cis* to the $^{119}SnCl_3^-$ and the other with $^{117}SnCl_3^-$ ligand *trans* to $^{119}SnCl_3^-$ ligand, are illustrated in Scheme 3.8b and c.

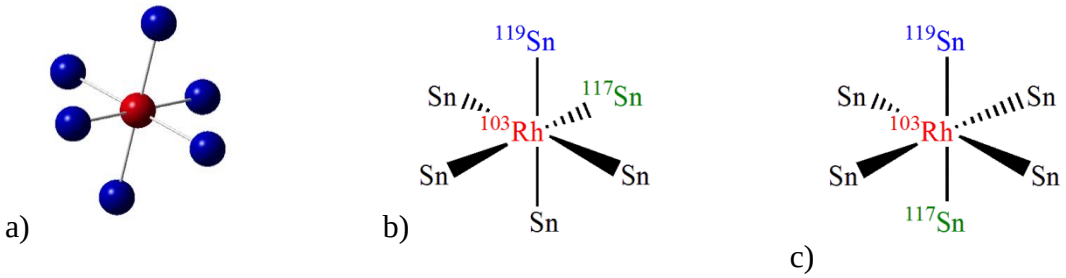

Scheme 3.8A schematic representation of a) the $Rh(SnCl_3)_6]^{3-}$ complex anion and its possible *isotopomers* where the ^{119}Sn nucleus is b) in the axial and c) in the equatorial position. All Cl^- ions are left out for clarity

Since all six $SnCl_3^-$ ligands in the octahedral $[Rh(SnCl_6)_6]^{3-}$ complex anion would be magnetically equivalent, only one set of ^{119}Sn NMR signals would be observed for this species, irrespective of the rigidity thereof. However, taking into consideration that it was just proven that the series of $[Rh(SnCl_3)_nCl_{6-n})]^{3-}$ (n = 1 – 3) complex anions are kinetically inert, it is reasonable to suggest the same for the $[Rh(SnCl_3)_6]^{3-}$ complex anion.

In Scheme 3.8b and c, two possible *isotopomers* of the $[Rh(SnCl_3)_6]^{3-}$ complex anion are illustrated. From these it is clear that coupling of the ^{119}Sn nucleus to ^{117}Sn (natural abundance = 7.61 %, I = ½) will result in two sets of doublet of doublet satellites: 1) $^2J(^{117}Sn\text{-}^{119}Sn)$ coupling to ^{117}Sn in the *cis* position (Scheme 3.8b) and 2) $^2J(^{117}Sn\text{-}^{119}Sn)$ coupling to ^{117}Sn in the *trans* position (Scheme 3.8c). This is consistent with the two types of $^2J(^{117}Sn\text{-}^{119}Sn)$ satellites observed for the species at $\delta(^{119}Sn)$ = 36.1 ppm that are indicated by ‘b’ and ‘c’ in Figure 3.11. From Figure 3.12b, the ^{119}Sn NMR signals indicated by ‘b’, with coupling constant of 1651 Hz, can be assigned to the $^2J(^{117}Sn\text{-}^{119}Sn)_{cis}$ satellites of the $[^{103}Rh(^{i}SnCl_3)_n(^{119}SnCl_3)_{5-n}(^{117}SnCl_3)]^{3-}$ (n = 0 – 4) isotopologue. The ^{119}Sn NMR signals indicated by ‘c’, with coupling constant of 22 585 Hz, are accordingly assigned to the $^2J(^{117}Sn\text{-}^{119}Sn)_{trans}$ satellites of the same isotopologue. The magnitude of these *trans*-satellites is expected to be about tenfold that of the *cis*-satellites.[14,19] Moreover, relative integration of the $^2J(^{117}Sn\text{-}^{119}Sn)_{cis/trans}$ satellites to the main set of ^{119}Sn NMR signals are measured to be 21 % which agrees well with the calculated NSA value, using Equation 3.1.5, of 22.4 %. Plotting the NSA of each of the $[Rh(SnCl_3)_nCl_{6-n}]^{3-}$ (n = 1 – 6) complex anions against the number of tin ligands bound to the rhodium results in a straight line, shown in Figure 3.13. It is thus suggested that the set of ^{119}Sn NMR resonance signals observed at -36.1 ppm should be assigned to the octahedral, kinetically inert $[Rh(SnCl_3)_6]^{3-}$ complex anion with 6 magnetically equivalent $SnCl_3^-$-ligands coordinated to Rh. Thus, the ^{119}Sn NMR resonance

signals observed at -36.0 ppm can unambiguously be assigned to the $[Rh(SnCl_3)_6]^{3-}$ complex anion, which has never been reported before.

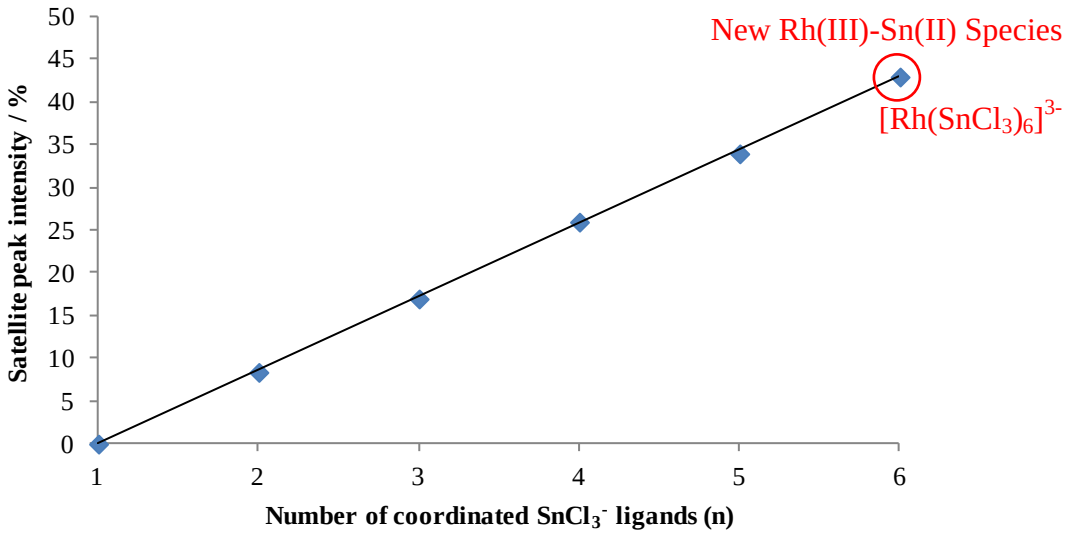

Figure 3.13 Plot of the NSA of each of the $[Rh(SnCl_3)_nCl_{6-n}]^{3-}$ (n = 1 – 6) complex anions against the number of tin ligands bound to the rhodium(III). $[Rh(SnCl_3)_6]^{3-}$ not previously reported.

In a recent study of the series of $[PtCl_{6-n}Br_n]^{3-}$ (n = 0 – 6) species, Koch and Kramer[101] reported that plotting the $\delta(^{195}Pt)$ against the 'n' of each species is a useful method to study the trend analysis of such species. Therefore, a similar approach was used for the Rh-Sn species and the resulting plot is given in Figure 3.14. As the number of coordinated $SnCl_3^-$-ligands in the series of $[Rh(SnCl_3)_nCl_{5-n}]^{3-}$ (n = 1 – 5) complex anions increase, the ^{119}Sn atom becomes less shielded indicated by the downfield shift of the ^{119}Sn NMR signals shown by the trend Figure 3.14. This is in agreement with what Moriyama *et. al.*[41] reported for these $[Rh(SnCl_3)_nCl_{6-n}]^{3-}$ (n = 1 – 5) species. Moreover, it is seen that two separate trends are obtained when plotting the number of tin-ligands coordinated to the central rhodium against the ^{119}Sn NMR chemical shift of that species; one where the $^{119}SnCl_3^-$-ligand is *trans* to the Cl^- ligand (indicated by the red trend in Figure 3.14) and the other where the $^{119}SnCl_3^-$-ligand is *cis* to a Cl^- ligand (shown by the blue trend if Figure 3.14). From the slopes of the two respective trends, it is evident that substitution of a Cl^- ligand by a $SnCl_3^-$ ligand *trans* to Cl^- results in a relatively greater shift of the $\delta(^{119}Sn)$ downfield as compared to substitution *cis* to a Cl^- ligand. This may be related to the *trans* influence of the $SnCl_3^-$ ligand.[58,59]

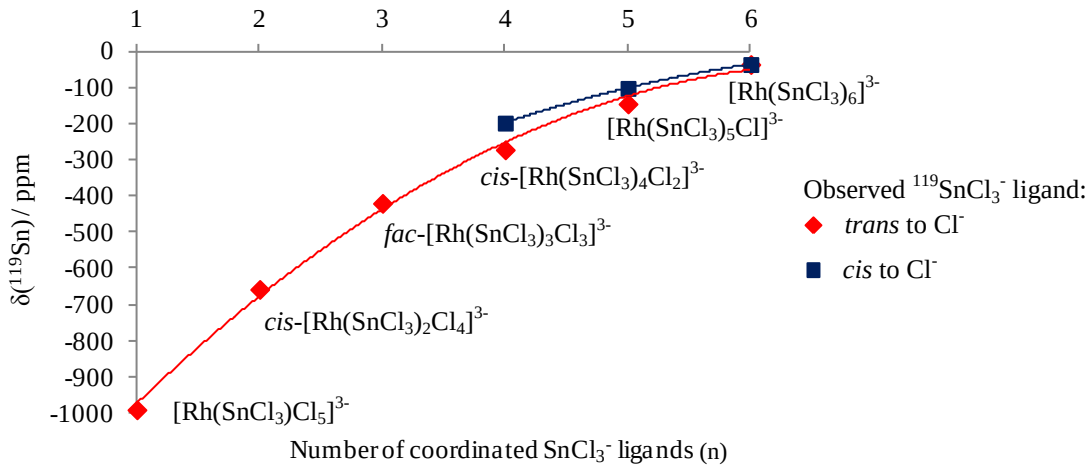

Figure 3.14 Plot of the $\delta(^{119}Sn)$ of the $[Rh(SnCl_3)_nCl_{5-n}]^{3-}$ (n = 1 – 6) complex anions as a function of the number of coordinated $SnCl_3^-$ ligands.

3.2.1.5 Conclusion

It is clear that previous assignments of these interesting, but deceptively simple $[Rh(SnCl_3)_nCl_{6-n}]^{3-}$ (n = 1 – 6) species were not complete. The reinvestigation of the stannous chloride complexes of rhodium(I/III) in acidic solution furnished the assignment of all 6 $[Rh(SnCl_3)_nCl_{6-n}]^{3-}$ (n = 1 – 6) species, listed in Table 3.5, as well as distinctive *isotopomer* pairs for the complex anions where n = 4 and 5. It is thus established that these species are kinetically inert and do not undergo rapid *intra*- or *inter*-molecular exchange on the NMR time-scale, as was previously proposed in literature.[41,98]

It is shown that individual sets of ^{119}Sn NMR resonance signals are observed for the respective *isotopomers* of the $[Rh^{III}(SnCl_3)_nCl_{6-n}]^{3-}$ (n = 3 – 5) species as shown in Table 3.3 and Table 3.4. Contrary to what is reported and assumed in the literature these Rh(III)-Sn(II) species is shown here not to undergo *inter*- or *intra*- molecular exchange on the NMR time scale, but to be kinetically inert. Moreover, each set of ^{119}Sn NMR signals observed in Figure 3.6, as well as its respective $^2J(^{119/117}Sn\text{-}^{119}Sn)$ satellites, has unambiguously been assigned to the respective *isotopologues* of the $[Rh(SnCl_3)_nCl_{6-n}]^{3-}$ (n = 1 – 6) complexes as listed in Table 3. 5.

Table 3. 5 ^{119}Sn NMR parameters of all the $[Rh(SnCl_3)_nCl_{6-n}]^{3-}$ (n = 1 – 6) species observed in acidic aqueous solutions and assignments of respective Rh-Sn *isotopologues*.

	Rigid Rh-Sn Complexes	δ(^{119}Sn)/ ppm	Rh-Sn isotopologue	$^1J(^{103}Rh-^{119}Sn)$/ Hz [c]	$^2J(^{117}Sn-^{119}Sn)$/ Hz
1[a]	$[Rh(SnCl_3)Cl_5]^{3-}$	-991.6	-	864	-
2[a]	*cis*-$[Rh(SnCl_3)_2Cl_4]^{3-}$ ($^{119}SnCl_3^-$ *trans* to Cl^-)	-657.5	-	791	-
3	*fac*-$[Rh(SnCl_3)_3Cl_3]^{3-}$ $^{119}SnCl_3^-$ *trans* to Cl^-	-411.3	$[^{103}Rh(^iSnCl_3)_2(^{119}SnCl_3)Cl_2]^{3-}$ $[^{103}Rh(^iSnCl_3)_1(^{119}SnCl_3)(^{117}SnCl_3)Cl_2]^{3-}$	716	[b] - $2817_{(cis)}$
4a	*cis*-$[Rh(SnCl_3)_4Cl_2]^{3-}$ equatorial ($^{119}SnCl_3^-$ *trans* to Cl^-)	-275.2	$[^{103}Rh(^iSnCl_3)_3(^{119}SnCl_3)Cl_2]^{3-}$ $[^{103}Rh(^iSnCl_3)_2(^{119}SnCl_3)_2Cl_2]^{3-}$ $[^{103}Rh(^iSnCl_3)_2(^{119}SnCl_3)(^{117}SnCl_3)Cl_2]^{3-}$	664	[b] - $^2J(^{119}Sn-^{119}Sn)_{(cis,eq-ax)} = 2240$ $2455_{(cis,eq-eq)}$ $2143_{(cis,ax-eq)}$
4b	***cis*-$[Rh(SnCl_3)_4Cl_2]^{3-}$ axial** ($^{119}SnCl_3^-$ *trans* to $SnCl_3^-$)	-202.5	$[^{103}Rh(^iSnCl_3)_3(^{119}SnCl_3)Cl_2]^{3-}$ $[^{103}Rh(^iSnCl_3)_2(^{119}SnCl_3)_2Cl_2]^{3-}$ $[^{103}Rh(^iSnCl_3)_2(^{119}SnCl_3)(^{117}SnCl_3)Cl_2]^{3-}$	589	-[b] $^2J(^{119}Sn-^{119}Sn)_{(cis,eq-ax)} = 2240$ $2140_{(cis,eq-ax)}$
5a	**$[Rh(SnCl_3)_5Cl]^{3-}$ axial ($^{119}SnCl_3^-$ *trans* to Cl^-)**	-146.2	$[^{103}Rh(^iSnCl_3)_4(^{119}SnCl_3)Cl]^{3-}$ $[^{103}Rh(^iSnCl_3)_3(^{119}SnCl_3)_2Cl]^{3-}$ $[^{103}Rh(^iSnCl_3)_3(^{119}SnCl_3)(^{117}SnCl_3)Cl]^{3-}$	627	-[b] $^2J(^{119}Sn-^{119}Sn)_{(cis,eq-ax)} = 1963$ $1883_{(cis,eq-ax)}$
5b	$[Rh(SnCl_3)_5Cl]^{3-}$ equatorial ($^{119}SnCl_3^-$ *cis* to Cl^-)	-98.3	$[^{103}Rh(^iSnCl_3)_4(^{119}SnCl_3)Cl]^{3-}$ $[^{103}Rh(^iSnCl_3)_3(^{119}SnCl_3)_2Cl]^{3-}$ $[^{103}Rh(^iSnCl_3)_3(^{119}SnCl_3)(^{117}SnCl_3)Cl]^{3-}$	555	[b] - $^2J(^{119}Sn-^{119}Sn)_{(cis,ax-eq)} = 1962$ $1883_{(cis,ax-eq)}$
6	**$[Rh(SnCl_3)_6]^{3-}$**	-36.1	$[^{103}Rh(^iSnCl_3)_5(^{119}SnCl_3)Cl]^{3-}$ $[^{103}Rh(^iSnCl_3)_4(^{119}SnCl_3)(^{117}SnCl_3)Cl]^{3-}$	518	[b] - 1650_{cis} $22\ 600_{trans}$
7	$[Rh(SnCl_3)_5]^{4-}$	9.4	$[^{103}Rh(^iSnCl_3)_n(^{119}SnCl_3)_{4-n}]^{4-}$ $[^{103}Rh(^iSnCl_3)_n(^{119}SnCl_3)_{3-n}(^{117}SnCl_3)Cl]^{3-}$	809	-[b] 3624

[a] The ^{119}Sn NMR parameters of these species are referenced from Moriyama *et. al.*[10] as these species were not observed in this work. Therefore no isotopologue assignments are given. [b] For these *isotopologues* there are no $^{117}SnCl_3^-$ to which ^{119}Sn can couple, thus not ^{2}J couplings are observed. [c] All *isotopologues* of respective species have the same $^1J(^{103}Rh-^{119}Sn)$ value.

Chapter IV

Speciation of stannous bromide complexes of rhodium(I/III) in acidic aqueous solutions with high-resolution ^{119}Sn NMR spectroscopy

Chapter IV

Speciation of stannous bromide complexes of rhodium(I/III) in acidic aqueous solutions with high-resolution ^{119}Sn NMR spectroscopy

4.1 Introduction

By contrast to the stannous chloride complexes of Rh(I/III), stannous bromide complexes of Rh(I/III) have received very little attention in the literature. In the 1960's Berman and co-workers[19,102] studied the spectrophotometric determination of rhodium with tin(II)bromide. It was reported that an intense yellow colour was obtained when rhodium salts were treated with solutions of tin(II)bromide in hydrobromic acid, however, the nature of the species responsible for the colour was unknown. Garralda *et. al*. studied the reaction of $[RhCl(NBD)]_2$ (NBD = norbordiene) with tertiary phosphine and tin(II) bromide using ^{119}Sn and ^{31}P NMR spectroscopy.[103] Based on the solution data obtained they suggested that halide scrambling occurs in the $SnCl_nBr_{3-n}$ ligand which resulted in scrambled 5-coordinate $[Rh(SnCl_nBr_{3-n})(norbornadiene)(tertiary\ phosphine)_2]$ complexes.[103] Moreover, the $^1J(^{103}Rh$-$^{119}Sn)$ coupling constants were found to vary from 452 to 580 Hz and were linearly related to the ^{119}Sn chemical shift of the $[Rh(SnCl_nBr_{3-n})(norbornadiene)(tertiary\ phosphine)_2]$ (n = 0 – 3) complex anions as well as the sum of the *Pauling* electronegativity for the halogens bonded to the tin nucleus.

Recently a detailed study of homoleptic $[Pt(SnX_3)_5]^{3-}$ as well as the series of heteroleptic $[Pt(Sn_5Cl_nBr_{15-n})]^{3-}$ (n = 0 – 15) species using high resolution ^{195}Pt and ^{119}Sn NMR spectroscopy,[58,59] showed that the $^1J(^{195}Pt$-$^{119}Sn)$ coupling constant was dependent on the configuration of the tin-halide ligands and decrease in the order $SnCl_3^- > SnCl_2Br^- > SnClBr_2^- > SnBr_3^-$. All possible *isotopologues* of these $[Pt(Sn_5Cl_nBr_{15-n})]^{3-}$ (n = 0 – 15) species could be resolved in detail using ^{195}Pt NMR if extracted into $CDCl_3$ with AQ336 as anion exchanger.

Furthermore, the nature of the Rh species responsible for the formation of the yellow solution as reported by Berman and co-workers[19,102] has not been yet been determined and no detailed study of the possible $[Rh^{III}(SnBr_3)_{6-n}Br_n]^{3-}$ or $[Rh(SnBr_3)_5]^{4-}$ are known. In view of this, a

detailed ^{119}Sn NMR study of the analogous stannous(II) bromide species of Rh(I/III) in hydrobromic acid solutions were undertaken and are discussed here.

4.2. Speciation of the series of $[Rh(SnBr_3)_nBr_{6-n}]^{3-}$ (n = 1 – 6) species in hydrobromic acid solutions

The analogous $[Rh(SnBr_3)_5]^{4-}$ complex anions were prepared by similar experimental conditions as used for the formation of the chlorido species, $[Rh(SnCl_3)_5]^{4-}$, shown in Section 3.2.1.1. The addition of commercial $SnBr_2$ to $RhCl_3 \cdot 3H_2O$ in HBr solutions proved to be unsuccessful. Therefore after several attempts, the reaction of a commercial $Rh(NO_3)_3$ solution with $SnBr_2$ in HBr was exammend. This proved to be successful and would not yield complexes with $SnCl_{3-n}Br_n^-$ ligands, which might be expected to result in very complex spectra. The treatment of $Rh(NO_3)_3$ solution with $SnBr_2$ in HBr results in a dark red solution as compared to the deep purple observed for the chlorido species. After 24 hour equilibration time under N_2 the ^{119}Sn NMR spectrum was recorded of this solution, shown in Figure 4.1.

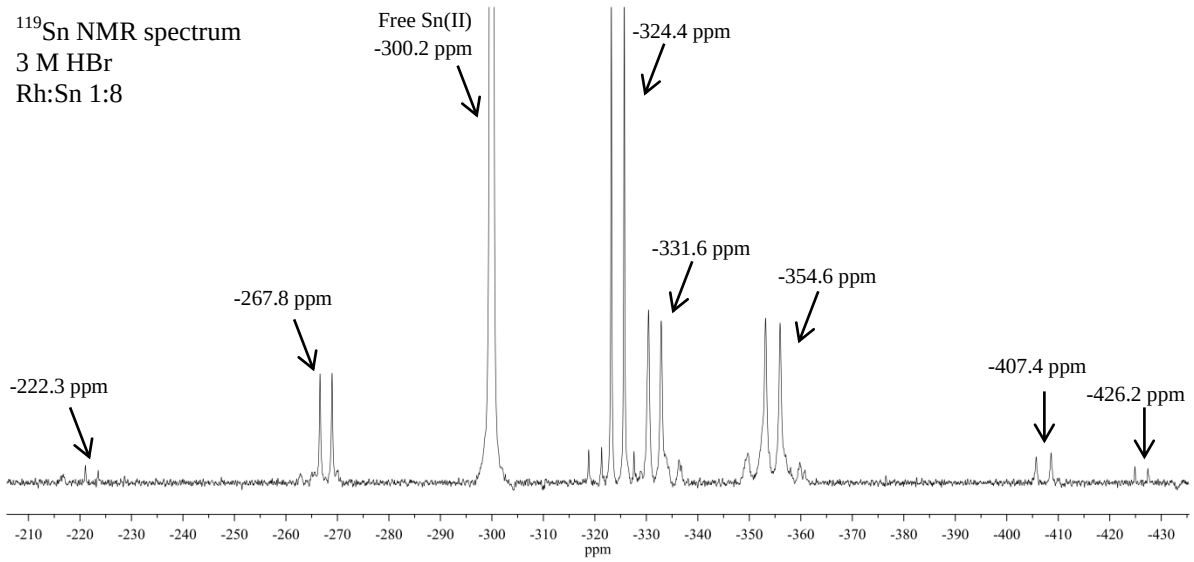

Figure 4.1 The ^{119}Sn NMR spectrum acquired for a 0.5 M $Rh(NO_3)_3$ solution with an effective $Rh:SnBr_3^-$ mole ratio of 1:8 in 3 M HBr at 25 °C. Seven main doublets are observed, each flanked by their respective satellites.

The ^{119}Sn NMR spectrum in Figure 4.1 with an effective Rh:Sn mole ratio of 1:8 in 3 M HBr shows seven sets of Rh-Sn complex signals, compared to only one set of ^{119}Sn signals that was obtained under similar conditions for the chlorido Rh-Sn solution and was assigned to

the $[Rh^{I}(SnCl_3)_5]^{4-}$ complex anion. From the equilibrium equations discussed in Chapter 3, Equation 3.1.1 to 3.1.4, it is clear that with an excess of tin(II) chloride the $[Rh^{I}(SnCl_3)_5]^{4-}$ species is the dominant species. Assuming that the bromido system is similar to the chlorido system, the possible equilibrium equations for the Rh(I/III)-$SnBr_3$ species in solution are given in Equations 4.1.1 to 4.15:

$$Rh^{III}(NO_3)_3 + 6HBr \rightleftharpoons [Rh^{III}Br_6]^{3-} + 3NO_3^- \quad 4.1.1$$

$$[Rh^{III}Br_6]^{3-} + SnBr_3^- \rightleftharpoons [Rh^{III}(SnBr_3)Br_5]^{3-} + Br^- \quad 4.1.2$$

$$[Rh^{III}(SnBr_3)Br_5]^{3-} + SnBr_3^- \rightleftharpoons \textit{cis/trans}\text{-}[Rh^{III}(SnBr_3)_2Br_4]^{3-} + Br^- \quad 4.1.3$$

$$\textit{c/t}\text{-}[Rh^{III}(SnBr_3)_2Br_4]^{3-} + SnBr_3^- \rightleftharpoons \textit{fac/mer}\text{-}[Rh^{III}(SnBr_3)_3Br_3]^{3-} + Br^- \quad 4.1.4$$

$$[Rh^{III}(SnBr_3)_5Br]^{3-} + SnBr_3^- \rightleftharpoons [Rh^{I}(SnBr_3)_5]^{4-} + Br^- \quad 4.1.5$$

As these bromido rhodium-tin(II) species have not previously been reported in literature, obtaining one obviously assignable species would assist in the assignment of all seven species in Figure 4.1. Subsequently, in order to encourage the formation of a single reduced $[Rh^{I}(SnBr_3)_5]^{4-}$ species, the HBr concentration was decreased to 0.5 M in order to decrease the total free Br^- concentration using effective Rh:Sn mole ratio of 1:10, Figure 4.2B. Further increases of the effective Rh:Sn mole ratio to 1:20 in 0.5 M HBr by adding additional amounts of $SnBr_2$ and allowing the solution to stand at room temperature under N_2 overnight for equilibration resulted in the ^{119}Sn NMR spectrum shown in Figure 4.2C. The ^{119}Sn NMR spectra all display a total seven main sets of ^{119}Sn resonances due to Rh-Sn species regardless, as is evidenced by the series of doublet resonances due to $^{1}J(^{103}Rh\text{-}^{119}Sn)$ spin coupling, flanked by their respective $^{2}J(^{119/117}Sn\text{-}^{119}Sn)$ satellites, Figure 4.2. The broad singlets at -300.0 ppm and -248.7 ppm in the 3 M and 0.5 M HBr solutions, respectively, are ascribed to excess free bromido Sn(II) species.

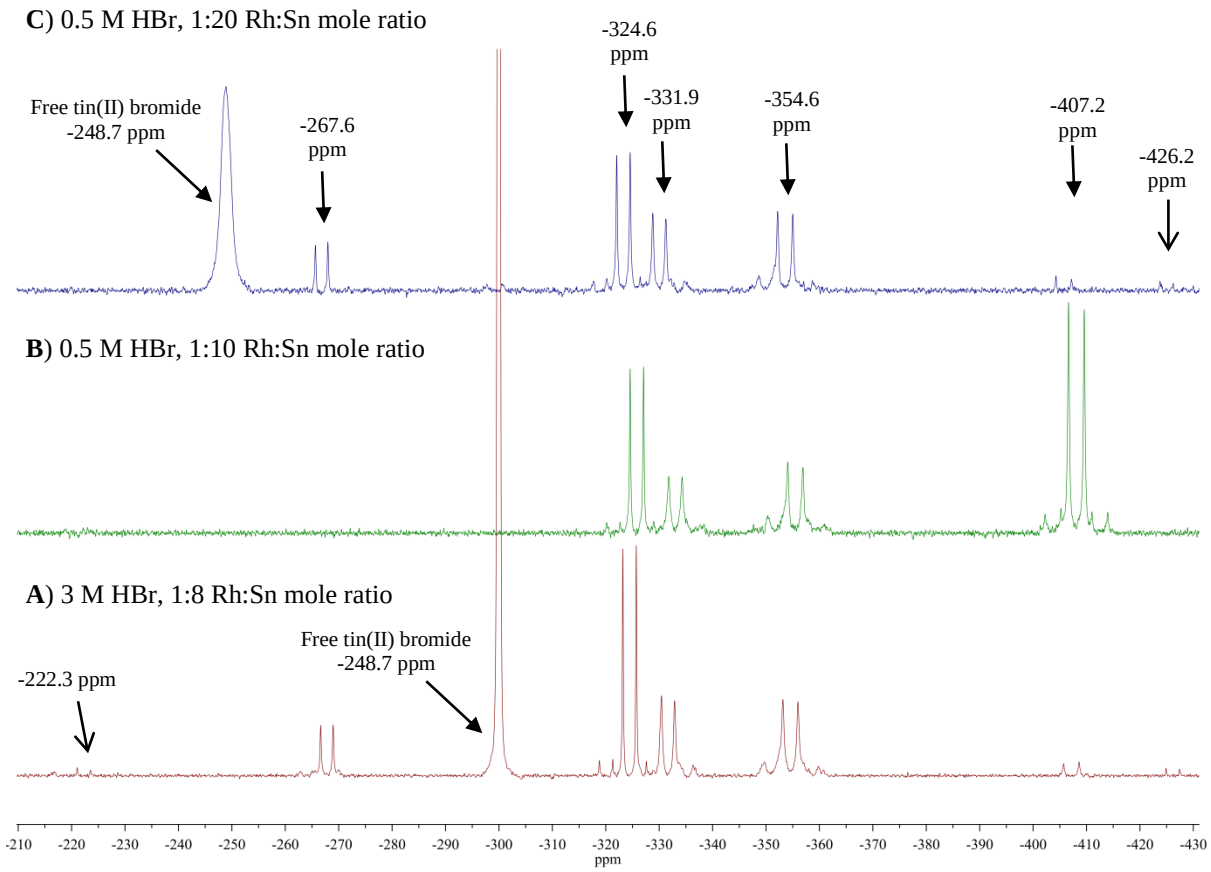

Figure 4.2 The ^{119}Sn NMR spectra acquired for a 0.5 M Rh(nitrate) solution with (A) an effective Rh:Sn mole ratio of 1:8 in 3 M HBr, (B) an effective Rh:Sn mole ratio of 1:10 in 0.5 M HBr and (C) and an effective Rh:Sn mole ratio of 1:20 in 0.5 M HBr at 25 °C. Seven main doublets are observed, each flanked by their respective satellites.

A similar methodology as used earlier for the assignment of the ^{119}Sn NMR spectra of the series of $[Rh(SnCl_3)_nCl_{6-n}]^{3-}$ (n = 1 – 6) complex anions in Sections 3.2 was applied to elucidate the ^{119}Sn NMR spectra of the bromido Rh-Sn species. The $\delta(^{119}Sn)$ chemical shift of each species may be plotted against the corresponding $^1J(^{103}Rh\text{-}^{119}Sn)$ coupling constant for that species, and compared to the trend observed for the series of $[Rh(SnCl_3)_nCl_{6-n}]^{3-}$ (n = 3 – 6) complex anions. The resultant trend shown if Figure 4.3 for the bromido $[Rh(SnBr_3)_nBr_{6-n}]^{3-}$ species is similar to the one obtained for the chlorido Rh-Sn species in particular those species that fall into the regions encircled in Figure 4.3. However, the scatter is larger and the chemical shift ranges narrower. This allows for the tentative assignment of 5 species of the series indicated by the roman numerals. The species indicated with the question marks, "?", however do not fall into the trend previously observed for the chlorido species and are therefore approached differently.

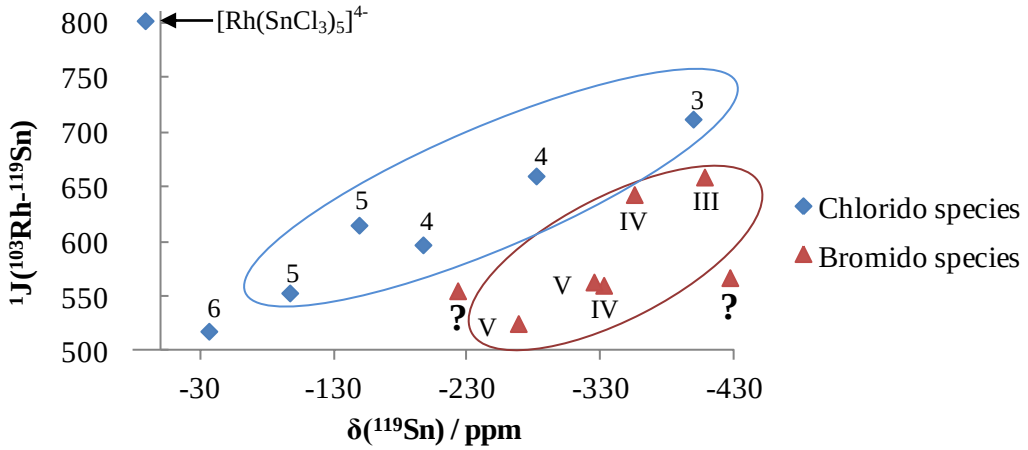

Figure 4.3 Comparison of the plots obtained for $^{1}J(^{103}Rh\text{-}^{119}Sn)$ as a function of $\delta(^{119}Sn)$ for the series of $[Rh(SnCl_3)_nCl_{6-n}]^{3-}$ (n = 3 – 6), given in blue, and the series of Rh-Sn species obtained for the bromido Rh-Sn species, given in red. The roman numerals indicate tentative assignments of the number of $SnBr_3^-$ ligands bound to Rh(III) in the series of $[Rh(SnBr_3)_nBr_{6-n}]^{3-}$ (n = 3 – 5) complexes.

The $\delta(^{119}Sn)$ and $^{1}J(^{103}Rh\text{-}^{119}Sn)$ coupling constants measured for each species is listed in Table 4.1 according to tentative assignments made from the comparative trend observed in Figure 4.3, together with the ^{119}Sn NMR parameters measured for the analogous chlorido Rh-Sn complexes from which the tentative assignment of the bromido Rh-Sn species are derived by comparison.

Table 4.1 ^{119}Sn NMR parameters and tentative assignments of the series of $[Rh(SnBr_3)_nBr_{6-n}]^{3-}$ (n = 3 – 5) complexes, as well as the ^{119}Sn NMR parameters of the series of $[Rh(SnCl_3)_nCl_{6-n}]^{3-}$ (n = 3 – 5) complexes.

		X = Cl⁻		**X = Br⁻**	
n	**Rh-Sn Complexes**	**$\delta(^{119}Sn)$/ ppm[a]**	**$^{1}J(^{103}Rh\text{-}^{119}Sn)$/ Hz[b]**	**$\delta(^{119}Sn)$/ ppm[a]**	**$^{1}J(^{103}Rh\text{-}^{119}Sn)$/ Hz[b]**
3	*fac*-$[Rh(SnX_3)_3X_3]^{3-}$	-420.2	714	-407.2	659
4	*cis*-$[Rh(SnX_3)_4X_2]^{3-}$ (eq)	-275.1	664	-354.6	630
4	*cis*-$[Rh(SnX_3)_4X_2]^{3-}$ (ax)	-193.8	589	-331.9	553
5	$[Rh(SnX_3)_5X]^{3-}$ (ax)	-145.1	620	-324.6	562
5	$[Rh(SnX_3)_5X]^{3-}$ (eq)	-102.3	555	-267.6	523
5	$[Rh^{I}(SnX_3)_5]^{4-}$	9.4	810	-	-

However, further analyses of the experimental ^{119}Sn NMR data of the bromido Rh-Sn species, $[Rh^{III}(SnBr_3)_nBr_{6-n}]^{3-}$ and $[Rh^{I}(SnBr_3)_5]^{4-}$, are necessary for the unambiguous assignment of these species. Assignment and discussion of the detailed ^{119}Sn NMR spectra will be approached in a similar manner as was done for the chlorido Rh-Sn species in Chapter III starting with the set of ^{119}Sn NMR signals at -407.2 ppm. The ^{119}Sn NMR signals at -

426.5 ppm and -222.6 ppm will be discussed later as they are present in only very low concentrations and do not conform to the trend.

4.2.1 Spectral section: δ(^{119}Sn) = - 407.2 ppm

First consider the set of ^{119}Sn NMR signals at -407.2 ppm which was tentatively assigned to the *fac*-$[Rh(SnBr_3)_3Br_3]^{3-}$ complex anion, Table 4.1. The main signal, split into a doublet with $^1J(^{103}Rh\text{-}^{119}Sn)$ = 659 Hz, is flanked by one set of $^2J(^{117}Sn\text{-}^{119}Sn)$ satellites with a coupling constant of 1960 Hz as shown in Figure 4.4. As baseline separation between the satellites and the main signals was not experimentally obtained, the areas of the respective signals were estimated by deconvolution of the spectrum.

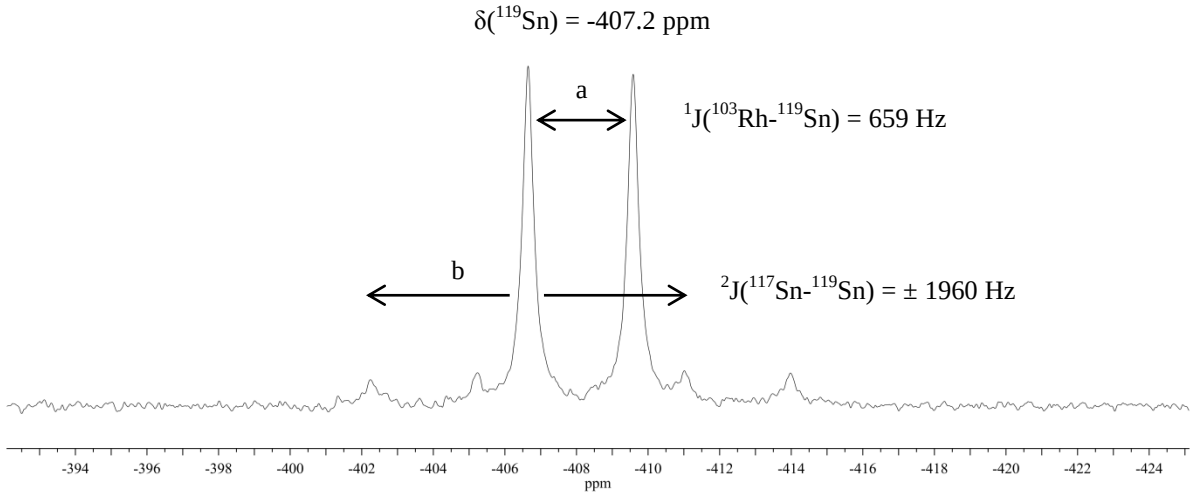

Figure 4.4 Expansion of the set of signals at δ(^{119}Sn) = -407.2 ppm. Symbol 'a' indicates $^1J(^{103}Rh\text{-}^{119}Sn)$ coupling and symbol 'b' indicates the $^2J(^{117}Sn\text{-}^{119}Sn)$ satellites.

The resultant intensity ratio, I(satellite)/I(main), was estimated (from the deconvoluted spectrum) to be 8.5 %, and is in good agreement with the natural statistical abundance (NSA) calculated, using Equation 3.1, for a Rh-Sn species with three magnetically equivalent tin-ligands bound to a central rhodium(III) ion, 8.3 %. This supports the assignment of the set of ^{119}Sn NMR signals at -407.2 ppm to the $[Rh(SnBr_3)_3Br_3]^{3-}$ complex anion. Using the same reasoning as in Section 3.2.1.3.1 for the analogous chlorido species, $[Rh(SnCl_3)_3Cl_3]^{3-}$, all three $SnCl_3^-$-ligands are magnetically equivalent and the set of ^{119}Sn resonance signals at -407.2 ppm can be assigned to the kinetically inert *fac*-$[Rh(SnBr_3)_3Br_3]^{3-}$ complex anion. The main set of signals is assigned to the $[^{103}Rh(^iSnBr_3)_n(^{119}SnBr_3)_{3-n}Br_3]^{3-}$ (n = 0 – 2)

isotopologues and the $^{2}J(^{117}Sn\text{-}^{119}Sn)_{cis}$ satellites are assigned to the $[^{103}Rh(^{i}SnCl_3)_n(^{119}SnCl_3)(^{117}SnCl_3)_{2-n}Cl_3]^{3-}$ (n = 0, 1) *isotopologues*, illustrated in Scheme 4.1.

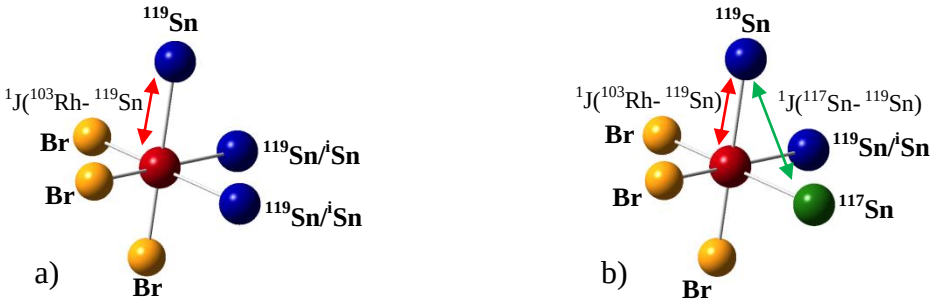

Scheme 4.1 Schematic representation of (a) the $[^{103}Rh(^{i}SnBr_3)_n(^{119}SnBr_3)_{3-n}Br_3]^{3-}$ (n = 0 – 2) and (b) the $[^{103}Rh(^{i}SnBr_3)_n(^{119}SnBr_3)(^{117}SnBr_3)_{2-n}Br_3]^{3-}$ (n = 0,1) *isotopologues* of *fac*-$[Rh(SnBr_3)_3Br_3]^{3-}$ complex anion resonating at $\delta(^{119}Sn)$ = -407.2 ppm. All coordinated bromido ligands of $SnBr_3^-$ are left out for clarity. The $^{119}Sn/^{i}Sn$ label on atoms means that that atom can represent either ^{119}Sn or ^{i}Sn in a specific *isotopologue*.

Comparison between the ^{119}Sn NMR spectra of the bromido and chlorido species showed that although the chemical shift difference between the ^{119}Sn NMR signals of *fac*-$[Rh(SnBr_3)_3Br_3]^{3-}$ complex anion and that of its chlorido analogue is not significant, the magnitude of the $^{1}J(^{103}Rh\text{-}^{119}Sn)$ coupling constant measured for the *fac*-$[Rh(SnX_3)_3X_3]^{3-}$ species decreases by *ca*. 8 % on passing from X = Cl^- to Br^- as shown in Table 4.1. This is similar to the trend observed for the $[Pt(SnX_3)_5]^{3-}$ (X = Cl^-/Br^-) species previously studied in our laboratory.[59] The decrease in the magnitude of the $^{1}J(^{119}Sn\text{-}^{195}Pt)$ coupling constant may be postulated to be due to the elongation of the Pt-Sn bond length on passing from X = Cl^- to Br^-. This postulation was based on a study by Nelson *et. al.*[58] of the $[PtX_n(SnX_3)_{4-n}]^{2-}$ (X = Cl^-/Br^-, n = 1 – 4) complex anions by means of ^{119}Sn and ^{195}Pt NMR as well as X-ray diffraction, wherein it was shown that the Pt-Sn bond lengths increased in the order *cis*-$[PtCl_2(SnCl_3)_2]^{2-}$ < $[PtBr_3(SnBr_3)]^{2-}$ < *cis*-$[PtBr_2(SnBr_3)_2]^{2-}$. It is thus reasonable to suggest that the decrease in the $^{1}J(^{103}Rh\text{-}^{119}Sn)$ coupling constants observed for the *fac*-$[Rh(SnX_3)_3X_3]^{3-}$ (X = Cl^-/Br^-) complex anions is due to a slight increase in the Rh-Sn bond length when going from X = Cl^- to X = Br^-. Nevertheless, the nature of the $SnCl_3^-$ compared to the $SnBr_3^-$ ligands for Rh^{III} may also play a role, so that this suggestion must remain tentative until further, preferably computational results are available.

4.2.2 Assignment of Species in the Spectral Range: $\delta(^{119}Sn)$ = -331.9 to -354.7 ppm

The two sets of ^{119}Sn NMR signals at -354.7 ppm and -331.9 ppm are both split into doublets due to $^{1}J(^{103}Rh\text{-}^{119}Sn)$ spin coupling with coupling constants of 630 Hz and 552 Hz, respectively, as is indicated by the symbols 'a' and 'c' in Figure 4.5B. Unfortunately, only broad, unresolved $^{2}J(^{119/117}Sn\text{-}^{119}Sn)$ satellite signals are obtained for both species, indicated by symbols 'b' and 'd', which makes it difficult to distinguish between different sets of satellites and subsequently hinders the assignment of the spectrum.

Based on their respective positions in the trend obtained when plotting the $\delta(^{119}Sn)$/ppm against the $^{1}J(^{103}Rh)$/Hz in Figure 4.3, the ^{119}Sn NMR resonance signals at -354.7 and -331.9 ppm may however tentatively be assigned to *stereo-isotopomers* of the *cis*-$[Rh(SnBr_3)_4Br_2]^{3-}$ species where the observed $^{119}SnBr_3^-$ ligand is in the equatorial (*trans* to Br^-) and axial (*trans* to $SnBr_3^-$ and *cis* to Br^-) positions, respectively. This assignment is based on the similarity of this ^{119}Sn NMR spectrum to that of the analogous chlorido *cis*-$[Rh(SnCl_3)_4Cl_2]^{3-}$ complex shown in Figure 4.5A, in which two different chemical shifts were reported for the *observed* $^{119}SnCl_3^-$ ligand in the axial (*cis* to Cl^-) and in the equatorial (*trans* to Cl^-) positions. Furthermore, the asymmetrical distribution of the $^{2}J(^{119}Sn\text{-}^{119}Sn)$ satellites around the main signals is similar to those that have previously been assigned in Chapter III which supports the tentative assignments of $\delta(^{119}Sn)$ = -354.7 and -331.9 ppm. Unfortunately, due to the broadness of the unresolved $^{2}J(^{119/117}Sn\text{-}^{119}Sn)$ satellites, these assignments cannot be made with absolute certainty.

It was shown for the chlorido Rh-Sn species (Chapter III, Section 3.2.1) that using the program gNMR50 to simulate the ^{119}Sn NMR spectra of these Rh-Sn species greatly facilitates the elucidation and assignment of the ^{119}Sn NMR spectra thereof. In this regard, the experimental NMR parameters ($\delta(^{119}Sn)$, $^{1}J(^{103}Rh\text{-}^{119}Sn)$, estimated $^{2}J(^{117}Sn\text{-}^{119}Sn)$ and $\Delta\nu_{1/2}$) measured in the ^{119}Sn NMR spectrum tentatively assigned to the *cis*-$[Rh(SnBr_3)_4Br_2]^{3-}$ species, Figure 4.5B, were used as input to simulate the ^{119}Sn NMR spectrum of these species as shown Figure 4.5C. The width at half height ($\Delta\nu_{1/2}$) of the ^{119}Sn signals of the simulated spectrum in Figure 4.5C was deliberately set to 132 Hz to approximate the experimentally obtained ^{119}Sn NMR spectrum.

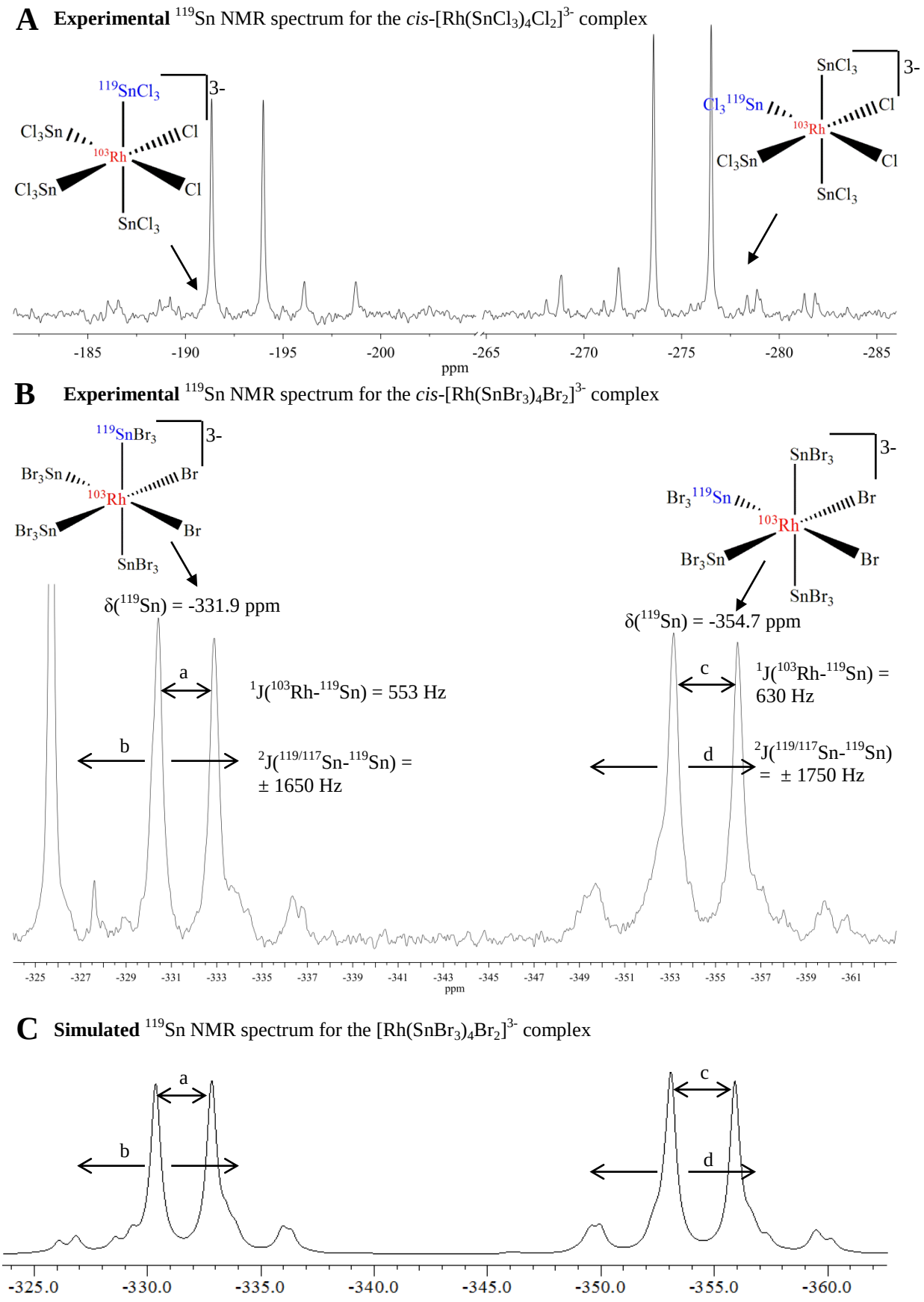

Figure 4.5 The ^{119}Sn NMR spectrum of the stereoisomers of the *cis*-$[Rh(SnCl_3)_4Cl_2]^{3-}$ species is given in (A) and the ^{119}Sn NMR spectrum of the stereoisomers of the *cis*-$[Rh(SnBr_3)_4Br_2]^{3-}$ species is given in (B). The NMR parameters measured in (B) were used as input to simulate the ^{119}Sn NMR spectrum in (C).

The spectral pattern of the simulated ^{119}Sn NMR spectrum for the *cis*-$[Rh(SnBr_3)_4Br_2]^{3-}$ species, Figure 4.5C, strongly resembles the experimentally spectrum with $\delta(^{119}Sn)$ peaks at -354.7 and -331.9 ppm shown in Figure 4.5B, both showing comparable asymmetrical $^2J(^{119/117}Sn\text{-}^{117}Sn)$ satellites. However, not much is achieved by simulating an ^{119}Sn spectrum with the same broad signals as was experimentally obtained, except for confirming spectral pattern obtained for a particular species. Therefore the width at half height ($\Delta\nu_{½}$) of the signals in the simulated ^{119}Sn NMR spectrum was changed from 132 Hz (which was experimentally obtained) in Figure 4.6A to 10 Hz in Figure 4.6B using gNMR50. This resulted in much better resolution of the signals and exposed the intricate underlying spectral pattern of the $^2J(^{119/117}Sn\text{-}^{119}Sn)$ satellites for the ^{119}Sn NMR resonances at -354.7 and -331.9 ppm tentatively assigned to the *cis*-$[Rh(SnBr_3)_4Br_2]^{3-}$ species, Figure 4.6B, which is not obtainable by any other method. Therefore, the simulated ^{119}Sn NMR spectrum in Figure 4.6B may be used to determine the values of the respective $^2J(^{119/117}Sn\text{-}^{117}Sn)$ coupling constants for the *cis*-$[Rh(SnBr_3)_4Br_2]^{3-}$ species, as was done for the corresponding chlorido species on page 54.

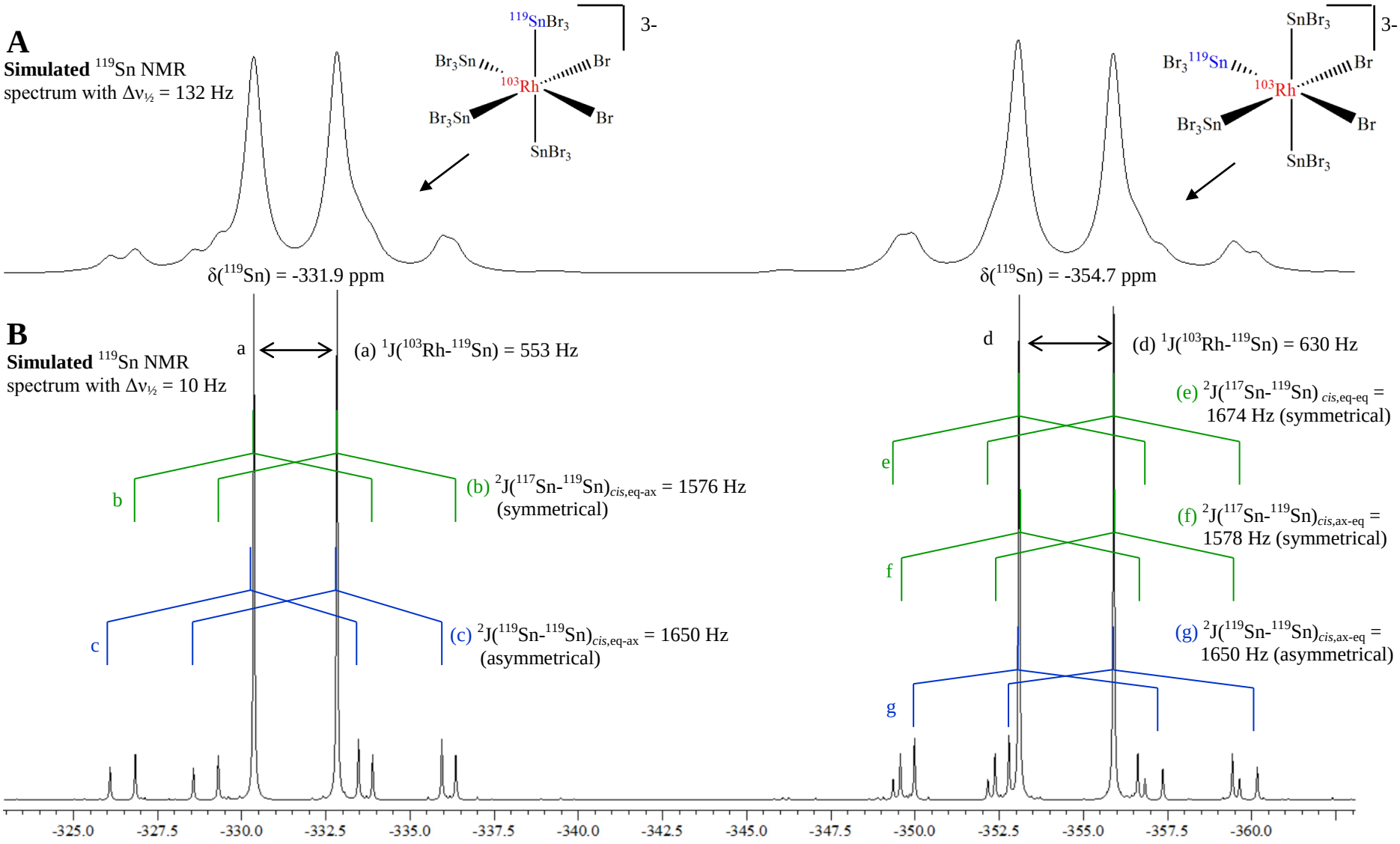

Figure 4.6 The simulated ^{119}Sn NMR spectrum of *cis*-$[Rh(SnBr_3)_4Br_2]^{3-}$ with the width at half height ($\Delta\nu_{½}$) of the ^{119}Sn NMR signals set to 132 Hz in (A) and reduced to 10 Hz in (B).

Two possible *isotopomers* of the *cis*-$[Rh(SnBr_3)_4Br_2]^{3-}$ species wherein the observed $^{119}SnBr_3^-$ ligand is either axial (*trans* to another $SnBr_3^-$ ligand) or equatorial (*trans* to Br^-) are shown in Scheme 4.2. Consider first the set of ^{119}Sn NMR signals at -331.9 ppm tentatively assigned to the the *cis*-$[Rh(SnBr_3)_4Br_2]^{3-}$ complex anion in which the observed $^{119}SnBr_3^-$ ligand is coordinated in the axial (*trans* to $SnBr_3^-$ and *cis* to Br^-) position, shown in Figure 4.2A.

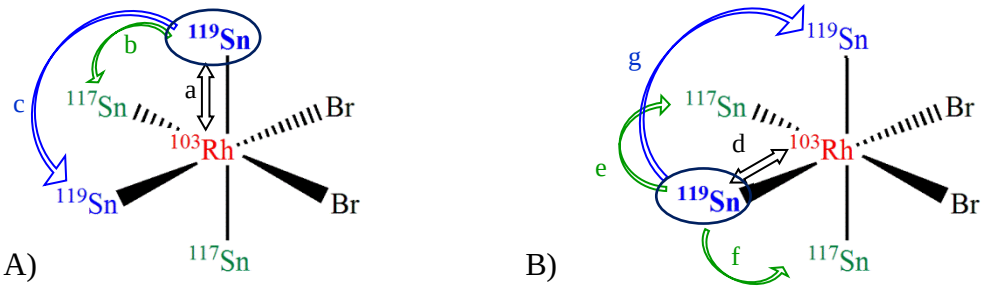

Scheme 4.2 A schematic representation of the *cis*-$[Rh(SnBr_3)_4Br_2]^{3-}$ complex where the observed $^{119}SnBr_3^-$ ligand is (A) in the axial position and (B) in the equatorial position. If the observed ^{119}Sn is in the axial position (*trans* to another $^{i}SnBr_3^-$ ligand) it has a different chemical shift to the case when it is in the equatorial (*trans* to a Br^-), supporting the suggestion that these species are kinetically inert. The $^1J(^{103}Rh\text{-}^{119}Sn)$ couplings in the different *isotopomers* are indicated with the symbols 'a' and 'd', respectively, which correspond to the splitting indicated by symbols 'a' and 'd' in Figure 4.6B. Similarly, the possible $^2J(^{119/117}Sn\text{-}^{119}Sn)$ scalar couplings are indicated with symbols 'b', 'c', 'e', 'f' and 'g' and correspond to respective satellites shown in Figure 4.6B. All coordinated bromido ligands of $SnBr_3^-$ are left out for clarity.

The signal is split into a doublet due to $^1J(^{103}Rh\text{-}^{119}Sn)$ spin coupling with a coupling constant of 552 Hz, indicated by the symbol 'a' in Figure 4.6B and Scheme 4.2A. Furthermore, from the well-resolved simulated ^{119}Sn NMR spectrum, Figure 4.6B, it is evident that the main signal at -331.9 ppm is flanked by two sets of $^2J(^{119/117}Sn\text{-}^{119}Sn)$ satellites; one symmetrically distributed set of satellites with a coupling constant of 1576 Hz ('b') and one asymmetrically distributed set of satellites with a coupling constant of 1650 Hz ('c'). This spectral pattern is consistent with the one observed for the analogous chlorido species, *cis*-$[Rh(SnCl_3)_4Cl_2]^{3-}$, in which the observed $^{119}SnCl_3^-$ ligand was in the axial position (*trans* to another $SnCl_3^-$), discussed in Section 3.2.1.3. It was attested that the asymmetrically distributed $^2J(^{119/117}Sn\text{-}^{119}Sn)$ satellites are due to scalar coupling between the $^{119}SnCl_3^-$ ligand in the axial position (*trans* to another $SnCl_3^-$) and a $^{119}SnCl_3^-$ ligand in the equatorial position (*trans* to Cl^-), which are not magnetically equivalent as this Rh(III)-Sn(II) species is kinetically inert. It is thus reasonable to assign the set of satellites indicated by 'c' in Figure 4.6B to the $^2J(^{119}Sn\text{-}^{119}Sn)_{cis,eq\text{-}ax}$ satellites of the *cis*-$[^{103}Rh(^{i}SnBr_3)_2(^{119}SnBr_3)_2Br_2]$ *isotopologue* of the *isotopomer* shown in Scheme 4.2A. The set of satellites indicated by 'b' in Figure 4.6B are

subsequently assigned to the $^{2}J(^{117}Sn\text{-}^{119}Sn)_{cis,eq\text{-}ax}$ satellites of the *cis*-[$^{103}Rh(^{i}SnBr_3)_2$-($^{119}SnBr_3$)($^{117}SnBr_3$)Br_2] *isotopologue* of the *isotopomer* shown in Scheme 4.2A. In both these *isotopologues* the observed $^{119}SnBr_3^-$ ligand is in the axial (*trans* to $SnBr_3^-$) position, as is indicated in Scheme 4.2A. This assignment is supported by the ratio of the coupling constants of the two sets of satellites, (1650 Hz/1576 Hz) = 1.047, which is proportional to the $\gamma(^{119}Sn)$ to $\gamma(^{117}Sn)$ ratio. As expected, the coupling constants of the $^{2}J(^{119}Sn\text{-}^{119}Sn)_{cis,eq\text{-}ax}$ and $^{2}J(^{117}Sn\text{-}^{119}Sn)_{cis,eq\text{-}ax}$ satellites are in accordance with the trend previously observed for $^{2}J(^{119/117}Sn\text{-}^{119}Sn)$ coupling constants of the corresponding chlorido complex: $^{2}J(^{119}Sn\text{-}^{119}Sn)_{cis,eq\text{-}ax} > {}^{2}J(^{117}Sn\text{-}^{119}Sn)_{cis,eq\text{-}ax}$, which further supports the assignments as stated.

The ^{119}Sn NMR set of peaks at $\delta(^{119}Sn)$ = -354.7 ppm is tentatively assigned to the the *cis*-$[Rh(SnBr_3)_4Br_2]^{3-}$ complex anion in which a observed $^{119}SnBr_3^-$ ligand is in the equatorial (*trans* to Br^-) position, as illustrated in Scheme 4.2B. The main ^{119}Sn NMR doublet, due to $^{1}J(^{103}Rh\text{-}^{119}Sn)$ = 630 Hz as indicated by the symbol 'd' in Figure 4.6B, is flanked by three sets of $^{2}J(^{119/117}Sn\text{-}^{119}Sn)$ satellites indicated by 'e', 'f' and 'g', respectively. The two sets of satellites, indicated by 'e' and 'f' with coupling constants of 1578 and 1674 Hz, respectively, are symmetrically distributed around the main signal, whereas the set of satellites indicated by 'g' with coupling constant of 1650 Hz is asymmetrically distributed around the main signal. This splitting pattern corresponds well with one expected for the *cis*-$[Rh(SnBr_3)_4Br_2]^{3-}$ complex anion where the $^{119}SnBr_3^-$ ligand is in the equatorial (*trans* to Br^-) position, as is shown in Scheme 4.2B.

The satellites indicated by 'e', 'f' and 'g' in Figure 4.6B are thus accordingly assigned to the $^{2}J(^{117}Sn\text{-}^{119}Sn)_{cis,ax\text{-}eq}$, $^{2}J(^{117}Sn\text{-}^{119}Sn)_{cis,eq\text{-}eq}$ and $^{2}J(^{119}Sn\text{-}^{119}Sn)_{cis,ax\text{-}eq}$ satellites of the respective *isotopologues* of the *cis*-$[Rh(SnBr_3)_4Br_2]^{3-}$ species as is listed in Table 4.2, respectively. For these *isotopologues*, the observed $^{119}SnBr_3^-$ ligand is in the equatorial position, *trans* to Br^-. The high degree of second order distortion obtained for the $^{2}J(^{119}Sn\text{-}^{119}Sn)_{cis,eq\text{-}ax}$ satellites is justified by $(\nu_A - \nu_B)/J_{AB}$ = 3.11, which is well below the value of 7 which is required for first order analysis as was discussed in Chapter III.

Table 4.2 ^{119}Sn NMR parameters of the *isotopologues* observed for the equatorial and axial *isotopomers* of the *cis*-$[Rh(SnBr_3)_4Br_2]^{3-}$ species.

Rh-Sn isotopologue	**$\delta(^{119}Sn)$ /ppm**	**$^1J(^{103}Rh\text{-}^{119}Sn)$ /Hz**	**$^2J(^{117}Sn\text{-}^{119}Sn)$ /Hz**
Isotopomer: Observed $^{119}SnBr_3^-$ ligand *trans* to $SnBr_3^-$, *cis* to Br^-			
$[^{103}Rh(^{i}SnBr_3)_3(^{119}SnBr_3)Br_2]^{3-}$	$-354.7_{(eq)}$	$630_{(eq)}$	-
$[^{103}Rh(^{i}SnBr_3)_2(^{119}SnBr_3)_2Br_2]^{3-}$	$-354.7_{(eq)}$	$630_{(eq)}$	$^2J(^{119}Sn\text{-}^{119}Sn)_{(cis,ax\text{-}eq)}$ = 1650
$[^{103}Rh(^{i}SnBr_3)_2(^{119}SnBr_3)(^{117}SnBr_3)Br_2]^{3-}$	$-354.7_{(eq)}$	$630_{(eq)}$	$1674_{(cis,eq\text{-}eq)}$ $1578_{(cis,ax\text{-}eq)}$
Isotopomer: Observed $^{119}SnBr_3^-$ ligand *trans* to Br^-, *cis* to $SnBr_3^-$			
$[^{103}Rh(^{i}SnBr_3)_3(^{119}SnBr_3)Br_2]^{3-}$	$-331.9_{(ax)}$	$553_{(ax)}$	-
$[^{103}Rh(^{i}SnBr_3)_2(^{119}SnBr_3)_2Br_2]^{3-}$	$-331.9_{(ax)}$	$553_{(ax)}$	$^2J(^{119}Sn\text{-}^{119}Sn)_{(cis,eq\text{-}ax)}$ = 1650
$[^{103}Rh(^{i}SnBr_3)_2(^{119}SnBr_3)(^{117}SnBr_3)Br_2]^{3-}$	$-331.9_{(ax)}$	$553_{(ax)}$	$1576_{(cis,eq\text{-}ax)}$

From the trend obtained in Figure 4.3, the good correlation between spectral pattern observed here and that of the *cis*-$[Rh(SnCl_3)_4Cl_2]^3$ species and the simulated ^{119}Sn NMR spectrum, the sets of ^{119}Sn NMR signals at -354.7 and -331.9 ppm are unambiguously assigned to a single species, *cis*-$[Rh(SnBr_3)_4Br_2]^{3-}$, in which the observed $^{119}SnBr_3^-$ ligand is in the *axial*, *trans* to another $^{i}SnBr_3^-$ ligand position and the *equatorial*, *trans* to a Br^- ion position, respectively. Moreover, the gNMR50 simulated ^{119}Sn NMR spectra have allowed for the accurate determination of the scalar couplings for each of the respective sets of $^2J(^{119/117}Sn\text{-}^{119}Sn)$ satellites of the *cis*-$[Rh(SnBr_3)_4Br_2]^{3-}$ species. Thus, from the results obtained it is reasonable to conclude that for both the *fac*-$[Rh(SnBr_3)Br_3]^{3-}$ and *cis*-$[Rh(SnBr_3)_4Br_2]^{3-}$ species the assignments suggested for these species as shown in Figure 4.5 and listed in Table 4.1 are confirmed. It has thus been shown for both the chlorido and bromido Rh(III)-Sn(II) species that different chemical shifts are observed for different *isotopomers* of a respective species, which supports our assignments overall and that these Rh(III)-Sn(II) species are kinetically inert.

4.2.3 Assignment of Species in the Spectral Range $\delta(^{119}Sn)$ = -267.6 ppm and -324.4 ppm

The ^{119}Sn NMR signals at -267.6 and -324.4 ppm as shown in Figure 4.7B are split into doublets with $^1J(^{103}Rh\text{-}^{119}Sn)$ = 523 Hz (a) and 562 Hz (c) respectively, each flanked by their corresponding $^2J(^{117}Sn\text{-}^{119}Sn)$ satellites with a coupling constants of ca. 1565 Hz (b) and 1970 Hz (d).

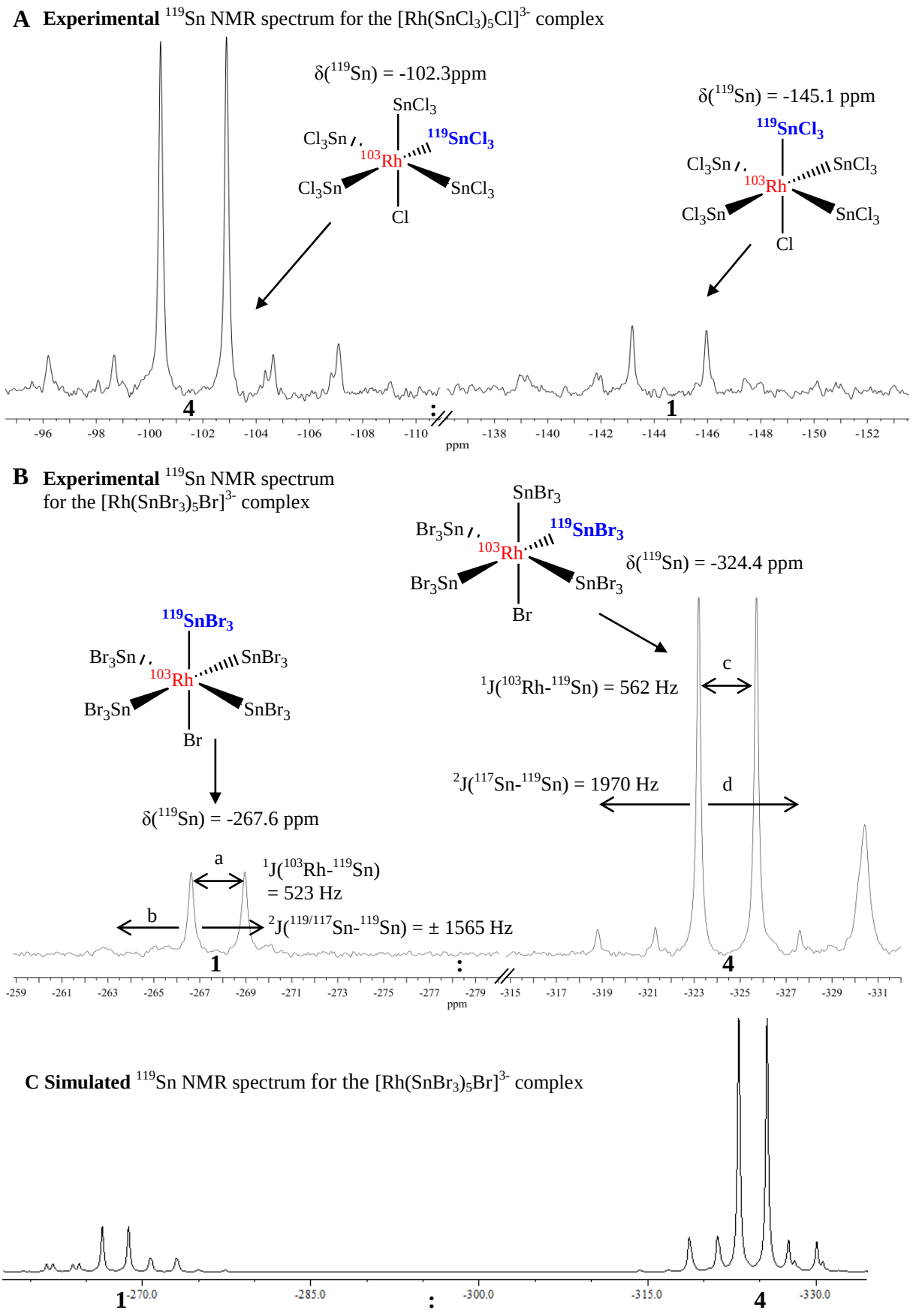

Figure 4.7 The ^{119}Sn NMR spectrum of (A) the $[Rh(SnCl_3)_5Cl]^{3-}$ species is shown, as well as the assignment of the two respective *isotopomers* and (B) the $[Rh(SnBr_3)_5Br]^{3-}$ species with $\delta(^{119}Sn)$ = -267.6 ppm and -324.4 ppm, split into doublets due to $^1J(^{103}Rh\text{-}^{119}Sn)$ = 523 Hz (a) and 562 Hz (b), respectively. The spectrum is tentatively assigned to the respective species as shown. (C) The simulated spectrum using gNMR50.

According to the trend in Figure 4.3, and its resemblance to that of the chlorido Rh(III)-Sn species, the two sets of signals at $\delta(^{119}Sn)$ = -267.6 ppm and -324.4 ppm were tentatively assigned to two *isotopomers* of the $[Rh^{III}(SnBr_3)_5Br]^{3-}$ complex anion where the observed $^{119}SnBr_3^-$ ligand is the equatorial (*trans* to $SnBr_3^-$) and the axial (*trans* to Br^-) positions, respectively, as shown in Scheme 4.3.

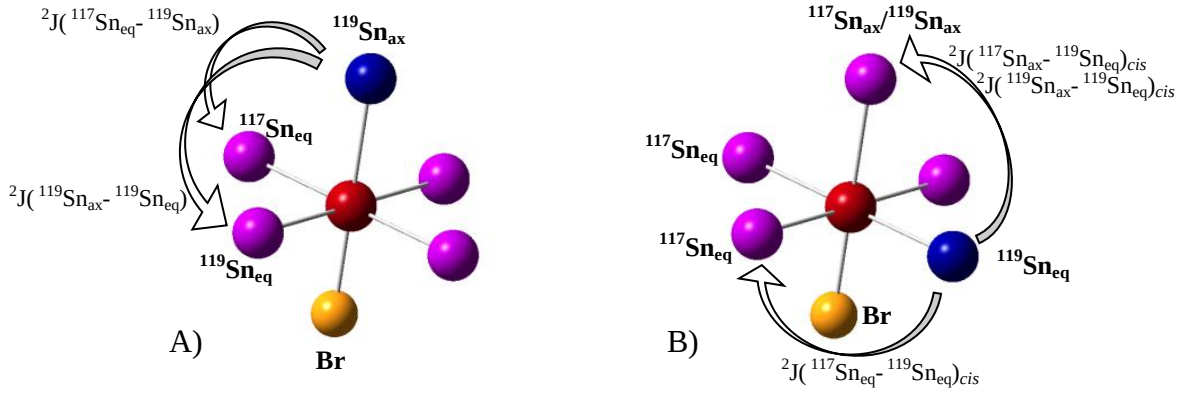

Scheme 4.3 A schematic representation of two *isotopomers* of $Rh(SnBr_3)_5Br]^{3-}$ complex anion where the observed $^{119}SnBr_3^-$ ligand is a) in the axial (*trans* to Br^-) and b) in the equatorial (*cis* to Br^-) position. Moreover, the expected $^2J(^{119/117}Sn-^{119}Sn)$ spin-couplings for each *isotopomer* are indicated on the scheme. All coordinated bromido ligands of $SnBr_3^-$ are left out for clarity.

The relative peak areas are in the ratio of $4Sn_{eq}$:$1Sn_{ax}$ in both the chlorido and bromido species, however, the relative chemical shifts are swopped around in the $[Rh(SnBr_3)_5Br]^{3-}$ species as is seen in Figure 4.7B. In other words, the chemical shift of (A) and (B) in Scheme 4.3 are different if rigid, with the set of signals at $\delta(^{119}Sn)$ = -267.6 ppm assigned to the axial *isotopomer* of $[Rh(SnBr_3)_5Br]^{3-}$, wherein the $^{119}SnBr_3^-$ ligand is *trans* to Br^-, and the set of signals at $\delta(^{119}Sn)$ = -324.4 ppm to the equatorial *isotopomer*, wherein the $^{119}SnBr_3^-$ ligand is *trans* to another $SnBr_3^-$ ligand, as is shown in Figure 4.7B. Moreover, the relative peak area ratio of (A) to (B) should be, and is, 1:4. Unfortunately, both the S/N ratio and the resolution obtained is not optimum to accurately measure the respective $^2J(^{119/117}Sn-^{119}Sn)$ coupling constants for the satellites observed. Therefore, the NMR parameters measured for the spectrum shown in Figure 4.7B was used to simulate the ^{119}Sn NMR spectrum of these species with gNMR50 and the resulting spectrum is shown in Figure 4.7C. The spectral pattern of the simulated spectrum resembles that of the experimental spectrum in Figure 4.7B which makes the assignment of signals as discussed above seem reasonable.

In order to analyse the $^{2}J(^{119/117}Sn\text{-}^{119}Sn)$ satellites of the respective *isotopomers*, the width at half height ($\Delta\nu_{½}$) of the signals in the simulated ^{119}Sn NMR spectrum in Figure 4.7C was changed from 64 Hz, which was experimentally obtained, to 10 Hz in order to increase the resolution of the signals; the resulting spectra of the two sets of signals are shown in Figure 4.8.

A: Simulated ^{119}Sn NMR spectrum of $[Rh(SnBr_3)_5Br]^{3-}$ with observed $^{119}SnBr_3^-$ *trans* to another $SnBr_3^-$ ligand

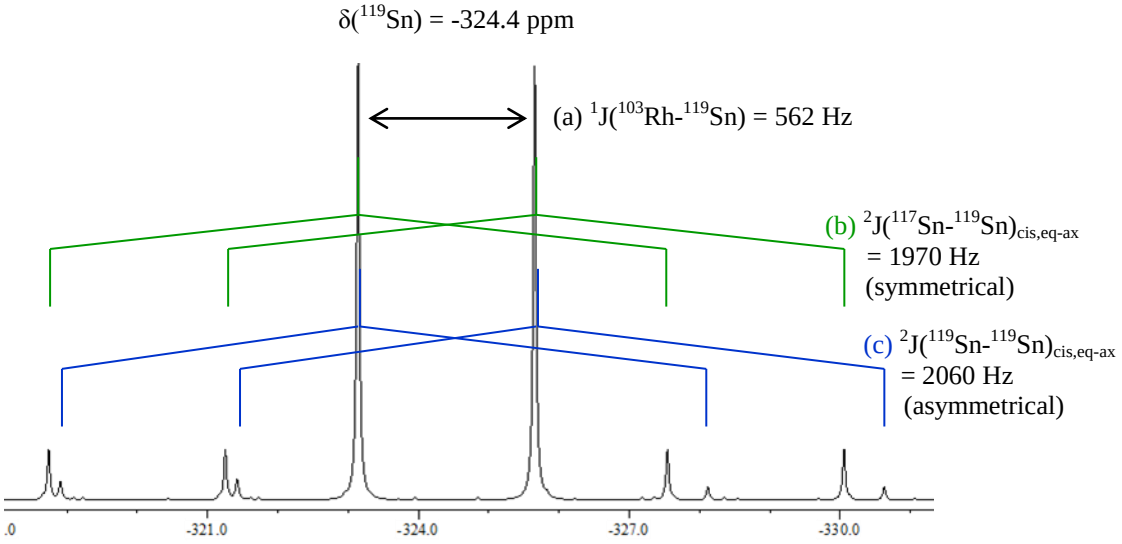

B: Simulated ^{119}Sn NMR spectrum of $[Rh(SnBr_3)_5Br]^{3-}$ with observed $^{119}SnBr_3^-$ *trans* to Br^-

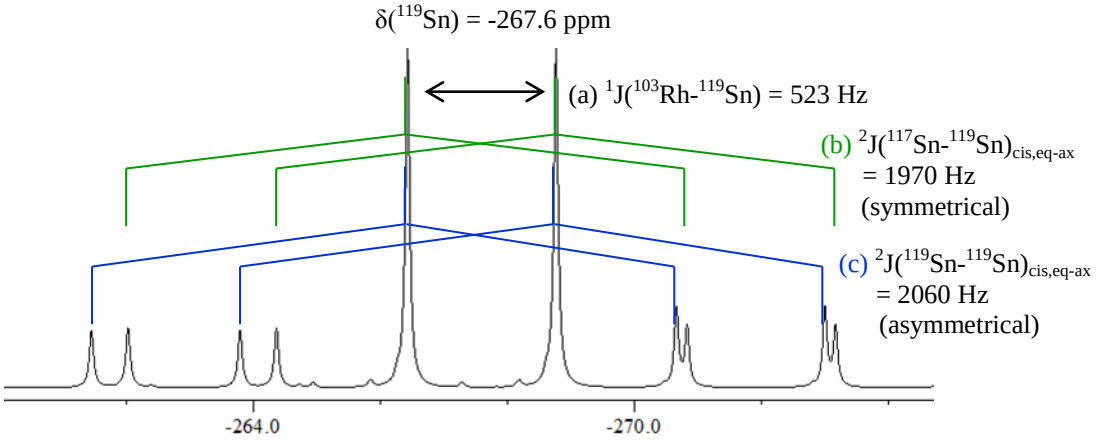

Figure 4.8 The simulated ^{119}Sn NMR spectrum of the $[Rh(SnBr_3)_5Br]^{3-}$ species and the respective $^{1}J(^{103}Rh\text{-}^{119}Sn)$ and $^{2}J(^{119/117}Sn\text{-}^{119}Sn)$ spin-couplings of the set of signals at (A) $\delta(^{119}Sn)$ = -324.4 ppm and at (B) $\delta(^{119}Sn)$ = -267.6 ppm. The $\Delta\nu_{½}$ is set to 10 Hz to increase resolution.

From the simulated ^{119}Sn NMR spectrum of the signals at $\delta(^{119}Sn)$ = -324.4 ppm shown in Figure 4.8A, there are two sets of $^{2}J(^{119/117}Sn\text{-}^{119}Sn)$ satellites: a symmetrically distributed set

of satellites with a coupling constant of 1970 Hz indicated by (b) in Figure 4.8A and an asymmetrically distributed set of satellites with a coupling constant of 2060 Hz indicated by (c) in the same Figure. Integration of the individual experimental ^{119}Sn NMR signals at $\delta(^{119}Sn)$ = -324.4 ppm, however, gave a I(satellite)/I(main) ratio of 7 %, which does not agree with the calculated NSA of 12.3 %, using Equation 3.1, for a Rh-Sn species with 4 magnetically equivalent tin-ligands coordinated to the central Rh. Rather, this ratio suggests that only 3 magnetically equivalent $SnBr_3^-$-ligands are bound to the central Rh. Unfortunately, the low S/N ratio obtained for the species at $\delta(^{119}Sn)$ = -267.6 ppm prevented the integration of those satellites. This, together with the overlapping of the ^{119}Sn NMR signals, causes difficulties in the unambiguous assignment of these species. However, from the trend obtained in Figure 4.3 and from the simulated ^{119}Sn NMR spectrum, these species are assigned to the axial and equatorial *isotopomers* of the $[Rh(SnBr_3)_5Br]^{3-}$ species as listed in Table 4.3.

Table 4.3 ^{119}Sn NMR parameters of the *isotopologues* observed for the equatorial and axial *isotopomers* of the $[Rh(SnBr_3)_5Br]^{3-}$ complex.

Rh-Sn isotopologue	**$\delta(^{119}Sn)$ /ppm**	**$^1J(^{103}Rh\text{-}^{119}Sn)$ /Hz**	**$^2J(^{117}Sn\text{-}^{119}Sn)$ /Hz**
Isotopomer: Observed $^{119}SnBr_3^-$ ligand *trans* to $SnBr_3^-$, *cis* to Br^-			
$[^{103}Rh(^{i}SnBr_3)_4(^{119}SnBr_3)Br]^{3-}$	$-324.4_{(eq)}$	$562_{(eq)}$	$^2J(^{119}Sn\text{-}^{119}Sn)_{(cis,ax\text{-}eq)} = 2060$
$[^{103}Rh(^{i}SnBr_3)_3(^{119}SnBr_3)_2Br]^{3-}$	$-324.4_{(eq)}$	$562_{(eq)}$	
$[^{103}Rh(^{i}SnBr_3)_3(^{119}SnBr_3)(^{117}SnBr_3)Br]^{3-}$	$-324.4_{(eq)}$	$562_{(eq)}$	$1970_{(cis,ax\text{-}eq)}$
Isotopomer: Observed $^{119}SnBr_3^-$ ligand *cis* to $SnBr_3^-$, *trans* to Br^-			
$[^{103}Rh(^{i}SnBr_3)_4(^{119}SnBr_3)Br]^{3-}$	$-267.6_{(ax)}$	$523_{(ax)}$	$^2J(^{119}Sn\text{-}^{119}Sn)_{(cis,eq\text{-}ax)} = 2060$
$[^{103}Rh(^{i}SnBr_3)_3(^{119}SnBr_3)_2Br]^{3-}$	$-267.6_{(ax)}$	$523_{(ax)}$	
$[^{103}Rh(^{i}SnBr_3)_3(^{119}SnBr_3)(^{117}SnBr_3)Br]^{3-}$	$-267.6_{(ax)}$	$523_{(ax)}$	$1970_{(cis,eq\text{-}ax)}$

The ^{119}Sn NMR parameters of the $[Rh(SnCl_3)_nCl_{6-n}]^{3-}$ (n = 1 – 6) and the $[Rh(SnBr_3)_nBr_{6-n}]^{3-}$ (n = 3 – 5) complexes are compared in Table 4.4.

Table 4.4 Comparison between the ^{119}Sn NMR parameters of the $[Rh(SnCl_3)_nCl_{6-n}]^{3-}$ (n = 1 – 6) and the $[Rh(SnBr_3)_nBr_{6-n}]^{3-}$ (n = 3 – 5) species observed in acidic aqueous solutions and assignments of respective Rh-Sn *isotopologues*

	Rigid Rh-Sn Complexes	**δ(^{119}Sn)/ ppm**		**^{1}J(^{103}Rh-^{119}Sn)/ Hz** [b]		**Rh-Sn isotopologue**	**^{2}J(^{117}Sn-^{119}Sn)/ Hz**	
		X = Cl	X = Br	X = Cl	X = Br		X = Cl	X = Br
3	*fac*-$[Rh(SnX_3)_3X_3]^{3-}$ *trans* to X^-	-411.3	-407.2	716	659	$[^{103}Rh(^{i}SnX_3)_2(^{119}SnX_3)X_2]^{3-}$ $[^{103}Rh(^{i}SnX_3)_1(^{119}SnX_3)(^{117}SnX_3)X_2]^{3-}$	[a] - 2817$_{(cis)}$	- 1960$_{(cis)}$
4a	*cis*-$[Rh(SnX_3)_4X_2]^{3-}$ equatorial (*trans* to X^-)	-275.2	-354.7	664	630	$[^{103}Rh(^{i}SnX_3)_3(^{119}SnX_3)X_2]^{3-}$ $[^{103}Rh(^{i}SnX_3)_2(^{119}SnX_3)_2X_2]^{3-}$ $[^{103}Rh(^{i}SnX_3)_2(^{119}SnX_3)(^{117}SnX_3)X_2]^{3-}$	[a] - 2240 2455$_{(cis,eq\text{-}eq)}$ 2143$_{(cis,ax\text{-}eq)}$	- 1650 1674$_{(cis,eq\text{-}eq)}$ 1578$_{(cis,ax\text{-}eq)}$
4b	*cis*-$[Rh(SnX_3)_4X_2]^{3-}$ axial (*cis* to X^-)	-202.5	-331.7	589	553	$[^{103}Rh(^{i}SnX_3)_3(^{119}SnX_3)X_2]^{3-}$ $[^{103}Rh(^{i}SnX_3)_2(^{119}SnX_3)_2X_2]^{3-}$ $[^{103}Rh(^{i}SnX_3)_2(^{119}SnX_3)(^{117}SnX_3)X_2]^{3-}$	- [a] 2240 2140$_{(cis,eq\text{-}ax)}$	 1650 1576
5a	$[Rh(SnX_3)_5X]^{3-}$ axial (*trans* to Cl^-)	-146.2	-267.6	627	523	$[^{103}Rh(^{i}SnX_3)_4(^{119}SnX_3)X]^{3-}$ $[^{103}Rh(^{i}SnX_3)_3(^{119}SnX_3)_2Cl]^{3-}$ $[^{103}Rh(^{i}SnX_3)_3(^{119}SnX_3)(^{117}SnX_3)X]^{3-}$	- [a] 1963 1883$_{(cis,eq\text{-}ax)}$	- 2060 1970 $_{(cis,eq\text{-}ax)}$
5b	$[Rh(SnX_3)_5X]^{3-}$ equatorial (*cis* to X^-)	-98.3	-324.4	555	562	$[^{103}Rh(^{i}SnX_3)_4(^{119}SnX_3)X]^{3-}$ $[^{103}Rh(^{i}SnX_3)_3(^{119}SnX_3)_2X]^{3-}$ $[^{103}Rh(^{i}SnX_3)_3(^{119}SnX_3)(^{117}SnX_3)X]^{3-}$	- [a] 1962 1883$_{(cis,ax\text{-}eq)}$	- 2060 1970 $_{(cis,eq\text{-}ax)}$
6	$[Rh(SnX_3)_6]^{3-}$	-36.1	-	518	-	$[^{103}Rh(^{i}SnX_3)_5(^{119}SnX_3)X]^{3-}$ $[^{103}Rh(^{i}SnX_3)_4(^{119}SnX_3)(^{117}SnX_3)X]^{3-}$	[a] - 1650$_{cis}$ 22 600$_{trans}$	
7	$[Rh(SnX_3)_5]^{4-}$	9.4	-	809		$[^{103}Rh(^{i}SnX_3)_n(^{119}SnX_3)_{4-n}]^{4-}$ $[^{103}Rh(^{i}SnX_3)_n(^{119}SnX_3)_{3-n}(^{117}SnCl_3)X]^{3-}$	- [a] 3624	

[a] For these *isotopologues* there are no $^{117}SnCl_3^-$ to which ^{119}Sn can couple, thus no ^{2}J(^{117}Sn-^{119}Sn) couplings are observed. [b] All *isotopologues* of respective species have the same ^{1}J(^{103}Rh-^{119}Sn) value.

4.3 Conclusion

Investigation of the stannous bromide complexes of rhodium(I/III) in acidic solution furnished the assignment of 3 new $[Rh^{III}(SnBr_3)_nBr_{6-n}]^{3-}$ (n = 3 – 5) species that has never been reported before, listed in Tables 4.1 to 4.3. Moreover, the distinctive *isotopomer* pairs of these complex anions were assigned. It is thus established that these species, as with the analogous chlorido species, are kinetically inert and do not undergo rapid *intra-* or *inter-*molecular exchange on the NMR time-scale. In contrast to the $[Rh^{I}(SnCl_3)_5]^{4-}$ species, no clear evidence of a similar $[Rh^{I}(SnBr_3)_5]^{4-}$ species could be found.

In Chapter III it was shown for the series of $[Rh(SnCl_3)_nCl_{6-n}]^{3-}$ (n = 1 – 6) species that the ^{119}Sn NMR signals becomes less shielded as 'n' increases which results in a downfield shift of the signals. A similar trend is observed for the $[Rh(SnBr_3)_nBr_{6-n}]^{3-}$ (n = 3 – 5) species. However, the difference between the $\delta(^{119}Sn)$ of the species are smaller than was observed with the chlorido species, which suggests that the observed ^{119}Sn nucleus is less influenced by changes in the bromido species than in the chlorido species. Moreover, the $^{1}J(^{103}Rh\text{-}^{119}Sn)$ coupling constant of the species listed in Table 4.4 are smaller for the bromido species than the chlorido species. This is in agreement with what was previously reported for the $[Pt(SnX_3)_5]^{3-}$ (X = Cl-, Br^-) species.[59] This suggests that the interaction between the ^{103}Rh and a $SnBr_3^-$ ligand is weaker than that between the ^{103}Rh and a $SnCl_3^-$ ligand. Unfortunately the peaks indicated with '?' in Figure 4.3 have not been assignable at this time.

Chapter V

Stannous chloride complexes of rhodium(I/III) extracted into non-aqueous solutions such as chloroform with AQ336 and methyl isobutyl ketone

Chapter V

Stannous chloride complexes of rhodium(I/III) extracted into non-aqueous solutions such as chloroform with AQ336 and methyl isobutyl ketone

5.1 Introduction

The importance of finding effective separation processes for the recovery of PGMs from diverse secondary resources is an ever growing industry, partly due to the natural resources of these metals being highly localized but also due to their greater use globally. The extraction of rhodium from hydrochloric acid solutions into an organic phase is a difficult process and few quantitative direct extraction methods of rhodium have been achieved. It has, however, been shown by various studies that with the addition of tin(II) chloride to the aqueous phase containing rhodium, the extraction of rhodium is greatly enhanced. Indeed this process could presumably have been used in the discovery of rhodium by Wollaston in the early 19th century.[1]

Koch *et. al.*[104,105] studied the extraction of rhodium with flexible polyurethane foams and found that rhodium(III)chlorides itself are not extracted from hydrochloric acid solutions, but in the presence of increasing quantities of tin(II) chloride a red complex is rapidly absorbed into the foam. Moreover, it was shown that almost quantitative separation of rhodium and iridium could be achieved by selective absorbtion of the chloro(trichlorostannato)-rhodium(III/I) complex anions by the polyurethane foam.[104,105] This is probably due to the fact that the corresponding chloro(trichlorostannato)iridium species do not form at room temperature so preventing the absorbtion of iridium by the polyurethane foam. The polyurethane immobilized chloro(trichlorostannato)rhodium(III/I) compounds may be readily stripped from the polyurethane foam with hot (60 °C) 2.5 – 5.0 % (v/v) concentrated HCl in ethanol, giving quantitative recovery of the noble metal.[105] However, with the Rh-Sn species sorbed into the solid polyurethane foam, the composition and structure of the Rh-Sn species was not established as shown in previous chapters and the literature. ^{119}Sn NMR spectroscopy has proven to be an indispensible tool for the characterization of such Rh-Sn species.

As part of an early study of the liquid-liquid extraction of PGMs in the presence of tin(II) chloride, Koch and Wyrley-Birch[98] investigated the extraction of rhodium with 4-methyl isobutyl ketone (MIBK) from aqueous hydrochloric acid solutions of various concentrations by means of ^{119}Sn NMR spectroscopy. At least seven sets of ^{119}Sn signals due to (Rh-$SnCl_3$) complexes were observed under various conditions, three of which could be assigned based on good agreement with those observed in 2 – 6 M HCl solutions by Moriyama *et. al.*[41] In a 2 M HCl solution containing rhodium(III) chloride and tin(II) chloride with a mole ratio of 1:5-6 and extracted into MIBK, a colour change from purple-red (aqueous) to pale yellow-orange (organic) was reported.

The ^{119}Sn NMR spectrum recorded for the bright yellow MIBK extract displayed only one predominant species ($\delta(^{119}Sn)$ = -14.6 ppm, $^{1}J(^{103}Rh\text{-}^{119}Sn)$ = 600 Hz, $^{2}J(^{117}Sn\text{-}^{119}Sn)$ = 1927 Hz and $^{2}J(^{1}H\text{-}^{119}Sn)$ = 57 Hz) assigned to the $[Rh^{III}H(SnCl_3)_4Cl]^{3-}$ complex anion based on the I(satellites)/I(main) ratio of 12.9 % measured which corresponded well with the statistically expected value of 12.3 %. Moreover, it was proposed that this hydrido Rh-Sn species is formed by oxidative addition of co-extracted HCl in MIBK to the red trichlorostannato-rhodium(I) anion, $[Rh^{I}(SnCl_3)_5]^{4-}$, in the MIBK phase, as no evidence of the yellow species in the aqueous phase prior/after extraction was found. On the other hand, during their study of the photo-enhanced catalytic dehydrogenation of propan-2-ol with rhodium-tin complexes, Saito *et. al.*[41,106,107] recorded a similar ^{119}Sn NMR spectrum (for the yellow solution obtained when mixing $RhCl_3 \cdot 3H_2O$, $SnCl_2 \cdot 2H_2O$, propan-2-ol and 3 M HCl) to the one reported by Koch and Wyrley-Birch.[98] However, Saito *et. al.*[107] assigned the set of signals at $\delta(^{119}Sn)$ = -14.6 ppm to the $[RhH(SnCl_3)_5]^{3-}$ complex anion. More specifically, the set of signals at $\delta(^{119}Sn)$ = -14.6 ppm was assigned to the $[Rh^{III}H(SnCl_3)_5]^{4-}$ complex anion where the observed ^{119}Sn nucleus is in the equatorial position.

In addition, a set of signals at $\delta(^{119}Sn)$ = 78.4 ppm, assigned to the axial $[Rh^{III}H(SnCl_3)_5]^{4-}$ complex anion, was reported.[107] These results thus suggest that the assignment made by Wyrley-Birch[98] may have been incorrect. In a subsequent ^{119}Sn NMR study by Koch and Hall,[8] a quaternary ammonium liquid anion exchanger, trioctylmethylammonium chloride (AQ-336) in chloroform was used to extract Rh-Sn complexes of the type $[Rh(SnCl_3)_nCl_{6-n}]^{3-}$ (n = 1 – 5) from hydrochloric acid solutions. Upon extraction of a Rh(III)chloride species in 0.5 M HCl solution with a Rh:Sn 1:10 mole ratio, the predominant species extracted into the

organic phase was assigned to presumably a Rh^{I} complex species, the deep red $[Rh(SnCl_3)_5]^{4-}$ complex anion. Moreover by either adding CF_3COOH directly to the organic phase or by increasing the HCl concentration of the aqueous phase to 5 M prior to extraction, a rapid colour change from purple-red to yellow was reported.[8] This yellow species at $\delta(^{119}Sn)_{eq}$ = -14.1 ppm and $\delta(^{119}Sn)_{ax}$ = 78.7 ppm relative to tetramethyltin at $\delta(^{119}Sn)$ = 0.0 ppm, was assigned to the $[Rh^{III}H(SnCl_3)_5]^{3-}$ complex anion by comparing the ^{119}Sn NMR parameters with the simulated parameters as obtained in the paper.[8] When the Rh^{III}-$SnCl_3^-$ complexes were extracted from strongly acidic solutions, 5 M HCl, into MIBK, a additional species with $\delta(^{119}Sn)$ at -92.5 ppm was reported, tentatively assigned to another possible hydride complex, $[RhH(SnCl_3)_4Cl]_3^-$. Due to the low concentration of this species however, it was not unambiguously assigned.

A liquid-liquid extraction study of rhodium(III) in the presence of tin(II) chloride using a 7-substituted hydroxyquinoline reagent, which is commonly used in the metallurgical industry, Kelex100 (7-(4-ethyl-1-methylocty)-8-hydroxyquinoline), Benguerel *et. al.*[108,109] reported that although very high distribution coefficients (> 100) were rapidly achieved for a single extraction for less than one minute contact time in an aqueous solution of Sn:Rh ≥ 2:1, the stripping of the rhodium from the organic phase with 1.7 M H_2SO_4 was only effective when Sn:Rh ≥ 6 :1 mole ratio was used. ^{119}Sn NMR spectroscopy was used to investigate the speciation in both the aqueous and the organic phases where the feed solutions contained a rhodium to tin mole ratio of either 1:3 or 1:12. In the former solution only one ^{119}Sn NMR signal assigned to $[Rh^{III}(SnCl_3)Cl_3]^{3-}$, was observed in both the aqueous and the organic phases. In contrast, there were some differences in the ^{119}Sn NMR spectra recorded for the aqueous feed solution with a Rh:Sn mole ratio of 1:12 and the corresponding organic phase. The ^{119}Sn NMR spectrum of the aqueous phase showed a doublet at $\delta(^{119}Sn)$ = 4.2 ppm ($^1J(^{103}Rh\text{-}^{119}Sn)$ = 811 Hz) assigned to the $[Rh^{I}(SnCl_3)_5]^{4-}$ complex anion. The ^{119}Sn NMR spectrum of the organic solution showed a doublet at $\delta(^{119}Sn)$ = - 9.1 ppm ($^1J(^{103}Rh\text{-}^{119}Sn)$ = 620 Hz). Dispite the large shift in peak position ($\Delta\delta(^{119}Sn$ = 13.3 ppm) and a difference of 191 Hz for the $^1J(^{103}Rh\text{-}^{119}Sn)$ coupling constant, this species was also assigned to the $[Rh(SnCl_3)_5]^{4-}$ complex anion.[109] The difference in $\delta(^{119}Sn)$ and $^1J(^{103}Rh\text{-}^{119}Sn)$ parameters were simply ascribed to the significantly different solvent environments and polarity of the aqueous phase *versus* the organic phase. Based on these results and assignments Benguerel *et. al.*[108,109] concluded that the oxidative addition of HCl, as reported by Koch *et. al.*[98] did not

occur in this extraction system. However, the assignment made by Benguerel *et. al.*[108,109] for the species at $\delta(^{119}Sn)$ = - 9.1 ppm in the organic phase and the justification of thereof does not seem reasonable and are at best questionable. Moreover, the chemical shift and $^{1}J(^{103}Rh\text{-}^{119}Sn)$ values obtained for the Rh-Sn species in the organic phase correlates very well to the values reported for the hydride Rh-Sn species by Koch *et. al.*[98] It is therefore reasonable to suggest that Benguerel *et. al.*[108,109] did not correctly assign these complexes.

Cyanex925, an organophosphine compound, has also been used to extract the Rh-Sn complexes into organic phases[110] which was shown to be useful for the separation of Rh(III) from Pt(IV) and Pd(II) as the order of extraction was found to be Pt > Rh and negligible in the case of Pd(II). Similarly, Sun and Lee[111] reported the use of Alamine336 and tri-butyl phosphate (TBP) as extractants to separate rhodium from iridium in the presence of tin(II) chloride. Addition of tin(II) chloride to hydrochloric acid solutions containing both iridium and rhodium surpressed the extraction of Ir whilst the extraction of Rh was promoted. However, the authors[111] were only interested in the concentration of the metal in the aqueous and organic phases (as determined by ICP-OES) and did not identify and characterize the Rh-$SnCl_3$ species extracted by either Alamine336 or TBP. It was suggested that the extraction reaction of the Rh-Sn species with TBP can be presented as:

$$[Rh_2Cl_{6-n}(SnCl_3)_n]^{4-}\,(aq) + 4(TBP\cdot HCl)\,(org) = (TBPH)_4[Rh_2Cl_{6-n}(SnCl_3)_n]^{4-}\,(org) + 4Cl^-$$

However, no evidence was given for the existence of the $[Rh_2Cl_{6-n}(SnCl_3)_n]^{4-}$ species. In contrast, it has been shown in literature[28,29,32,33,41] that a binuclear Rh-Sn species, such as the one proposed, does not exist is solution. Therefore the suggested extraction reaction as given above is questionable and it is much more likely that it is the $[Rh(SnCl_3)_5]^{4-}$ species that is being extracted as a Rh:Sn 1:10 mole ratio was used.

Okamoto *et. al.*[112] was the first group to report a detailed X-ray absorption fine structure (XAFS) study for these Rh-Sn species. They studied the extractability of Rh and Sn by solvent extraction methods using N,N-dioctyl hexanamide (DOHA). The change in the valences and local structures of Rh, in both the aqueous and the organic phases, were measured by means of XAFS. It was reported that rhodium was highly extractable from

solutions with various HCl concentrations (ranging from 1 to 10.5 M) when the Rh to Sn mole ratio was 1 to 12. Moreover, from the Rh K-edge XAFS measurements for Rh in 1 M HCl solution it was confirmed that the $[Rh^{III}Cl_5(H_2O)]^{2-}$ complex anion was reduced to the $[Rh^{I}(SnCl_3)_5]^{4-}$ complex anion with addition of excess tin(II) chloride.[112] The coordination number of Rh-Sn in this complex anion was reported to be 5.3(6) with a bond distance of 2.54(1) Å. The XAFS measurements of the corresponding DOHA complex also revealed that the $[Rh^{I}(SnCl_3)_5]^{4-}$ complex anion predominates in the organic phase. The coordination number of Rh-Sn in this complex anion was reported to be 4.7(8) with a bond distance of 2.56(1) Å. It is thus shown that in the presence of excess tin(II) chloride, the $[Rh^{I}(SnCl_3)_5]^{4-}$ species are predominant in both the aqueous and organic phases. Thus, as the Rh-Sn species did no undergo any structural changes on extraction with DOHA, the Rh-Sn species is extracted by an anion-exchange mechanism.

These studies show that the extraction of rhodium(III/I) from acidic HCl solutions into an organic phase can be greatly increased by the addition of tin(II) chloride to the aqueous phase using various different organic extractants. The 8-hydroxyquinoline,[108,109] Alamine336[111] and DOHA[112] acts as anion exchangers, i.e. it is protonated by HCl + Lig $\leftrightarrow$LigH$^+$ + Cl$^-$ and this behaves just like Aliquat336 used in this work, whereas TBP is similar to MIBK which is also used in this work. Although the extraction of the series of $[Rh^{III}(SnCl_3)_nCl_{6-n}]^{3-}$ (n = 1 – 5) and $[Rh^{I}(SnCl_3)_5]^{4-}$ complex anions, as well as the formation of the $[Rh^{III}H(SnCl_3)_5]^{3-}$, has been well documented,[8,98,104,105] there are some uncertainty about the exact nature of the species in the respective organic phases.[108-112] Moreover, the $[Rh^{III}(SnCl_3)_nCl_{6-n}]^{3-}$ (n = 1 – 5) complex anions were until now thought to be kinetically labile, however, in Chapter 3 of this thesis it was unambiguously proven that these species are kinetically inert and several new species were assigned. In light of this, the speciation of the Rh(III/I)-Sn(II) species extracted into organic phases was reinvestigated and is discussed below. Chapter V focuses on the extraction of the series of $[Rh(SnCl_3)_nCl_{6-n}]^{3-}$ (n = 1 – 5) and $[Rh(SnCl_3)_5]^{4-}$ complex anions using (1) MIBK and (2) AQ-336 in chloroform. In addition the speciation of the Rh-Sn complex anions in propan-2-ol is discussed.

5.2 Results and Discussion

5.2.1 ^{119}Sn NMR of Rh-Sn complexes extracted into methyl-isobutyl-ketone

A 0.1 M rhodium-tin solution with a Rh:Sn ratio of 1:10 was prepared by dissolving 0.1803 g $SnCl_2$ (anhydrous) in 0.6 mL conc. HCl and after the initially formed cloudiness (due to hydrolysis products) had disappeared the required amount of $RhCl_3 \cdot 3H_2O$ was added to the solution. The solution was diluted to 1 mL to obtain a final HCl concentration of 6 M and was left to equilibrate overnight. Methyl-isobutyl-ketone (MIBK) was added to the resulting deep purple solution, indicative of the formation of the $[Rh(SnCl_3)_5]^{4-}$ species, in a 1:1 volume:volume ratio and was stirred for 30 minutes. During the extraction, the aqueous phase went colourless whilst the organic, MIBK phase turned bright yellow. The ^{119}Sn NMR spectrum recorded for the bright yellow solution is shown in Figure 5.1.

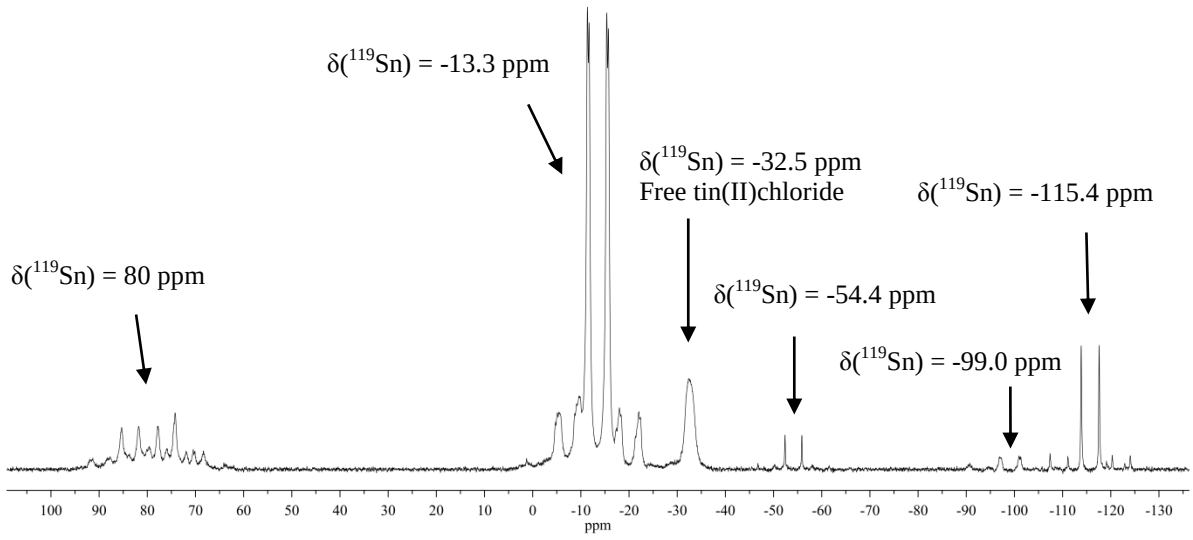

Figure 5.1 ^{119}Sn NMR spectrum of the $[RhH(SnCl_3)_5]^{3-}$ species that was extracted into methyl isobutylketone (MIBK) from an aqueous solution containing $[Rh(SnCl_3)_5]^{4-}$ at 25 °C.

The ^{119}Sn NMR spectrum shown in Figure 5.1 consists of six sets of signals at δ(^{119}Sn) = 80, -13.3, -32.5, -54.4, -99.0 and -115.4 ppm, each flanked by its respective ^{2}($^{117/119}$Sn-^{119}Sn) satellites. The chemical shift values of the species observed in Figure 5.1 are comparable to the findings of Koch *et. al.*[98] for similar solutions as listed in Table 5.1.

Table 5.1 ^{119}Sn NMR parameters and assignments reported by Koch *et. al.*[98] for MIBK solution.*

Rh-Sn complex	δ(^{119}Sn)/ppm	^{1}J(^{103}Rh-^{119}Sn)/Hz	^{2}J(^{117}Sn-^{119}Sn)/Hz	^{2}J(^{1}H-^{119}Sn)/Hz
$[RhH(SnCl_3)_4Cl]^{3-}$	-13.3 (-14.6)	600 (600)	1900 (1927)	57 (57)
Unassigned#	-54.4 (-54.7)	520 (522)	1670 (1691)	-
$[Rh(SnCl_3)_5Cl]^{3-}$	-115.4 (-117.5)	567 (558)	1930 (1943)	-
$[Rh(SnCl_3)_3Cl_3]^{3-}$	(-370.0)	(732)	(3023)	-
Sn(IV) species	(-640.2)	-	-	-

* The values in parenthesis are the experimental values reported in litaruter. # This species is tentatively proposed to be formulated as $[Rh^{III}(SnCl_3)_5X]^{3-}$ in which a solvent molecule, X, loosely occupies a vacant coordination site (see text).

5.2.1.1 Spectral section of resonances at δ(^{119}Sn) = -13.3 ppm and 80.0 ppm

Yamakawa *et. al.*[113] assigned the species at both δ(^{119}Sn) = -13.7 ppm and 77.58 ppm to the $[RhH(SnCl_3)_5]^{3-}$ species. The signals at δ(^{119}Sn) = -13.7 ppm were assigned to the *isotopomer* in which the observed ^{119}Sn nucleus is in the equatorial position, *trans* to another $SnCl_3^-$ ligand, and the signals at δ(^{119}Sn) = 77.58 ppm to the *isotopomer* in which the observed ^{119}Sn nucleus is in the axial, *trans* to ^{1}H, position. The ^{119}Sn NMR parameters of the species observed at δ(^{119}Sn) = -13.3 and 80.0 ppm in Figure 5.2 agree well with the values reported by Koch and Hall[8] and Yamakawa *et. al.*[113]

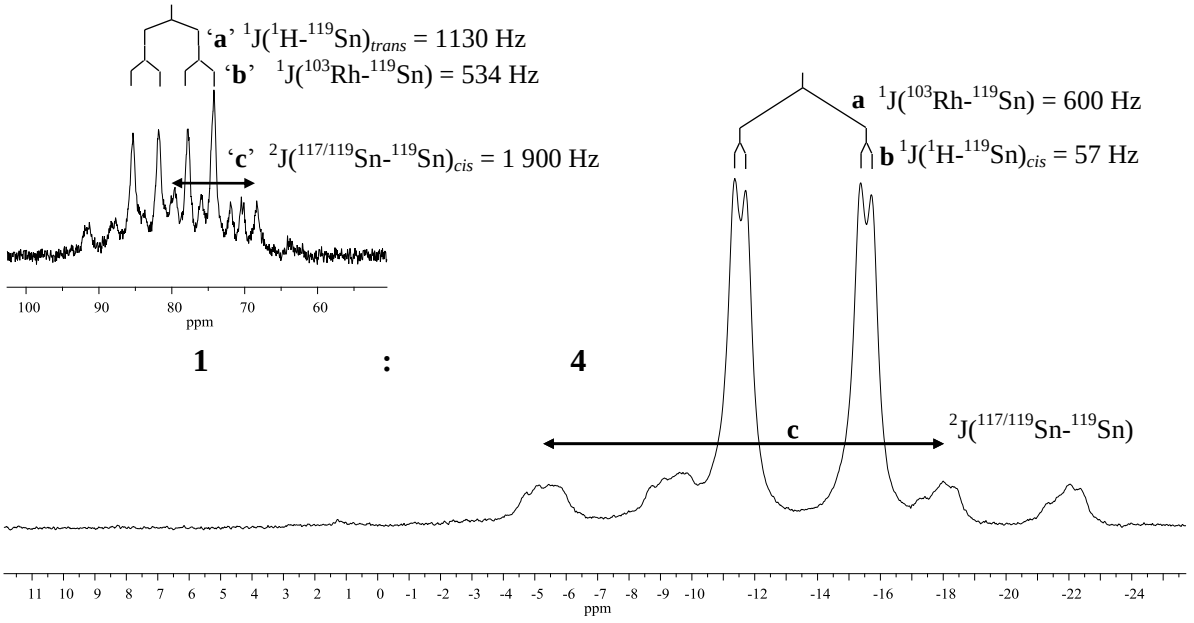

Figure 5.2 The expanded ^{119}Sn NMR spectra of the sets of signals at -13.3 ppm and 80 ppm. The ^{1}J(^{1}H-^{119}Sn)$_{cis}$ and ^{1}J(^{1}H-^{119}Sn)$_{trans}$ spin couplings are indicated by symbols a and 'a' respectively. The ^{1}J(^{103}Rh-^{119}Sn) spin couplings are indicated by the symbols b and 'b' and the ^{2}J($^{119/117}$Sn-^{119}Sn) spin couplings are indicated by the symbols c and 'c'. The relative integrals of the respective peaks are 1 to 4.

The set of signals at -13.3 ppm is split into a doublet due to $^{2}J(^{103}Rh\text{-}^{119}Sn)$ spin coupling with a coupling constant of 600 Hz and is further split into a doublet of doublets with a coupling constant of $^{2}J(^{1}H\text{-}^{119}Sn)$ = 57 Hz as illustrated by symbols **a** and **b** in Figure 5., respectively. Unfortunately, the $^{2}J(^{117/119}Sn\text{-}^{119}Sn)_{cis}$ satellites observed for this species are broad, possibly due to dynamic processes, with an average coupling constant of 1900 Hz, indicated by the symbol **c** in Figure 5., making the measurement of individual sets of satellites difficult. Similarly, the $^{2}J(^{117/119}Sn\text{-}^{119}Sn)_{cis}$ satellites observed for the signals at 80.0 ppm are broad and ill-defined. To assist with the assignment of the satellites, the ^{119}Sn NMR spectrum of the species at -13.3 ppm and 80.0 ppm was simulated with gNMR50 using the ^{119}Sn NMR parameters given in Figure 5.3. Previously, Hall *et. al.*[8] reported a $^{2}J(^{117}Sn\text{-}^{119}Sn)_{trans,eq\text{-}eq}$ coupling with a coupling constant of 25344 Hz for the $[Rh(H(SnCl_3)_5]^{3-}$ complex anion in MIBK, illustrated in Scheme 5.1A.

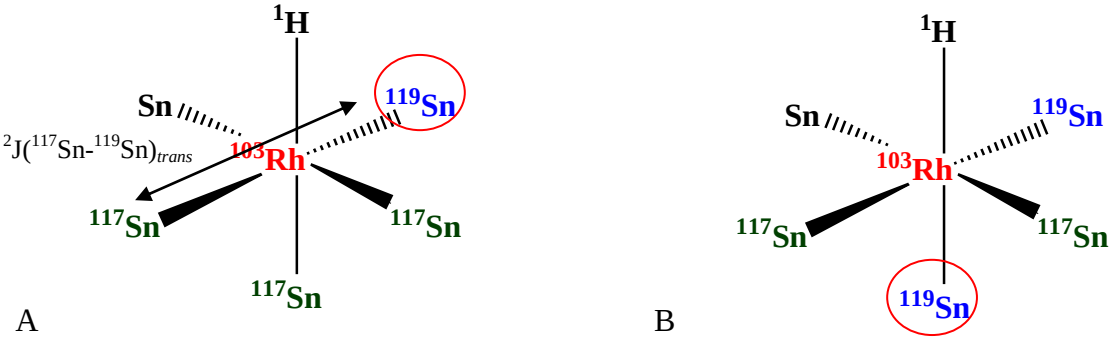

Scheme 5.1 Schematic representation of two *isotopomers* and *isotopologues* of the $[RhH(SnCl_3)_5]^{3-}$ species. The observed ^{119}Sn nucleus is encircled. All Cl^- ligands of the $SnCl_3^-$ ligand are left out for clarity.

Due to a possible overlap of the ^{119}Sn signals of the $[RhH(SnCl_3)_5]^{3-}$ species with the observed $^{119}SnCl_3^-$ *trans* to ^{1}H and the $^{2}J(^{117}Sn\text{-}^{119}Sn)_{trans,eq\text{-}eq}$ satellites of the species at $\delta(^{119}Sn)$ = -13.3 ppm, it was difficult to identify the $^{2}J(^{117}Sn\text{-}^{119}Sn)_{trans,eq\text{-}eq}$ satellites. Therefore the magnitude of the coupling constant reported for the $^{2}J(^{117}Sn\text{-}^{119}Sn)_{trans,eq\text{-}eq}$ satellites by Hall *et. al.*,[8] 25334 Hz, was used to simulate the $^{2}J(^{117}Sn\text{-}^{119}Sn)_{trans,eq\text{-}eq}$ satellites in the ^{119}Sn spectrum of the $[RhH(SnCl_3)_5]^{3-}$ species. However, this value proved to be too small and was increased to 25 600 Hz. The re-simulated ^{119}Sn NMR spectrum is shown in Figure 5.3B and compares well to the experimental ^{119}Sn NMR spectrum recorded, shown in Figure 5.3A. The good correlation obtained between the two spectra allows for the assignment of the sets of signals at $\delta(^{119}Sn)$ = 71.8 and -99.0 ppm to the $^{2}J(^{117}Sn\text{-}^{119}Sn)_{trans,eq\text{-}eq}$ satellites of the $[RhH(SnCl_3)_5]^{3-}$ *isotopomer* shown in Scheme 5.1A.

Furthermore, the $^{1}J(^{103}Rh\text{-}^{119}Sn)$ coupling constant measured for the set of signals at $\delta(^{119}Sn)$ = -99.0 ppm is 600 Hz which is identical to that of the main set of signals. This confirms the assignment of these signals to the $^{2}J(^{117}Sn\text{-}^{119}Sn)_{trans,eq\text{-}eq}$ = 25 600 Hz satellites of the $[RhH(SnCl_3)_5]^{3-}$ (eq) complex anion.

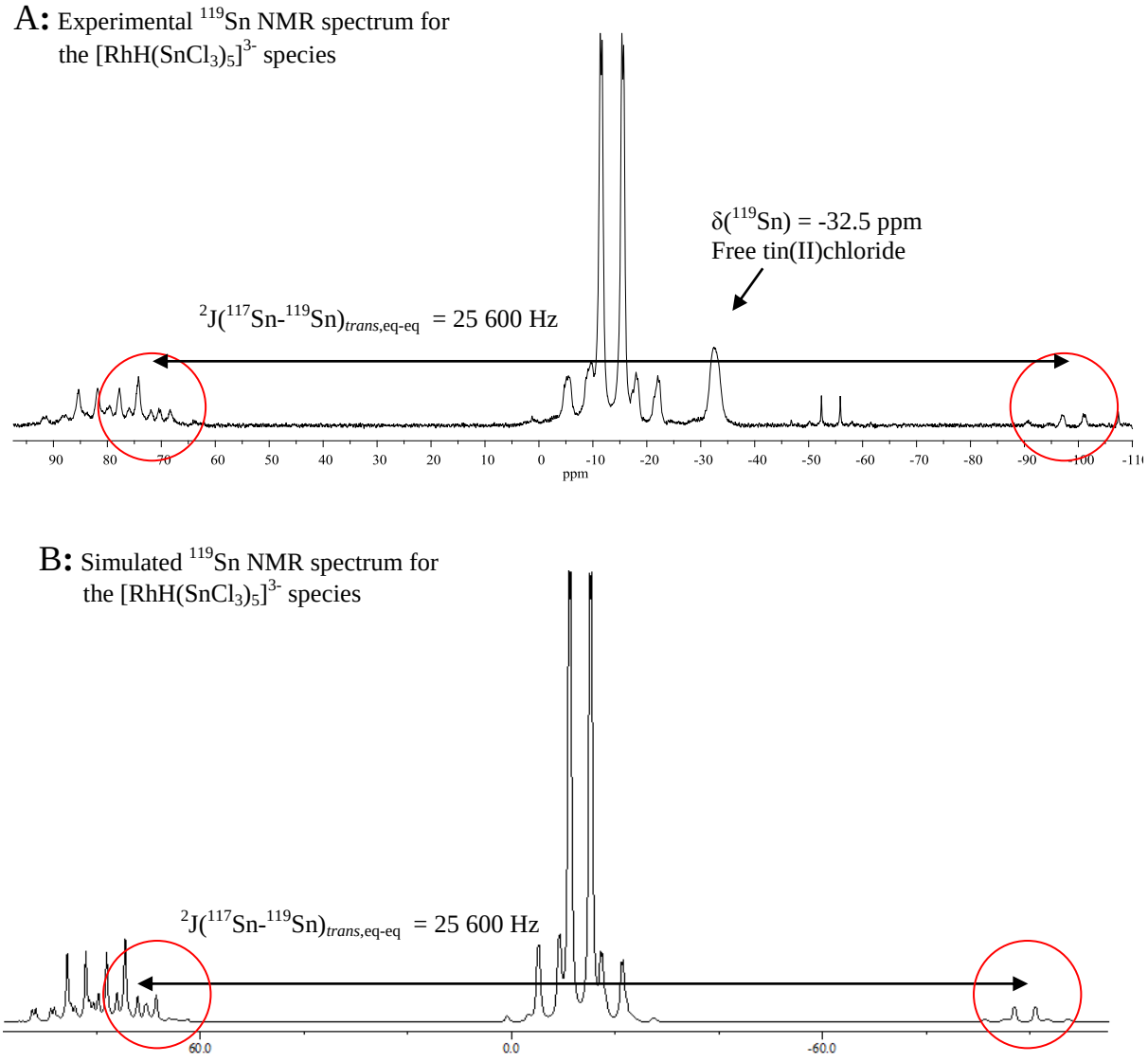

Figure 5.3 The ^{119}Sn NMR spectra of the sets of signals at -13.3 ppm and 80 ppm obtained (A) experimentally and (B) simulated using gNMR50. The good correlation between the experimental and simulated spectra allowed for the assignment of the $^{2}J(^{117}Sn\text{-}^{119}Sn)_{trans,eq\text{-}eq}$ satellites of the $[RhH(SnCl_3)_5]^{3-}$ complex anion, which was complicated by the overlap of these satellites with the set of signals at $\delta(^{119}Sn)$ = 80.0 ppm assigned to the $[RhH(SnCl_3)_5]^{3-}$ *isotopomer* where the observed $^{119}SnCl_3^-$ ligand is *trans* to ^{1}H.

In order to assign the respective sets of $^{2}J(^{117/119}Sn\text{-}^{119}Sn)$ satellites of the species at $\delta(^{119}Sn)$ = -13.3 and 80.0 ppm and determine the coupling constants thereof, the width at half height ($\Delta\nu_{1/2}$) of the signals was adjusted from 70 Hz (which was experimentally obtained) to 5 Hz

using gNMR50. The expansions of the simulated sets of signals at -13.3 and 80.0 ppm are shown in Figure 5.4 A and B.

A: Simulated ^{119}Sn NMR spectrum of signals at δ(^{119}Sn) = -13.3 ppm

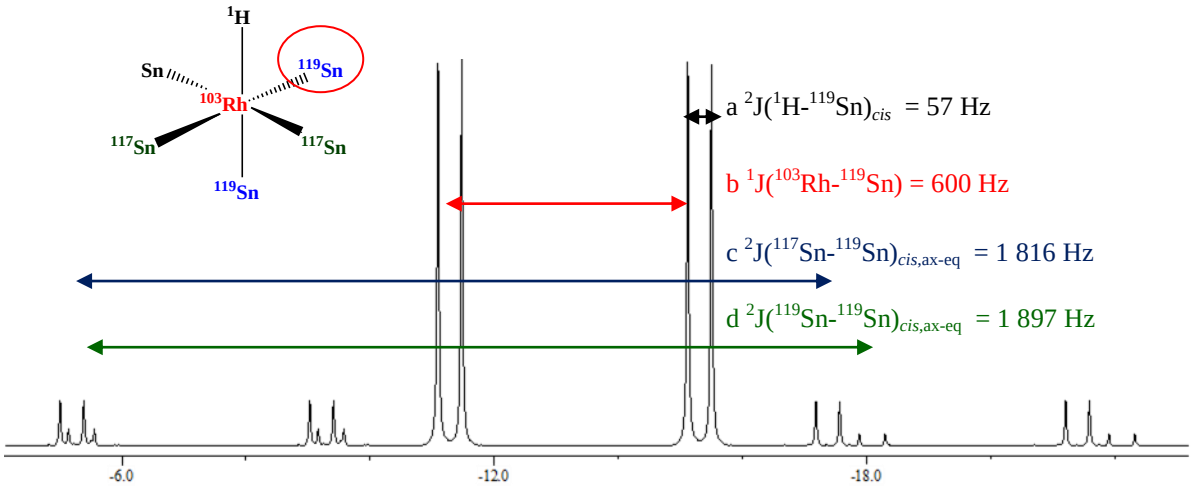

B: Simulated ^{119}Sn NMR spectrum of signals at δ(^{119}Sn) = 80.0 ppm

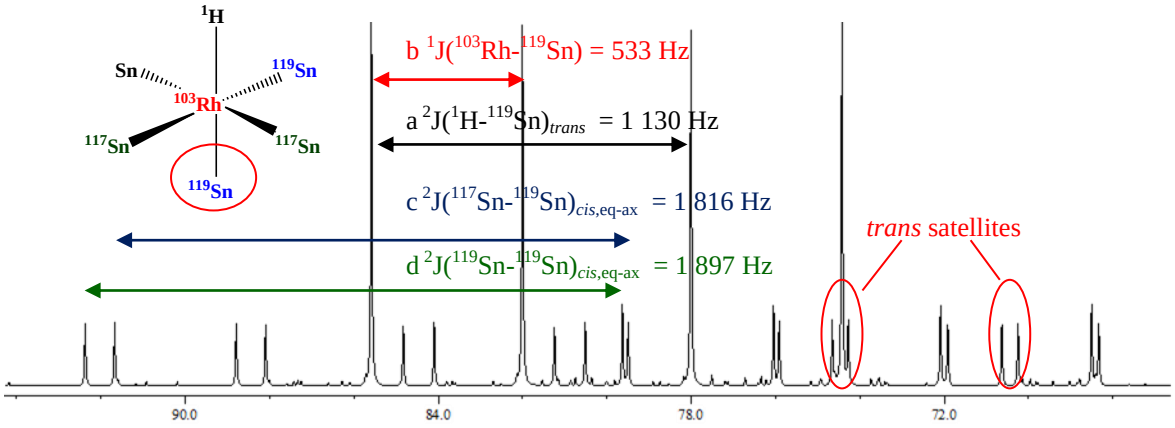

Figure 5.4 The simulated ^{119}Sn NMR spectrum of (A) the set of signals at δ(^{119}Sn) = -13.3 ppm assigned to the 'equatorial' $[RhH(SnCl_3)_5]^{3-}$ complex anion where the observed $^{119}SnCl_3$ ligand is *trans* to another $^{119}SnCl_3$ ligand and (B) the set of signals at δ(^{119}Sn) = 80.0 ppm assigned to the 'axial' $[RhH(SnCl_3)_5]^{3-}$ complex anion where the observed $^{119}SnCl_3$ ligand is *trans* to H. The width at half height of the signals was set to 5 Hz to improve the resolution of the signals in order to assign the all the respective ^{1}J and ^{2}J spin couplings, indicated by symbols **a** to **d**.

The ^{1}J(^{103}Rh-^{119}Sn) and ^{2}J(^{1}H-^{119}Sn) spin couplings for the two respective *isotopomers* of the $[Rh^{III}H(SnCl_3)_5]^{3-}$ species are indicated by the symbols **a** and **b** in Figure 5.4A and B. With the improved resolution, two sets of ^{2}J($^{117/119}$Sn-^{119}Sn)$_{cis}$, indicated by the symbols **c** (1816 Hz) and **d** (1897 Hz) in Figure 5.4A and B, are observed for both *isotopomers*. The ratio between these two sets of signals is 1897 Hz/1816 Hz = 1.045 which is equal to the ratio of the magnetogyric ratios, γ(^{119}Sn)/γ(^{117}Sn) = 1.046. This suggests that the set of signals

indicated by symbol **c** is due to $^{2}J(^{117}Sn\text{-}^{119}Sn)_{cis,eq\text{-}ax}$ spin coupling, and the set of signals indicated by symbol **d** is due to $^{2}J(^{119}Sn\text{-}^{119}Sn)_{cis,eq\text{-}ax}$ spin coupling within the $[Rh^{III}H(SnCl_3)_5]^{3-}$ species. The assignment of the axial and equatorial $[Rh^{III}H(SnCl_3)_5]^{3-}$ species, as well as its respective *isotopologues*, are summarized in Table 5.2.

Table 5.2 Summary of the ^{119}Sn NMR parameters and assignments of the Rh-Sn species extracted with MIBK.

Rh-Sn isotopologue	**$\delta(^{119}Sn)$/ ppm**	**$^{1}J(^{103}Rh\text{-}^{119}Sn)$/ Hz**	**$^{2}J(^{117/119}Sn\text{-}^{119}Sn)$/ Hz**	**$^{2}J(^{1}H\text{-}^{119}Sn)$/ Hz**
$[Rh^{III}H(SnCl_3)_5]^{3-}$				
Isotopomer: Observed $^{119}SnCl_3^-$ ligand in the axial position, *trans* to H^1				
$[^{103}Rh^{III}H(^{i}SnCl_3)_4(^{119}SnCl_3)]^{3-}$	80	533	-	$1130_{trans,ax\text{-}ax}$
$[^{103}Rh^{III}H(^{i}SnCl_3)_3(^{119}SnCl_3)_2]^{3-}$	80	533	$^{2}J(^{119}Sn\text{-}^{119}Sn)_{cis,ax\text{-}eq} = 1897$	$1130_{trans,ax\text{-}ax}$
$[^{103}Rh^{III}H(^{i}SnCl_3)_3(^{119}SnCl_3)(^{117}SnCl_3)]^{3-}$	80	553	$1816_{cis,ax\text{-}eq}$	$1130_{trans,ax\text{-}ax}$
Isotopomer: Observed $^{119}SnCl_3^-$ ligand in the equatorial position, *trans* to $SnCl_3$-				
$[^{103}Rh^{III}H(^{i}SnCl_3)_4(^{119}SnCl_3)]^{3-}$	-13.3	600	-	$57_{cis,ax\text{-}eq}$
$[^{103}Rh^{III}H(^{i}SnCl_3)_3(^{119}SnCl_3)_2]^{3-}$	-13.3	600	$^{2}J(^{119}Sn\text{-}^{119}Sn)_{cis,ax\text{-}eq} = 1897$	$57_{cis,ax\text{-}eq}$
$[^{103}Rh^{III}H(^{i}SnCl_3)_3(^{119}SnCl_3)(^{117}SnCl_3)]^{3-}$	-13.3	600	$1816_{cis,ax\text{-}eq}$ $25600_{trans,eq\text{-}eq}$	$57_{cis,ax\text{-}eq}$
$[Rh^{III}(SnCl_3)_6]^{3-}$				
$[^{103}Rh^{III}(^{i}SnCl_3)_5(^{119}SnCl_3)]^{3-}$	-54.4	520	-	-
$[^{103}Rh^{III}(^{i}SnCl_3)_4(^{119}SnCl_3)_2]^{3-}$	-54.4	520	-	-
$[^{103}Rh^{III}(^{i}SnCl_3)_4(^{119}SnCl_3)(^{117}SnCl_3)]^{3-}$	-54.4	520	1670_{cis}	-
$[Rh^{III}(SnCl_3)_5Cl]^{3-}$				
$[^{103}Rh^{III}(^{i}SnCl_3)_4(^{119}SnCl_3)Cl]^{3-}$	$-115.4_{(eq)}$	$567_{(eq)}$	-	-
$[^{103}Rh^{III}(^{i}SnCl_3)_3(^{119}SnCl_3)_2Cl]^{3-}$	$-115.4_{(eq)}$	$567_{(eq)}$	$^{2}J(^{119}Sn\text{-}^{119}Sn)_{(cis,ax\text{-}eq)} = 1775$	-
$[^{103}Rh^{III}(^{i}SnCl_3)_3(^{119}SnCl_3)(^{117}SnCl_3)Cl]^{3-}$	$-115.4_{(eq)}$	$567_{(eq)}$	$1930_{(cis,ax\text{-}eq)}$	-

5.2.1.1.a Characterization of $[RhH(SnCl_3)_5]^{3-}$ in MIBK with ^{1}H and 2D HMQC NMR

Obtaining the ^{103}Rh NMR spectra of these species should be possible, however ^{103}Rh NMR spectroscopy has long been considered difficult due to the low gyromagnetic ratio of the nucleus (Ξ = 3.16 MHz)[14] and the experimental aspects thereof tend to be tedious as large volumes of sample, high concentrations and long recording times are required. Moreover, the

chemical shift of Rh-Sn species of this nature has never been reported before and with the wide chemical shift range of ^{103}Rh (15 000 Hz) it will be like looking for a needle in a hay stack, and as mentioned, with the long acquisition times required, this can become a cumbersome venture. Fortunately, the hydrido species, $[Rh^{III}H(SnCl_3)_5]^{3-}$, contains both ^{103}Rh and ^{1}H nuclei, in addition to the ^{119}Sn nucleus, which makes 2D NMR spectroscopy possible. Moreover, when a rhodium-bound proton is used for the detection of ^{103}Rh an enhancement of $(\gamma H/\gamma Rh)^{5/2}$ = 5635 can be achieved in ^{1}H, ^{103}Rh HMQC.[14] Therefore the triple resonance probe at the University of Witwatersrand (WITS) was used to indirectly detect the ^{103}Rh using two-dimensional ^{103}Rh-^{1}H NMR spectroscopy.

In order to obtain a proper 2D NMR spectrum, certain NMR parameters such as the exact ^{1}H chemical shift of the $[Rh^{III}H(SnCl_3)_5]^{3-}$ species, the 90° pulse widths of the proton and of the rhodium must first be determined and optimized. Subsequently, the ^{1}H NMR spectrum of the hydrido species, $[Rh^{III}H(SnCl_3)_5]^{3-}$, was recorded and is shown in Figure 5.5A. The ^{1}H NMR spectrum proved to be more complicated than expected. It shows a doublet at -12.77 ppm, indicated by symbol **a** in Figure 5.5A, flanked by two different sets of $^{2}J(^{119/117}Sn\text{-}^{1}H)$ satellites as indicated by the symbols **b** and **c** in Figure 5.5A.

The main ^{1}H NMR resonance signal is split into a doublet with a coupling constant of 9.70 Hz due to $^{1}J(^{103}Rh\text{-}^{1}H)$ coupling, indicated by the symbol **a** in Figure 5.5A. The signal is flanked by two sets of $^{2}J(^{119/117}Sn\text{-}^{1}H)$ satellites; one with a coupling constant of 58.3 Hz and the other with a coupling constant of 1 100 Hz, indicated by symbols **b** and **c**, respectively. Once again the usefulness of the dependence of $^{2}J(^{119}Sn\text{-}^{1}H)$/Hz on the complex geometry, such that the *trans* coupling is always much larger than the *cis* coupling, is noted.[114] This allows for the assignment of the $^{2}J(^{119}Sn\text{-}^{1}H)$ satellites indicated by the symbol **b** in Figure 5.5A to the *cis* satellites and those indicated by the symbol **c** to the *trans* satellites of the $[Rh^{III}H(SnCl_3)_5]^{3-}$ species, as is indicated in Scheme 5.2.

A) Experimental ^{1}H NMR spectrum of $[RhH(SnCl_3)_5]^{3-}$

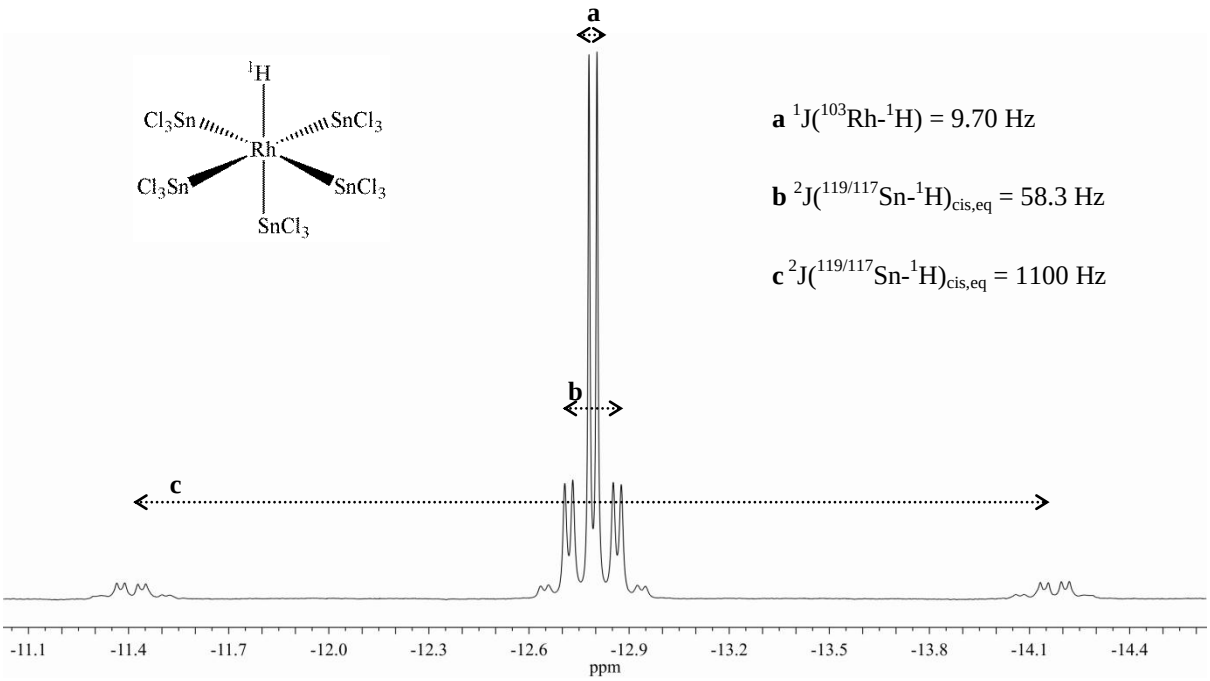

B) Simulated ^{1}H NMR spectrum of $[RhH(SnCl_3)_5]^{3-}$

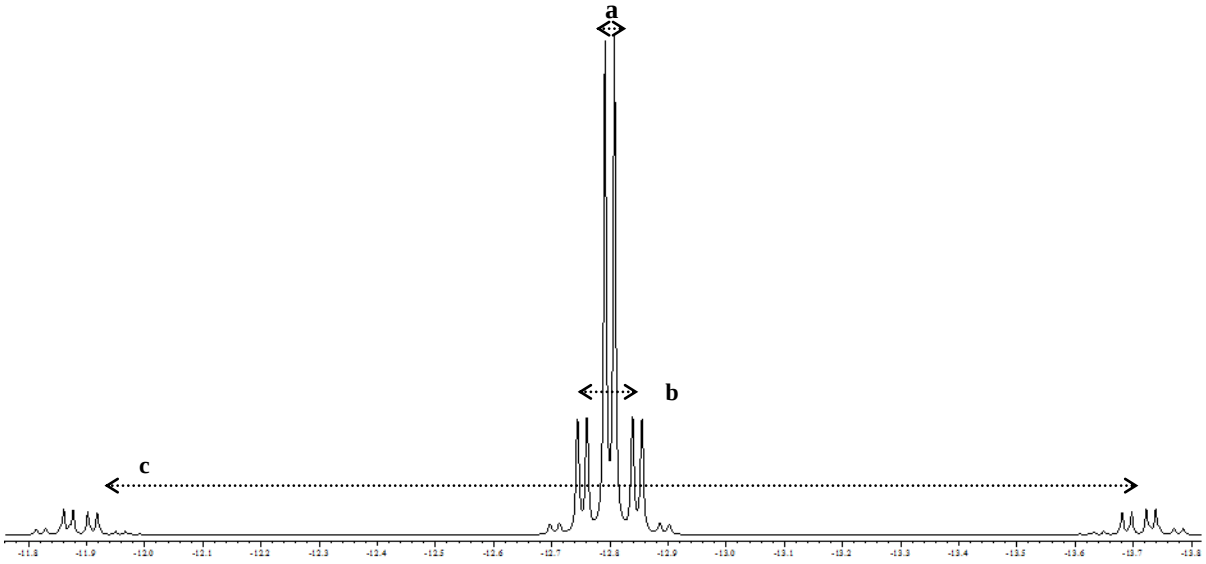

Figure 5.5 ^{1}H NMR spectrum of A) the $[Rh^{III}H(SnCl_3)_5]^{3-}$ species that was extracted into methyl isobutylketone (MIBK) from an aqueous solution containing $[Rh^{I}(SnCl_3)_5]^{4-}$ at 25 °C. The symbol **a** indicates the $^{1}J(^{103}Rh\text{-}^{119}Sn)$ spin coupling, and symbols **b** and **c** indicates the $^{2}J(^{119/117}Sn\text{-}^{1}H)$ spin couplings. B) Simulated ^{1}H NMR spectrum of the $[RhH(SnCl_3)_5]^{3-}$ species using the NMR parameters obtained from the experimental spectrum.

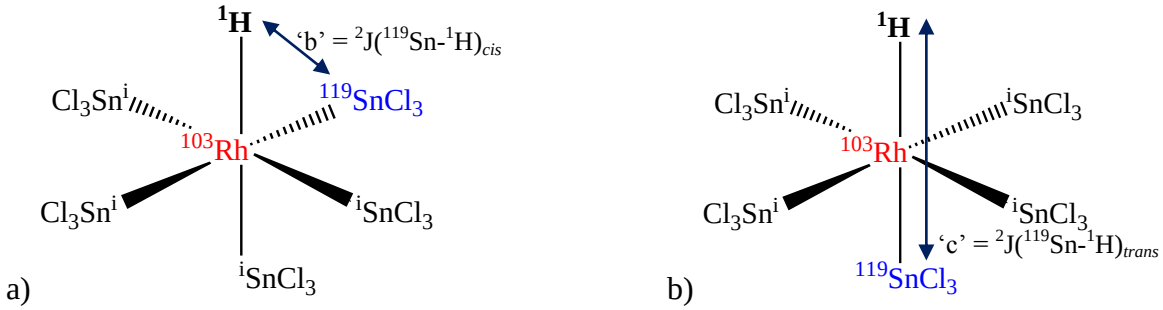

Scheme 5.2 Schematic representation of two different *isotopomers* of the $[Rh^{III}H(SnCl_3)_5]^{3-}$ species where the $^{119}SnCl_3^-$-ligand is (a) *cis* and (b) *trans* to the observed ^1H nucleus.

On closer investigation of the respective signals it was noted that the width at half height ($\Delta\nu_{1/2}$) of the main signals is measured to be 2.9 Hz, whereas that of the *cis* satellites are measured to be 5.7 Hz, almost double that of the main signals. As ^{117}Sn has a natural abundance of 7.67 % compared to the 8.68 % of ^{119}Sn one would also expect to see $^2J(^{117}Sn\text{-}^1H)$ satellites in addition to $^2J(^{119}Sn\text{-}^1H)$ satellites. Moreover, the gyromagnetic ratios of ^{119}Sn and ^{117}Sn are very similar, thus one would expect the magnitude of their coupling to ^1H to be similar in magnitude. It is thus reasonable to suggest that the satellites indicated by the symbol **b** in Figure 5.5A are due to both $^2J(^{119}Sn\text{-}^1H)$ and $^2J(^{117}Sn\text{-}^1H)$ coupling. Unfortunately better resolution could not experimentally be obtained. Therefore, the experimental data obtained were used to simulate the ^1H NMR spectrum of the $[Rh^{III}H(SnCl_3)_5]^{3-}$ species with the computer program gNMR50 and is shown Figure 5.5B.

The simulated ^1H NMR spectrum is identical to the experimentally obtained spectrum when the half width at half height is set to 2.7 Hz (as is obtained experimentally), Figure 5.5B. However, when the $\Delta\nu_{1/2}$ of the signals is manually set to 0.5 Hz the ^1H NMR spectrum shown in Figure 5.6A is obtained. The rather more complicated spectrum shows the central doublet of ^1H NMR signals at -12.78 ppm that is now flanked by several resolved $^2J(^{119/117/115}Sn\text{-}^1H)$ coupling satellites. As mentioned before, tin has three magnetically active isotopes (^{119}Sn, ^{117}Sn and ^{115}Sn) which result in several different *isotopologues* of the $[Rh^{III}H(SnCl_3)_5]^{3-}$ species being observed with ^1H NMR spectroscopy.

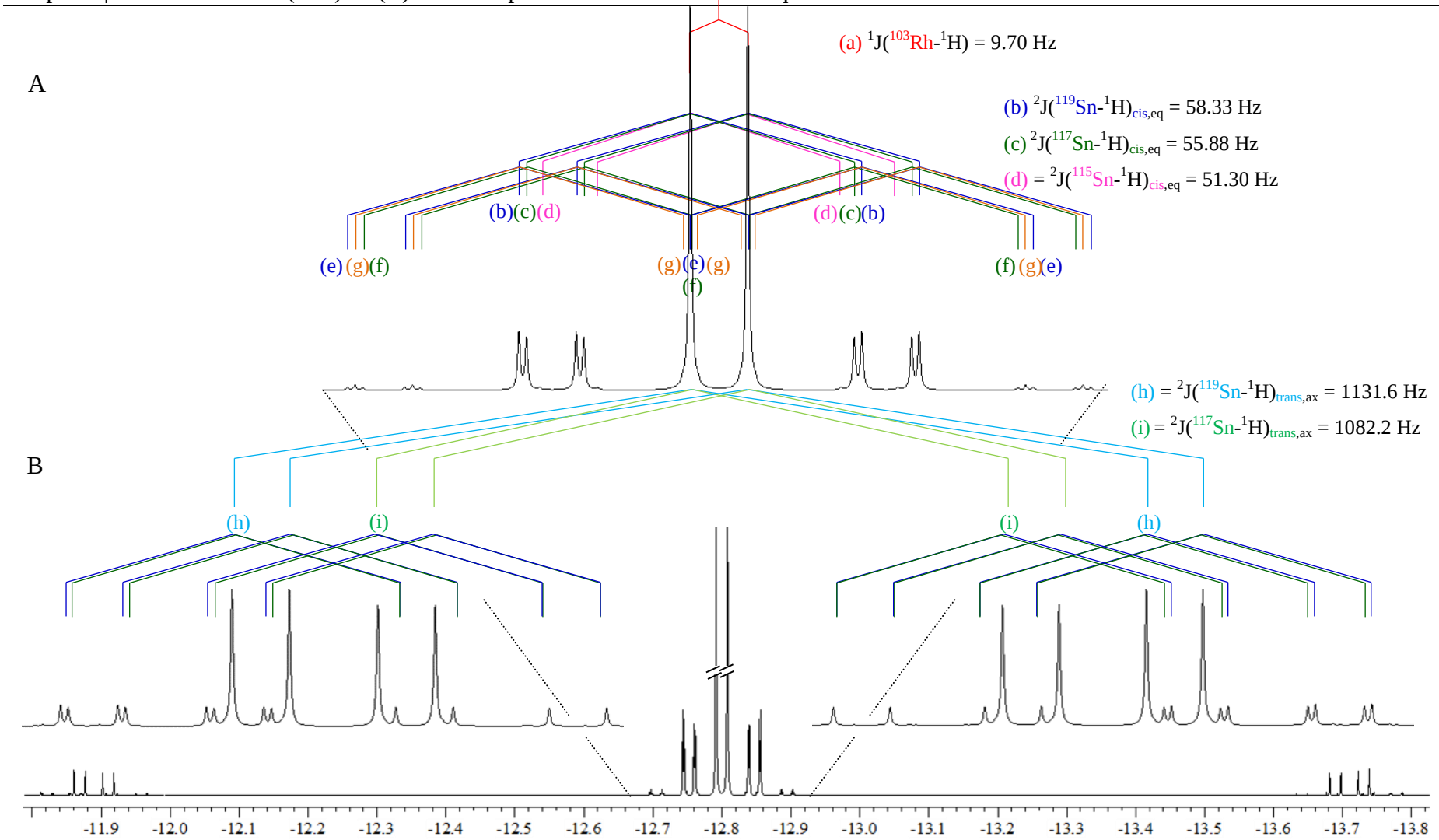

Figure 5.6 The simulated ^{1}H NMR spectrum of the set of signals at $\delta(^{1}H)$ = -12.78 ppm assigned to the $[Rh^{III}H(SnCl_3)_5]^{3-}$ complex anion where (A) shows an expansion of the $^{2}J(^{119/117}Sn\text{-}^{1}H)_{cis}$ satellites and (B) an expansion of the $^{2}J(^{119/117}Sn\text{-}^{1}H)_{trans}$ satellites. The width at half height of the signals was set to 0.5 Hz to improve the resolution of the signals.

The splitting pattern obtained is reminiscent to the one previously reported by this group for the ^{195}Pt NMR spectrum of the $[Pt(SnCl_3)_5]^{3-}$ species, after which a detailed analysis of all the possible *isotopologues* of the species were performed.[59] To the best of our knowledge a detailed investigation of the many possible *isotopologues* and *isotopomers* of the $[Rh^{III}H(SnCl_3)_5]^{3-}$ complex anions have not been done. Similar methodology to what was used in the Pt-Sn study would be applied here.

The central doublet of ^{1}H NMR signals is assigned to the $[^{103}Rh^{III}H(SnCl_3)_5]^{3-}$ *isotopologue* which contains no magnetically-active tin nuclei, ^{119}Sn, ^{117}Sn, ^{115}Sn. The satellites indicated by symbols **b** to **i**, on the other hand are due to *isotopologues*/*isotopomers* of the hydrido species that do contain one or more magnetically-active tin isotope. First consider the satellites due to ^{1}H coupling to Sn in the *cis* position as indicated by the splitting diagram labelled A in Figure 5.6. From the ^{119}Sn NMR spectrum it is known that the $^2J(^1H\text{-}^{119}Sn)$ coupling constant has a magnitude of 57 Hz and from the gyromagnetic ratios of ^{119}Sn and ^{117}Sn, the $^2J(^{117}Sn\text{-}^1H)$ coupling constant should be the smaller of the two. Thus, the doublet of doublet set of satellites indicated by the symbol **b**, with coupling constant of 58.3 Hz, can be assigned to the $^2J(^{119}Sn\text{-}^1H)_{cis}$ satellites of the *cis*-$[^{103}Rh^{III}H(^{119}SnCl_3)(SnCl_3)_4]^{3-}$ *isotopologue* which contains only one magnetically active ^{119}Sn nucleus. Similarly the doublet of doublet (dd) satellites indicated by the symbols **c** and **d** can be assigned to the *cis*-$[^{103}Rh^{III}H(^{117}SnCl_3)(SnCl_3)_4]^{3-}$ and *cis*-$[^{103}Rh^{III}H(^{115}SnCl_3)(SnCl_3)_4]^{3-}$ *isotopologues* of the hydrido species. For *isotopologues* containing two magnetically-active tin nuclei, the method of successive splitting is used to elucidate the respective satellites. Consider the $[^{103}Rh^{III}H(^{119}SnCl_3)_2(SnCl_3)_3]^{3-}$ *isotopologue* wherein the ^{1}H nucleus can couple to two ^{119}Sn nuclei (both in the *cis* position). The main doublet will be split into a doublet of doublets due to coupling to one ^{119}Sn nucleus, $^2J(^{119}Sn\text{-}^1H)$ = 58.3 Hz, as indicated by symbol **b**, followed by successive splitting with the same coupling constant, 58.3 Hz, due to coupling to the second ^{119}Sn nucleus, resulting in the doublet of doublet of triplets (ddt) indicated by the symbol **e** in Figure 5.6, and the assignment is made accordingly. Similarly the set of 'ddt' satellites indicated by the symbol **f** in Figure 5.6 is assigned to the *cis*-$[^{103}Rh^{III}H(^{117}SnCl_3)_2(SnCl_3)_3]^{3-}$ *isotopologue*. The 'ddd' satellites indicated by the symbol **g** in Figure 5.6 are observed due to both $^2J(^{119}Sn\text{-}^1H)$ and $^2J(^{117}Sn\text{-}^1H)$ coupling in the *cis*-$[^{103}Rh^{III}H(^{119}SnCl_3)(^{117}SnCl_3)(SnCl_3)_3]^{3-}$ *isotopologue*. Thus, the satellites indicated by the symbols **b** – **g** has been assigned to 6 different *isotopologues* of the $[Rh^{III}H(SnCl_3)_5]^{3-}$ species

wherein both magnetically-active tin nuclei are *cis* to the ^{1}H nucleus, Table 5.3. Using the same methodology, the doublet of doublet satellites indicated by the symbols **h** and **i** in Figure 5.6 have been assigned to the $[^{103}Rh^{III}H(^{119}SnCl_3)(SnCl_3)_4]^{3-}$ and $[^{103}Rh^{III}H(^{117}SnCl_3)(SnCl_3)_4]^{3-}$ *isotopologues* of the *trans* stereoisomer of the $[Rh^{III}H(SnCl_3)_5]^{3-}$ species, respectively. The four remaining 'ddd' sets of satellites are assigned to *isotopologues*/*isotopomers* of the $[Rh^{III}H(SnCl_3)_5]^{3-}$ species containing two magnetically active tin nuclei, ^{119}Sn or ^{117}Sn, of which one must be in the position *trans* to ^{1}H and the other one *cis*: $[^{103}Rh^{1}H(^{119}SnCl_3)_{trans}(^{119}SnCl_3)(SnCl_3)_3]^{3-}$, $[^{103}Rh^{1}H(^{119}SnCl_3)_{trans}$-$(^{117}SnCl_3)(SnCl_3)_3]^{3-}$, $[^{103}Rh^{1}H(^{117}SnCl_3)_{trans}(^{119}SnCl_3)(SnCl_3)_3]^{3-}$, and $[^{103}Rh^{1}H(^{117}SnCl_3)_{trans}$-$(^{117}SnCl_3)(SnCl_3)_3]^{3-}$.

Table 5.3 Assignment of the respective *isotopologues* and *isotopomers* of the $[Rh^{III}H(SnCl_3)_5]^{3-}$ complex anion.

^{2}J sat	***Isotopologue/isotopomer***	**$^{2}J(^{119}Sn$-$^{1}H)$ /Hz**	**$^{2}J(^{117}Sn$-$^{1}H)$ /Hz**	**Mult.**
a	$[^{103}Rh^{III}H(SnCl_3)_5]^{3-}$	-	-	d
b	$[^{103}Rh^{III}H(^{119}SnCl_3)(SnCl_3)_4]^{3-}$	58.3		dd
c	$[^{103}Rh^{III}H(^{117}SnCl_3)(SnCl_3)_4]^{3-}$	55.9		dd
d	$[^{103}Rh^{III}H(^{115}SnCl_3)(SnCl_3)_4]^{3-}$	51.3		dd
e	$[^{103}Rh^{III}H(^{119}SnCl_3)_{2(cis)}(SnCl_3)_3]^{3-}$	58.3; 58.3		ddt
f	$[^{103}Rh^{III}H(^{117}SnCl_3)_{2(cis)}(SnCl_3)_3]^{3-}$	55.9; 55.9		ddt
g	$[^{103}Rh^{III}H(^{119}SnCl_3)_{cis}(^{117}SnCl_3)_{cis}(SnCl_3)_3]^{3-}$	58.3	55.9	ddd
h	$[^{103}Rh^{III}H(^{119}SnCl_3)_{trans}(SnCl_3)_4]^{3-}$	1131.6		dd
i	$[^{103}Rh^{III}H(^{117}SnCl_3)_{trans}(SnCl_3)_4]^{3-}$		1082.2	dd
j	$[^{103}Rh^{III}H(^{119}SnCl_3)_{trans}(^{119}SnCl_3)_{cis}(SnCl_3)_3]^{3-}$	1131.6; 58.3		ddd
k	$[^{103}Rh^{III}H(^{119}SnCl_3)_{trans}(^{117}SnCl_3)_{cis}(SnCl_3)_3]^{3-}$	1131.6	55.9	ddd
l	$[^{103}Rh^{III}H(^{117}SnCl_3)_{trans}(^{119}SnCl_3)_{cis}(SnCl_3)_3]^{3-}$	58.3	1082.2	ddd
m	$[^{103}Rh^{III}H(^{117}SnCl_3)_{trans}(^{117}SnCl_3)_{cis}(SnCl_3)_3]^{3-}$		1082.2; 55.9	ddd

To summarize, it has once again been shown how valuable NMR spectroscopy is for the structural assignment of these Rh-Sn complex anions. With the aid of the simulated ^{1}H NMR spectrum, the complex splitting pattern observed for the $[RhH(SnCl_3)_5]^{3-}$ complex anion has fully been elucidated and assigned to 12 respective *isotopologues* and *isotopomers*, given in Table 5.3.

With the $\delta(^{1}H)$ accurately determined, a pw90 experiment was setup and the 90° pulse of the ^{1}H nucleus was determined to be 13.7 µs. The ^{103}Rh-^{1}H HMQC recorded for this solution, using the HMQCf3ph pulse sequence, is given below in Figure 5.7. The spectral widths in the

f2 and f1 dimensions were set to 3 ppm and 20 ppm, respectively. After the spectrum was left to record over night, a broad ^{103}Rh signal was generated in the f1 dimension, and shows good correlation with the ^{1}H NMR spectrum shown in the f2 dimension. The ^{103}Rh-^{1}H HMQC spectrum has enabled the determination of ^{103}Rh chemical shift of the $[Rh^{III}H(SnCl_3)_5]^{3-}$ species to be between δ(^{103}Rh) = -1190 and -1192 ppm. Unfortunately, better resolution of the ^{103}Rh signal could not be obtained, but further studies should be done using this technique.

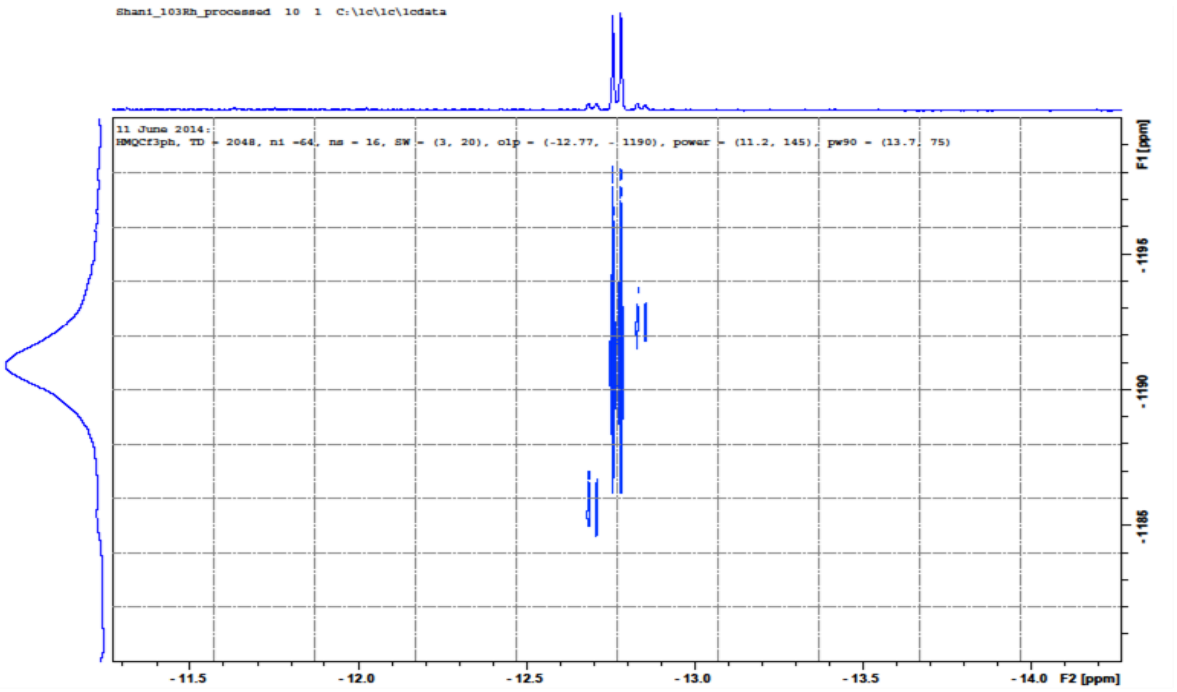

Figure 5.7 The ^{103}Rh-^{1}H HMQC recorded for the $[RhH(SnCl_3)_5]^{3-}$ complex anion. The δ(^{1}H) and ^{1}J(^{103}Rh-^{119}Sn) values used to generate the ^{103}Rh spectrum are -12.78 ppm and 58.3 Hz, respectively. The 90° pulse values were determined to be 13.7 μs for the proton and 75 μs for rhodium. The HMQCf3ph pulse sequence was used.

The ^{103}Rh chemical shift value of this species has never before been determined. The large upfield shift of the δ(^{103}Rh) suggests that coordination of the $SnCl_3$-ligands to the rhodium nucleus has resulted in the ^{103}Rh nucleus being less shielded that an uncoordinated nucleus. However, this is only speculative and further investigations are required to determine the effect of the $SnCl_3$-ligand on the shielding of the ^{103}Rh nucleus.

5.2.1.2 Spectral section of resonances at δ(^{119}Sn) = -54.4 ppm

An expansion of the set of signals at δ(^{119}Sn) = -54.5 ppm in Figure 5.1 is given below in Figure 5.8A. The main signal is split into a doublet due to ^{1}J(^{103}Rh-^{119}Sn) = 520 Hz, as indicated by symbol **a** in Figure 5.8A and is flanked by a set of ^{2}J(^{117}Sn-^{119}Sn) satellites,

indicated by symbol **b**, with a coupling constant of 1670 Hz. These ^{119}Sn NMR parameters are in good agreement with the ^{119}Sn NMR parameters of a set of signals previously reported by Koch and Hall[8] for a similar solution. However, there was some ambiguity regarding the assignment of these signals and only tentative assignments were proposed. Based on the good correlation obtained with the plot of $^{1}J(^{103}Rh\text{-}^{119}Sn)/Hz$ as a function of $\delta(^{119}Sn)/ppm$ for the series of $[Rh(SnCl_3)_nCl_{6-n}]^{3-}$ (n = 1 – 5) complex anions in 3 M HCl as found by Moriyama *et. al.*,[41] as well as the integrated peak ratios, I(sat)/I(main), Koch and Hall[8] suggested that the set of signals at -54.5 ppm is due to the $[Rh^{III}(SnCl_3)_4Cl_2]^{3-}$ species. However, neither the chemical shift parameter, nor the magnitude of the coupling constant agrees with the values reported for this species in the aqueous phase, discussed in Chapter III Section 3.2.3.2. It was postulated that strong solvent effects (aqueous media *versus* MIBK) could account for the differences in the NMR parameters. Alternatively, it was suggested by Koch and Hall[8] that one of the chlorido ligands was substituted with an oxygen donor solvent molecule, MIBK; a phenomenon similar to the one that was suggested by Saito *et. al.*[107,113] to occur for these species in propan-2-ol.

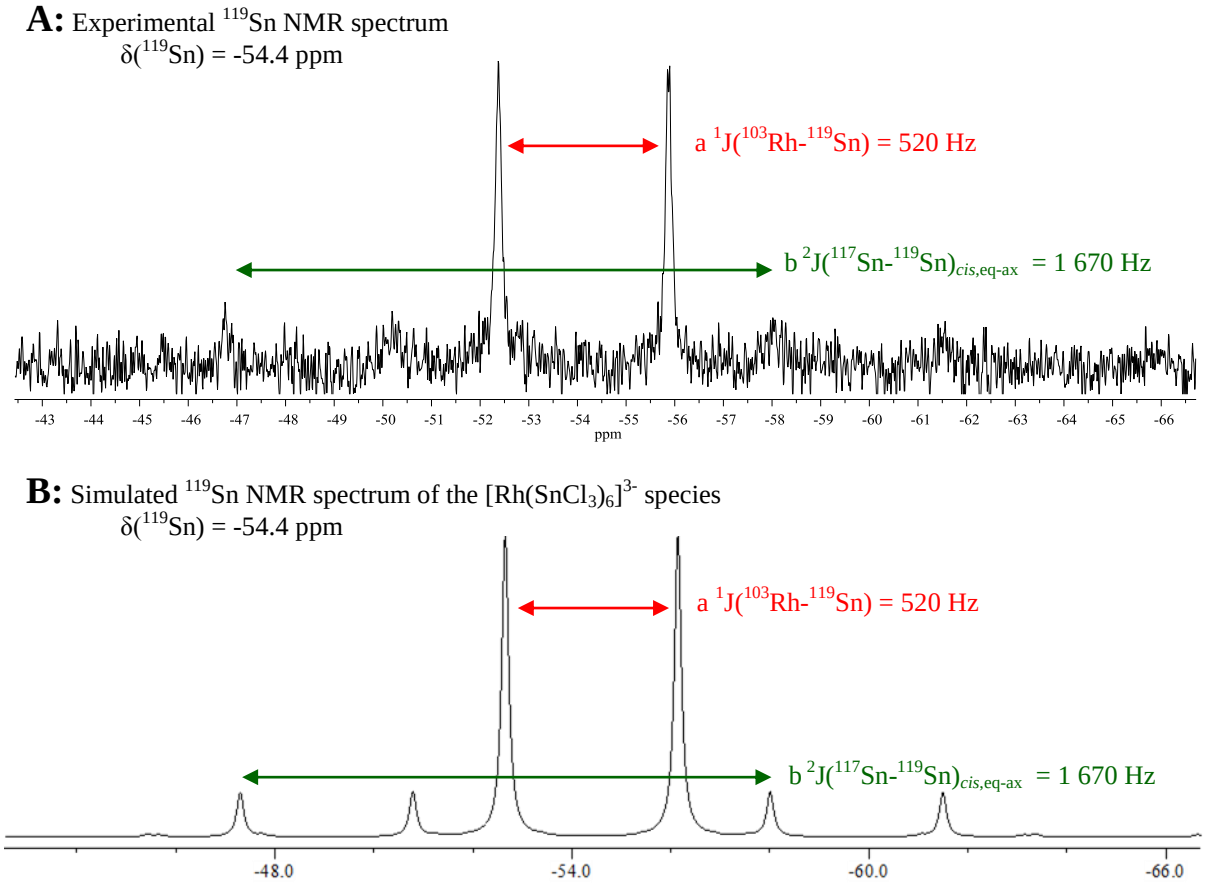

Figure 5.8 The ^{119}Sn NMR spectra of the sets of signals at $\delta(^{119}Sn)$ = -54.4 ppm obtained (A) experimentally and (B) by simulating the spectrum for a $[Rh(SnCl_3)_6]^{3-}$ species using gNMR50.

Although both these propositions seem feasible, no concrete evidence is provided for either one. On the other hand, in Chapter III Section 3.2.1.4 of this thesis, a new $[Rh(SnCl_3)_nCl_{6-n}]^{3-}$ (n = 1 – 6) species, the $[Rh(SnCl_3)_6]^{3-}$ species, were identified and characterized. The $[Rh(SnCl_3)_6]^{3-}$ complex anion resonated at -36.1 ppm, was split into a doublet due to $^1J(^{103}Rh\text{-}^{119}Sn)$ = 518 Hz and was flanked by $^2J(^{117}Sn\text{-}^{119}Sn)$ satellites with a coupling constant of 1651 Hz. From the good agreement between the ^{119}Sn NMR parameters, it is reasonable to suggest that the set of signals at $\delta(^{119}Sn)$ = -54.4 ppm in the MIBK solution can tentatively be assigned to the $[Rh(SnCl_3)_6]^{3-}$ species, shown in Scheme 5.3.

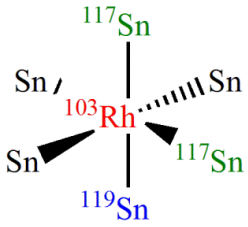

Scheme 5.3 Schematic representation of the kinetically inert $[Rh(SnCl_3)_6]^{3-}$ species.

According to Equation 3.1.5 the NSA of the $[^{103}Rh(^{i}SnCl_3)_n(^{119}SnCl_3)_{5-n}(^{117}SnCl_3)]$ *isotopologue* is 22.4 %, which should be reflected in the I(sat)/I(main) ratio of the set of signals at $\delta(^{119}Sn)$ = -54.4 ppm. Moreover, from Scheme 5.3 as well as the discussion in Section 3.2.1.4, $^2J(^{117}Sn\text{-}^{119}Sn)_{trans}$ satellites should also be observed for the $[Rh(SnCl_3)_6]^{3-}$ species. Unfortunately, the signal to noise ratio obtained in Figure 5.8A is too low to either accurately measure the I(sat)/I(main) ratio or to observe the $^2J(^{117}Sn\text{-}^{119}Sn)_{trans}$ satellites. Therefore, the ^{119}Sn NMR parameters given in Figure 5.8A, together with the $^2J(^{117}Sn\text{-}^{119}Sn)_{trans}$ coupling constant measured for the species in the aqueous solution, were used to simulate the ^{119}Sn NMR spectrum for the $[Rh(SnCl_3)_6]^{3-}$ species. The resulting simulated spectrum is shown in Figure 5.8B and is in excellent agreement with the experimental ^{119}Sn NMR spectrum. Moreover, integration of the $^2J(^{117}Sn\text{-}^{119}Sn)_{trans/cis}$ satellites in the simulated spectrum gave a I(sat)/I(main) ratio of 22.3 % which agrees well with the 22.4 % NSA calculated for a Rh-Sn species with 6 Sn-ligands coordinated to the rhodium. Subsequently, the set of signals at (^{119}Sn) = -54.4 ppm is unambiguously assigned to the $[Rh^{III}(SnCl_3)_6]^{3-}$ complex anion as listed in Table 5.2. The upfield shift of 18.3 ppm obtained when going from aqueous perchloric acid solution to MIBK is indicative of the observed ^{119}Sn nucleus being less shielded in the MIBK solution and can probably be ascribed to solvent effects. Moreover, only one set of signals are observed and no second order coupling effects are observed, which

suggests that all 6 $SnCl_3$-ligands are magnetically equivalent. As it has been shown in this dissertation that the series of $[Rh(SnCl_3)_nCl_{6-n}]^{3-}$ (n = 1 – 6) species are kinetically inert, it is reasonable to postulate that the Rh-Sn bond lengths of all 6 $SnCl_3^-$-ligands are equivalent. However, further studies are required to confirm this postulation.

5.2.1.2 Spectral section of resonances at δ(^{119}Sn) = -115.7 ppm

The set of ^{119}Sn NMR signals at -115.7 ppm is split into a doublet due to $^1J(^{103}Rh\text{-}^{119}Sn)$ = 567 Hz and is flanked by two sets of $^2J(^{117/119}Sn\text{-}^{119}Sn)$ satellites, one with a coupling constant of 1930 Hz and the other with a coupling constant of 1775 Hz, Figure 5.9.

Experimental ^{119}Sn NMR spectrum of the species at δ(^{119}Sn) = -115.7 ppm

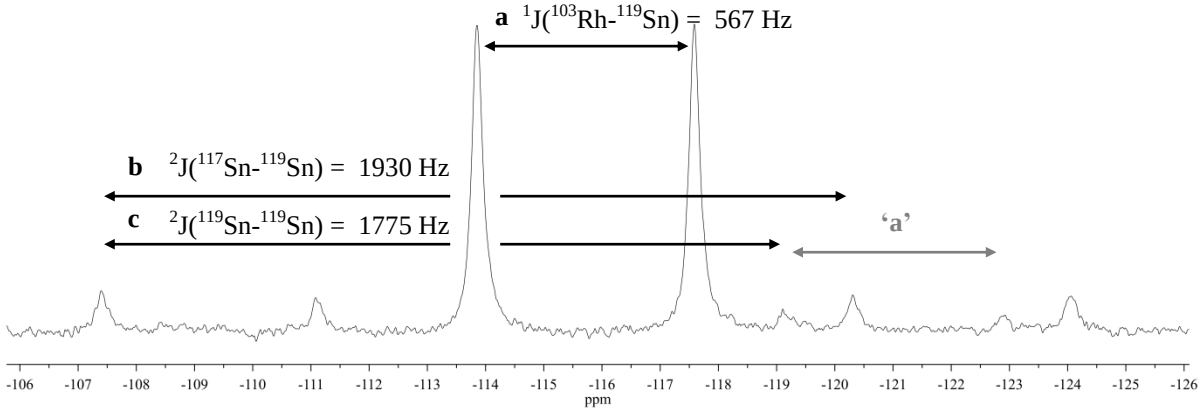

Figure 5.9 The expanded ^{119}Sn NMR spectrum of the set of signals at -115.7 ppm. The $^1J(^{103}Rh\text{-}^{119}Sn)$ spin couplings are indicated by the symbols **a** and **'a'** and the $^2J(^{119/117}Sn\text{-}^{119}Sn)$ spin couplings are indicated by the symbols **b** and **c**.

Hall *et. al.*[8] previously reported a Rh-Sn species at δ(^{119}Sn) = -117.5 ppm with $^1J(^{103}Rh\text{-}^{119}Sn)$ = 558 Hz and $^2J(^{117}Sn\text{-}^{119}Sn)$ = 1943 Hz, which correspond very well with the NMR parameters given in Figure 5.9. In a separate study Yamakawa *et. al.*[113] also reported a set of ^{119}Sn NMR signals with similar NMR parameters after using a solution of $RhCl_3{\cdot}3H_2O$ and $SnCl_2{\cdot}2H_2O$ as catalyst for the dehydrogenation of propan-2-ol to acetone. Regardless of the similarities in the NMR parameters reported by these authors, there was a discrepancy regarding the number of $SnCl_3^-$ ligands coordinated to the central rhodium: Hall *et. al.*[8] reported 3 $SnCl_3^-$-ligands coordinated to the central rhodium, whereas Yamakawa *et. al.*[113] reported the presence of 4 $SnCl_3^-$-ligands. Both authors proposed that the Cl^- ligands were

substituted with one or more solvent molecule; however no clear evidence was given for this proposal and necessitated further investigations. A closer examination of the $^{2}J(^{117}Sn\text{-}^{119}Sn)$ satellites of the signal at -115.7 ppm in Figure 5.9 revealed that the main doublet is flanked by two sets of satellites; one symmetrically distributed set of satellites with a coupling constant of 1930 Hz and one asymmetrically distributed set of satellites with a coupling constant of 1755 Hz, as indicated by the symbols **b** and **c** in Figure 5.9, respectively. The $^{1}J(^{103}Rh\text{-}^{119}Sn)$ coupling constant of the asymmetrically distributed satellites, indicated by the symbol **'a'**, are of equal magnitude as that of the main set of signals, 567 Hz, which is indicative of these signals being satellites and not a different rhodium-tin species. This splitting pattern, as well as the measured ^{119}Sn NMR parameters, are reminiscent of those reported in Chapter III Section 3.2.1.3.3 for the $[Rh^{III}(SnCl_3)_5Cl]^{3-}$ complex anion where the observed ^{119}Sn nucleus in the equatorial position *trans* to another $SnCl_3$-ligand as shown in Scheme 5.4.

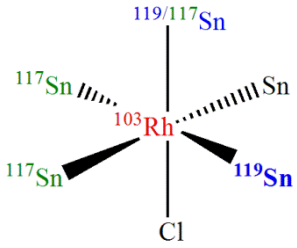

Scheme 5.4 Schematic representation of the *isotopomer* of the $[Rh^{III}(SnCl_3)_5Cl]^{3-}$ complex anion where the observed ^{119}Sn nucleus is in the equatorial position. The ligand labelled $^{119/117}Sn$ represents either an $^{119}SnCl_3$ ligand or an $^{117}SnCl_3$ ligand. All coordinated chlorido ligands of $SnCl_3^-$ are left out for clarity.

From the $[Rh^{III}(SnCl_3)_5Cl]^{3-}$ complex anion shown in Scheme 5.4 one would expect to see 4 sets of $^{2}J(^{119/117}Sn\text{-}^{119}Sn)$ satellites with their coupling constants decreasing in the order $^{2}J(^{117}Sn\text{-}^{119}Sn)_{trans} > {}^{2}J(^{117}Sn\text{-}^{119}Sn)_{cis,eq\text{-}eq} > {}^{2}J(^{119}Sn\text{-}^{119}Sn)_{cis,ax\text{-}eq} > {}^{2}J(^{117}Sn\text{-}^{119}Sn)_{cis,ax\text{-}eq}$ as was discussed in Chapter III. Furthermore, it has been shown that it is the $^{2}J(^{119}Sn\text{-}^{119}Sn)_{cis,eq\text{-}ax}$ coupling that results in second order distortions which causes the occurrence of asymmetrically distributed satellites, such is observed for the set of satellites indicated by the symbol **c** in Figure 5.9. Subsequently, the set of symmetrical satellites indicated by the symbol **b** in Figure 5.9 is assigned to the $^{2}J(^{117}Sn\text{-}^{119}Sn)_{cis,eq\text{-}eq}$ satellites of the $[Rh^{III}(SnCl_3)_5Cl]^{3-}$ complex anion and more specifically the *isotopomer* in which the observed $^{119}SnCl_3^-$ ligand is in the equatorial, *trans* to another $SnCl_3^-$ ligand, position. However, the $^{2}J(^{119}Sn\text{-}^{119}Sn)_{cis,ax\text{-}eq}/{}^{2}J(^{117}Sn\text{-}^{119}Sn)_{cis,ax\text{-}eq}$ = 1.100 ratio is not equal to the $\gamma(^{119}Sn)/\gamma(^{117}Sn)$ = 1.047. This discrepancy between the two values can however be ascribed

to the low resolution obtained. Considering the other evidence, it is reasonable to suggest that the tentative assignment as stated in Table 5.2 is indeed the correct assignment.

5.2.2 ^{119}Sn NMR of Rh-Sn complexes extracted into AQ336 in chloroform-*d*

A 0.1 M rhodium-tin solution with a Rh:Sn ratio of 1:10 was prepared by dissolving 0.1803 g $SnCl_2$ (anhydrous) in 0.6 mL conc. HCl and after the initially formed cloudiness (due to hydrolysis products) had disappeared the required amount of $RhCl_3 \cdot 3H_2O$ was added to the solution. The solution was diluted to 1 mL to obtain a final HCl concentration of 3 M and was left to equilibrate overnight. AQ336 (30 %, v/v) in chloroform-*d* was added to the resulting deep purple solution, indicative of the formation of the $[Rh^{I}(SnCl_3)_5]^{4-}$ species, in a 1:1 volume:volume ratio and was stirred for 30 minutes. During the extraction, the aqueous phase went colourless whilst the organic phase turned pale yellow-orange. The ^{119}Sn NMR spectrum recorded for the yellow solution is shown in Figure 5.10A. In a similar manner a 0.1 M Rh-Sn solution with a Rh:Sn mole ratio to 1:7 was prepared and extracted into chloroform using AQ336, the ^{119}Sn NMR spectrum of which is shown in Figure 5.10B.

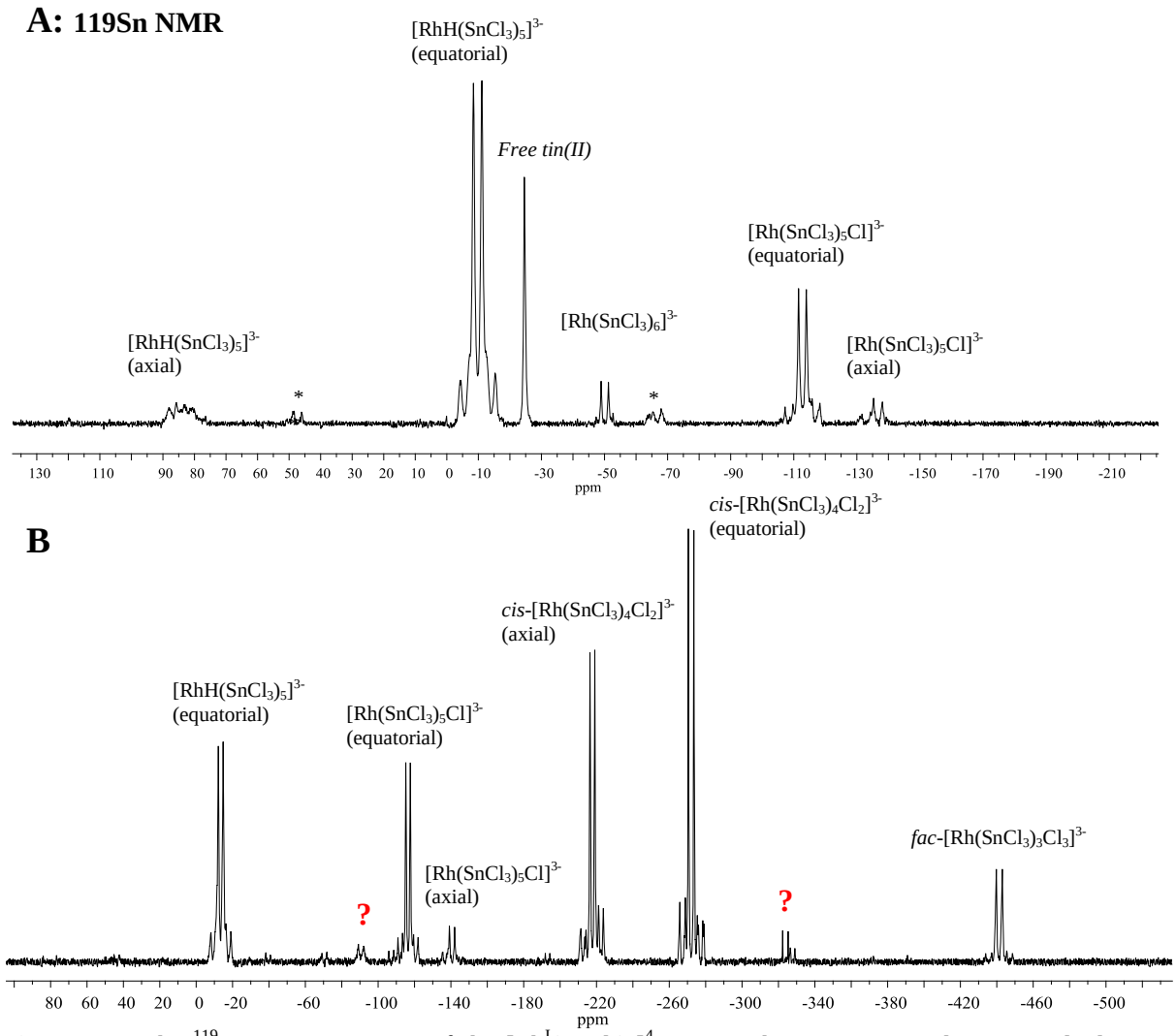

Figure 5.10 The ^{119}Sn NMR spectrum of the $[Rh^{I}(SnCl_3)_5]^{4-}$ species that was extracted into $CDCl_3$-*d* using AQ336 as anion exchanger from a 3 M HCl solution containing (A) a Rh:Sn mole ratio of 1:10 and (B) a Rh:Sn mole ratio of 1:7. The spectra were recorded at 25 °C. No other ^{119}Sn NMR signals were observed for the spectrum shown in A, whereas free Sn(IV) signals were observed at -665.9 and – 729.5 ppm in spectrum (B). The ^{119}Sn signals marked with (*) in A is assigned to the $^{2}J(^{117}Sn\text{-}^{119}Sn)_{trans,eq\text{-}eq}$ satellites of the *cis*-$[RhH(SnCl_3)_5]^{3-}$ complex anion at $\delta(^{119}Sn)$ = -9.7 ppm.

The $\delta(^{119}Sn)$/ppm *vs* $^{1}J(^{103}Rh\text{-}^{119}Sn)$/Hz trend obtained for the ^{119}Sn NMR signals observed in Figure 5.10 corresponds very well to the trend obtained for the ^{119}Sn NMR signals observed in the aqueous solutions, Figure 5.11, which aided the assignment of the some of the ^{119}Sn NMR signals that has not been previously assigned. The assignments of the Rh-Sn species are listed in Table 5.4.

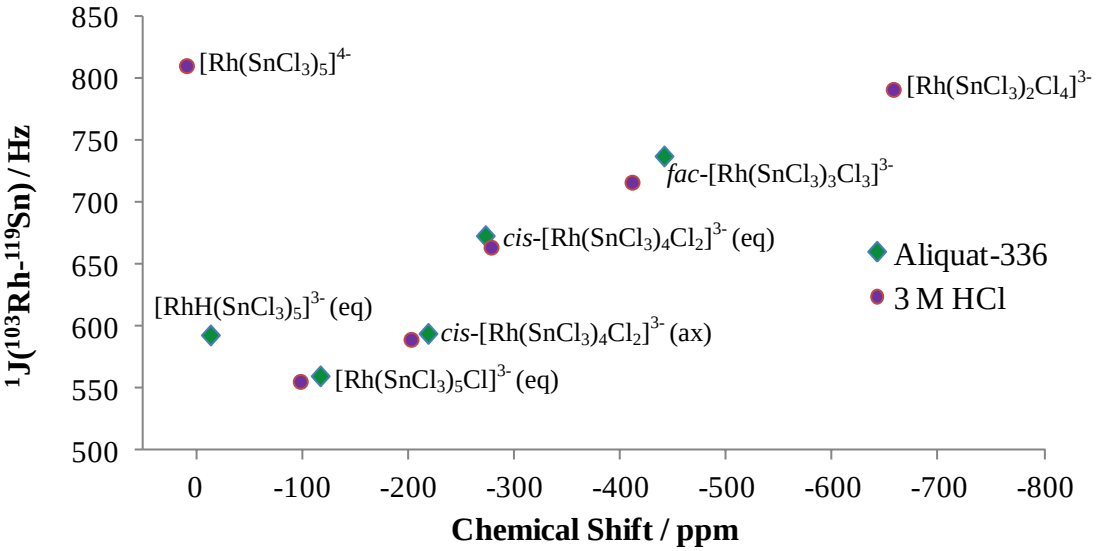

Figure 5.11 Comparison of the δ(^{119}Sn) vs ^{1}J(^{103}Rh-^{119}Sn) trends observed for the ^{119}Sn NMR signals observed for the 3 M HCl aqueous solution and those observed for the species extracted into chloroform-*d* using Aliquat-336 as anion exchanger.

Table 5.4 Comparison between the ^{119}Sn NMR parameters of the Rh-Sn species in aqueous HCl solution and extracted into chloroform-*d* using AQ336.

Rh-Sn Complexes	**δ(^{119}Sn)/ppm$^{\#}$**		**^{1}J(^{103}Rh-^{119}Sn)/Hz$^{\#}$**	
	AQ336	**HCl**	**AQ336**	**HCl**
***fac*-$[Rh(SnCl_3)_3Cl_3]^{3-}$** ($^{119}SnCl_3^-$ *trans* to Cl^-)	-441.1	-411.3	735	716
?*	-323.9		672	
***cis*-$[Rh(SnCl_3)_4Cl_2]^{3-}$** ($^{119}SnCl_3^-$ *trans* to Cl^-) equatorial	-272.1	-275.2	668	664
***cis*-$[Rh(SnCl_3)_4Cl_2]^{3-}$** ($^{119}SnCl_3^-$ *trans* to $SnCl_3^-$) axial	-217.7	-202.5	589	589
$[Rh(SnCl_3)_5Cl]^{3-}$ ($^{119}SnCl_3^-$ *trans* to Cl^-) axial	-140.6	-146.2	623	627
$[Rh(SnCl_3)_5Cl]^{3-}$ ($^{119}SnCl_3^-$ *trans* to $SnCl_3^-$) equatorial	-116.4	-98.3	557	555
?*	-90.5		700	
$[Rh(SnCl_3)_6]^{3-}$	-50.1	-36.1	522	518
$[RhH(SnCl_3)_5]^{3-}$ ($^{119}SnCl_3^-$ *trans* to $SnCl_3^-$)	-9.7		597	
$[Rh(SnCl_3)_5]^{4-}$		9.4		809

*These species have not been assigned. Due to the low S/N ratio enough information to make assignments of these species are not available.

Full elucidation of all the respective $^{2}J(^{117/119}Sn\text{-}^{119}Sn)$ spin couplings of the Rh-Sn have been given and discussed in Chapter 3 and is therefore not discussed in detail here. However, in Section 3.1.2.3.2 it was mentioned that one would expect to see $^{2}J(^{117}Sn\text{-}^{119}Sn)_{trans,ax\text{-}ax}$ spin coupling for the *cis*-$[Rh^{III}(SnCl_3)_4Cl_2]^{3-}$ (^{119}Sn, axial) complex anion, however, none was observed. This was attributed to the low S/N ratio obtained. In Figure 5.10B the $^{1}J(^{103}Rh\text{-}^{119}Sn)$ coupling constants of the sets of signals at $\delta(^{119}Sn)$ = -107.1 ppm and -327.8 ppm are both measured to be 589 Hz, which is equal to that of the $^{1}J(^{103}Rh\text{-}^{119}Sn)$ spin coupling measured for the *cis*-$[Rh^{III}(SnCl_3)_4Cl_2]^{3-}$ complex anion at $\delta(^{119}Sn)$ = -217.7 ppm, Table 5.4. Moreover, these two sets of signals are symmetrically distributed about the signal $\delta(^{119}Sn)$ = -217.7 ppm. It is thus reasonable to assign these two sets of signals to the $^{2}J(^{117}Sn\text{-}^{119}Sn)_{trans,ax\text{-}ax}$ satellites, with a coupling constant of 49320 Hz, of the *cis*-$[Rh^{III}(SnCl_3)_4Cl_2]^{3-}$ (^{119}Sn, axial) complex anion. These satellites have not been reported in literature before. The coupling constant measured is quite large, almost double that of the *trans* satellites reported for the hydrido Rh-Sn species. This may be indicative of the bond between the two tin nuclei *trans* to each other in the *cis*-$[Rh^{III}(SnCl_3)_4Cl_2]^{3-}$ complex anion has considerably higher *s*-character than those in the $[Rh^{III}H(SnCl_3)_5]^{3-}$ complex anion. However, further studies are required to elucidate the large coupling constant obtained.

It is thus evident that the $[Rh^{III}(SnCl_3)_nCl_{6-n}]^{3-}$ (n = 1- 6) complex anions retain their *stereo-chemical* rigidity in the organic phase. Moreover, the same $[Rh^{III}(SnCl_3)_nCl_{6-n}]^{3-}$ (n = 1- 6) complex anions were reported in both the aqueous and the organic phase, thus confirming that these species are extracted by AQ336 through an ion-exchange mechanism. It is only the $[Rh\mathit{I}(SnCl_3)_5]^{4-}$ species that was converted into the $[Rh^{III}H(SnCl_3)_5]^{3-}$ species, but this is ascribed to the co-extraction of HCl followed by the direct oxidative addition thereof to form the hydride species.

5.2.3 ^{119}Sn NMR of the Rh-Sn complex anions in propa-2-nol

A 0.5 M rhodium solution with a Rh:Sn mole ratio of 1:3 was prepared in pure propa-2-nol. 3 M LiCl was also added to the solution to ensure the formation of $SnCl_3^-$ from $SnCl_2$, after which the solution was left to equilibrate for 24 hours under N_2 before the ^{119}Sn NMR spectrum was acquired, Figure 5.12. A very complicated spectrum with 14 distinguishable set of ^{119}Sn signals were obtained of which the NMR parameters are summarized in Table 5.5.

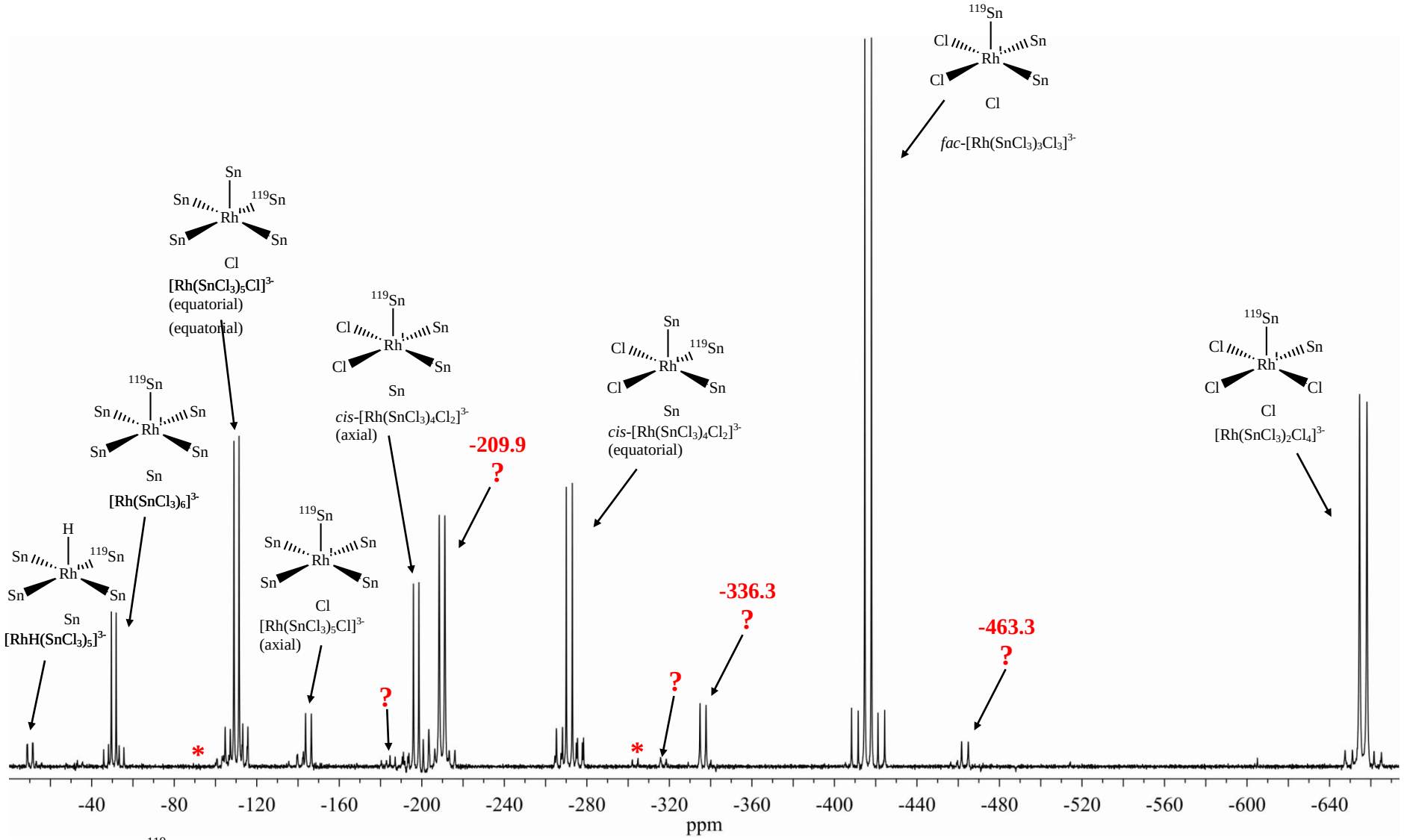

Figure 5.12 The ^{119}Sn NMR spectrum recorded for the propan-2-ol solution with a rhodium concentration of 0.5 M and a Rh:Sn mole ratio of 1:3 at 25 °C. The spectrum shows 13 respective Rh-Sn species, as identified by the characteristic doublet formation due to $^{1}J(^{103}Rh\text{-}^{119}Sn)$ spin coupling. Eight of these signals have been assigned, whereas the signals labelled with '?' have not yet been assigned. The signals labelled with '*' has been assigned to the $^{2}J(^{117}Sn\text{-}^{119}Sn)_{trans,ax\text{-}ax}$ satellites of the *cis*-$[Rh(SnCl_3)_4Cl_2]^{3-}$ (axial) complex anion.

The assignment of the species labelled in Figure 5.12, as listed in Table 5.5, are based on the good agreement of the measured ^{119}Sn NMR parameters ($\delta(^{119}Sn)$/ppm, $^{1}J(^{103}Rh\text{-}^{119}Sn)$/Hz, $^{2}J(^{117/119}Sn\text{-}^{119}Sn)$/Hz) with those of the corresponding species discussed and assigned in Chapter 3. The $\delta(^{119}Sn)$/ppm of these species were plotted against the number of $SnCl_3^-$ ligands coordinated to the central rhodium, 'n', of each species in the series of $[Rh(SnCl_3)_nCl_{5-n}]^{3-}$ (n = 1 – 5) complex anions and resulted in the two trends shown in Figure 5.13. As discussed in Chapter 3, these two trends are ascribed to the *isotopomers* where the $^{119}SnCl_3^-$-ligand is either *trans* (indicated by the red trend in Figure 5.13) or *cis* (indicated by the blue trend in Figure 5.13) to a Cl^- ligand. In Figure 5.13 the trend of the *trans* $^{119}SnCl_3^-$-ligand is extrapolated to where the number of $SnCl_3^-$ ligands coordinated to the central rhodium is equal to 1, n = 1.

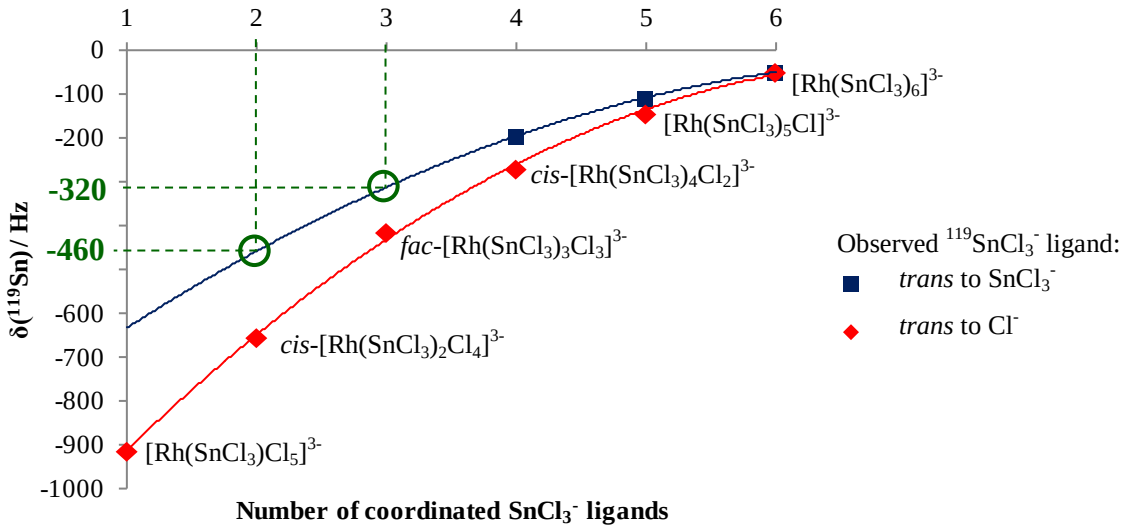

Figure 5.13 Plot of the $\delta(^{119}Sn)$ of the $[Rh^{III}(SnCl_3)_nCl_{5-n}]^{3-}$ (n = 1 – 6) complex anions as a function of the number of coordinated $SnCl_3^-$ ligands.

From the extrapolated trend, one might expect to see signals at $\delta(^{119}Sn)$ = -320 and - 460 ppm for the species with n = 3 and 2, respectively, where the observed $^{119}SnCl_3^-$ ligand is *trans* to a Cl^- ligand. These chemical shift values correspond well with the unidentified signals at $\delta(^{119}Sn)$ = -336.3 and - 463.3 ppm, Figure 5.12. Subsequently, these signals were tentatively assigned to the $[Rh(SnCl_3)_3Cl_3]^{3-}$ and $[Rh(SnCl_3)_2Cl_4]^{3-}$ complex anions where the observed $^{119}SnCl_3$- ligand is *trans* to a chlorido ligand, as listed in Table 5.5. Although the signal to noise ratio obtained in this spectrum is too low to observe the $^{2}J(^{117/119}Sn\text{-}^{119}Sn)$ satellites of these species, thus preventing the determination of the I(sat)/I(main) ratio, the $^{1}J(^{103}Rh\text{-}^{119}Sn)$

was measured and given in Table 5.5. Plotting the $^{1}J(^{103}Rh\text{-}^{119}Sn)$ *versus* the number of coordinated $SnCl_3^-$ ligands (n) for the species listed in Table 5.5 results in the two distinctive, very systematic, trends shown in Figure 5.14. Similarly to the trends in Figure 5.13, these two trends are ascribed to the *isotopomers* where the observed $^{119}SnCl_3^-$-ligand is either *trans* (indicated by the red trend in Figure 5.14) or *cis* (indicated by the blue trend in Figure 5.14) to a Cl^- ligand. The data points obtained for the species at (^{119}Sn) = -336.3 and - 463.3 ppm, tentatively assigned to the $[Rh(SnCl_3)_3Cl_3]^{3-}$ and $[Rh(SnCl_3)_2Cl_4]^{3-}$ complex anions, are encircled in Figure 5.14.

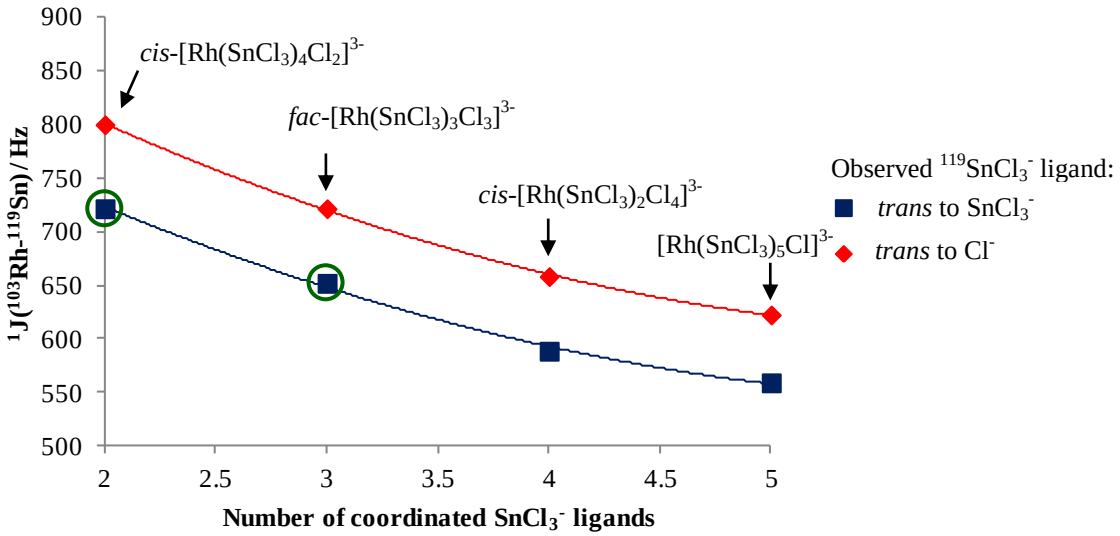

Figure 5.14 Plot of the $^{1}J(^{103}Rh\text{-}^{119}Sn)$ coupling constants measured for the $[Rh(SnCl_3)_nCl_{5-n}]^{3-}$ (n = 2 – 5) complex anions as a function of the number of coordinated $SnCl_3^-$ ligands.

From Figure 5.14 these two data points clearly form part of the trend where the observed $^{119}SnCl_3^-$ ligand is *trans* to another $SnCl_3^-$ ligand, which greatly supports the assignment given in Figure 5..

The signal at (^{119}Sn) = -209.9 ppm does not conform to either of the trends shown in Figure 5.14 or Figure 5.15. However, from its chemical shift and $^{1}J(^{103}Rh\text{-}^{119}Sn)$ coupling constant it does form part of the series of Rh(III)-Sn(II) species and deconvolution of the signals suggests that there are two $SnCl_3^-$ ligands coordinated to the central rhodium. Therefore, the set of signals (^{119}Sn) = -209.9 ppm at this time can only be tentatively assigned to a $[Rh(SnCl_3)_2Cl_4]^{3-}$complex anion, with no further additional information available. Unfortunately, no assignment could be made of the minor Rh-Sn species observed in Figure 5.12 and listed in Table 5.5. Nonetheless, using the trend analyses in Figures 5.14 and 5.15

eleven species could be assigned and characterized, two of which (*fac*-$[Rh(SnCl_3)_3Cl_3]^{3-}$ with the observed $^{119}SnCl_3^-$ ligand *trans* to Cl^- and *cis*-$[Rh(SnCl_3)Cl_4]^{3-}$ with observed $^{119}SnCl_3^-$ ligand *trans* to Cl^-) has never been assigned before

Table 5.5 Summary of the ^{119}Sn NMR parameters for the Rh-Sn species obtained in propan-2-ol.

Rh-Sn Complex*	**δ(^{119}Sn)/ppm**	**^{1}J(^{103}Rh-^{119}Sn)/Hz**	**No. $SnCl_3^-$ ligands**	
$[RhH(SnCl_3)_5]^{3-}$	-10.1	596	5	mi
$[Rh(SnCl_3)_6]^{3-}$	-50.7	521	6	ma
$[Rh(SnCl_3)_5Cl]^{3-}$ (eq) (*cis* to Cl^-)	-110.2	555	5	ma
-#	-141.1	616		mi
$[Rh(SnCl_3)_5Cl]^{3-}$ (ax) (*trans* to Cl^-)	-145.1	624	5	ma
-	-185.9	562		mi
cis-$[Rh(SnCl_3)_4Cl_2]^{3-}$ (*cis* to Cl^-)	-197.2	591	4	ma
$[Rh(SnCl_3)_2Cl_4]^{3-}$$	-209.8	616	2	ma
cis-$[Rh(SnCl_3)_4Cl_2]^{3-}$ (*trans* to Cl^-)	-271.5	659	4	ma
-	-303.4	605		mi
-	-317.1	625		mi
***fac*-$[Rh(SnCl_3)_3Cl_3]^{3-}$** (*trans* to Cl^-)	**-336.3**	**654**	**3**	**ma**
fac-$[Rh(SnCl_3)_3Cl_3]^{3-}$ (*cis* to Cl^-)	-416.3	721.9	3	ma
***cis*-$[Rh(SnCl_3)_2Cl_4]^{3-}$** (*cis* to Cl^-)	**-463.3**	**722**	**2**	**mi**
cis-$[Rh(SnCl_3)_2Cl_4]^{3-}$	-656.3	793	2	ma

* Assignments are based on the correlation of the ^{119}Sn NMR parameters to those previously discussed for either the aqueous phase, Chapter 3, or for the Rh-Sn complexes extracted with MIBK. # No assignment has been made. The intensities of the signals are indicated by **minor (mi)** or **major (ma)** where the former indicates species that are present at < 10 %. $ This is a tentative assignment based on the I(sat)/I(main) ratio obtained.

5.3 Conclusion

In this chapter the speciation of the series of $[Rh(SnCl_3)_nCl_{6-n}]^{3-}$ (n = 1 – 6) complex anions, as well as the $[Rh(SnCl_3)_5]^{4-}$ and $[RhH(SnCl_3)_5]^{3-}$ complex anions, extracted into various non-aqueous phases were studied using modern 1D and 2D ^{1}H, ^{103}Rh and ^{119}Sn NMR spectroscopy.

Plotting the $\delta(^{119}Sn)$/ppm of a species against the $^{1}J(^{103}Rh\text{-}^{119}Sn)$/Hz thereof, as well as plotting the $\delta(^{119}Sn)$/ppm against the number of Sn-ligands coordinated to the central Rh, together with the comparison of the $^{2}J(^{119}Sn\text{-}^{119}Sn)/^{2}J(^{117}Sn\text{-}^{119}Sn)$ ratios to the $\gamma(^{119}Sn)/\gamma(^{117}Sn)$ and applying the method of successive splitting allowed for the unambiguous assignment of the series of $[Rh(SnCl_3)_nCl_{6-n}]^{3-}$ (n = 1 – 6) complex anions, the $[Rh(SnCl_3)_5]^{4-}$ complex anion and the $[RhH(SnCl_3)_5]^{3-}$ complex anion. Additionally, having proven in Chapter III that these Rh(III)-Sn(II) species are kinetically inert, allowed for the identification and characterization of *isotopomers* of the series of $[Rh(SnCl_3)_nCl_{6-n}]^{3-}$ (n = 1 – 6) complex anions, which have never been reported before.

The $[Rh(SnCl_3)_nCl_{6-n}]^{3-}$ (n = 1 – 6) complex anions, as well as the $[Rh(SnCl_3)_5]^{4-}$ were successfully extracted into an organic phase by using either MIBK or Aliquat336 in chloroform-*d*. Re-investigation of the Rh(III/I)-Sn(II) species extracted into MIBK, with the new knowledge that these Rh(III)-Sn(II) complex anions are kinetically inert, has lead to the assignment of 3 species in the ^{119}Sn NMR spectrum, $[RhH(SnCl_3)_5]^{3-}$ and $[Rh(SnCl_3)_nCl_{6-n}]^{3-}$ (n = 5, 6), as well as their respective *isotopomers (*with the observed $^{119}SnCl_3^-$ ligand either *trans* to another $SnCl_3^-$ ligand or *trans* to Cl^-). Full elucidation of the ^{119}Sn NMR spectrum is thus achieved, compared to previous reports in the literature where the signals were either unassigned or incorrectly assigned.[98,111] Moreover, it was proven that the predominant species in the bright yellow MIBK solution is the $[RhH(SnCl_3)_5]^{3-}$ species. The $\delta(^{1}H)$ and $^{2}J(^{1}H\text{-}^{119}Sn)$ parameters obtained from the ^{1}H NMR spectrum of thereof were used to generate the ^{103}Rh, ^{1}H HMQC NMR spectrum, which facilitated the determination of the $\delta(^{103}Rh)$ = -1191 ppm for these Rh(III)-Sn(II) species. This is the first ^{103}Rh chemical shift ever reported for these Rh(III/I) species.

The ^{119}Sn NMR parameters of the Rh(III/I)-Sn(II) species extracted into chloroform-*d* using Aliquat336 corresponded very well with both that reported for the aqueous solutions (discussed in Chapter 3) and that reported in the literature for chloroform-*d* (Aliquat336) extracts, for these species. This confirms that the species are extracted by Aliquat336 through an ion-exchange mechanism. The formation of the $[RhH(SnCl_3)_5]^{3-}$ species is ascribed to the HCl that is co-extracted with the species which results in the oxidative addition (still speculative) reaction of HCl to the species, giving the hydride. The spectra were unambiguously assigned to 6 respective $[Rh(SnCl_3)_nCl_{6-n}]^{3-}$ (n = 3 – 6), $[RhH(SnCl_3)_5]^{3-}$

complex anions and their respective *isotopomer* pairs. Again several of these assignments have not previously been reported for the Aliquat336 extracts, as it was generally accepted that these $[Rh(SnCl_3)_nCl_{6-n}]^{3-}$ (n = 1 – 6) species were *stereo*-chemically non-rigid, which lead to each species being assigned to a resonance signal in stead of a specific *isotopomer* of that species.

The ^{119}Sn NMR spectrum obtained for the propan-2-ol solution showed 13 signals due to Rh-Sn species. From the results obtained in this work, 11 of those signals was assigned two of which has never been assigned before. The $\delta(^{119}Sn)$ and $^{1}J(^{103}Rh\text{-}^{119}Sn)$ was respectively plotted against the number of coordinated $SnCl_3^-$ ligands of a species in order to study the trend analyses of these complex anions. From the trends obtained, two of the unknown species were assigned to the *isotopomers* of the $[Rh(SnCl_3)_nCl_{6-n}]^{3-}$ (n = 2 and 3) species where the observed $^{119}SnCl_3^-$ ligand are *trans* to another $SnCl_3^-$ ligand, respectively. These species have never been reported. Thus all possible *isotopomer* pairs for the series of $[Rh(SnCl_3)_nCl_{6-n}]^{3-}$ (n = 2 – 6) have been identified and characterized in the propan-2-ol solution using high resolution ^{119}Sn NMR.

Chapter VI

General Discussions and Conclusions

Chapter VI

General Discussions and Conclusions

6.1 General Discussions and Conclusions

The detailed high-resolution multi-nuclear 1 and 2D NMR study of the stannous halide complexes of Rh(I/III) in aqueous and non-aqueous solutions has emphasized the power of NMR spectroscopy and the advantages the advances in NMR spectroscopy holds.

Re-investigation of the chlorido Rh(III/I)-Sn(II) species by means of high resolution ^{119}Sn NMR at high magnetic fields proved to be worthwhile. From the detailed high-resolution ^{119}Sn NMR study it was shown that both Rh(I)-Sn(II) and Rh(III)-Sn(II) can simultaneously be present in hydrochloric acid solutions, depending on the experimental conditions used and is in agreement with what is reported in literature.[41] The signal at $\delta(^{119}Sn)$ = -9.39 ppm is assigned to the *stereo*-cehmically non-rigid 5 -coordinated Rh(I)-Sn(II) species, $[Rh^{I}(SnCl_3)_5]^{4-}$. This is in agreement with what is reported in literature.

However, for the series of $[Rh^{III}(SnCl_3)_nCl_{6-n}]^{3-}$ (n = 1 – 6) complex anions in hydrochloric acid solutions, it was explicitly shown that the Rh(III)-Sn(II) species, previously tacitly believed to be *stereo-chemically non-rigid*, do not undergo any *inter*- or *intra*- molecular scrambling on the NMR time-scale and are in fact kinetically inert. This is evidenced by the two separate ^{119}Sn NMR signals obtained for *isotopomer*- pairs where the observed $^{119}SnCl_3^-$ coordinated to the rhodium is either in a position *trans* to a Cl^- or in a position *trans* to another $^{i}SnCl_3^-$ ligand. This is the first time that *isotopomer*-pairs such as these are reported for the series of $[Rh^{III}(SnCl_3)_nCl_{6-n}]^{3-}$ (n = 1 – 6) complex anions.

Thus, prior to this breakthrough, speciation of these $[Rh^{III}(SnX_3)_nX_{6-n}]^{3-}$ (X = Cl^-/Br^-, n = 1 – 6) species using ^{119}Sn NMR could not be fully elucidated as the respective *isotopomer* pairs were not taken into consideration. Until now 5 Rh(III)-$SnCl_3^-$ species have been identified and characterized in literature,[8,41] however, these assignments for these $[Rh^{III}(SnCl_3)_nCl_{6-n}]^{3-}$ (n = 1 – 6) species can no longer be accepted to be correct, as the assignments are made to specific species and not respective *isotopomers*. In the work presented here, 9 of the possible 10 $[Rh^{III}(SnCl_3)_nCl_{6-n}]^{3-}$ (n = 1 – 6) *isotopomers* have been identified and charactarized using high resolution ^{119}Sn NMR spectroscopy.

This is the first *isopomer* study reported for these Rh(III)-Sn(I)species. Additionally, the $[Rh(SnCl_3)_6]^{3-}$ species was identified for the first time and characterized using ^{119}Sn NMR spectroscopy. A simulation program, gNMR50, was used to simulate each set of ^{119}Sn NMR signals in order to confirm the assignments. From the excellent agreements obtained between the experimental and gNMR50 simulated ^{119}Sn NMR spectrum, these assignments could be considered unambiguous.

Investigation of the analogous stannous bromide complexes of rhodium(I/III) in HBr solutions furnished the assignment of 3 $[Rh(SnBr_3)_nBr_{6-n}]^{3-}$ (n = 3 – 5) species that has never been reported before. Moreover, 2 distinctive *isotopomer* pairs of these complex anions (with n = 3, 4) were assigned. It is thus established that these species, as with the analogous chlorido species, are kinetically inert and do not undergo rapid *intra*- or *inter*-molecular exchange on the NMR time-scale. Comparison between the ^{119}Sn NMR parameters of the stannous chlorido and stannous bromido species has shown that for the series of $[Rh(SnX_3)_nX_{6-n}]^{3-}$ (X = Cl^-, Br^-, n = 1 – 6) complex anions that the ^{119}Sn NMR signals becomes less shielded as 'n' increases which results in a downfield shift of the signals. This suggests that the interaction between the ^{103}Rh and a $SnBr_3^-$ ligand is weaker than that between the ^{103}Rh and a $SnCl_3^-$ ligand. Several attempts were made to obtain the mixed chlorido/bromido species, however they were not observed with ^{119}Sn NMR spectroscopy. The difference between the $\delta(^{119}Sn)$ of the species are smaller than was observed with the chlorido species, which suggests that the observed ^{119}Sn nucleus is less influenced by changes in the bromido species than in the chlorido species. Moreover, the $^1J(^{103}Rh\text{-}^{119}Sn)$ coupling constant of the species are smaller for the bromido species than the chlorido species. This is in agreement with what was previously reported for the $[Pt(SnX_3)_5]^{3-}$ (X = Cl-, Br^-) species. Thus it is reasonable to suggest that the interaction between the ^{103}Rh and a $SnBr_3^-$ ligand is weaker than that between the ^{103}Rh and a $SnCl_3^-$ ligand.

With the new knowledge of the *stereo*-chemical rigidity of the Rh(III)-Sn(II) species, the speciation of the Rh(IIII)-Sn(II) species extracted into organic solutions was re-investigated using multi-nuclear NMR spectroscopy. These species were either extracted from hydrochloric acid solutions into MIBK or into chloroform-*d* using Aliquat336. The species were assigned using same methodology that was used to assign these species in the aqueous solutions. The ^{119}Sn NMR parameters of the Rh(III/I)-Sn(II) species extracted into

chloroform-*d* using Aliquat336 corresponded very well with those previously reported by Koch et. al.[8] However, all the ^{119}Sn NMR signals were re-assigned to the respective *isotopomers* of the species in the kinetically inert $[Rh^{III}(SnCl_3)_nCl_{6-n}]^{3-}$ (n = 3 – 6) series. Moreover, the Rh(III)-Sn(I) species extracted into chloroform-*d* using Aliquat336 corresponded well to the species in the aqueous solution, which confirms that the species are extracted by Aliquat336 through an ion-exchange mechanism. The $[Rh^{I}(SnCl_3)_5]^{4-}$ species, on the other hand, is not observed in the extracted solutions, but is replaced with the $[Rh^{III}H(SnCl_3)_5]^{3-}$ complex anion. The latter is proposed to be formed by the oxidative addition of HCl, which is co-extracted, to $[Rh^{I}(SnCl_3)_5]^{4-}$. The ^{119}Sn NMR spectrum of the chloroform-*d* (AQ336) has been fully elucidated with all the signals being assigned.

For the MIBK extract it was found that $[Rh^{III}H(SnCl_3)_5]^{3-}$ was the predominant species in solution which is in agreement with what was reported by Koch *et. al*.[98] for these solutions. A detailed *isotopomer/isotopologue* study of this species was performed by means of ^{1}H and ^{119}Sn NMR spectroscopy. From the elucidation of the ^{119}Sn NMR spectrum, and with the aid of gNMR50 simulated spectra, two *isotopomers* ($^{119}SnCl_3^-$ *trans* to Cl^- and *trans* to $SnCl_3^-$) and six *isotopologues* were identified and characterized. Twelve respective *isotopologues* and *isotopomers* were assigned in the ^{1}H NMR spectrum of the $[RhH(SnCl_3)_5]^{3-}$ complex anion. However, this was only achieved by simulating the ^{1}H NMR spectrum with gNMR50 and setting the $\Delta(\nu_{½})$ = 0.5 Hz. The recorded ^{1}H NMR parameters were used to record the ^{103}Rh,^{1}H HMQC NMR spectrum for this species and the $\delta(^{103}Rh)$ was determined to be -1191 ppm. This is the first ^{103}Rh chemical shift value reported for these Rh(III)-Sn(II) species.

As mentioned, two types of *isotopomers* are observed for these $[Rh^{III}(SnX_3)_nX_{6-n}]^{3-}$ (n = 1 – 6, X = Cl^-/Br^-) species: one where the observed $^{119}SnX_3^-$ ligand is coordinated to the rhodium in a position *trans* to a X^- or in a position *trans* to another $^{i}SnX_3^-$ ligand. Execellent second order correlation is obtained for both these types of *isotopomers* when plotting the $\delta(^{119}Sn)$ of a specific *isotopomer* against the Number of Coordinated SnX_3^- ligands for that *isotopomer*. Similarly, great second order correlation is obtained when plotting the $^{1}J(^{103}Rh\text{-}^{119}Sn)$ of an *isotopomer* against the Number of Coordinated SnX_3^- ligands for that *isotopomer*. Both these methods of trend analysis for these $[Rh^{III}(SnX_3)_nX_{6-n}]^{3-}$ (n = 1 – 6, X = Cl^-/Br^-) species are a great improvements on the method previously used in literature[41] where the $\delta(^{119}Sn)$ was plotted against the $^{1}J(^{103}Rh\text{-}^{119}Sn)$ of a species. With the *isotopomer* trend analysis described in this work, the correlations obtained are good enough to predict the chemical shift of a specific *isotopomer*, which makes it a great

method to study the speciation of these Rh(III)-Sn(II) species. Using this method of trend analysis, 5 $[Rh^{III}(SnCl_3)_nCl_{6-n}]^{3-}$ (n = 2 – 6) species (one has never been reported before), 5 *isotopomer* pairs which has never been reported and 27 *isotopologues* could be assigned

Once again high-resolution NMR spectroscopy has proven to be an indispensible tool for the identification and characterization of these Rh-Sn species, having enabled the unambiguous assignment of the respective *isotopomers* and *isotopologues* of the series of $([Rh(SnCl_3)_nCl_{6-n}]^{3-}$ (n = 1 – 6) complex anions, thus proving the *stereo-chemical* rigidity of these species.

References

References

1. Wollaston, W. H., *Philosophical Transactions*, of the Royal Society of London, 419 (1804)
2. Barbalace, K., *Periodic Table of Elements*, http://EnvironmentalChemistry.com (1995 – 2015)
3. Cowley, A., *Platinum 2013*, Johnson MattheyPLC, Royston, UK, 8 (2013)
4. Diamantatos, A., *Anal. Chim. Acta*, **131**, 53 (1981)
5. Gindin, L. M., *Ion Exch. Solvent Extr.*, **8**, 311 (1981)
6. Benguerel, E., Demopoulos, G. P. and Harris, G. B., *Hydrometallurgy*, **40**, 135 (1996)
7. Cox, M., *Principles and Practices of Solvent Extraction*, ed. J. Rydberg, Cox, M., Musikas, C. and Choppin, G. R., 2nd Ed. Marcel Dekker, Inc., New York, 445 (2004)
8. Hall, I. and Koch, K. R., *Polyhedron*, **10**(14), 1721 (1991)
9. Hall, I., *PhD Thesis*, University of Cape Town (1990)
10. Ivanov, V. N., *J. Russ. Phys-Chem. Soc*., **50**, 460 (1913)
11. Thompson, S. O., Beamish, F. E., and Scott, M., *Ind. Eng. Chem. Anal*. Ed., **9**, 420 (1937).
12. Wöbling, H., *Ber*., **67**, 773 (1934)
13. Bouvet, P., *Ann. pharm. franc*., **5**, 293, (1947)
14. Sandell, E. B., *Colorimetric Determination of Traces of Metals'*, Interscience, New York, Vol 3, 384 (1944)
15. Ayres, G. H., and Young, J. F., *Anal. Chem.*, **34**, 949 (1952)
16. Ayres, G. H., Tuffly, B. L., and Forrester, J. S., *Anal. Chem*., **27**(11), 1742 (1955)
17. Ayres, G. H., and Meyer, A. S., Jr., *Anal. Chem.*, **23**, 299 (1955)
18. Meyer, A. S., Jr., and Ayres, G. H., *J. Am. Chem. Soc.*, **77**, 2671(1955)
19. Berman, S. S. and Ironside, R., *Can. J. of Chem.*, **36**(8), 1151 (1958)
20. Maynes, A. D. and McBryde, *Analyst*, **79**, 230 (1954)
21. Gardner, R. D., and Hues, A. D., *Anal. Chem*., **31**, 1488 (1959)
22. Sandell, E. B., "*Chemical Analysis v3: Colorimetric Determination of Traces of Metals"*, Interscience, New York, 2nd Ed, 523 (1950)
23. Davies, A. G., Wilkinson, G., and Young, J. F., *J. Am. Chem. Soc*., **85**, 1692 (1963)
24. Young, J. F., Gillard, R. D., and Wilkinson, G., *J. Chem. Soc*., **12**, 5176 (1964)
25. Adams, D. M., and Chandler, P. J., *Chem. Ind*. (London), 269 (1965)
26. Gorsich, R. D., *J. Am. Chem. Soc*., **84**, 2486 (1962)
27. Bonati and Wilkinson, J., *J. Am. Chem. Soc*., 179 (1964)
28. Furlani, C., Zinato, E., and Furlan, F., *Atti Accad. Naz. Lincei, Rend. Sc. Fis. Mat. e Nat.*, **38**, 517 (1965)
29. Furlani, C., Zinato, E., and Culot, G., *Atti. Accad. Nazl. Lincei, Rend., Classe Sci. Fis., Mat. Nat.* **41**, 69 (1966)
30. Young, J. F., *Adv. Inorg. Chem. Radiochem.*, **11**, 91 (1968)
31. Kingston, J. V., and Scollarly, G. R., *J. Chem. Soc. (A)*, 3399 (1971)
32. Kimura, T., Miki, E., Mizumachi, K., and Ishimori, T., *Chem Lett*, 1325 (1976)
33. Kimura, T., *Sci. Papers I.P.C.R.*,**73**(3) (1979)
34. Parish, R. V., and Rowbotham, P. J., *J. Chem. Soc.(Dalton Trans.)*, 37 (1973)

35. Antonov, P. G., Kukushkin, Yu. N., Anufriev, V. I., Vasil'ev, L. N., and Konovalov, L. V., *Russ. J. Inorg. Chem.*, **24** (2) (1979)

36. Kukushkin, Yu. N., Antonov, P. G., Dubonos, K. I., and Konovalov, L. V., *Russ. J. Inorg. Chem.*, **11** (1973)

37. Yurchenko, E. N., Antonov, P. G., Varnek, V. A., Konnov, V. I., Shan'ko, A. N., and Kukushkin, Yu. N., *Koord. Khim.*, **2**, 1632 (1976)

38. Varnek, V. A., Yurchenko, E. N., Elizarova, G. L., Shan'ko, A. N., Matvienko, L. G., Antonov, P. G., and Kukushkin, Yu. N., *Koord. Khim.*, **1**, 161 (1975)

39. Kimura, T., and Sakurai, T., *J. Solid State Chem.*, **34**, 369 (1980)

40. Lassigne, C. R. and Wells, E. J., *Can. J. Chem.*, **55** (6), 927 (1977)

41. Moriyama, H., Aoki, T., Shinoda, S., and Saito, Y., *J. Chem. Soc. (Dalton Trans.)*, 639 (1981)

42. Chernyaev, I. I., *Ann. Inst. Platine (U.S.S.R)*, **1**, 243 (1926)

43. Huheey, J. E., *Inorg. Chem.*, Harper & Row, New York, 2nd Ed. (1978)

44. Holt, M. S., Wilson, W. L., and Nelson, J. H., *Chem. Rev.*, **89**,11 (1989)

45. Cramer, R. D., Lindsey, R. V., Jr., Jenner, E. L., Prewitt, C. T., and Stolberg, U. G., *J. Am. Chem. Soc.*, **87** (3), 658 (1965)

46. Kukushkin, Yu. N., Antonov, P. G., Dubonos, K. I., and Konovalov, L. V., *Russ. J. Inorg. Chem.*, **18**, 1604 (1973)

47. Usón, R., Oro, L. A., Reyes, J., Carmona, D. and Lahuerta, P., *Transition Met. Chem.*, **8**, 46 (1983)

48. Albinati, A., Pregosin, P. S., and Rüegger, H.J, *Inorg. Chem.*, **23**, 3223 (1984)

49. Parshall, G. W., *J. Am. Chem. Soc*., **86**, 3567 (1964)

50. Parshall, G. W., *J. Am. Chem. Soc*., **88**, 704 (1966)

51. Graham, W. A. G, *Inorg. Chem.*, **7**, 315 (1968)

52. Cotton, F. A., and Kraihanzel, C. S., *J. Am. Chem. Soc*., **84**, 4432 (1962)

53. Cotton, F. A., and Kraihanzel, C. S., *Inorg. Chem*., **2**, 533 (1963)

54. Cotton, F. A., *Inorg. Chem*., **3**, 702 (1964)

55. Hartley, F. R., *Chem. Soc. Rev.*, **2**, 287 (1973)

56. L. E. Orgel, "An Introduction to Transition Metal Chemistry," John Wiley and Sons, Inc,. New York, N. Y, **9**, 137 (1960)

57. Bryan, R. F., Greene, P. T., Melson, G. A., and Stokely, P. F., *Chem. Commun*., 722 (1969)

58. Nelson, J. H., Wilson, W. L., Wilson, Cary, L. W., Alcock, N. W., Clase, H. J., Jas, G. S., Ramsey-Tassin, L., and Kenney, J. W., *Inorg. Chem.*, **35** (4), 883 (1996)

59. Barkhuysen, S., MSc Thesis, University of Stellenbosch, 2012

60. Taylor, R. C., Young, J. F., amd Wilkinson, G., *Inorg. Chem.*, **5**, 20 (1966)

61. Lindsey, R. V. Jr., Parshall, G. W., and Stolberg, U. G., *J. Am. Chem. Soc*., **87**, 658 (1965)

62. Chatt, J., Duncanson, L. A., and Shaw, B. L., *Chem. Ind.* (London), 859 (1958)

63. Chatt, J. and Shaw, B. L., *J. Chem. Soc.*, 5075 (1962)

64. Chatt, J., Duncanson, L. A., and Venanzi, L. M., *J. Chem. Soc.*, 4456 (1955)

65. Kretschmer, M., Pregosin, P. S., and Rüegger, H.J., *J. Organomet. Chem.*, **241**, 87 (1983)

66. Albinati, A., von Gunten, U., Pregosin, P. S., and Rüegger, H. J., *J. Organomet. Chem.*, **295**, 239 (1985)

67. Anderson, K. M., and Orpen, A. G., *Chem. Commun.*, 2682 (2001)

68. Coe, B. J., and Glenwright, S. J., *Coord. Chem. Rev.*, **203**, 5 (2000)

69. Rabi, I. I., Zacharais, J. R., Millman, S. and Kusch, P., *Phys. Rev.*, **53**, 318 (1938)

70. Proctor, W. G., and Yu, F. C., *Phys. Rev.*, **77**, 717 (1950)

71. Dickenson, W. C., *Phys. Rev.*, **77**, 736 (1950)

72. Lindstrom, G., *Phys. Rev.*, **78**, 817 (1950)

73. Thomas, H. A., *Phys. Rev.*, **80**, 901 (1950)

74. Kessler, H., Gerke, M., and Griesinger, C., *Angew. Chem. Int. Ed. Engl.*, **27**, 500 (1988)

75. Morris, G. A., *Magn. Res. Chem.*,**24**, 371 (1986)

76. Benn, R, and Günther, H., *Angew. Chem. Int. Ed. Engl.*, **22**, 350 (1983)

77. Freeman, R. and Morris, G. A., *Bull. Magn. Reson.*, **1**, 5 (1979)

78. Ernst, R., *Angew. Chem. Int. Ed. Engl.*, **31**, 805 (1991)

79. Becker, E. D., *High Resolution NMR: Theory and Chemical Applications*, 3rd Ed., Academic Press, New York (2000)

80. Hani, R. and Geanangel, R. A., *Coord. Chem. Rev.*, **44**, 229 (1982)

81. Ramsey, N. R., *Phys. Rev.*, **78**, 699 (1950)

82. Juranic, N., *Coord. Chem. Rev.*, **96**, 253 (1989)

83. Pople, J. A. and Santry, D. P., *Mol. Phys.*, **8**, 1 (1964)

84. Moriyama, H., Aoki, T., Shinoda, S., and Saito, Y., *J. Chem. Soc. (Dalton Trans.)*, 639 (1981)

85. Bax, A., Griffey, R. H., and Hawkins, B. L., *J. Magn. Reson.*, **55**, 301 (1983)

86. von Philipsborn, W., *Chem. Soc. Rev.*, **28**, 95 (1999)

87. Carlton, L, *Inorg. Chem.*, **39**(20), 4510 (2000)

88. Mason, J., *Chem. Rev.*, **87**, 1299 (1987)

89. Mann, B. E., *Transition Metal NMR*, Pregosin, P. S., Ed., Elsevier, Amsterdam, 177 – 215 (1991)

90. Kidd, R. G. and Goodfellow, R. J., *NMR and the Periodic Table*, Harris, R. K. and Mann, B. E., eds., Academic Press, London (1978)

91. Geswindt, T. E., Gerber, W. J., Brand, D. J., and Koch, K. R., *Anal. Chim. Acta*, **730**, 93 (2012)

92. Budzelaar, P. H. M., *Simulation of one-dimensional NMR spectra*, IvorySoft (1995-2006)

93. Klinskaya, I. Yu., Rosenkevich, M. B. and Sakaharovski, Yu. A., *Kinet. Katal*., **19**, 329 (1978)

94. Parish, R. V., *Prog. Inorg. Chem.*, **18**, 101 (1972)

95. Burke, J. J. and Lauterbur, M. F., *J. Am. Chem., Soc.*, **83**, 326 (1961)

96. Gerber, W. J, Murray, P. and Koch, K. R., *Chem. Soc. (Dalton Trans.)*, **31**, 4113 (2008)

97. IUPAC. Compendium of Chemical Terminology, 2nd edition (the "Gold Book"). Compiled by A. D. McNaught and A. Wilkonson. Blackwell Scientific Publications. Oxpord (1997)

98. Koch, K. R. and Wyrley-Birch, J. M., *Inorg. Chim. Acta*, **L5**, 102 (1985)

99. Krut'ko, D. P., Permin, A. B., Petrosyan, V. S. and Reutov, O. A., *Izv. Akad. Nauk SSSR, Ser. Khim.* (Engl. Trans.), **12**, 2553 (1984)

100. Moriyama, H., Aoki, T., Shinoda, S., and Saito, Y., *J. Chem. Soc., Chem. Commun*., 500 (1982)

101. Koch, K. R. and Kramer, J., *Inorg. Chem.*, **45**, 7843 (2006)

102. Berman, S. S. and McBryde, W. A. E., *Analyst*, **81**, 566 (1956)

103. Garralda, M., Garcia, V., Kretschmer, M., Pregosin, P. S. and Rüegger, H., *Helv. Chim. Acta*, **64**(4), 1150 (1981)

104. Jones, L., Nel, I. and Koch, K. R., *Anal. Chim. Acta*, **182**, 61 (1986)

105. Brackenbury, K. F. G., Jones, L., Nel, I., Koch, K. R. and Wyrley-Birch, J. M., *Polyhedron*, **6(1)**, 71 (1987)

106. Shinoda, S., Moriyama, H., Kise, Y.and Saito, Y., *J. Chem. Soc., Chem. Commun.*, 348 (1978)

107. Moriyama, H., Aoki, T., Shinoda, S. and Saito, Y., *J. Chem. Soc., Perkin Trans.*, **2**, 369 (1982)

108. Benguerel, E., Cote, G., Lautie, A., Demopoulos, G. and Bauer, D., *J. Chem. Tech. Biotechnol.*, **62**, 380 (1995)

109. Benguerel, E., *PhD Thesis*, McGrill University (1996)

110. Mhaske, A. and Dhadke, P, *Separ. Sci.Technol.*, **36(14)**, 3235 (2001)

111. Sun, P. P. and Lee, M. S., *Hydrometallurgy*, **105**, 334 (2011)

112. Narita, H., Tanaka, M., Yaita, T. and Okamoto, Y., *Solvent Extr. Ion Exc.*, **22(5)**, 853 (2004)

113. Yamakawa, T., Shinoda, S., Saito, Y, Moriyama, H. and Pregosin, P. S., *Mag. Res. Chem.*, **23** (1985)

114. Kretschmer, M. and Pregosin, P. S., *Inorg. Chim. Acta*, **61**, 247 (1982)